FREEBOARD PHENOMENA IN A FLUIDIZED BED COAL COMBUSTOR

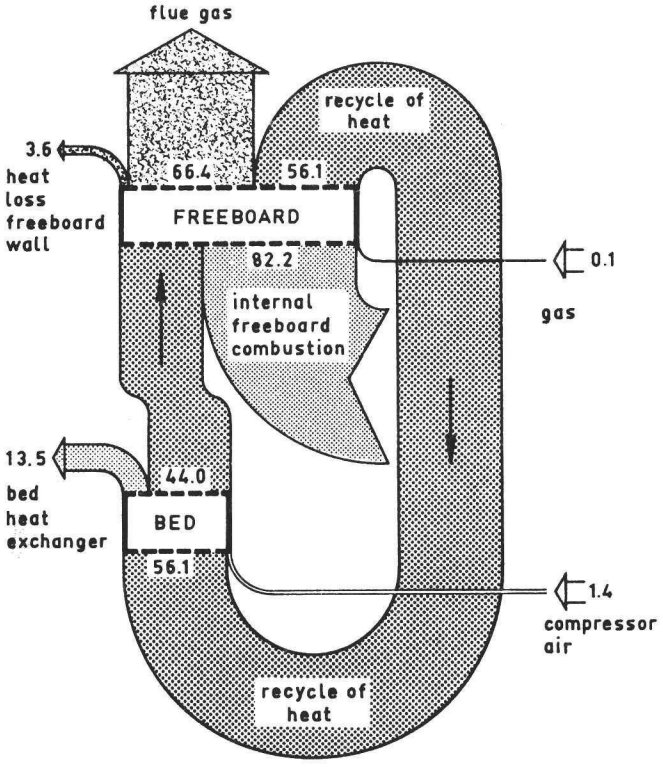

F.J.A. Martens

FREEBOARD PHENOMENA IN A FLUIDIZED BED COAL COMBUSTOR

Proefschrift

Ter verkrijging van de graad van doctor in de
technische wetenschappen aan de Technische Hogeschool Delft,
op gezag van de Rector Magnificus,
prof. ir. B.P.Th. Veltman voor een commissie aangewezen
door het College van Dekanen, te verdedigen op
dinsdag 4 december 1984 om 14.00 uur.

door

FRANCISCUS JOHANNA ARNOLDUS MARTENS
geboren te Meerssen
werktuigkundig ingenieur

Dit proefschrift is goedgekeurd door de promotoren
PROF.IR. C.W.J. VAN KOPPEN
PROF.DRS. P.J. VAN DEN BERG

Aan de medewerkers van het
Laboratorium voor Energievoorziening

SUMMARY

A steady state, one-dimensional model of the freeboard is developed. The model consists of the connection of many simplified phenomenological descriptions and results in a comprehensive model.

Starting from the fluidized bed surface and provided with the proper boundary conditions the model is able to predict solids behaviour, mixing, chemical reactions and heat transfer along the freeboard as a function of height.

The solids behaviour is based on ballistic considerations, i.e. inertia, drag and gravity. The particle trajectory calculations provide for mass flux and holdup of particles along the freeboard which are key parameters for the heterogeneous chemical reactions and the heat economy.

The model of a cascade of perfectly stirred reactors is taken to represent the gas phase flow. In the freeboard the mixing of the oxygen-rich gas from the bubbling phase and the CO-rich emulsion phase of the fluidized bed is treated by a mixing parameter. The conversion rate of O2, CO2 and NOx with char follows from the mechanisms of diffusion and first order chemical reaction.

The quasi steady state heat economy comprises the contributions of the chemical heat release, of the enthalpy flow of the gas and the solids, and of the convective and radiative heat transfer from both the gas and the solids to the wall. The net conductive heat transfer of a single particle during its freeboard trajectory is governed by the external and internal resistances to heat-up, the changing temperatures and the residence time.

The literature on freeboard phenomena is reviewed in connection with the various assumptions made in the model. The general scarcity of experimental data does not permit a more complex approach to be taken.

One model calculation is treated in detail. The boundary conditions are based on experiments carried out in an experimental fluidized bed coal combustor. A fairly coherent picture of the various phenomena in the freeboard can be developed in this way. Further, the model results on chemical conversion and heat transfer compare quite well with the experimental results.

The freeboard is shown to be an integral part of the fluidized bed system. The processes occurring contribute essentially to the total combustion and NOx reduction. Most of the chemical heat release is found to be transported upwind towards the fluidized bed by recirculating particles.

TABLE OF CONTENTS

1 INTRODUCTION

1.1 Fluidization and combustion

Fluidization occurs when a gas (fluid) passes a bed of particles at such a rate that the gravity force acting on the bed is in a dynamic balance with the overall drag force. The gas passes the bed via voids between moving agglomerations of particles at a low relative velocity and via particle lean voids at a much higher velocity. The stability of the lean voids and the agglomerations of particles depends on the physical properties of the gas and the solids but most of all on the gas velocity and the particles' size and distribution. When averaged with respect to time and space the gravity has a dominating influence on the behaviour of the moving agglomerations of particles resulting in a relatively dense and uniformly packed volume. The region here-above is called the 'free board' or generally 'freeboard'. The aerodynamical behaviour of the gas voids in the bed, assisted by the decrease of static pressure head when rising, results in mixing of solids in the fluidized bed and projecting and/or dragging particles into the freeboard. Consequently the freeboard is not free of particles. The function of the freeboard is to provide for space for the (gravity) separation of particles from the gas stream. The fine particles may be dragged upward overcoming the gravity force and ultimately leave the freeboard at the top side. They are elutriated.

In a fluidized bed coal combustor the fluidized bed is a reservoir of chemical active solids: the fuel to be burned and absorbents for minimizing emissions of e.g. SO2 and NOx. For having adequate chemical and/ or physical processes the bed should provide for:

* solid-gas contacting,
* gas-phase macro- and micro-mixing,
* residence time of the particles and the gas,
* proper temperature.

As far as known the gas-phase macro-mixing is limiting some of the chemical conversions considerably. Consequently emissions of partly or even totally unconverted products in the freeboard occur. This and the presence of particles in the freeboard may lead to further conversions and consequently to chemical heat release. Favourable conversions in the gas phase could be the oxidation of CO, H2, CH4 and other combustible products from coal volatiles. Favourable conversions of particles in the freeboard could be:

* combustion of char,
* reduction of NOx by char,
* absorption of SO2 by calcined limestone or dolomite.

Elutriation of solids from the freeboard has a critical impact on fluidized bed efficiency, because:

* elutriation of coal from the freeboard represents the main source of loss in combustion efficiency,
* elutriation affects the utilization of the limestone or dolomite.

Several measures have been or are being investigated to counteract these effects. The earlier developed carbon-burn-up-cell is found less and less. The recycling of the elutriated fines into the fluidized bed by auxiliaries is presently accepted.

1.2 Background and objective

The objective is to contribute to the understanding of the phenomena occuring in the freeboard of a pressurized fluidized bed coal combustor.

The study requires the hypothetical separation of the freeboard from the fluidized bed with respect to the fluid and solid flow, the chemical conversions and the heat economy. Consequently the boundary conditions at the fluidized bed surface have to be known. For proper and comprehensive freeboard analysis a complete set of data has to be available. Unfortunately

the literature scoping the regime of fluidization to be investigated is scarce and if available it turns out to be far from complete. Experimental investigation becomes necessary.

A coal fired pressurized semi-pilot plant was programmed by the university and some industries, being sponsored by the Ministry of Economic Affairs. The design succeeded the engineers' table only. Changing priorities and futher budget restrictions led to canceling of the plan.

Instead, the university succeeded to realize the experimental 'pressurized' fluidized bed coal combustor 'MAGMA' to be operated at atmospheric pressure. A main difference of this 'pressurized' unit compared to an atmospheric one is found in the final combustor freeboard temperature. The high temperature in a 'pressurized' unit follows from gas turbine requirements. The temperature for the atmospheric unit is low to reduce heat losses by stack gases. The combustor 'MAGMA' and the experiments executed were reported in detail by Martens (1984). For information here the lay out of the test-rig is given in figures 1-1 and 1-2. The main dimensions of the combustor are: inner diameter 0.39 m, expanded bed height 0.6 m and freeboard height 2.75 m. The combustor should provide for the detailed information at the boundaries (i.e. at the fluidized bed surface) to be input data for a comprehensive freeboard model.

It is the objective of this thesis to describe the theoretical basis of this model. The program description, the users hand guide and the evaluation of the numerical error analysis can be found in Op den Brouw (1984). The model is called 'FAME' derived from 'Freeboard Analysing Model and Evaluation'.

The performance of the model 'FAME' and of the experiment in the 'MAGMA' should be compared and evaluated.

It was not yet the objective to provide for scaling-up and/or engineering rules in order to build and operate pressurized fluidized beds with optimal freeboard performance in future.
Such a study should follow this primary, although detailed investigation.

1.3 References

Martens, F.J.A.
Experiments with the atmospheric fluidized bed combustor 'MAGMA'.
Rapport EV-1333, Laboratory for Thermal Power Engineering.
Delft University of Technology, Delft, The Netherlands (1984).

Op den Brouw, H.
'FAME' program description (Freeboard Analysing Model and Evaluation).
Rapport EV-1293, Laboratory for Thermal Power Engineering.
Delft University of Technology, Delft, The Netherlands (1984).

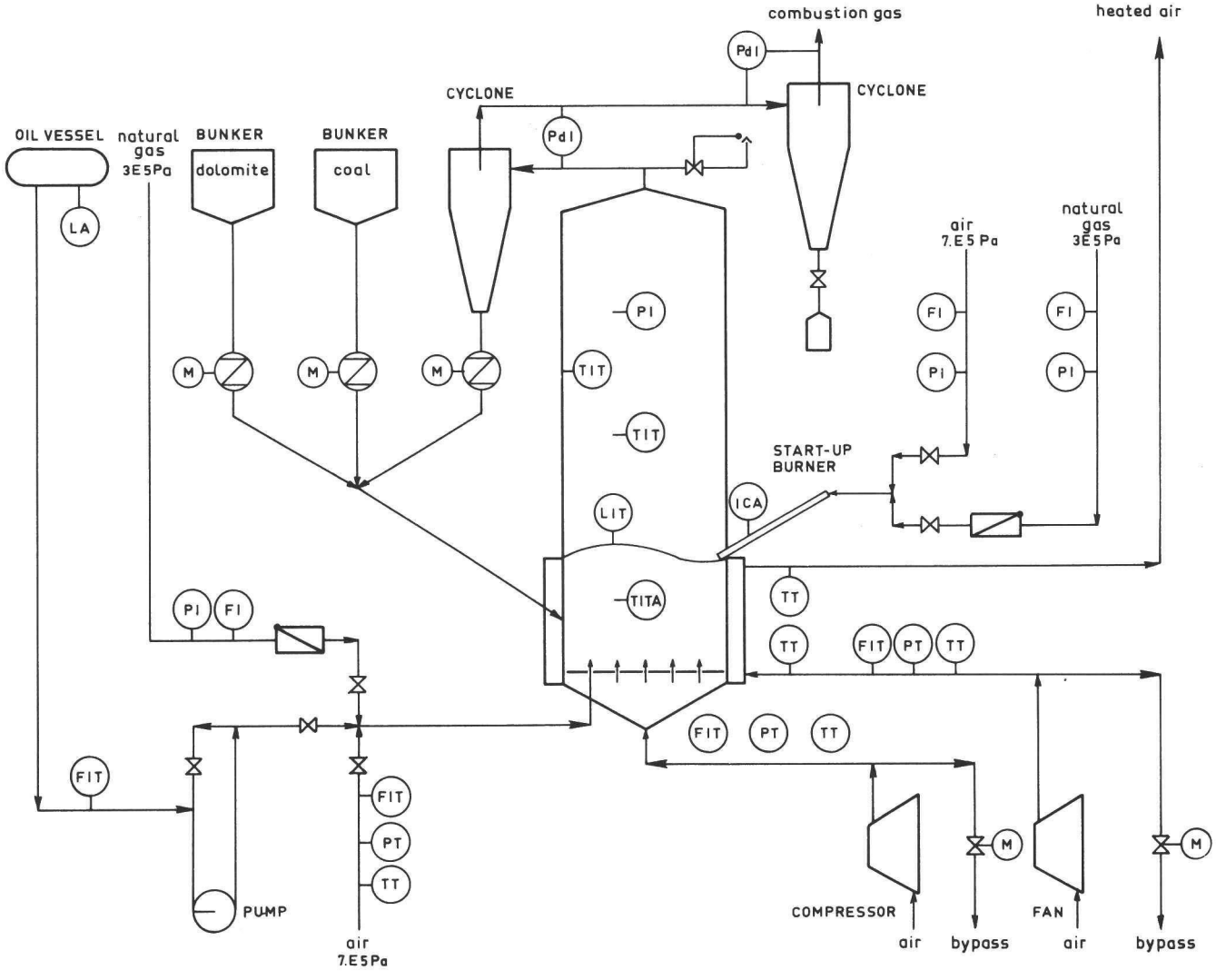

Figure 1-1.
Lay out of test rig with the experimental fluidized bed combustor 'MAGMA' (from Martens (1984)).

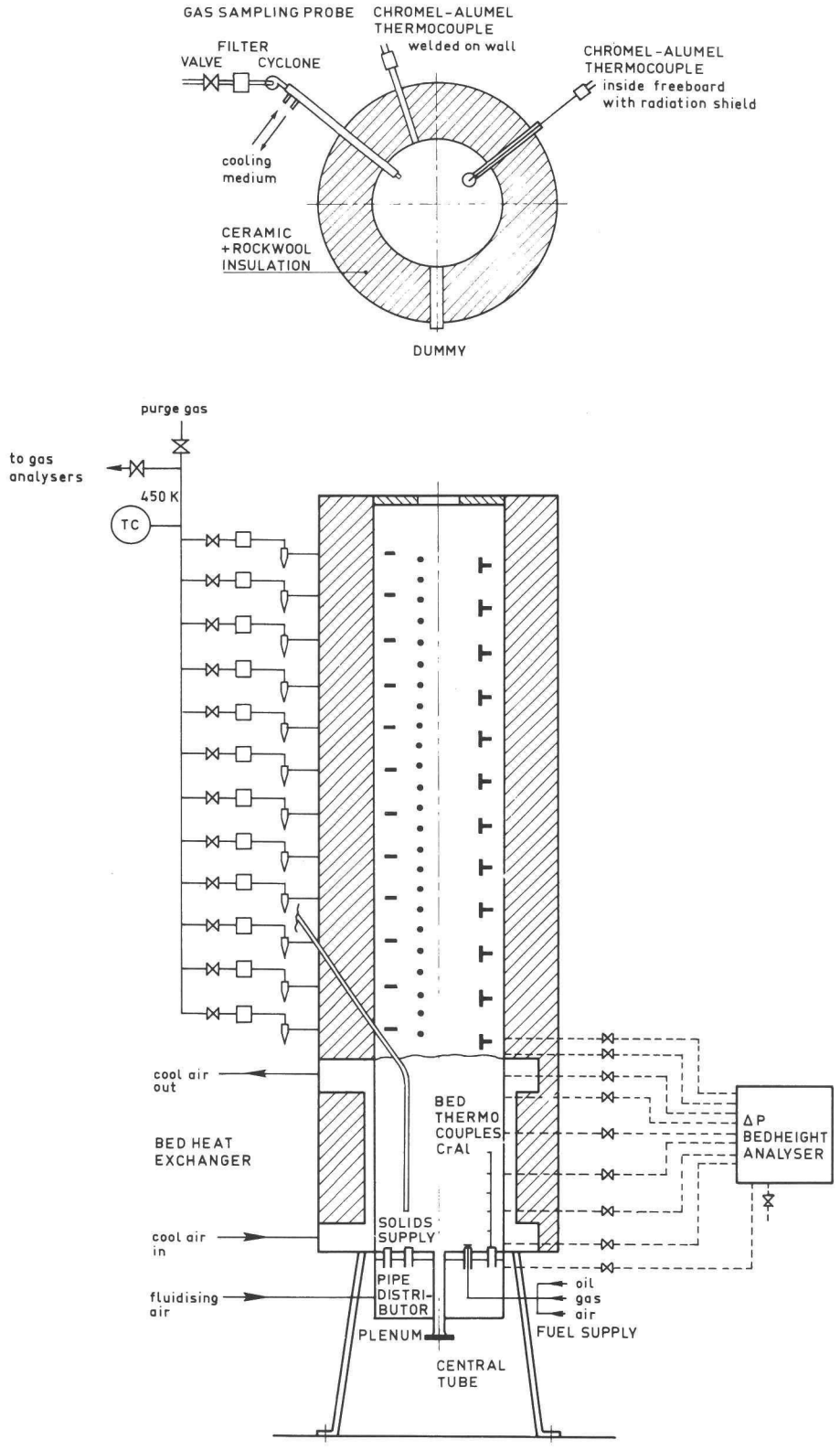

Figure 1-2.
Scheme of the 'MAGMA'; some measuring and sampling provisions (from Martens (1984)).

2 BEHAVIOUR OF SOLID PARTICLES IN THE FREEBOARD

2.1 Introduction

In the freeboard, the region above the fluidized bed, particles are always present. The origin of these particles is the fluidized bed where the bubbling or turbulent action of the gas gives initial upward velocity to the particles. The flux of ascending particles at the fluidized bed surface is here denominated as the initial entrainment. The classical function of the freeboard is to disengage the solids from the fluidizing medium. In simple terms it can be stated that in a fluidized bed system where the free fall velocity of the bulk of the particles is well above the superficial gas velocity and where the freeboard is high enough most of the particles finally will descend and return to the fluidized bed. However, particles with a free fall velocity lower than the superficial gas velocity mostly are carried away by the gas, i.e. they are elutriated.

2.2 Prior studies of entrainment phenomena

2.2.1 Models

Mechanistic solids transport models for calculating entrainment, particles concentration and particle residence time have been developed by Zenz and Weil (1958), Do et al. (1972), George and Grace (1978), Wells and al. (1981), Chaung (1982), Martens (1982), Martens et al. (1983) and Van Rhijn (1983). All models are of a ballistic nature and consider the motion of particles under the influence of inertia force, drag force and gravity force. Zenz and Weil (1958) adopted a modified Stokes-law expression for the drag coefficient permitting an analytical solution for the particle trajectory. Do, Grace and Clift (1972) used a standard-drag-curve relationship and concluded that the discrepancies from the Zenz and Weil prediction can be serious; for example for relatively large particles.

The greatest uncertainties for modeling the freeboard lie with the prediction of the particle-particle and particle-wall interactions and the boundary conditions at or near the fluidized bed surface. Important aspects in this connection are:

* The mass fluxes of solids.
* The solids size and density distribution.
* The initial particle velocities and the get-away angle.
* The particle coherence (aggregates or individual particles).
* The initial gas velocity (jetting velocity) and the gas turbulence.

These aspects will be discussed below.

2.2.2 Gas-solid flow regimes

Fluidized beds under combustion conditions operate with particle sizes in the order of 1.E-3 m and with superficial gas velocities around or above 5 times the minimum to fluidization. The regime of operation is then "slow bubble" or "turbulent". "slow bubble" meaning: slow relative to the interstitial gas velocity. In the turbulent regime there are no well defined bubbles but unsteady aggregates of particles (Van Deemter (1983)). Since the nature of the particle movement will be different for fluidized beds operating in the fast bubble regime, slow bubble regime and turbulent regime uncertainty exists as to the origin of the entrained particles under different regimes. The bubbling regimes are mainly determined by particle size and gas velocity.

Chitester et al. (1984) report that the turbulent flow regime is reached at lower gas velocities as the pressure is increased. The turbulence first reduces the stability of the clear gas-voids and then the stability of the agglomeration of solids. At high pressure the bed appears to be homogeneous with the voids of solid phase and the emulsion phase becoming practi-

cally indistinguishable.

The reader will find that there is only limited experimental data available for the fluidized bed combustion regime. Extrapolation to other fluidization regimes has to be carried out with care.

2.2.3 Origin of the entrained particles

Do et al. (1972) showed with a photographic technique in a two-dimensional bed that particles originate from the nose of the bubble when reaching the fluidized bed surface and that the velocities of injection are somewhat higher than the rise velocity of the corresponding bubble. When bubbles coalesce right at the bed surface ejection velocities are much higher. Further, ejected particles move quite individually and not as aggregates. These experiments were executed in a fluidized bed (bed height 2.44 m, bed width 0.01 m) at ambient temperature with relatively small particles (< 250.E-6 m), v_{mf} = 0.036 m/s, and with low gas velocities: 1.5 $v_{mf} < v_s < 3.0\ v_{mf}$. Saxena and Mathur (1983) gave additional direct experimental evidence of this mechanism of solids projection for their two-dimensional bed of milled seeds (d_p=2.064E-3 m, v_{mf} not reported), v_s=0.96 m/s) and of green peas (d_p=4.578E-3 m, v_{mf} not reported, v_s=1.83 m/s).

Extrapolation of the two-dimensional results to three dimensional fluidized beds is doubtful because in the two-dimensional bed the particle motion in the wake of a bubble is hindered by the presence of the wall, whereas in a three dimensional bed the wake particles can move freely and exchange momentum with dense phase particles (Chaung (1982)).

From experiments executed in a three-dimensional bed under "fast bubbling" conditions, with small coke and sand particles (< 500.E-6 m) at ambient temperature and low gas velocity (v_s=1.05 v_{mf}) George and Grace (1978) concluded that a substantial fraction of the ejected particles comes from below the bed surface, presumably the bubble wake. Peters et al. (1983) studied single bubble ejections from the centre of a fluidized bed consisting of glass ballotines with an image carrying probe. Their conditions were: D_{bed} = 0.152 m, d_p = 0.5E-3 - 0.6E-3 m (v_{mf} about 0.24 m/s), v_s just above v_{mf}, air at ambient temperature. They observed from a sequence of bubble eruptions (no coalescence):

* a growth of the bubble dome (nose)
* drainage of solids along the dome
* lateral movement of solids along the surface of the dome
* an increase in voidage of the dome until bubble eruption or break-up occurs
* solids are being ejected radially in all directions with respect to the centre of the bubble.

Based on the above observations they concluded that because of the net lateral movement of solids away from the eruption site towards the wall of the vessel, ejected particles from the eruption of a trailing bubble must come, for the most part, from beneath the original surface. Thus the freeboard region represents an integral part of the gross circulation in the bed. Levy et al. (1983) performed: controlled bubble injection experiments with superficial gas velocities up to 1.08 times the minimum to fluidization, and free-bubbling experiments with superficial gas velocities up to 3.44 times the minimum to fluidization. The cross sectional dimensions of the bed were 0.144 * 0.610 m. They defined the following mechanisms:

* The bulge bursting mechanism: Particles are thrown up by the bubble bulge and fall back to the bed surface after reaching a maximum height of approximately the bubble diameter. The bubble wake remains intact.
* The midlayer burst: When a pair of bubbles coalesce just below the bed surface bulge material of the leading bubble is thrown above the bed (bulge bursting mechanism). The layers of solids between the bubbles combine with the leading bulge layer. The resulting particle cloud

expands upward and outward and falls back to the bed (mid layer burst).

* The wake spike: The wake of the trailing bubble forms a spike which is projected above the bed surface reaching a height in excess of the height reached by the bulge and mid layers.
* The jet spray: This occurs when two or more bubbles coalesce. In this case a flow passage develops between the bubbles, allowing a jet of gas to form, which entrains particles and carries them to relatively large distances above the bed surface.

They further noticed for fluidization velocities above 3.44 the minimum to fluidization, that the diameter of the erupting bubbles became large enough to set up waves at the bed surface. These waves reflected at the walls and interfered with the eruption process.

Our current interest is focussed on conditions far above the fluidization regime discussed here. Extrapolation of results at least increases the uncertainty due to possible changes in the bubbling or ejection mechanism. Although no specific experimental data exist for the flow regimes where the superficial gas velocity exceeds 5 times the minimum to fluidization one still might expect that the bubbling or turbulent action of the gas in the bed is responsible for the majority of the solid entrainment at the bed surface, and further that the particles ejected from three-dimensionless beds represent an integral part of the particles circulating in the fluidized bed.

2.2.4 Entrainment and initial particle velocity at the bed surface

The physical properties of the gas and the particles, the fluidizing velocity and the bed height affect the hydrodynamic behaviour of the bed directly. Geometric factors such as bed diameter, distributor type and internal objects have a smaller effect on the hydrodynamic behaviour of the bed. As the bed hydrodynamics are responsible for the initial freeboard entrainment the value of the latter will be directly dependent on the operating conditions and somewhat less on the type of the individual combustor.

For the initial entrainment rate (the entrainment rate at the fluidized bed surface) Wen, Chen, George and Grace have obtained correlations. Pemberton and Davidson distinguished between the initial entrainment from the bubble roof and the bubble wake. George and Grace (1978) found:

$$F_0 = 0.5\ (1.42\ D_b - 0.091)\ \rho_p\ (1 - \varepsilon_{mf})\ (v_s - v_{mf}) \qquad (2\text{-}1)$$

This result was obtained for: silica sand with d_p= 350.E-6 m (v_{mf} about 0.1 m/s), 0.064 m < D_b < 0.15 m, D_{bed} = 0.457 m. More recently Chen (1981), Wen (1981), Wen and Chen (1981) and Wen and Chen (1982) proposed:

$$F_0 = 3.07E\text{-}9\ \frac{D_b\ A_{bed}\ \rho_g^{3.5}\ g^{0.5}\ (v_s - v_{mf})^{2.5}}{\eta^{2.5}} \qquad (2\text{-}2)$$

for: 0.051 m < D_{bed} < 0.61 m, 840 kg/m3 < ρ_p < 2650 kg/m3, 0.12 m/s < v_s < 0.9 m/s, 59 E-6 m.< d_p < 450.E-6 m. Both correlations were obtained for fluidization with bubbling beds, small particle sizes and low superficial gas velocities (relative to combustion conditions) and at ambient temperature and pressure. Pemberton and Davidson (1983) gave the initial entrainment of all particles from the bubble roof, assuming a hemispherical bubble cap as:

$$F_0 = \frac{3\ D_b\ \rho_p\ (1 - \varepsilon_{mf})\ (v_s - v_{mf})}{d_p} \qquad (2\text{-}3)$$

and the initial entrainment, assuming ejection of the bubble wake, as:

$$F_0 = 0.1\ \rho_p\ (1 - \varepsilon_{mf})\ (v_s - v_{mf}) \qquad (2\text{-}4)$$

Note that the ratio of the initial entrainment from the bubble roof and the bubble wake is $30\ D_b/d_p$. Published data from Pemberton (1982) show the following trends:

* at low bubble flows equation (2-3) applies for $F_0 < 10$ kg/(s.m2),
* equation (2-4) is relevant for $F_0 > 50$ kg/(s.m2),
* for $10 < F_0 < 50$ kg/(s.m2) a transition occurs, suggesting a change in the origin of ejected particles commensurate with an increase in bubble coalescence.

Figure 2-1a shows that applying the initial entrainment equations (2-1) and (2-2) to values, all lying in the appropriate regimes, result in a difference of more than one order of magnitude for the smaller bubble sizes. A deviation of a factor of ten is observed between Wen and Chen (1980) and equation (2-2) but probably this is a typing error. For comparison values from equation (2-3) and (2-4) are given in figure 2-1b for the same input as figure 2-1a. The initial entrainment obtained from equation (2-2) and (2-4) is of the same order of magnitude only for the larger bubble size.

Because of the uncertainties (extrapolation to regimes with higher fluidization velocities, determination of the bubble size, effects of bubble coalescence, reflected surface waves interfering with the erupting process) the foregoing correlations are not yet suitable for the modeling of the fluidized bed coal combustor.

Under fluidized bed combustion conditions Martens (1983) and Martens and Van Koppen (1983) have obtained experimental data on the descending solids flux in the centreline of a coal combustor. The lateral distribution of the descending solids flux was obtained by Martens (1984). The operating conditions were: T_{bed} = 1145 K, v_s = 1.0 m/s, d_p = 750.E-6 m (v_{mf} = 0.16 m/s), D_{bed} = 0.39 m, h_{bed} = 0.6 m, P = 1.023E5 Pa. The overall initial entrainment, which virtually equals the overall descending solids flux, was found to be 50 - 70 kg/(s.m2). Due to the limited number of experiments no correlation has been obtained. Walsh et al. (1983) analysed Martens' data (obtained in the centreline of the fluidized bed combustor, see figure 2-2) and found that:

* extrapolation of these data from the region 1.4 - 0.7 m above the bed to the bed surface yields an initial entrainment of 4 kg/(s.m2) which is consistent with their experimental results.
* in the region closer to the bed surface (0.7 - 0.3 m) Martens' data extrapolate to 500 kg/(s.m2), which is of the same order of magnitude as the predictions of equation 2-2 (assuming bubble diameters similar to those in the MIT AFBC).

Evidently, they concluded, some of the variations in the initial fluxes by different investigators may therefore be the result of a determination by extrapolation from different heights above the bed.

As regards the initial velocity distribution of particles at the fluidized bed surface George and Grace (1978) performed experiments in a slugging bed with size controlled single bubbles injected from the bottom of the three dimensional bed. The operating conditions were: $v_s = 1.05\ v_{mf}$, d_p= 250.E-6 - 300.E-6 m (v_{mf} = 0.052 m/s), glass ballotines, D_{bed} = 0.1 m, ambient temperature. They used a catching device along the freeboard height and back-calculated the distribution of the initial particle velocity by integrating the particle momentum equation. The initial velocity distribution found has a geometric mean of 2.1 times the bubble velocity. The maximum velocity found was as high as 8 times the bubble velocity and the minimum 1.5 times. Martens and Van Koppen (1983) recalculated from their experiment (described above) the axial particle velocity distribution

at the bed surface. From the gradient in the downward particle flux along the freeboard and a ballistic model they conclude that a minor fraction (< 25%) of the ejected particles have initial velocities below the superficial gas velocity and that the major fraction of the ejected particles have initial velocities in between 1 to 7 times the superficial gas velocity, the mean being 2.4 times that velocity. See figure 2-3. Applying the correlation of Mori and Wen (1975) for the bubble diameter and the correlation of Davidson and Harrison (1963) for the bubble velocity at the bed surface leads to: D_b = 0.1 m and v_b = 1.5 m/s. Starting from these values the experimental results can be expressed as: 0 m/s < $v_{p,0}$ < 4 v_b m/s, and $v_{p,0,50\%}$ = 1.53 v_b m/s. Peters et al. (1983) analysed motion pictures of erupting bubbles in a three-dimensional bed at minimum fluidization (no bubble coalescence). They concluded that the particle ejection velocities along the spherical radius of the bubble are approximately equal to the rise velocity at the surface. Under the simple assumption that the radial velocities are identical to the bubble velocity at the surface of the fluidized bed, solids velocities along the axial direction of the bed would be distributed according to the law of co-sines. They observed a critical angle beyond which particles are not ejected.

According to Chaung (1982) the experimental results from George and Grace (1978) compared quite well with his theoretical analysis. His analysis complies with the conservation of energy, when equating the energy associated with the initial bubble at the bed surface before, and the energy of the ejected particles and the jetted air after collapse. Unfortunately he provides no numerical data for comparison.

2.2.5 Entrainment at higher levels in the freeboard

The entrainment (ascending solids flux) in the freeboard is often held to decay exponentially with respect to height in the freeboard.

* Andrews (1960) was able to deduce this relationship by assuming that the energy distribution of the particles at the bed surface follows the Maxwell-Boltzmann distribution law.
* Kunii and Levenspiel (1969) explained the exponential decay rate based on the solids interchange between three distinct phases: 1) upward moving dispersed solids corresponding to a fully developed pneumatic transport regime and 2) the descending and 3) the ascending particle agglomerates, corresponding to the particles moving upward and downward above the bed.
* Zenz and Weil (1958) argued the exponential decay to result from the exponential dissipation of the true gas velocity with freeboard height and the velocity distribution of the solid particles being ejected from the bed.

Following the approach of others, Wen (1982) defined the entrainment rate of solids in the freeboard by the following equation:

$$F_h = F_\infty + (F_0 - F_\infty) \exp(-a\, h_f) \qquad (2\text{-}5)$$

F_∞ is the entrainment rate of particles at the exit of a very long freeboard or the entrainment rate after the transport disengaging height (TDH). The TDH is the level in the freeboard at which the rate of solids entrainment becomes essentially constant (changes maximally 1% f.i.).

The experimental data of Martens (1983) and Martens and Van Koppen (1983) obtained on the downward solids flux in the centre of a fluidized bed combustor indicate that, for the pertinent conditions (given before), there is not a simple exponential decay of the solids entrainment with freeboard height. See figure 2-2.

For the solids entrainment three distinct zones were designated as follows:

* a splash zone (freeboard height 0 - 0.3 m),
* a dense disengaging zone (freeboard height 0.3 - 0.7 m,
* a dilute disengaging zone (freeboard height 0.7 - 1.5 m).

In the splash zone the solids entrainment is almost constant (the decay exponent a=2.0 1/m). Both disengaging zones show an exponential decay, but with different exponents (the decay exponent a=11.8 1/m and 4.3 1/m of the dense and dilute disengaging zone respectively).

The experiments executed by Large et al. (1978) with a nearly isokinetic suction probe in the freeboard of a large fluidized bed (0.6 m I.D., bed height 1.03 m and superficial gas velocities between 0.2 and 0.3 m/s.) with rather small silica sand particles (d_p<250.E-6 m, $v_{mf} \leq$0.036 m/s) indicate that, regarding the solids motion, there are three freeboard regions:

* A region near the bed, where entrainment (upward solids flux) varies exponentially with height above the bed.
* A region far above the bed where entrainment is constant with height.
* A transition region between these two.

The data of Large et al. were taken at freeboard levels above 0.3 m (ref. bed level) and those from Martens and Van Koppen at levels below 1.5 m. So the possible existence of another region more close to the bed could not be observed by Large et al. and the region at higher freeboard levels not by Martens and Van Koppen.

From the experiments one may conclude that the models of Zenz and Weil(1958), Andrews (1960) and Kunii and Levenspiel (1969) are not adequate for detailed freeboard analysis.

2.2.6 Particle-particle interactions.

Particle-particle interactions have been largely ignored in fluidization research, especially for solids with a wide size distribution. Recently some experimental data have been obtained by Geldart (1982) and the first step to a quantitative model has been made by Van Rhijn (1983).

The one-dimensional vertical computations of particle trajectories by Van Rhijn were based on ballistic considerations (model 'FAME', described in section 2.3), on the particle mean free path theory and on the momentum interchange at particle-particle interaction. An illustration of some computational results is given in figure 2-4. The results concern a one-dimensional gas-particle flow where all the particles are assumed to be in a dynamic balance situation with respect to drag, inertia, gravity and collision force. The physical properties taken for the gas are: ρ_g= 0.339 kg/m3, η_g= 4.778E-5 kg/(m.s), and the superficial gas velocity: v_s = 1.0 m/s. Two groups of spherical mono-size particles are considered with: ρ_p = 2600 kg/m3, $d_{p,A}$ = 100.E-6 m, $d_{p,B}$ = 700.E-6 m. The free fall velocities of the spheres are: $v_{bal,A}$ = -0.8 m/s, $v_{bal,B}$ = -9 m/s. The particle flux of mono-size B is 25 kg/(s.m2), corresponding to the initial entrainment of Martens' experiments at similar conditions (discussed in 2.2.5). The initial flux of particles A varies. The collision efficiency is taken at 1 and the coefficient of restitution at 0 (perfect non-elastic), 0.5 and 1 (perfect elastic) respectively. The average particle velocities obtained indicate that:

a) Particles with a free fall velocity less than the superficial gas velocity (fines) may be carried back into the bed by collisions with the descending coarse particles (free fall velocity above the superficial gas velocity). In particular so if the flux of fine particles is low.
b) Coarse particles may be entrained (upward) due to the collisions with the ascending fine particles, in particular if the flux of fine particles is high.

As to be expected the effect of the collisions is strongly dependent on the concentrations of particles, i.e. the entrainment:

* For fluidized bed combustor operation the initial entrainment of the

coarse particles (based on mass) exceeds the initial entrainment of fine particles by several orders of magnitude. Then phenomenon a) dominates. Martens (1984) found that the maximal elutriation of fines in the 'MAGMA' is in the order of 10.E-3 kg/(s.m2). This will be typical for fluidized bed coal combustion without fines recycle. For recycle of fines and the use of natural sorbents for SO2 capture the flux of fines will increase with a factor of ten, roughly.

* For fluidized beds in which there is a large production or a large feed of fine particles phenomenon b) affects the entrainment of coarse particles.

Geldart verified the last mentioned phenomenon experimentally. The flux of fines fed to the bed varied from 1.5 to 7.9 kg/(s.m2). Geldart even concluded that under the conditions investigated there is in no case any evidence to support the idea of a TDH, except when the gas velocity is below the terminal velocity of all particles present in the bed. Consequently the TDH only will exist when there is no elutriation at all. This finding is in conflict with the idea of a saturation carrying capacity of the gas stream under pneumatic transport conditions.

2.2.7 The wall layer

The existence of a dense layer of solid particles descending along the freeboard wall is supported by Wen (1981), Pemberton and Davidson (1983), Morooka et al. (1983), Horio and al. (1982) and (1983), Van Rhijn (1983) and Martens (1984).

Pemberton and Davidson, and Horio et al. (1980) postulated the freeboard gas turbulence (low frequency eddies) to cause small particles to diffuse to the vessel wall. There particles descend. The motion of large particles is thought to be largely unaffected by the gas turbulence. They performed hot-wire-anemometer experiments in the freeboard at ambient temperature and found that:

* the turbulence intensity in the freeboard is proportional to the erupting bubble size,
* according to Horio et al. the turbulence intensity is inversely proportional to the distance above the bed, and according to Pemperton and Davidson it decays approximately in an exponential manner.

The turbulence intensity of the gas as a function of freeboard height, according to the empirical correlation of Horio et al. (1980) reads:

$$v^{*\prime}_{g,h} = v^{*\prime}_{g,0}\,\frac{D_b}{h_f} + v^{*\prime}_{g,\infty} \qquad 0.015 < (D_b/h_f) < 0.12 \qquad (2\text{-}6)$$

where:

$$v'_g = \sqrt{(v_g - \bar{v}_g)^2} \qquad (2\text{-}7)$$

Similarity has been found by Havenaar (1982) who performed laser doppler anemometer experiments at ambient temperature. With regard to the turbulence intensity Horio's model prediction gave too low a value. Probably the bubble diameter taken for Havenaars' calculation is under-estimated (see table 2-1). However under combustion conditions Havenaar found that the turbulence intensity can not be fitted to a correlation like Horio's. Post combustion is thought to have an influence by generation of turbulence. Thus more parameters are involved. The velocity and turbulence intensity profiles (axial gas velocity component only) obtained by Havenaar are illustrated in figures 2-5a and b. The decrease of the gas velocity near the wall can clearly been seen, although only measurements were possible up to 0.025 m from the wall. At ambient temperature a turbulent flow

type develops. At combustion conditions there are structural changes. A more laminar flow type develops, although the turbulence intensity remains high. At all heights investigated the average gas velocity in the vicinity of the wall is much lower compared to that in the centre. As could be expected the gas turbulence increases near the wall.

Morooka et al. hypothesized a solid recirculation flow from accumulation of solid particles in the wall layer. There the more densely packed particles may descend as a consequence of gravity force , withstanding the upward movement of the gas at some distance from the wall. Horio et al. (1982) and Morooka and al. (1983) determined with fiber optics the lateral distribution of the time-average (axial) particle velocity. In the central core this velocity was positive and relatively constant. The velocities declined laterally to become negative near the wall.

According to Wen (1981), at low gas velocity (particle Reynolds number less than a critical Reynolds number), the friction between the particles and the column wall is important. Thus, a significant wall effect is observed. However, at a high gas velocity (particle Reynolds number higher than a critical Reynolds number), the friction between the particles themselves is more important, and the wall effect diminishes. Unfortunately no values of the critical Reynolds number are reported.

With cracking catalyst Fournol et al. (1973) performed measurements of the lateral distribution of the entrainment (upward flux) in the freeboard at two different heights. The profiles were relatively flat. These experiments, however, do not exclude the existence of a wall return layer (downward particle flux) because of the isokinetic suction technique used for the flow rate in upward direction.

Particle-wall interactions have been theoretically investigated by Van Rhijn (1983). The model 'FAME' (described in section 2.3) has been used for the particle trajectory calculation in vertical i.e. axial direction. The particle trajectory in the lateral direction was based on ballistic considerations independently from the axial velocity component. The gravity force and any lateral gas velocity component did not occur in the calculation of the particle trajectory in lateral direction. The assumptions made at the fluidized bed level were:

* uniform distribution of particle entrainment,
* a get-away particle velocity of 3 times the superficial gas velocity,
* a distribution of the get-away angle of the particle velocity vector with the axis of the combustor after table 2-2.

A further assumption was:

* no particle-particle interactions in the freeboard region.

For the freeboard the following geometry was taken: ID of 0.39 m, height 2.75 m. The physical properties and superficial gas velocity were identical to that of the calculations of this reference mentioned in section 2.2.5. The two-dimensional particle trajectory was determined until 1) elutriation or 2) its return to the bed or 3) collision with the wall. The model results are visualized in figures 2-6a and b for coal particles (ρ=960 kg/m3) and inert particles (ρ=2600 kg/m3) respectively. The following conclusions can be drawn:

* The fraction of particles that collide with the wall increases for increasing particle diameter and density.
* A significant wall effect has to be expected, especially for the larger particles.
* If the lateral velocity component governs the particle to wall interaction then (for equal initial particle conditions) increasing the fluidized bed cross section area leads to a diminishing of the wall effect.

Martens (1984) measured the lateral distribution of the downward solids flux in the freeboard at various heights. The experimental conditions were close to those of the theoretical investigations of Van Rhijn (1983). Mar-

tens found the solids flux to be relatively constant in the central region and to increase near the wall up to 4 times the flux in the centre. See figure 2-7. Further and more detailed measurements would be required, however, to obtain quantitative insight in the phenomena leading to wall layer formation.

2.2.8 Obstacles in the freeboard

The existence of a wall layer is probably related to the effect of obstacles in the freeboard. Experiments by Pemberton (1982) with and without vertical plates in the freeboard indicate that the total elutriation rate is almost unaffected. However one may benefit from a reduction in freeboard height or an increase of residence time and burnout of char particles.

2.3 The one-dimensional particle trajectory model

This part of the model 'FAME' has been developed for prediction of the overall freeboard solid particle behaviour in a pressurized fluidized bed combustor.

For reasons of simplicity the model is kept one-dimensional, which implies that all lateral differences are ignored, the (axial) velocities and the solids volume fraction are uniform over a cross-section, and the wall-layer not taken into account.

The boundary conditions, assumptions and approximations of the freeboard model related to particle movement are the following:

* Gas phase
  - The freeboard is divided into a number of perfectly stirred disk-like compartments in series. Plug flow is approximated by forward (upward) gas transfer between compartments.
  - Turbulence and any back-mixing resulting from it are ignored because of the relatively low turbulence intensity measured by Havenaar (1982).
  - Since the fluid density is much less than that of the particles, added mass and history effects may be ignored.
* Solids
  - The size distribution of the particles ejected from the bed into the freeboard is assumed to be identical to the size distribution in the well mixed bed, obtained by in-bed-sampling, sieving, and a burn-off technique for determination of the carbon content. The sampling technique used (Martens (1984)) may have a preference to the middle and larger class of particles. The sieving technique used is expected to give only a rough estimation on the aerodynamical size distribution of the particles, because of the influences of the shape and density. Due to the chemical reactions and the attrition, a wide distribution in particles shape and density exists. The smaller the particles are, the more influence these phenomena have on elutriation modeling.
  - Particles are ejected from the bed surface with an upward velocity distribution as derived from combining experimental results from a particle catching device in the freeboard of the 'MAGMA' with a model calculation under the assumption of negligible gas jetting and / or particle-particle interaction.
  - The total flux of particles ejected from the bed is taken from experiments with catching devices in the freeboard of the 'MAGMA'.
  - Optionally the dissipation of unsteady state gas jets resulting from erupting bubbles as modified by Do et al. (1972) can also be used to calculate the true gas velocity for particles in upward direction.

This implies the following relation:

$$v_j = v_b \qquad h < 4.7\ d_b \qquad (2\text{-}8a)$$

$$v_j = v_s + (1.35 - 0.0744\ h/d_b)\ (v_b - v_s) \qquad 4.7 < h/d_b < 18.2 \qquad (2\text{-}8b)$$

$$v_j = v_s \qquad h < 18.2\ d_b \qquad (2\text{-}8c)$$

When particles reverse, as a result of the gravity force overcoming the drag force, they are assumed to emerge from the gas jet and to encounter the superficial gas velocity.

- Particle-particle and particle-wall interactions are neglected and it is assumed that the particles move quite individually and not as aggregates.
- The influence of gas turbulence on particle motion is neglected. The experimental work of Havenaar (1982) shows that the turbulence intensity is in the order of 20% of the average gas velocity. Ignoring the gas turbulence will most of all affect the details, but much less the average of the motion of fine particles.
- Starting from these assumptions and approximations vertical particle trajectories are obtained by numerical solution of the equation of motion (See Zenz and Weil (1958) and Do et al. (1972)).

$$\frac{dv_p}{dt} = \frac{1/4\ C_D\ \Delta_p\ \rho_g\ v_r\ |v_r|}{\rho_p\ d_p} - \frac{(\rho_p - \rho_g)\ g}{\rho_p} \qquad (2\text{-}9)$$

and:

$$v_p = \frac{dh}{dt} \qquad (2\text{-}10)$$

where:

$$C_D = \frac{24}{Re_{p,ev}} (1.0 + 0.15\ Re_{p,ev}^{0.687}) \qquad 0 < Re_{p,ev} < 1000 \qquad (2\text{-}11)$$

and:

$$v_r = v_p - v_j \qquad (2\text{-}12)$$

$$Re_{p,ev} = \frac{\rho_f\ v_r\ d_{p,ev}}{\eta_f} \qquad (2\text{-}13)$$

In calculating the particle trajectories it is necessary to take into account the loss of carbonaceous material by combustion. For a pressurized fluidized bed combustor this is particularly important as the combustion may proceed at such a rate that initially non-elutriable particles become of an elutriable size or even may be consumed completely (see Martens (1982)). For the char combustion a combination of a shrinking density and a shrinking core model can be used in 'FAME'. For details see chapter 3.

An additional important point is the shape of the particles. Analysis of coal and ash particles taken from the fluidized bed and the cyclones lead to the conclusion that the smaller the particles the

more roughly shaped and flat they are (Van Rhijn (1983)). Following the approach of Van Rhijn (1983) (that contains an extrapolation of the theoretical work of Clift et al. (1978)) this is taken into account by assuming the particles to be spheroidal. The spheroid may take shapes ranging from slightly deformed spheres to disks and needles. The aspect ratio E_p of a spheroid is defined as:

$$E_p = \frac{b_p}{a_p} \qquad (2\text{-}14)$$

where b is the maximum axial dimension and a is the maximum dimension normal to the axis of symmetry. The volume-equivalent sphere diameter is:

$$d_p = a_p \, E_p^{0.33} \qquad (2\text{-}15)$$

The drag-ratio based on the sphere with equal volume is approximated by:

$$\Delta_p = 0.2 \, (4 + E_p) \, E_p^{-0.33} \, \frac{1 + 0.15 \, Re_{p,ep}^{0.687}}{1 + 0.15 \, Re_{p,ev}^{0.687}} \qquad Re_p < 10 \qquad (2\text{-}16)$$

where:

$$Re_{p,ep} = \frac{\rho_f \, v_r \, d_{p,ep}}{\eta_f} \qquad (2\text{-}17)$$

- Because of the one-dimensionality of the model some numerical problems may occur for particles of near critical size, i.e. with a free fall velocity close to the superficial gas velocity. If inert, such a particle may start 'oscillating' between two adjacent compartments differing slightly in gas viscosity, density and or gas velocity. Near critical char particles will gradually be consumed and dragged upward but may behave similarly in the beginning. Such 'instabilities' must be avoided. A solution for the academic question whether the critical particle is elutriated or not is found in the hypothesis that such a particle gradually will be transported to the wall. There, in the boundary layer, the absolute gas velocity is near zero. Consequently the particle will descend.

Admittedly these simplifications limit the applicability of the model considerably, but at present the general scarcity of the data on a.o. two-dimensional effects in the freeboard does not permit a more complete approach to be taken.

In this thesis the model is predominantly used for a further analysis of the experimental result obtained from the 'MAGMA'. Thus some of the lacking data could be replaced by values obtained from measurements. This applies to particle movement, as will be discussed first, as well as to chemical reactions and heat losses, to be discussed in chapter 3 and 4 respectively. As will be shown a fairly coherent picture of the various phenomena in the freeboard can be developed in this way. This lends confidence to the basic reliability of the model.

2.4 Model predictions

2.4.1 Numerical set-up and boundary conditions

To illustrate the use of the model and the various effects influencing the particle trajectories in the freeboard the results of a model trial are presented in this section.

The model trial comprises division of the total freeboard height into 11 compartments of 0.25 m each and particle trajectory calculations for 9 particle sizes, ranging from 26.E-6 m upto 925.E-6 m for the inert and 11 particle sizes ranging from 0.125E-3 m upto 3.2E-3 m for the coal. To each particle size 7 initial particle velocities, ranging from 1 m/s to 7 m/s, were assigned. For convenience the level of the compartment boundary was taken coincident with the mesh point for the particle trajectory calculation. The freeboard boundary conditions are closely related to the experiments executed in the 'MAGMA', described in Martens and van Koppen (1983) and Martens (1984). Values are summarized in table 2-3. All physical properties not mentioned are calculated accordingly appendix 1.

2.4.2 Particle trajectories

For fluidized bed combustion solids with a wide size distribution are common. The ballistic forces on a particle depend strongly on particle size. Figures 2-9a through g visualize some inert and coal particle trajectories for various initial velocities. The maximum penetration height and the residence time of particles in the freeboard as a function of particle size is shown in figures 2-10a and b and 2-11a and b. For the small particle sizes the initial velocity is immaterial with respect to both the maximum height of rise and the residence time. The drag force governs the particle trajectory. For the particle of medium and under critical size for elutriation the influence of the inertia force increases. This leads to some lag in time for the particle having a lower initial particle velocity. For the medium above critical particle size the (changing) relative velocity of the gas and the particle influences the drag force considerably. Relative to the ascending particle, the descending particle with the same absolute velocity notices a stronger drag force. The upward gas velocity causes the asymmetrical particle trajectory. The drag and the gravity force are of the same order of magnitude. This results in a relatively long freeboard residence time. Both the freeboard residence time and the height of rise are strongly dependent on initial particle velocity. For coal particles the residence time may be such that sufficient combustion occurs, leading to an elutriable particle. See figure 2-9e. For the larger particles the inertia force and gravity force dominate and the drag force is of minor importance. Coal particles are more prone to elutriation (finer critical size) because of the lower density and the shape factor to be less than unity. As could be expected, the critical size for elutriation is hardly affected by the initial particle velocity distribution. See figure 2-9e. The critical size for the inert particle is 180.E-3 m and for the coal particle 400.E-3 m, roughly.

2.4.3 Entrainment

The spatially resolved entrainment along the freeboard for the conditions considered is shown in figure 2-12. The flux at the fluidized bed surface is several orders of magnitude larger than the elutriation. The entrainment decreases only 30% in the region 0 - 0.25 m (splash zone). Most particles disengage in the region 0.25 m - 0.5 m (dense disengaging zone). Above this region minor disengagement takes place (dilute disengaging zone). The entrainment becomes constant, for the inert material 0.03 kg/(s.m2) at a height beyond 1.25 m and for the coal 0.07 kg/(s.m2) beyond

0.75 m. Comparison from elutriation data from the experimental and the computational result (Martens(1984)) shows that the model over-estimates the elutriation by a factor of 10 and over-estimates the critical size for elutriation of the coal by a factor of 0.25. These differences may be due to:

* the bed material sampling technique used, or any non-homogeneous mixing state of the fluidized bed,
* the particle-particle or particle-wall interaction, or other two-dimensional effects,
* the gas turbulence,
* the vena contracta at the freeboard outlet, which is not considered in the model.

Further research on these points is required.

2.4.4 Particle volume fraction

The particle volume fraction in a compartment of the freeboard results from the volume flow rate of the particles, the particles' residence time and the compartment volume. Particles reverting direction especially contribute to the value of the particle volume fraction as their residence times become relatively long. The spatially resolved particle volume fraction is visualized in figure 2-13. Near the fluidized bed surface the particle volume fraction of the inert and the coal are about 2% and 0.26% respectively, remaining approximately constant in the splash zone and decreasing with height similar to the entrainment curve.

2.5 Conclusions and recommendations

* Information on bubble eruption, initial particle velocity and initial entrainment is becoming available at an increasing rate, especially for single bubbles and coalescing bubbles at fluidization velocities just above v_{mf} up to 3 v_{mf}. Experiments executed in fluidized beds for combustion purposes ($v_s > 5\ v_{mf}$) remain rare however.
* The freeboard wall layer has been shown to be significant, even for an I.D. 0.4 m fluidized bed. The dense layer of descending coarse particles near the wall results from the lateral movement of the particles caused by the bubbling behaviour of the bed and, possibly, the turbulence of the gas flow. The magnitude of the layer compared to the overall solids flux decreases when the freeboard cross sectional area increases. The dense layer of descending particles helps the gas-wall boundary layer to develop.
* The turbulence intensity is dominated by the bubbling phenomena of the bed. The intensity decays along the freeboard. The turbulence probabely causes small particles to collect in the wall layer where conditions are more favourable for descending.
* Particle-particle interactions counteract the inertia, the slip and the gravity force and lead to some dispersion of particles throughout the freeboard. Fine particles tend to lift descending coarse particles and coarse particles may cause fine particles to move upwind. For fluidized bed combustion conditions the latter effect may dominate in the splash zone.
* Modeling the wall layer and particle-particle interactions has still to be based on crude assumptions. Further, even when simplified, it will lead to many numerical complications. Uncertainties in calculating particle motion such as gas-jetting, turbulence, true initial particle velocity, particle-particle collision and deviations on drag relation can, at present, only be 'lumped' in the model by introduction of an apparent initial particle velocity distribution using experimental results.
* Modeling fine particles is prone to great uncertainty because of the effect of the wall layer, gas turbulence, and particle-particle interac-

tion. The model results on elutriation phenomena are not reliable.

* Further experimental results on particle motion and gas flow will be necessary to cover the whole regime of atmospheric and pressurized fluidized bed combustion. Until more experimental data for verification become available there is no urgent need to modify the model presented, as the effect caused by particle behaviour can be estimated satisfactorily via indirect measurement of chemical reaction and heat transfer (see chapter 3 and 4).

2.6 List of symbols

A	surface area	m2
a	constant in the entrainment equation	1/m
	maximum dimension spheroid normal to the axis of symmetry	m
b	maximum axial dimension spheroid	m
C_D	drag coefficient	-
D	diameter	m
d	diameter	m
E	aspect ratio spheroid	-
F	entrainment rate	kg/(s.m2)
g	acceleration of gravity	m/s2
h	axial distance	m
P	pressure	Pa
Re	Reynolds number	-
T	Temperature	K
t	time	s
v	velocity	m/s
v'	turbulence intensity	m/s
TDH	transport disengaging height	m

GREEK SYMBOLS

Δ	drag ratio	-
ρ	density	kg/m3
ε	porosity	-
η	viscosity	kg/(s.m)

SUBSCRIPTS

b	bubble
bal	balancing
bed	fluidized bed
ep	related to the projected equivalent sphere
ev	related to the volume equivalent sphere
f	mean physical properties in gas film
	freeboard
g	gas
j	gas jet
mf	minimum fluidization
p	particle
r	relative
s	superficial
0	initial condition
∞	infinity

OVERLINES

*	average over the cross section
-	time average

2.7 References

Andrews, J.M.
Fluidized solids entrainment.
Industrial and Engineering Chemistry, Vol. 52, No. 1 (1960),

Chaung, T.Z.
Particle entrainment and chemical reaction in the freeboard of a fluidized bed coal combustor.
Dissertation. Massachusetts Institute of Technology. Cambridge, MA., USA (1982).

Chen, L.
Fluidized bed freeboard phenomena.
Dissertation. West Virginia University. Morgantown, W-VA., USA (1981).

Chitester, D.C., Kornosky, R.M., Fan, L.S., Danko, J.P.
Characteristics of fluidization at high pressure.
Chemical Engineering Science, Vol. 39, No. 2, pp. 253/261 (1984).

Clift, R., Grace, J.R., Weber, E.
Bubbles, drops and particles.
Academic Press, New York, USA (1978).

Davidson, J.F. and Harrison, D.
Fluidized particles.
Cambridge University Press (1963).

Deemter, J.J. Van
Fluide bed verbranding, algemeen.
Lecture notes "College Steenkooltechnologie M18", pp. 9.1/9.12.
Delft University of Technology. Delft, The Netherlands (1983).

Do, J.R., Grace, J.R., Clift, R.
Particle ejection and entrainment from fluidized beds.
Powder Technology, 6, pp. 195/200 (1972).

Fournol, A. B., Bergougnou, M.A., Baker, C.G.J.
Solids entrainment in a large gas fluidized bed.
Can. J. Chem. Eng. Vol., pp. 401/404 (1973).

Geldart, D. and Pope, D.J.
Interaction of fine and coarse particles in the freeboard of a fluidized bed. Short communication.
Post Graduate School of Powder Technology. University of Bradford.
Bradford, West Yorkshire, UK (1982).

George, S.E. and Grace, J.R.
Entrainment of particles from aggregative fluidized beds.
AIChE Symposium Series, No 176, Vol. 74, pp. 67/74 (1978).

Havenaar, P.
Theoretisch en experimenteel stromings onderzoek in het vrijboord van een AFBC.
Rapport EV-1248, Laboratory for Thermal Power Engineering.
Delft University of Technology. Delft, The Netherlands (1982).

Horio, M., Taki, A., Hsieh, Y.S., Muchi, I.
Elutriation and particle transport through the freeboard of a gas-solid fluidized bed.
'Fluidization', Grace and Matsen (eds.), Plenum Press, pp 509/518 (1980).

Horio, M., Shibata, T., Muchi, I.,
Design criteria for the fluidized bed freeboard.
Proc. 4th Int. Conf. on Fluidization, pp. 307/314.
Eds. Kunii, D. and Toei, R., Publications Department AIChE, New York (1983).

Kunii, D. and Levenspiel, O.
Journal of Chemical Engineering of Japan, Vol. 2, No. 1, pp. 85/88 (1969).

Large, J.F., Martinie, Y., Bergounou, M.A.
Interpretative model for entrainment in a large gas- fluidized bed.
Journal of Powder & Bulk Solids Technology, pp. 15/21 (1978).

Levy, E.K., Caram, H.S., Dille, J.C., Edelstein, S.
Mechanisms for solid ejection from gas fluidized beds.
AIChE Journal, Vol. 29, No. 3, pp. 383/388 (1983).

Martens, F.J.A., Op den Brouw, H., Van Koppen, C.W.J.
The performance of the freeboard region of a fluidized bed coal combustor: model and experiments.
Proc. of the 1st Colloquium on Pressurized Fluidized Bed Combustion, pp. III1/21.
Delft University of Technology. Delft, The Netherlands (1982).

Martens, F.J.A., Op den Brouw, H., Van Koppen, C.W.J.
The behaviour of the freeboard region of a fluidized bed coal combustor.
Proc. of the 7th Int. Conf. on Fluidized Bed Combustion, pp. 1054/1063. National Technical Information Service, US Department of Commerce. Springfield, VA., USA (1983).

Martens, F.J.A.
The freeboard region in a fluidized bed combustor: experiments.
Proc. of the 2nd Colloquium on Pressurized Fluidized Bed Combustion, pp. IV 1/31.
Delft University of Technology. Delft, The Netherlands (1983).

Martens, F.J.A., Van Koppen, C.W.J.
Experimental study of the freeboard region in a fluidized bed coal combustor.
Verbrennung und Feuerungen, 11. Deutscher Flammentag.
VDI-Bericht Nr. 498, pp. 101/106. VDI-Verlag, Duesseldorf, BRD (1983).

Martens, F.J.A.
Experiments with the atmospheric fluidized bed combustor 'MAGMA'.
Rapport EV-1333, Laboratory for Thermal Power Engineering.
Delft University of Technology, Delft, The Netherlands (1984).

Mori, S. and Wen, C.Y.
Estimation of bubble diameter in gaseous fluidized beds.
AIChE Journal, No. 21, pp. 109 (1975).

Morooka, T., Kago, T., Kato, Y.
Flow pattern of solid particles in freeboard of fluidized bed.
Proc. 4th Int. Conf. on Fluidization, pp. 291/298.
Eds. Kunii, D. and Toei, R., Publications Department AIChE, New York (1983).

Peters, M.H., Fan, L.S., Sweeney, T.L.
Study of particle ejections in the freeboard region of a fluidized bed with an image carrying probe.
Chem. Eng. Sci., Vol. 38, No. 3, pp. 481/485 (1983).

Pemberton, S.T.
Entrainment from fluidized beds.
Dissertation. Cambridge University. Cambridge, UK (1982).

Pemberton, S.T., Davidson, J.F.
Elutriation of fine particles from bubbling fluidized beds.
Proc. 4th Int. Conf. on Fluidization, pp. 275/282.
Eds. Kunii, D. and Toei, R., Publications Department AIChE, New York (1983).

Rhijn, W.T.B. Van
De invloed van deeltjesvormen en deeltjesbbotsingen op het deeltjestransport in het vrijboord boven een wervelbed.
Rapport EV-1295, Laboratory for Thermal Power Engineering.
Delft University of Technology. Delft, The Netherlands (1983).

Saxena, S.C. and Mathur, S.C.
On the origin of solids projected from the surface of a gas-fluidized bed.
Dept. of Chem. Eng., University of Illinois, Chicago, USA (1983).
Will appear in Chem. Eng. Sci.

Walsh,P.M., Mayo, J.E., Beer, J.M.
Refluxing particles in the freeboard of a fluidized bed.
AIChE Annual Meeting, Session on fundamentals of fluidization and fluid-particles systems.
Washington, DC., USA (1983).

Wells, J.W., Culver, M.H., Krishnan, R.P.
Tennesee Valley Authority atmospheric fluidized bed combustor simulation interim annual report 1980.
Freeboard subcode, pp. 87/118.
Oak Ridge National Laboratory. Oak Ridge, Tennesee, USA (1981).

Wen, C.Y. and Chen, L.H.
A fluidized bed combustor freeboard model.
Proc. of the 6th. Conf. on Fluidized Bed Combustion. pp. 1115/1130.
National Technical Information Service, US Department of Commerce.
Springfield, VA, USA (1980).

Wen, C.Y.
Solid-gas reactions in the fluidized bed combustor freeboard.
Department of Chemical Engineering, West Virginia University.
Morgantown, W-VA., USA (1981).

Wen, C.Y. and Chen, L.H.
Fluidized bed freeboard phenomena: entrainment and elutriation.
AIChE J., Vol.28, No. 1, pp. 117/128 (1982).

Zenz, F.A. and Weil, N.A.
Theoretical-empirical approach to mechanism of particle entrainment from fluidized beds.
Am. Inst. Chem. Engrs. J., 4, p. 472 (1958).

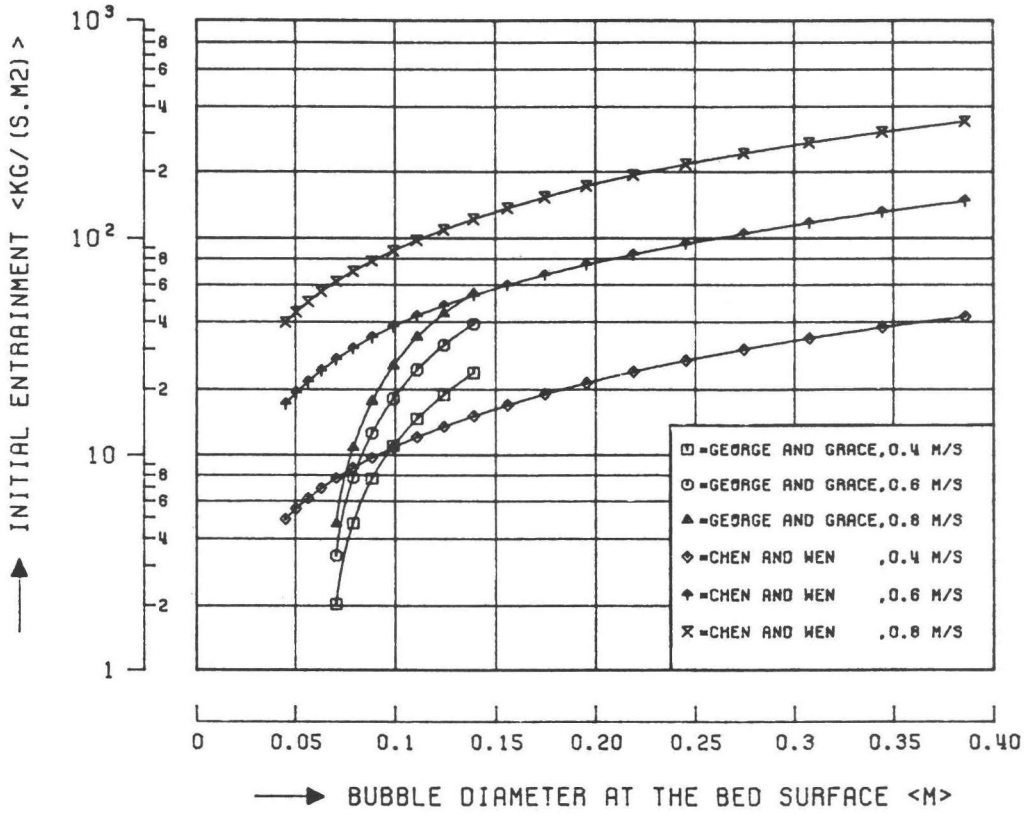

Figure 2-1a.
Calculated entrainment rate at the fluidized bed surface as a function of the bubble diameter, using correlations of George and Grace (1978), and Wen and Chen (1982).

minimum fluidization velocity	0.093	m/s
porosity at minumum fluidization	0.45	-
mean particle diameter	0.35E-3	m
particle density	2640	kg/m3
bed diameter	0.16	m
density of gas	1.188	kg/m3
viscosity of gas	1.798E-5	kg/(m.s)
accelaration from gravity	9.81	m/s2
superficial gas velocities	0.4 0.6 0.8	m/s

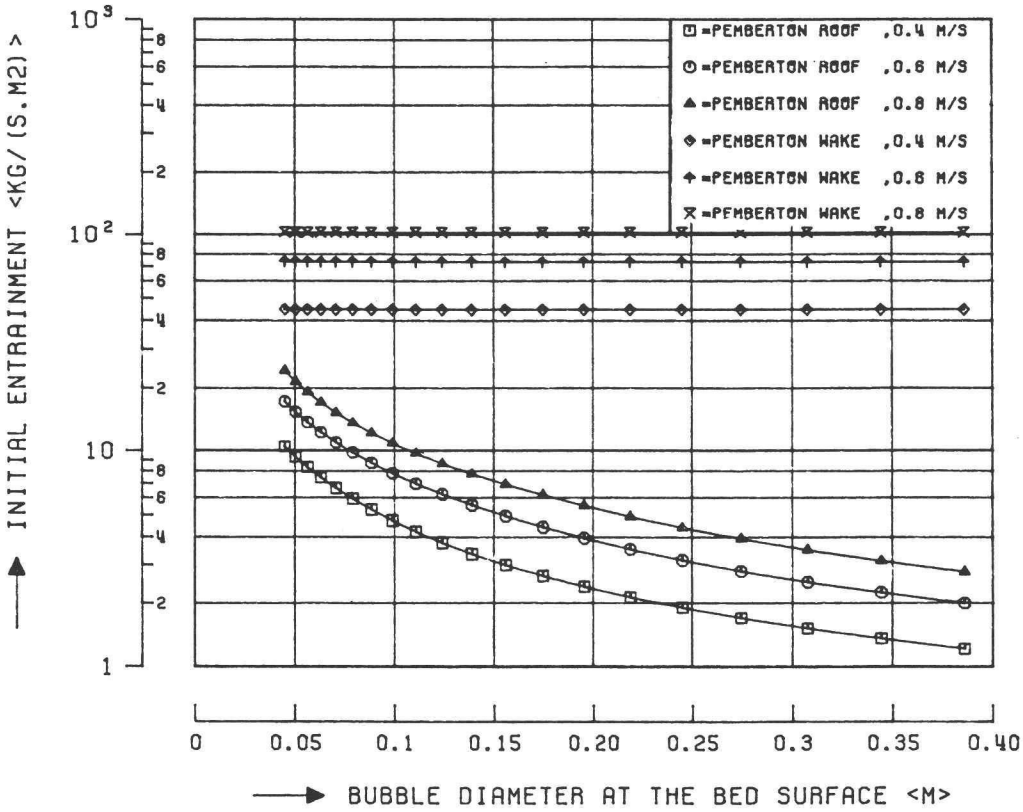

Figure 2-1b.
Calculated entrainment rate at the fluidized bed surface as a function of the bubble diameter, using correlations of Pemberton and Davidson (1983).

minimum fluidization velocity	0.093	m/s
porosity at minumum fluidization	0.45	-
mean particle diameter	0.35E-3	m
particle density	2640	kg/m3
bed diameter	0.16	m
density of gas	1.188	kg/m3
viscosity of gas	1.798E-5	kg/(m.s)
accelaration from gravity	9.81	m/s2
superficial gas velocities	0.4 0.6 0.8	m/s

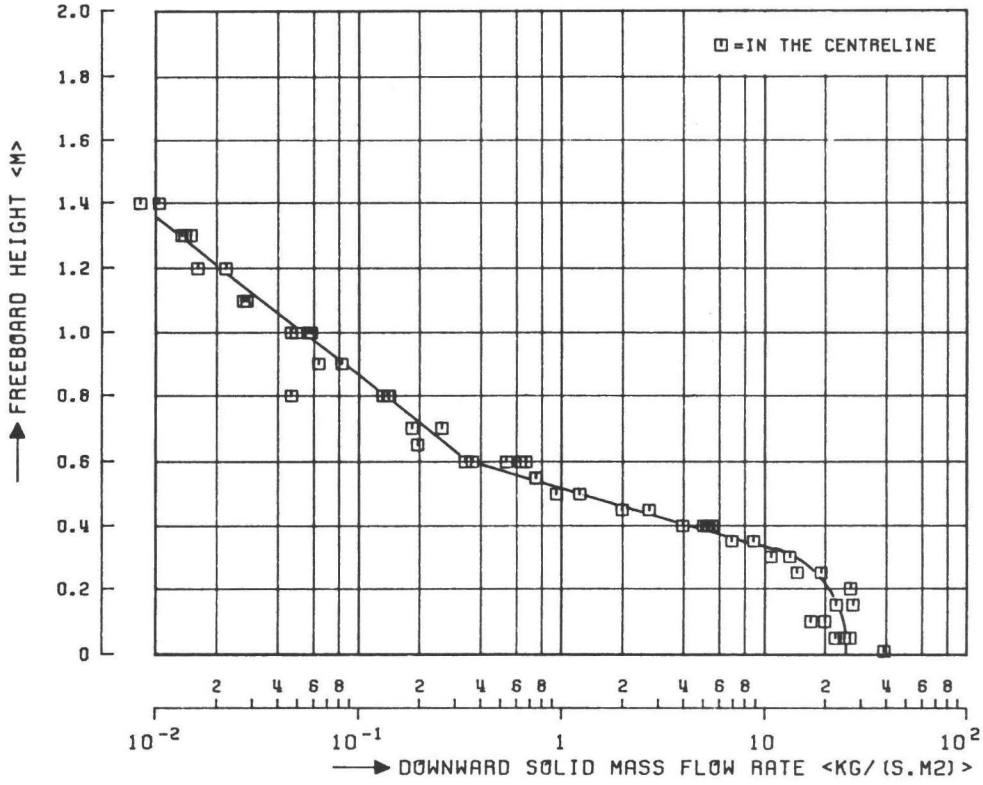

Figure 2-2.
Downward flux of solids in the centreline of the freeboard (Martens (1983)).

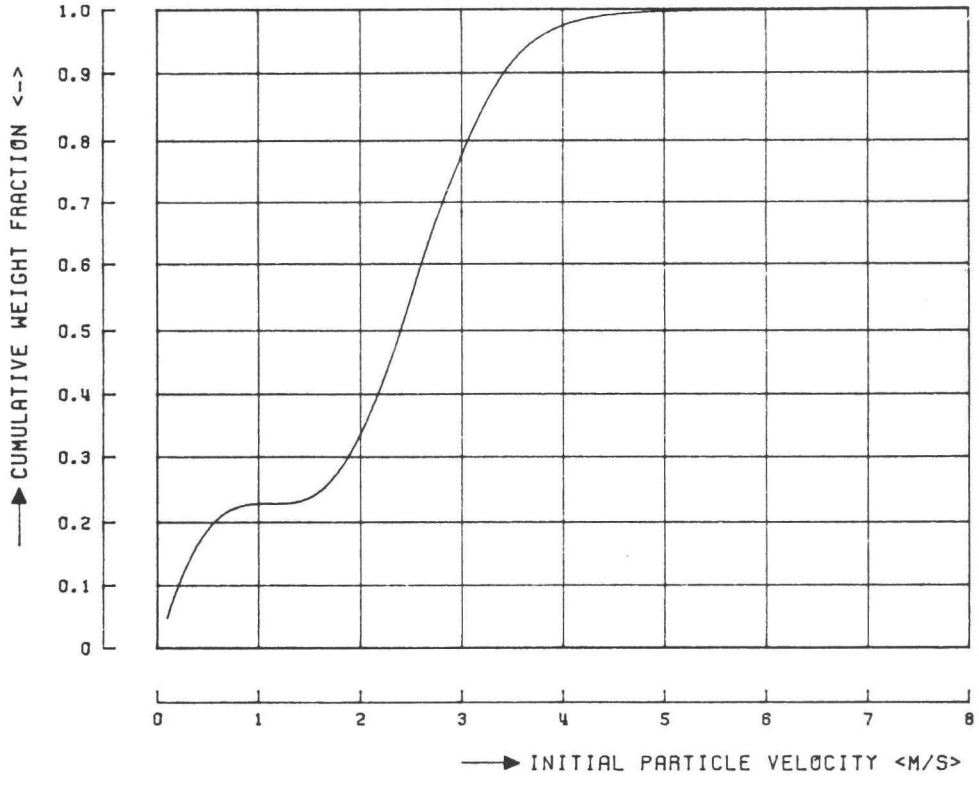

Figure 2-3.
Initial particle velocity distribution (after Martens and Van Koppen (1983)).

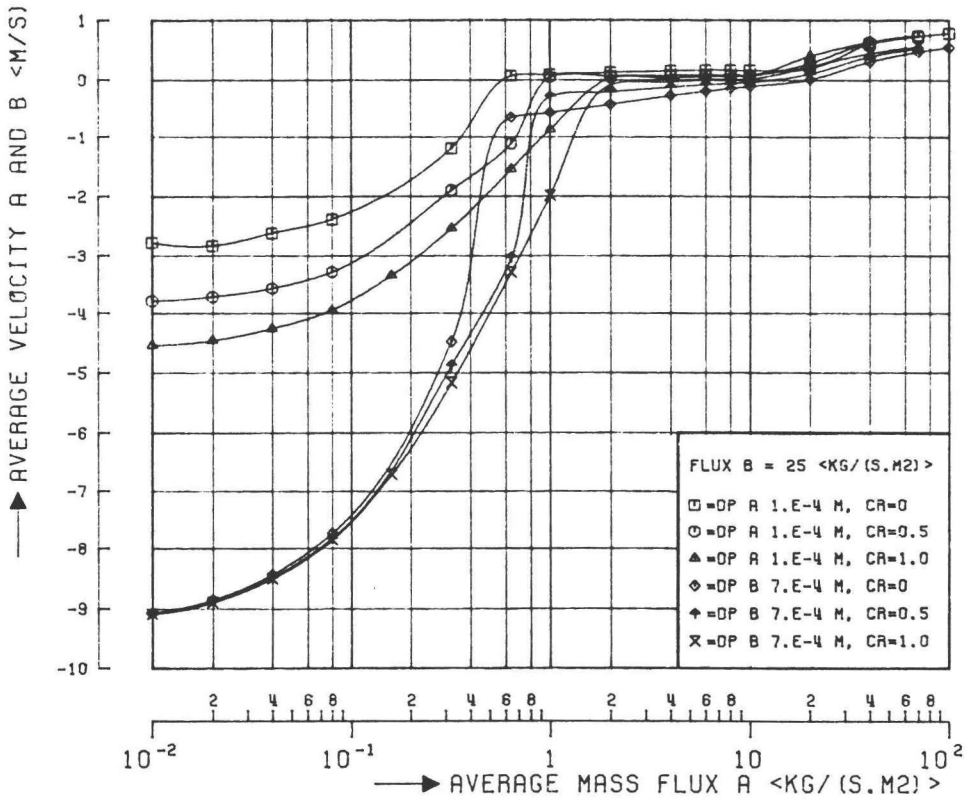

Figure 2-4.
Calculated average balancing particle velocities resulting from ballistic considerations and particle-particle collisions for two mono-size particle groups and for various mass fluxes.
From Van Rhijn (1983).

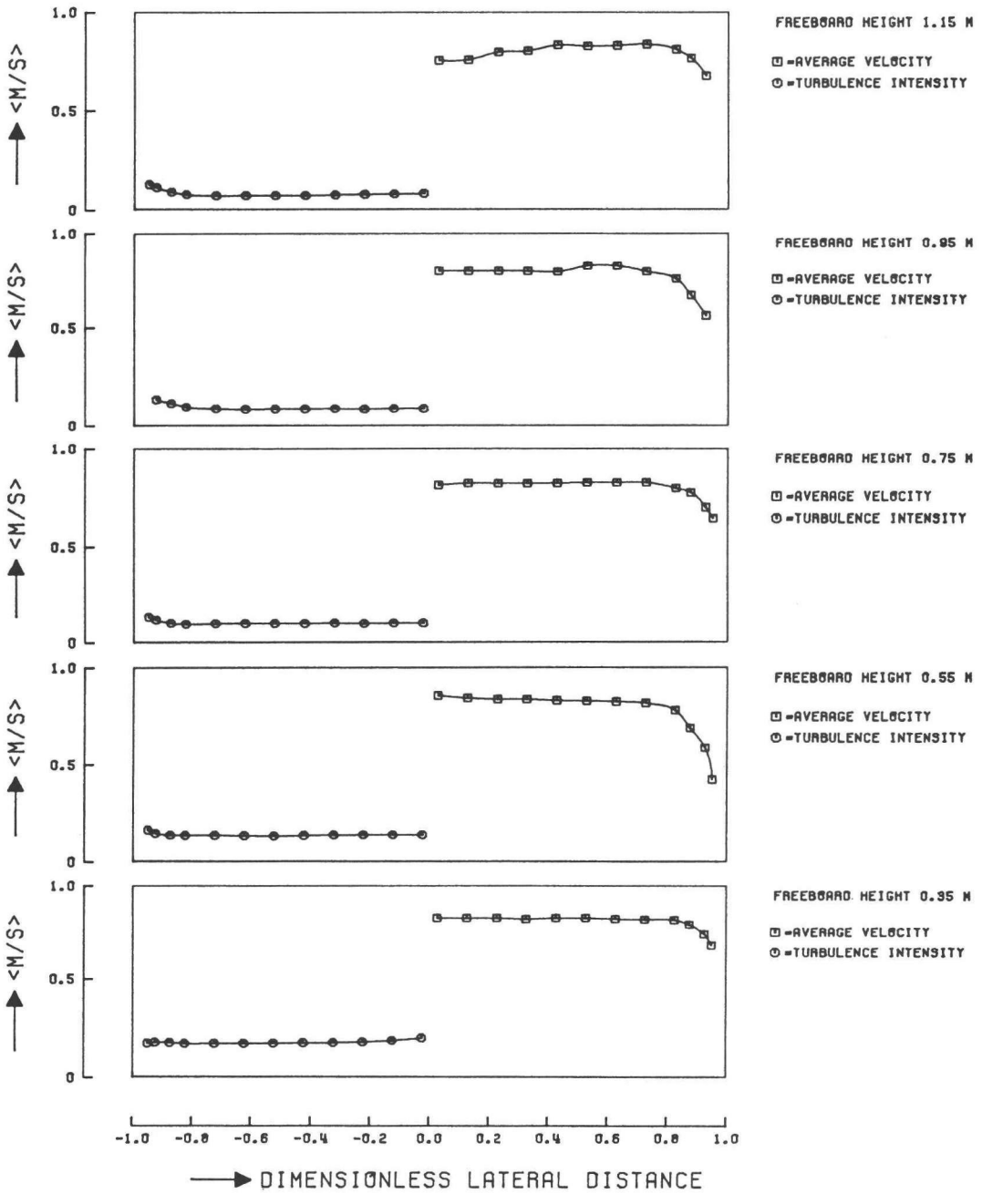

Figure 2-5a.
Axial gas velocity and turbulence intensity in the freeboard at various lateral positions and various heights.
From Havenaar (1981); run at ambient temperature.

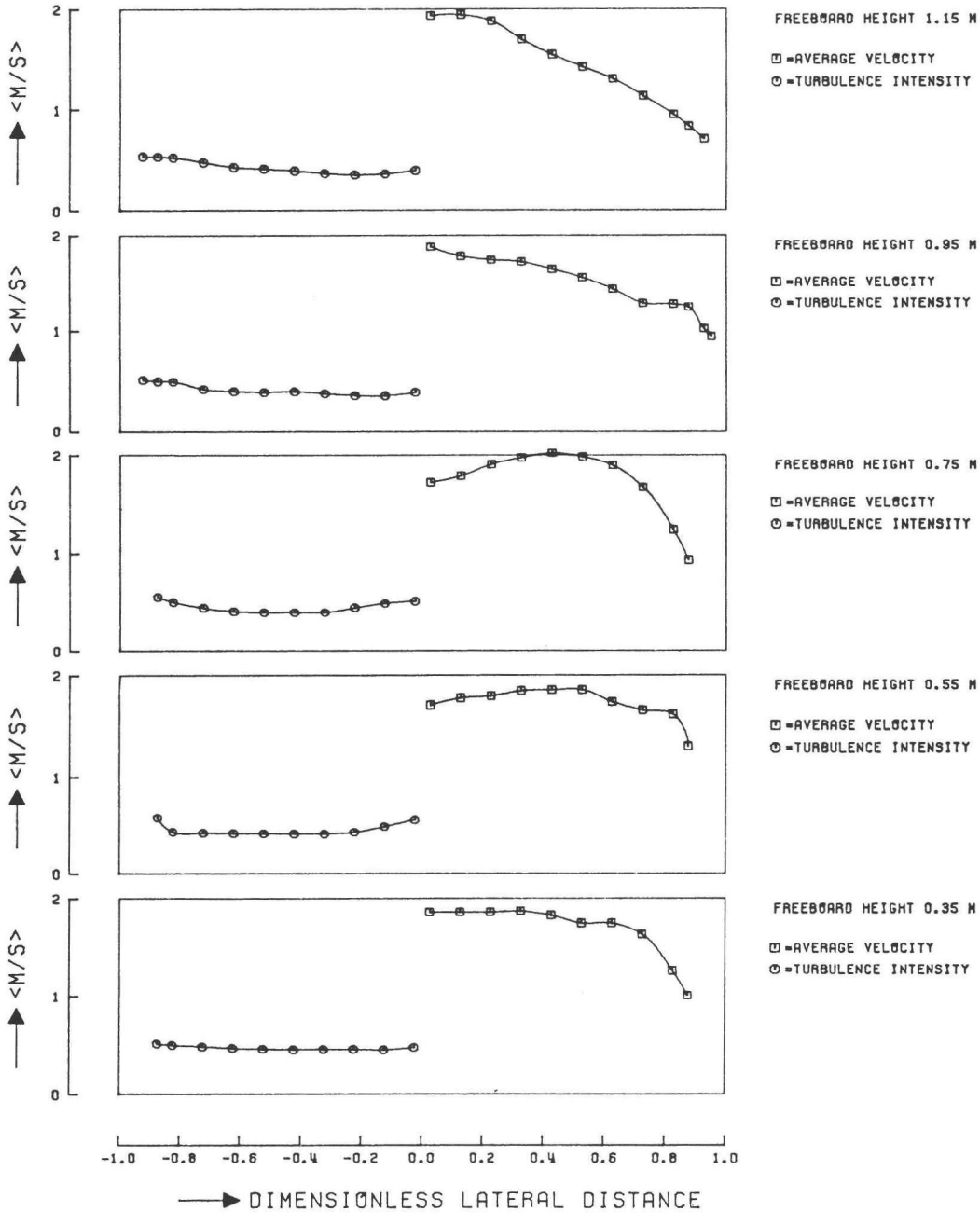

Figure 2-5b.
Axial gas velocity and turbulence intensity in the freeboard at various lateral positions and various heights.
From Havenaar (1981); run at 1150 K, combustion of anthracite.

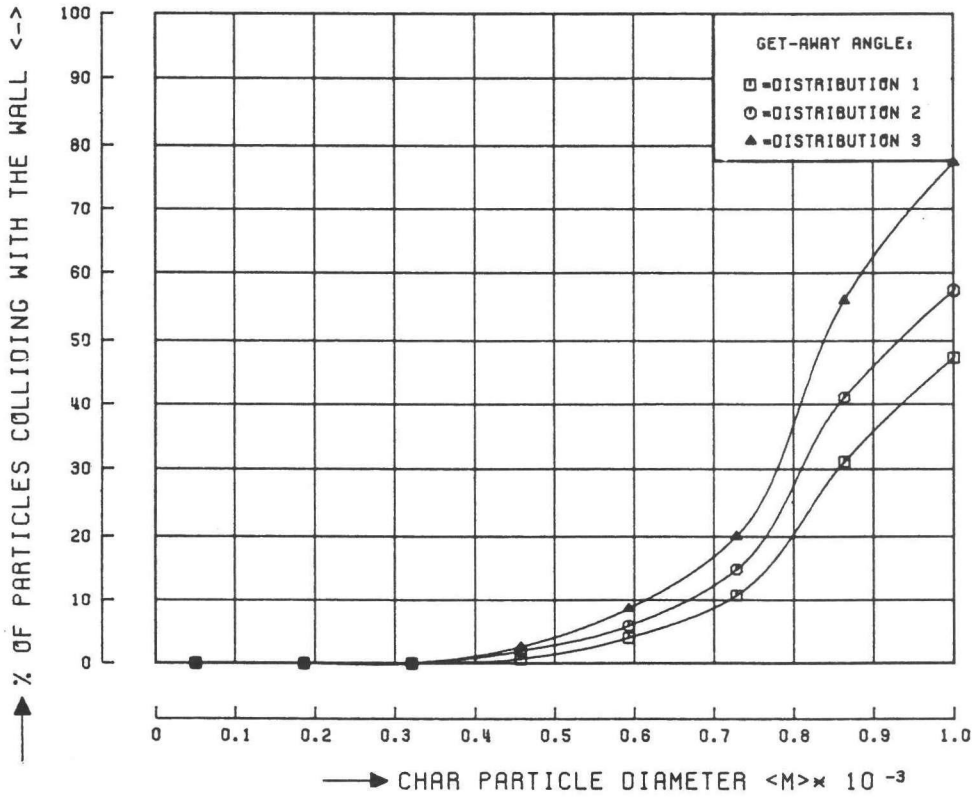

Figure 2-6a.
Percentage of char particles colliding with the freeboard wall.
From Van Rhijn (1983).

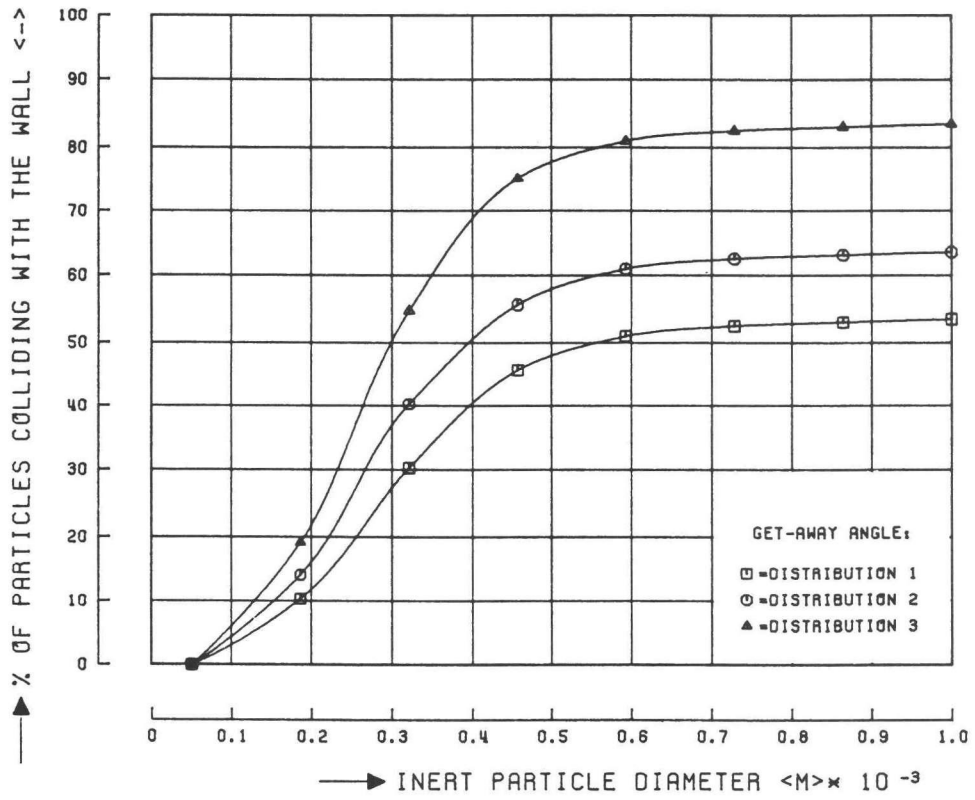

Figure 2-6b.
Percentage of inert particles colliding with the freeboard wall.
From Van Rhijn (1983);

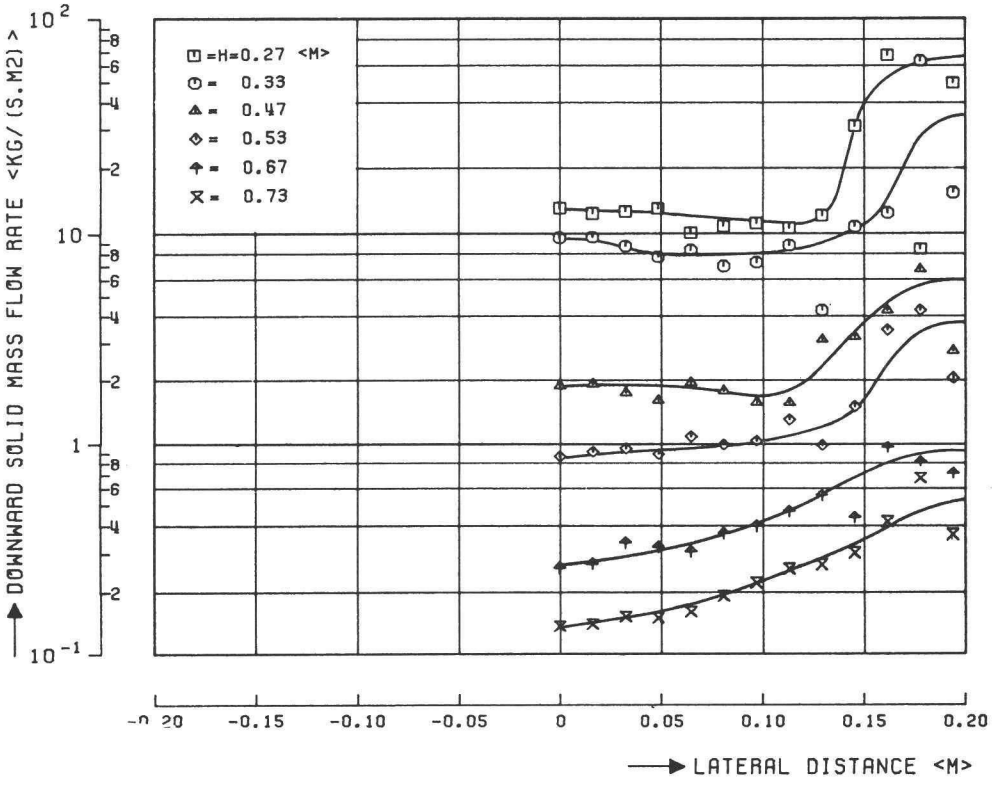

Figure 2-7.
Measured lateral distribution of the descending solids flux in the freeboard at various heights (after Martens (1984)).

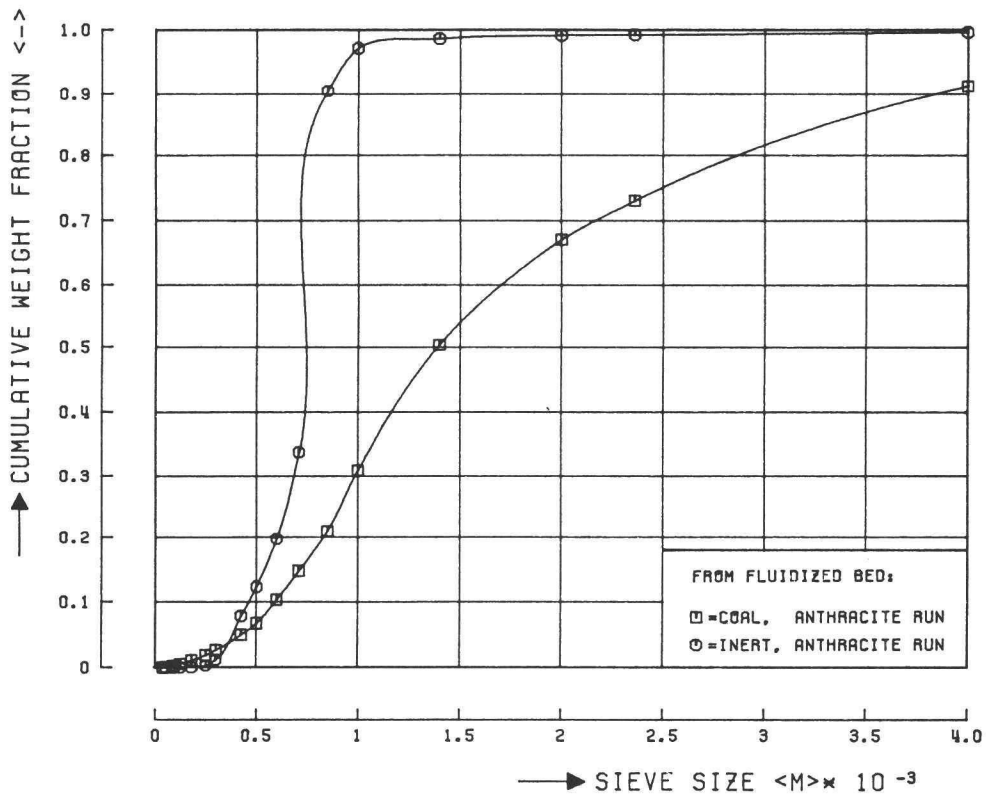

Figure 2-8.
Particle size distribution of the fluidized bed material (obtained from experiment, Martens (1984)).

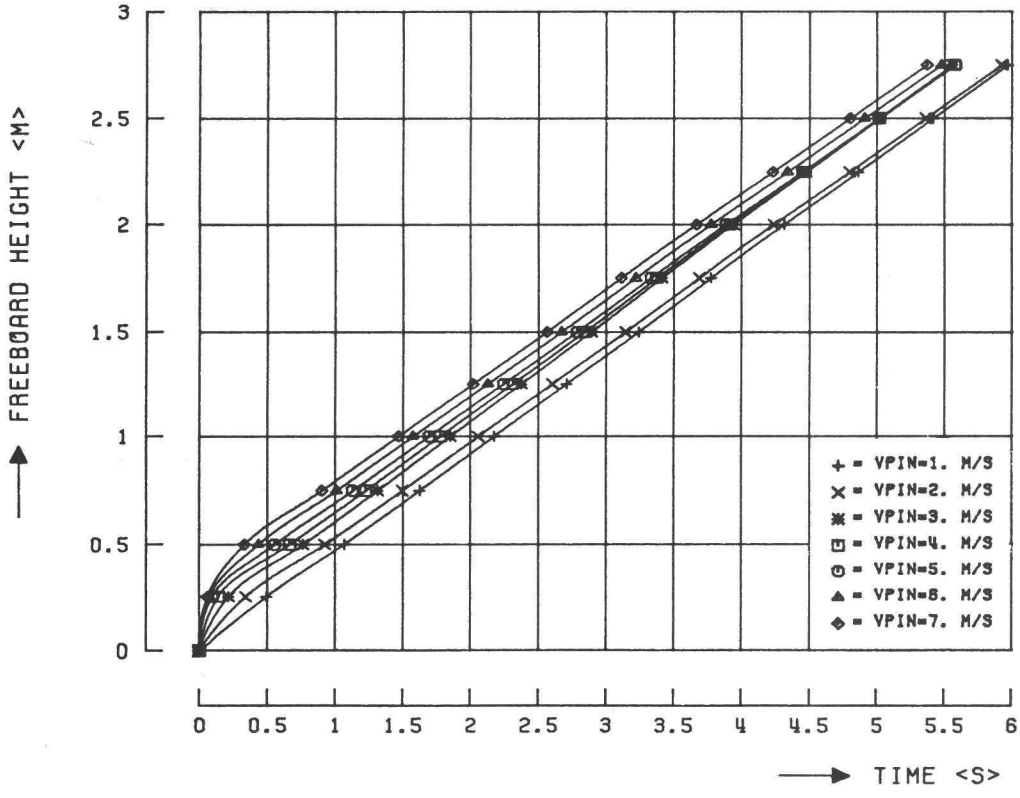

Figure 2-9a.
Some particle trajectories for various initial velocities. Ascending medium size inert particle (152.5E-6 m).

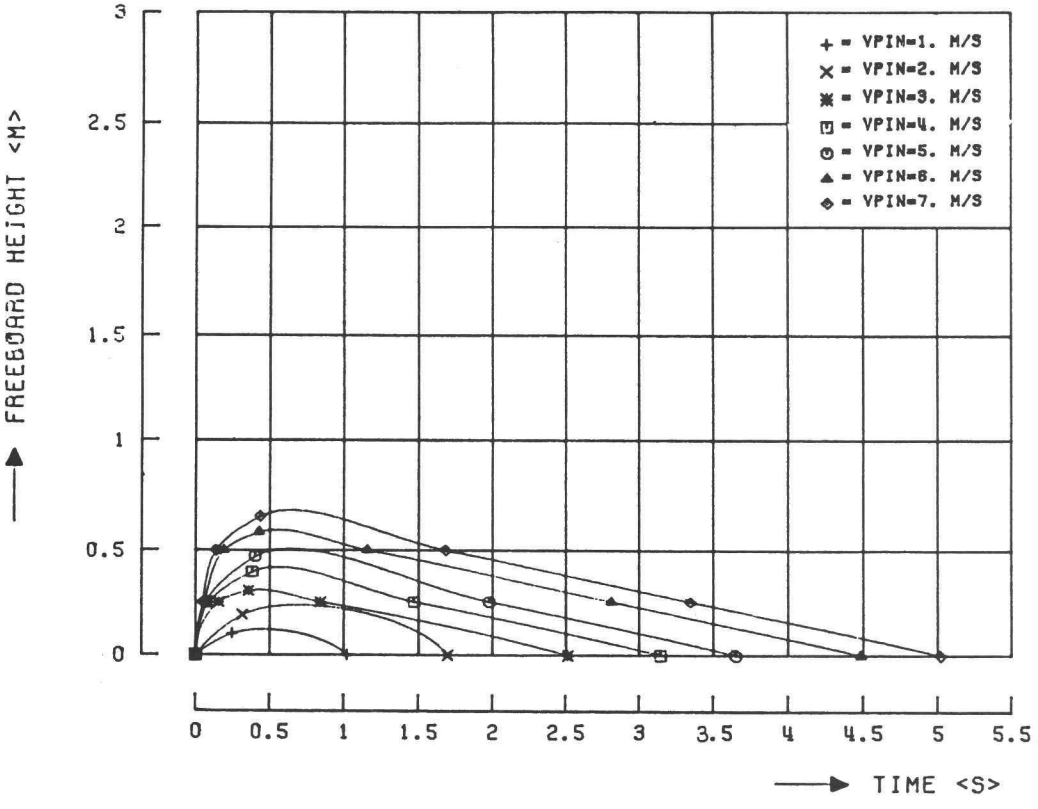

Figure 2-9b.
Some particle trajectories for various initial velocities. Medium size inert particle (215.E-6 m), finally descending.

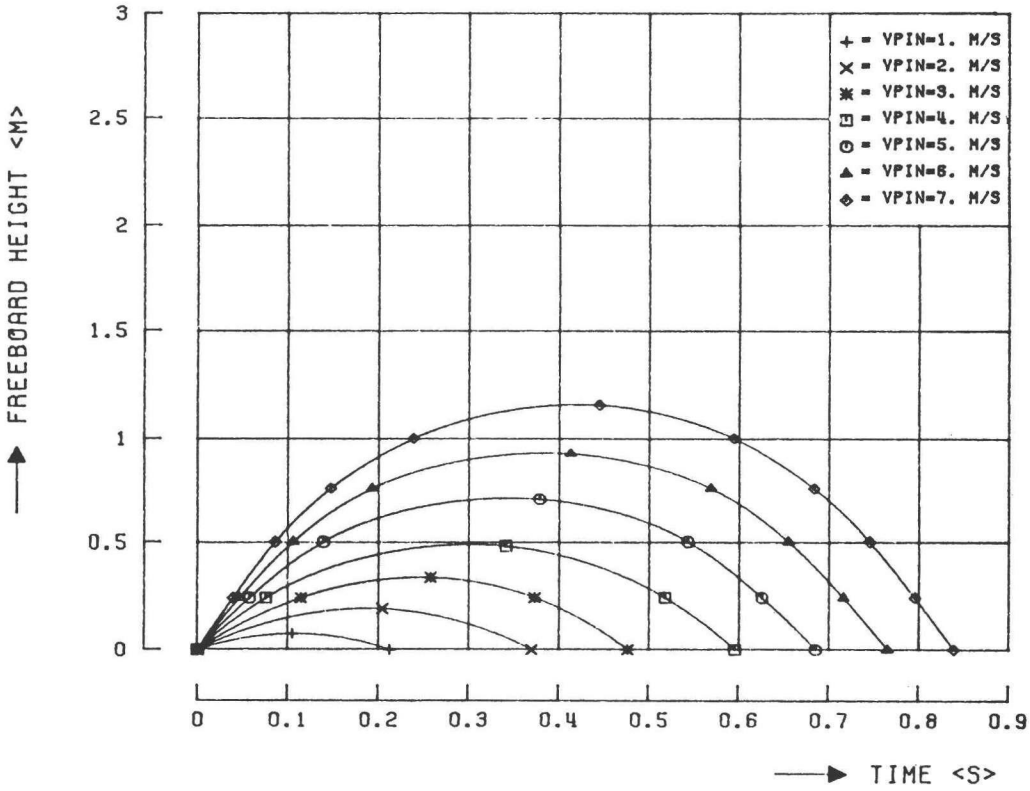

Figure 2-9c.
Some particle trajectories for various initial velocities. Large size inert particle (925.E-6 m), finally descending.

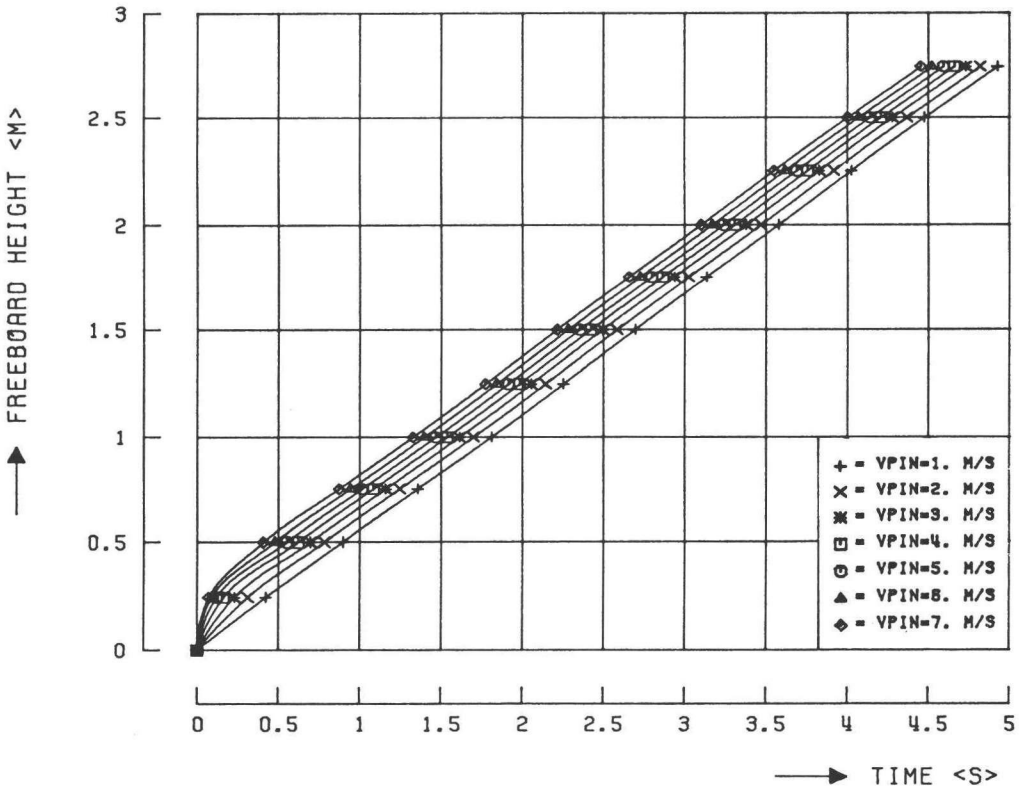

Figure 2-9d.
Some particle trajectories for various initial velocities. Ascending medium size coal particle (337.5E-6 m).

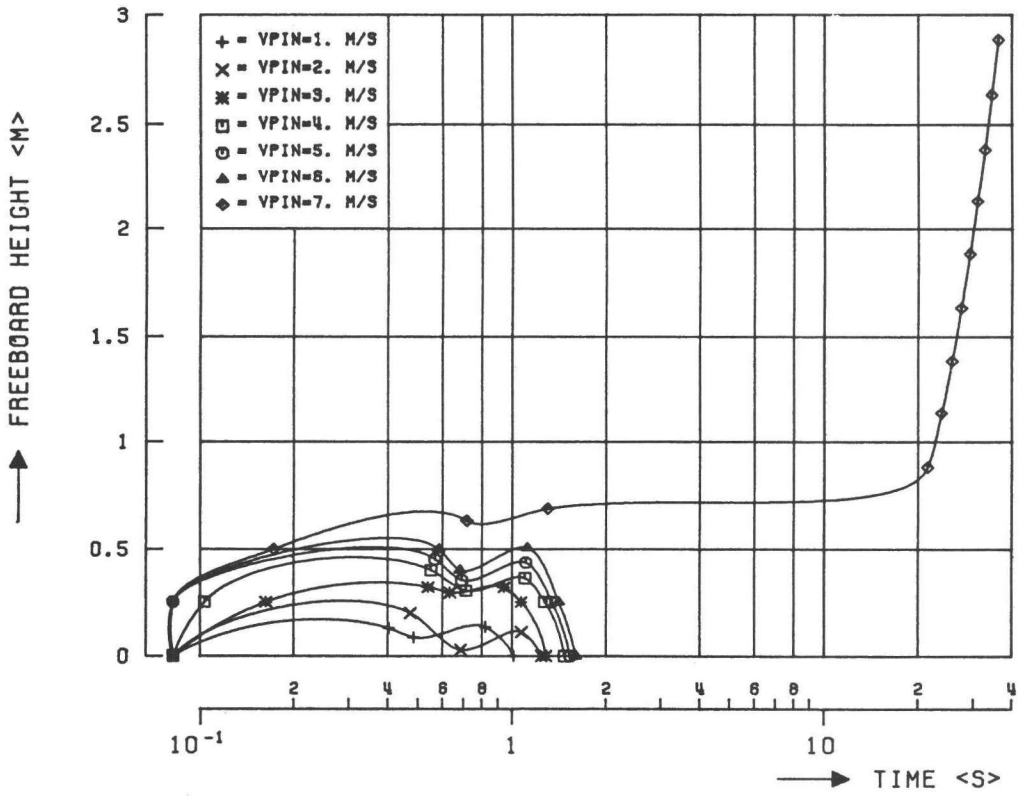

Figure 2-9e.
Some particle trajectories for various initial velocities. Critical size coal particle (400.E-6 m).

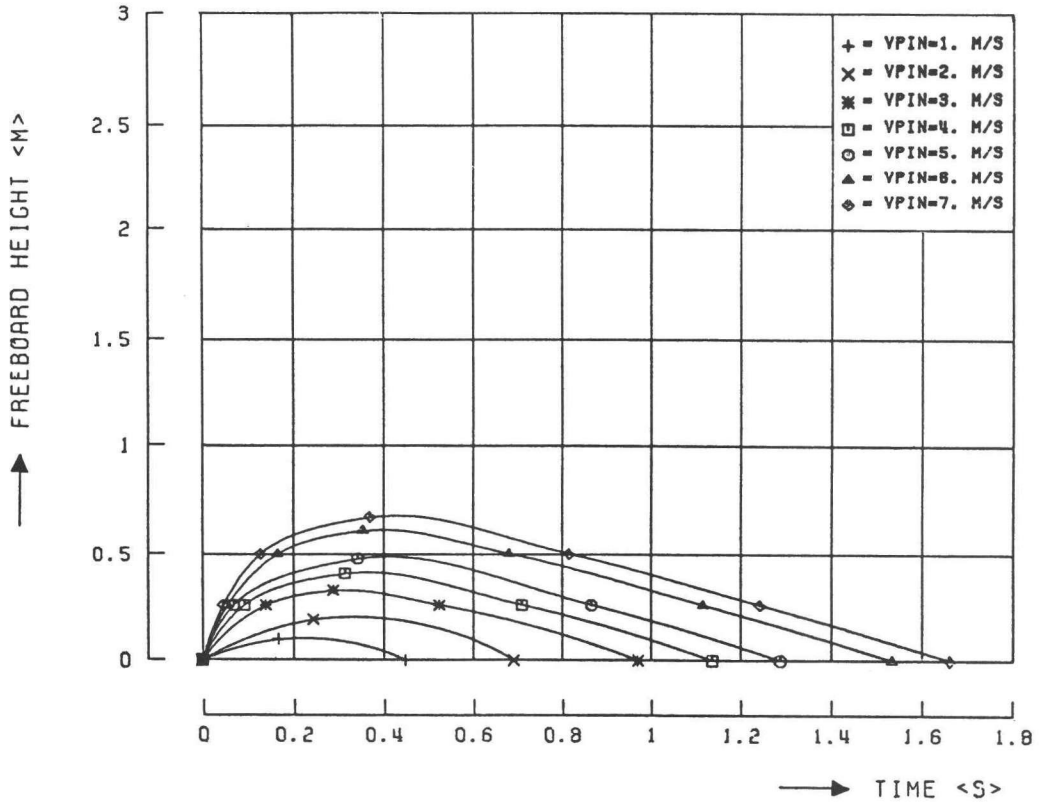

Figure 2-9f.
Some particle trajectories for various initial velocities. Medium size coal particle, finally descending (426.5E-6 m).

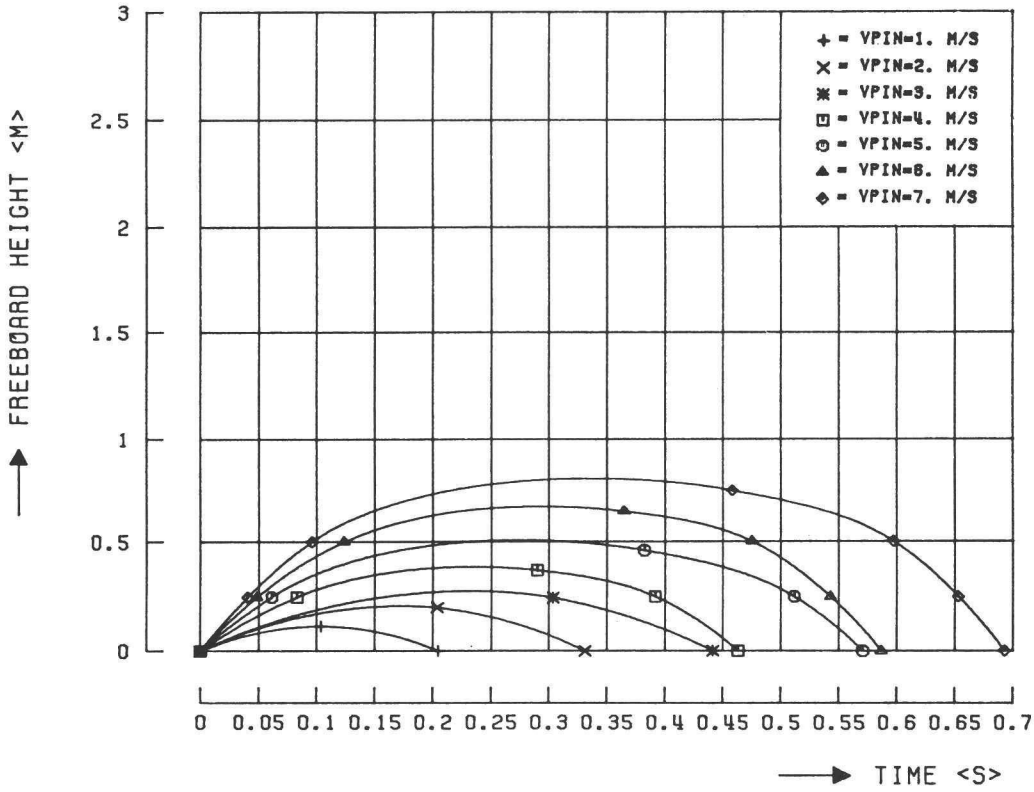

Figure 2-9g.
Some particle trajectories for various initial velocities. Large size coal particle (3.18E-3 m).

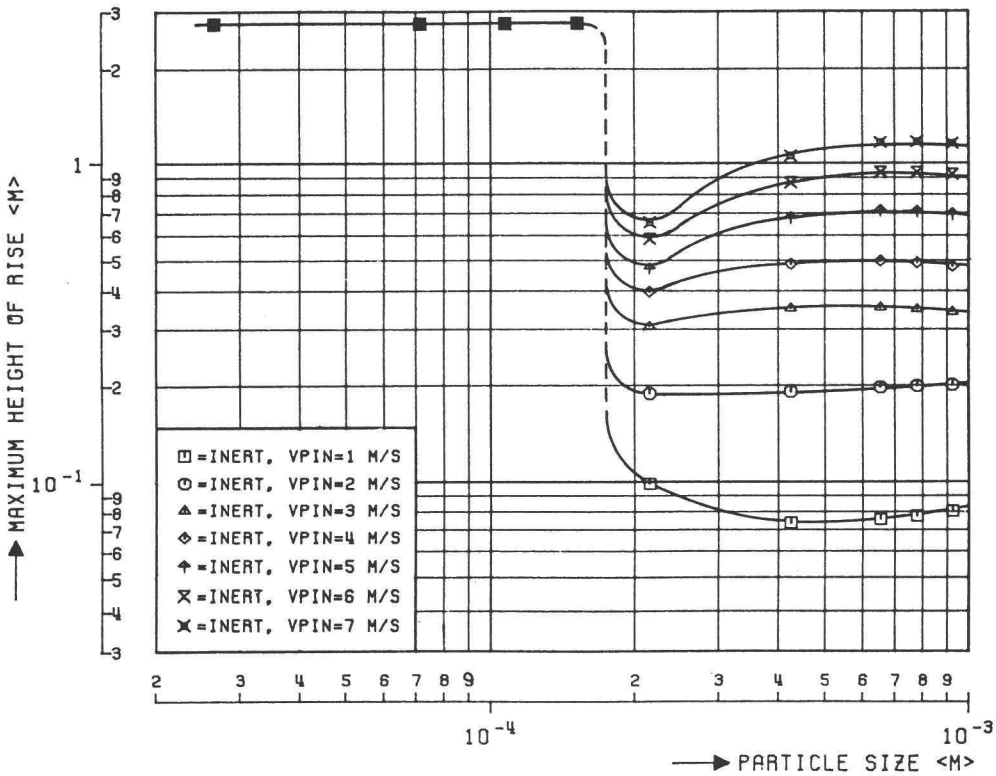

Figure 2-10a.
Maximum particle penetration height as a function of inert particle size for various initial velocities.

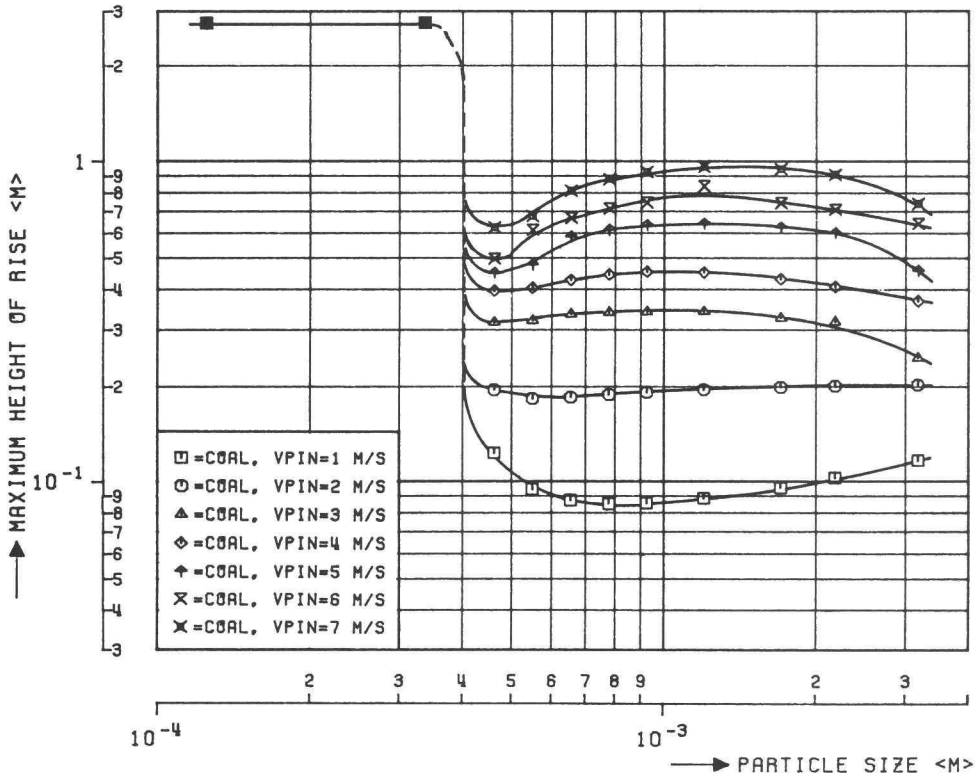

Figure 2-10b.
Maximum particle penetration height as a function of coal particle size for various initial velocities.

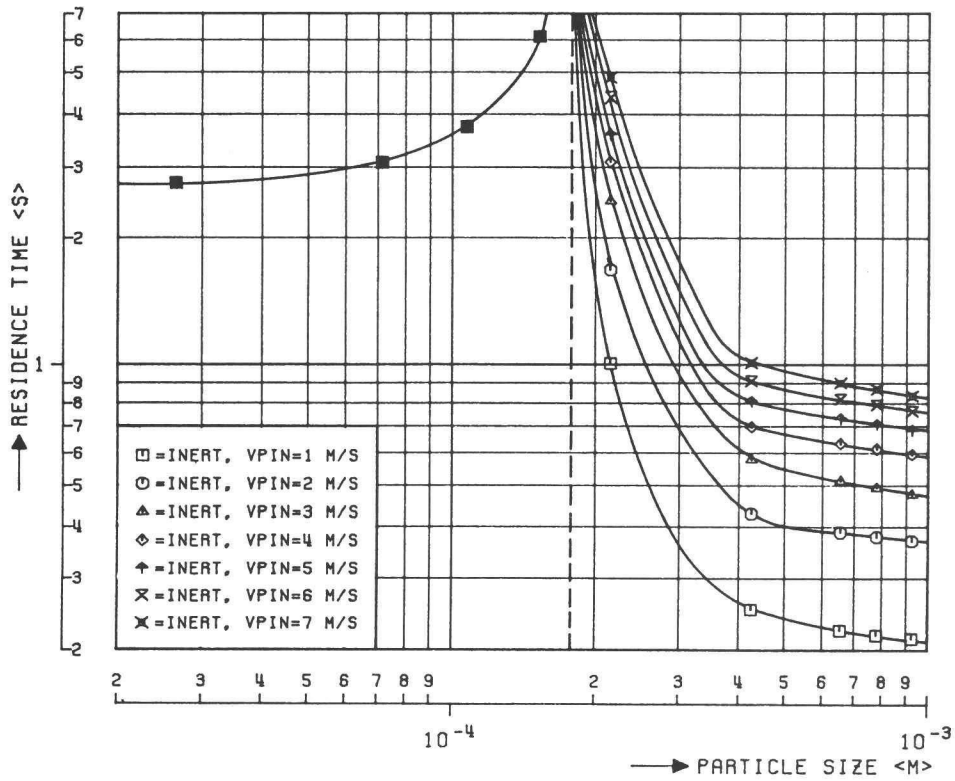

Figure 2-11a.
Particle residence time as a function of inert particle size for various initial velocities.

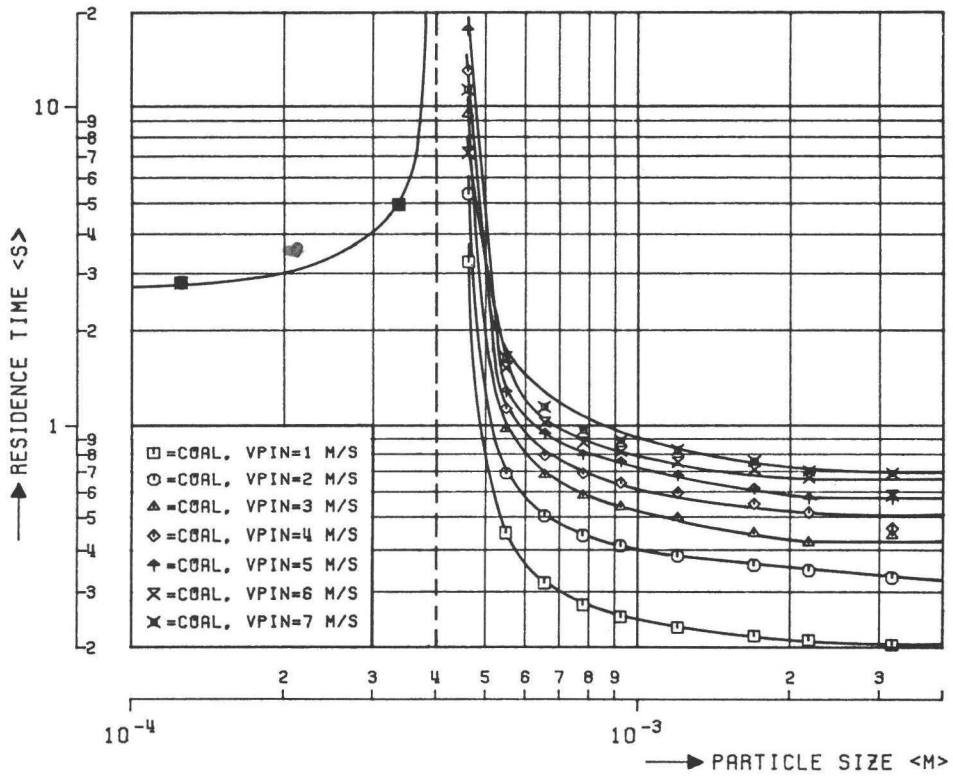

Figure 2-11b.
Particle residence time as a function of coal particle size for various initial velocities.

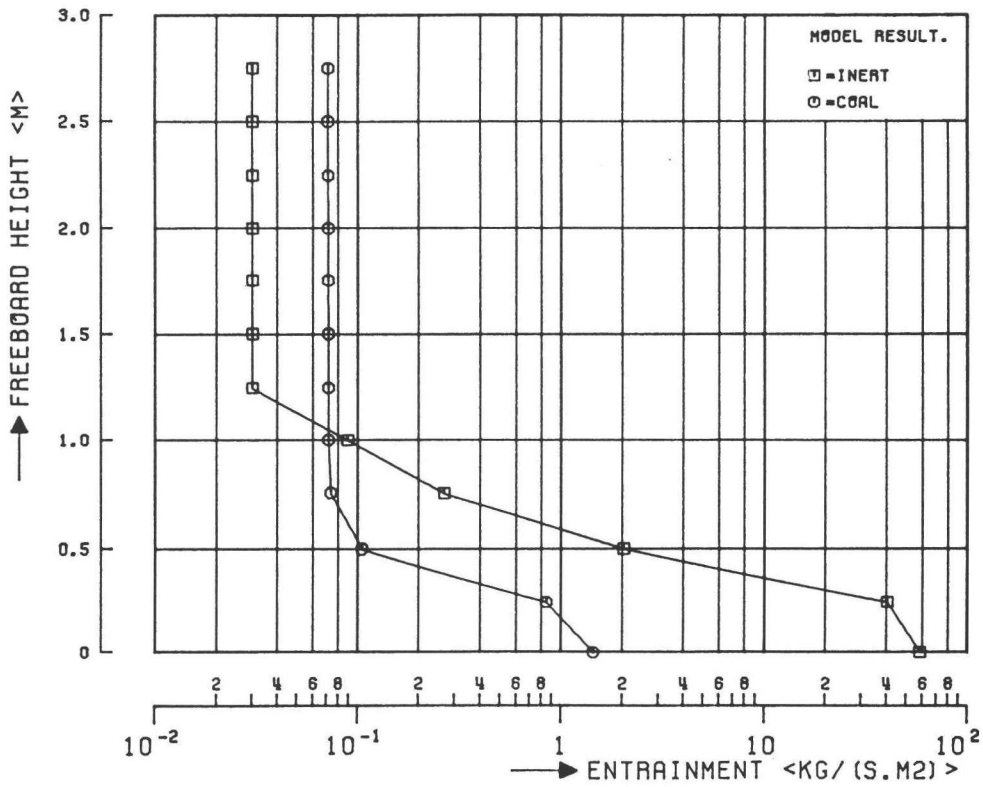

Figure 2-12.
Spatially resolved particle entrainment as a function of the freeboard height. Inert and coal particles; model calculation.

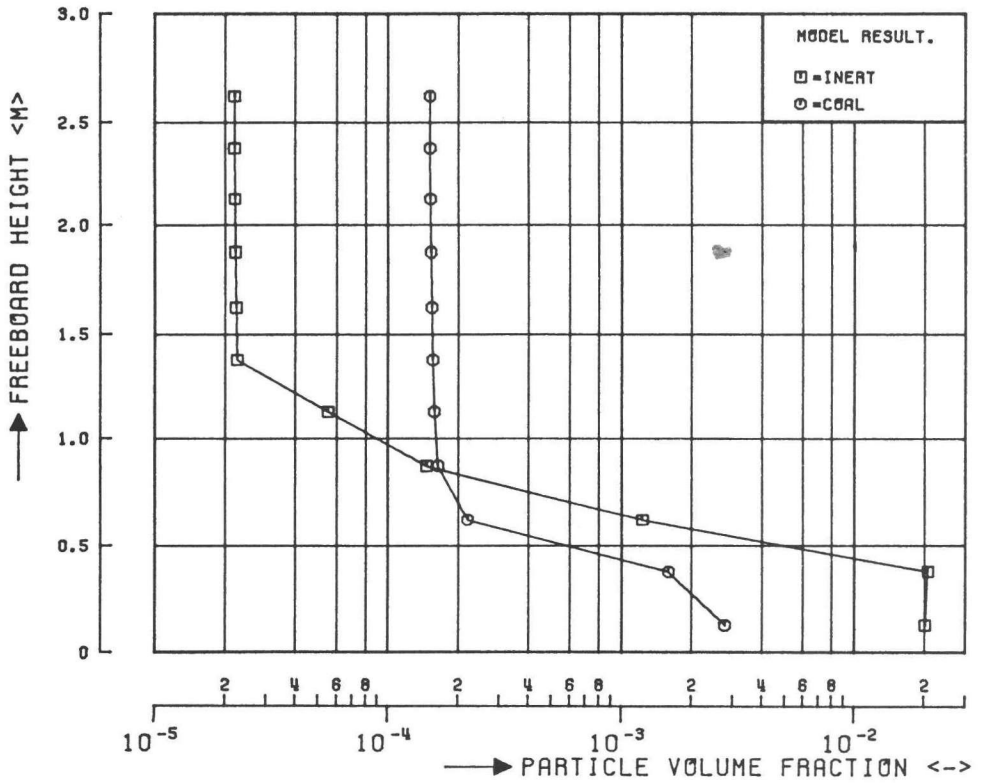

Figure 2-13.
Spatially resolved particle volume fraction as a function of the freeboard height. Inert and coal particles; model calculation.

Table 2-1.
Parameters for turbulence intensity correlation and operating conditions.

reference	$v_{0}^{*'}$ <m/s>	$v_{\infty}^{*'}$ <m/s>	D_b <m>	v_s <m/s>	$\bar{d}_p$ <m>	v_{mf} <m/s>	D_f <m>
Horio et al. (1980)	0.565	0.016	accord. Mori and Wen (1975)	0.3-0.6 air at ambient temp.	glas beads 270E-6 to 1.1E-3		0.24
Havenaar (1982)	0.866	0.036	0.05 exp. bed height= 0.6 m	0.8 air at ambient temp.	silica sand 750E-6	0.35	0.39

Table 2-2.
Get-away angular distribution for initial particle entrainment (according Van Rhijn (1983)).

particle get-away angle in degree <->	mass distribution 1	mass distribution 2	mass distribution 3
0	40 %	30 %	10 %
10	30 %	30 %	30 %
20	20 %	20 %	30 %
30	10 %	10 %	20 %
40	0 %	10 %	10 %

Table 2-3.
Input values for the model trial, respectively calculated physical properties.

pressure	1.013E5	Pa
fluidized bed temperature	1132	K
superficial gas velocity (Tbed)	1	m/s
gas density (Tbed)	0.34	kg/m3
gas viscosity (Tbed)	4.76E-5	kg/(m.s)
density of inert material	2600	kg/m3
density of coal	800	kg/m3
shape factor E_p of inert particles	1	-
shape factor E_p of coal particles (see equation (2-14))	$0.1518+1507.5\ d_p - 837300\ d_p^2$	-
cumulative particle size distribution inert (distribution reduced to 9 part. sizes)	figure 2-8	
coal (distribution reduced to 11 part. sizes)	figure 2-8	
cumulative initial particle velocity distribution (reduced to 7 values)	figure 2-3	
average initial entrainment (inert+coal)	60	kg/(s.m2)
mass fraction coal	0.024	-
freeboard height	2.75	m
compartment height	0.25	m

3 CHEMICAL REACTIONS AND MASS TRANSFER IN THE FREEBOARD

Chemical reactions and mass transfer in the freeboard of a fluidized bed coal combustor are still far from understood. To arrive at a somewhat better understanding experiments on the development of the gas composition were carried out in the 'MAGMA' freeboard. The results were analysed against the background of a fairly extensive literature review. In order to bridge the apparent inconsistencies a simple one-dimensional model was constructed, incorporating both homogeneous and heterogeneous chemical reactions and physical mixing of different gas streams in the lower part of the freeboard. In this chapter the available data and insights regarding gas and solids motion, the particle history and chemical reactions are discussed first (par 3.1 and 3.2). Thereafter the one-dimensional physico-chemical model is elucidated (par 3.3) and compared with experiments (par 3.4).

3.1 Overall gas and solids motion

The gas and solids motion in the freeboard results primarily from the fluid dynamic behaviour of the bed. The bubbling or turbulent behaviour of the bed is generally held to be sufficient for good overall in-bed particle mixing. Yet lateral differences in solids conditions may exist in the freeboard due to the effects from the wall, (as outlined in chapter 2), and from any internals in bed and or freeboard. Some of these effects will be touched upon below. The gas in the fluidized bed is mostly considered to percolate intermittently with or via a particle lean phase (bubble or gas-void phase) and, in parallel but more smoothly via a particle dense phase (emulsion or condensed phase). Because of these differences in origin the gas status at the bed-freeboard interface can be typefied by fluctuations of the gas flow (a sequence of gas eruptions) with different velocities and gas species compositions, that also may vary with lateral distance and time. The change of the gas composition in both gas phases in the fluidized bed results from:

* volatile evolution (coal or sorbent characteristics, particle size, temperature),
* gas-gas reactions (in-phase mixing, kinetics, temperature),
* gas-solid reactions (solid holdup, diffusion, kinetics, temperature),
* inter-phase mixing (fluid dynamics, diffusion).

At the bed freeboard interface the gas status can therefore be typified by fluctuations of the gas flow (a sequence of gas eruptions) with different velocities and gas species composition that both may vary with lateral distance and time.

The bubbles or jets project particles in the freeboard and cause low frequency (gas) eddies. Most of the particles ejected return to the fluidized bed. The low frequency eddies dissipate along the freeboard with height. Both phenomena can be seen as macro-mixing processes, however, none will be fully developed. The macro-mixing of the gas leads to the recombination of the two different gas phases originating from the fluidized bed surface. The macro-mixing of the particles in the freeboard can lead to dispersion. Then a gas-particle cloud results.

Under sufficient micro-mixing and favourable kinetics and temperature gas-gas reactions and gas-particle reactions result. The rate of the reactions will be affected by solids hold-up and gas species concentrations that on one position can vary with time, and on average may vary along the lateral distance and height (macro-mixing not complete or even segregation).

A particle that is fed into the fluidized bed heats up and traverses through the bed and the freeboard and is exposed to desintegrating forces. Eventually the solid is elutriated, taken from the bed overflow, or con-

sumed by reactions and transformed into the gas phase.

The particle trajectories and the disintegrating forces result directly from the fluid dynamic and thermal behaviour of the bed. The overall reaction rate results from the concentration of solid and gaseous reactants and the gasmixing induced by the fluid dynamic behaviour of the bed. Small particles, having a balancing velocity less than the superficial gas velocity, have a residence time in the system not much longer than the gas residence time, such contrary to the larger particles. Excluding the shallow- and fast-fluidized-bed type, the larger particles spend more time in the bed than in the freeboard, whereas for small particles the residence times in the bed and in the freeboard are of the same order. The trajectory of a small particle can roughly been seen as a once-through process. The larger particles mostly traverse many times through the bed and the freeboard.

When coal is fed into the fluidized bed a process of heat-up, swelling, devolatilization and pyrolysis can be observed, followed by relatively slow heterogeneous char reaction in the bed and the freeboard. As a result of thermal and tensional stress, the coal particle may break up into pieces. This process of fragmentation, that is dependent on the coal type, has almost exclusively been observed in the field of fluidized bed combustion and results primarily from the larger resistance to heating and devolatilization of the larger coal particle sizes. Before devolatilization the pore structure undergoes little change. When volatiles escape porosity develops. The knowledge of the char-pore structure becomes important when chemical kinetics or both diffusion and kinitics control the overall reaction rate. This is likely the case for the reactions of O2, CO2 and NO with char in a fluidized bed system, because of the relatively low temperatures. Then combustion in the pores may exceed the combustion at the external particle surface. Via pore enlargement the decomposition of the char leads to formation of numerous needles and finally to detachment of fines. This process can be enhanced by attrition, where forces resulting from the contacting of the coal with the gas, other particles or the bed internals and walls may cause coal and ash needles to break off. Therefore the visual result of attrition is the formation of fines and the counteracting of the internal decomposition by smoothening of the coal particle surfaces. When there is no pore formation attrition is merely the result of a rubbing and impinging process. Because of the much lower particle volume fraction in the freeboard, compared to the bed, one may expect that attrition in the freeboard can be neglected.

Concerning NOx it is known that during the rapid devolatilization substantial amounts of fuel nitrogen are driven out from the coal particles in the form of ammonia, amines and cyanides. These nitrogen species are converted into NOx or N2 depending on the local availability of oxygen. It is therefore possible that the homogeneous reduction of NOx plays an important role in the bed and in some cases in the splash zone (Chaung (1982)).

Substantial amounts of fuel sulfur products are driven out from the coal particles during the devolatilization stage. When dolomite or limestone is fed into the fluidized bed the heat-up results in a calcination step and CO2 evades from the particles. This goes with fragmentation of solid material and pore formation. During the life-time of the solid sulfation may lead to pore blockage. Attrition then will lead to renewal of active particle surface area.

From the considerations above it will be clear that a steady state of a fluidised bed combustor is realised at a balancing situation of particles and gas flow, each having its own status of development resulting from many, more or less stochastic phenomena. Consequently a comprehensive analysis of the gas and the particles' course of life in the reactor is extremely complex and as yet beyond reach. Because of lack of information about most important phenomena occuring in the bed and the transition region between the bed and the freeboard a general and simple approach of

the freeboard is proper.

3.2 Prior studies and experiments

In literature one can find various models that include the effect of diffusion in pore structures and ash layers and combine the physical transport rate with the reaction rate (Laurendeau (1978)). The treatment may lead to many mathematical complexities. Moreover application of the models requires detailed information from specialised and time consuming experiments. Concerning the modeling of the freeboard region of a fluidized bed coal combustor these techniques are not used yet. There are already too many uncertainties to cope with, f.i. regarding particle concentration, particle size and density distribution and the gas species concentrations. However literature gives several overall-reactions from bench-scale experiments in which for a specified type of material and specific conditions the physical internal transport rate and the reaction rate are related to the external or internal particle surface area. To utilize these data the mathematical representation of the freeboard reactions has to be accomodated to this simplified approach. For a better understanding and interpretation of the experimental and model results, at least qualitatively, the factors dominating the progress of the reactions are reviewed.

3.2.1 Coal combustion and gasification

When the diffusion- and chemical reaction-rate are of the same order of magnitude or when reaction is the rate determining step knowledge of the true intrinsic reactivity and char pore structure leads to a better understanding of the combustion process.

In fluidized bed systems the devolatilization time of a coal is found to exhibit a power law relationship with initial particle size. For various types of coal this relationship has been determined by Pillai (1981). The devolatilization time, at T=1150 K, is between 4 s and 10 s for a particle size of 0.5E-3 m, the coal being Niederberg anthracite and bituminous Ohio coal respectively. For a particle size of 5.E-3 m these devolatilization times read 10 s up to 40 s. The devolatilization time is found to be a function of the bed temperature. The heating of small particles in a fluidized bed is considered to be slow compared to f.i. the heating by laser, plasma jet and tube furnace (Thurgood and Smooth (1979)). For large particles, due to the low solid thermal conductivity, heat-up takes more time and a temperature gradient develops. The temperature gradient, the swelling and the devolatilization results in tensional stresses and fragmentation may occur. By fragmentation new and more particle external surface area is formed. In general the larger the particle size, the more fragmentation is observed (Chirone et al. (1983)). Fragmentation experiments on various coals are reported by Chirone and Paulillo (1981). During devolatilization and swelling the porosity develops. The intrinsic reactivity of a char after the devolatilization step is primarily determined by:

* the concentration of active carbon sites,
* mineral matter and trace elements,
* oxygen and hydrogen content.

The heating history and the temperature of the coal affect the intrinsic reactivity by:

* cluster reorganisation of molecules,
* the conversion of mineral matter into metal oxides that have catalytic activity,
* the oxygen and hydrogen concentration.

For further details on these matters the reader is referred to the review article of Laurendeau (1978).

The time for combustion of a shrinking char particle in a stagnant atmosphere, under diffusional control (fast reaction rate and no boundary layer combustion), can be written as (see f.i. Laurendeau (1978)):

$$t_{cp} = \frac{\rho_p \, d_p^2}{8 \, M_c \, \Phi_p \, C_{O2} \, \mathbb{D}_{O2-N2}} \qquad (3\text{-}1)$$

for the reaction:

$$\Phi_p \, C + O2 \longrightarrow (2\Phi_p - 2) \, CO + (2 - \Phi_p) \, CO2$$

Φ_p is the so-called mechanism factor. When, additional to diffusion, chemical kinetics become controling the time for complete combustion will be longer than indicated in (3-1). From this one can show that for fluidized bed combustion conditions the time for char combustion exceeds the time for devolatilization by roughly one order of magnitude.

The global reactions occurring during char gasification and combustion are:

$$C + CO2 \longrightarrow 2 \, CO \qquad \text{(endothermal)}$$

$$C + H2O \longrightarrow CO + H2 \qquad \text{(endothermal)}$$

$$C + 2 \, H2 \longrightarrow CH4 \qquad \text{(exothermal)}$$

$$C + O2 \longrightarrow CO2 \qquad \text{(exothermal)}$$

For almost all applications the carbon-hydrogen reaction is too slow to be of practical importance, unless under pressure. For fluidized bed combustion in particular (at 1150 K) even the C - H2O and C - CO2 reactions are relatively slow. The C - O2 reaction is probably the least understood (Laurendeau (1978)):

1) The exothermicity of the C - O2 reaction causes uncertainty in both particle temperature and active site concentration.
2) The rapid rate of this reaction obscures mechanistic studies due to mass transfer effects, pore structure changes, swelling and cenosphere formation (not important for FBC because the temperature is well below the fusion temperature).
3) As the experimental conditions (T, P, d) vary, the effect of secondary reactions in the boundary layer surrounding the particle layer change. At the carbon surface both CO and CO2 are formed as primary products. CO is favoured at the higher temperatures. A possible explanation is that CO is formed at the carbon edges, while CO2 is formed at inorganic sites. Lower temperatures favour CO2 due to thermodynamic equilibrium and catalytic activity; higher temperatures promote utilization of carbon edges. In the boundary layer the overall reaction

   $$CO + 1/2 \, O2 \longrightarrow CO2$$

   is possible. The elementary step controlling this global reaction is:

   $$CO + OH \longrightarrow CO2 + H$$

   The fundamental question is the relative location of the CO conversion process. The overall stochiometry and surface temperature depend on whether CO is converted to CO2 at the particle surface, within the boundary layer or outside the boundary layer. In general the location of the CO oxidation front is regulated by the particle size and the bulk gas temperature. Large particles and higher temperatures favour conversion near the surface; smaller particles and lower temperatures favour conversions outside the boundary layer. The boundary layer phe-

nomenon is often simplified by using either a single film or a double film model. In the single film model both CO and CO2 are considered primary products and no reaction occurs within the boundary layer, but CO oxidation may occur outside the layer. In the double film model, CO oxidation consumes all incoming oxygen before reaching the surface. The resulting CO2 diffuses from the reaction front in two directions. At high temperatures (that is probabely not the case for fluidized bed combustion) the reaction:

$$C + CO2 \longrightarrow 2\ CO$$

is the only heterogeneous step.

Because of these uncertainties and in spite of studies available on coal combustion rates, the understanding of 1) reactant-chemisorption, 2) migration of intermediates and 3) product desorption is poor. However, the simplified models with their overall kinetic rates give reasonable results for the appropriate regimes. Extrapolations, for instance to pressurised conditions, have to be done with care.

3.2.2 NOx reduction with coal (abstract of the literature review from Chaung (1982))

During the combustion of char particles (after the devolatilization stage has been completed), char bound nitrogen is converted to NO by reaction with oxygen diffusing into the pores of the solid. On the other hand NO can be reduced by ammonia, amines, CO, hydrocarbons and char to become molecular nitrogen.

Nitric oxide can be reduced either homogeneously or heterogeneous. The heterogeneous NO reduction reaction may belong to two different types: true catalytic or solid-gas reactions.

* Homogeneous NO reduction reactions.
  Duxbury and Pratt (1975) propose the following reduction step:

$$NO + NH3 \longrightarrow H2O + N2 + 1/2\ H2$$

  and De Soete (1980):

$$NH3 + O2 \longrightarrow NO + products$$

$$NH3 + NO \longrightarrow N2 + products$$

  Yamazaki et al. (1979), Meyerson (1975) and (not reported by Chaung (1982)) Paauw et al. (1979) find that in hydrocarbon combustion proceses many effective free radicals are formed that can reduce NO.

* Heterogeneous NO reduction reactions.
  De Soete et al. (1980) conclude that, except in cases where noble metals or typical metal oxide catalysts are present, direct transformation of NOx into molecular nitrogen in the absence of any reducing agent is a relatively slow process. When <NO> is larger than 300 ppm the NO reduction rate is zero order with respect to <NO>, when <NO> is less it becomes dependent on <NO>. In the presence of reducing agents, such as solid bound carbon atoms, CO and hydrogen, the direct transformation of nitric oxide into molecular nitrogen is significantly enhanced. Increase in reaction rate of 3 to 12 times dependent on <CO> or <H2> have been determined. In the presence of hydrogen (hydrogen atoms, molecular hydrogen, hydro-carbons) an indirect transformation of nitric oxide into molecular nitrogen with ammonia as an intermediate is observed. Edwards (1972) showed that five reactions of the form:

$$C + a\ NO \longrightarrow b\ CO + c\ CO2 + d\ N2$$

  are thermodynamically favourable. It is found that CO2 prevails at low temperatures (1100 K). The first step in NO carbon reaction is the

chemisorption of NO on the carbon surface, accompanied by the immediate release of N2. The desorption of surface oxide follows, resulting in the production of CO2 or CO depending on the reaction temperature. Another mechanism proposed by Beer (1980) is the adsorption of NO molecules on two adjacent active sites of the carbon surface resulting in a carbon complex and a loosely adsorbed nitrogen atom. Due to the subsequent fast surface diffusion, the N-atoms recombine into molecular nitrogen. The chemisorbed oxygen can either desorb to produce CO or react with CO to form CO2. This mechanism can be used to explain the observed increase of the NO conversion due to the presence of carbon monoxide. It is found that the overall reaction rate is first order with respect to the NO concentration.

3.2.3 NOx - char reactions; influence of CO and O2

During the combustion process reducing agents (such as CO) are formed as primary products. In 3.2.2 is reported that CO is an important species in the catalytic NO reduction reaction. The concentration of CO is determined by the mechanism of the reactions, that itself is dependent on the reaction rates and the diffusional rates. When for combustion the O2-chemisorption at the char surface is the rate determining step, changing oxygen concentration leads to a different rate of the NO reduction than for the case when the desorption of CO or CO2 from the char surface is the rate determining step. It is reported by Chan et al. (based on the kinetics of Horio et al. (1977)) that the rate of O2 - char reaction is approximately two orders of magnitude larger than that of the NO - char reaction. For this reason in major diffusional resistance of oxygen the O2 is consumed close to the particle surface (except for the smaller particles or for low temperatures) to produce CO. CO and NO co-diffuse into the pore structure to accelerate the rate of NO reduction. Comparison of the overall combustion rate with the overall NO reduction rate (both from Horio et al. (1977)), at 1100 K, do not lead to this finding. (The rate of NO reduction of Horio et al. (1977) can be found in table 3-1. For the combustion reaction used by Horio et al. take the Field and al. (1967) equation from table 3-1, with Φ_p=2). Then, although diffusion via the particle boundary layer is found to be the controlling step (for particles with d_p> 4.E-3 m), it both influences the O2 and NO diffusion equally.

3.2.4 NOx reactions with limestone and dolomite

Reactions of NOx with calcined limestones under fluidized bed combustion conditions have not been studied thoroughly yet. Furusawa et al. (1983) performed experiments in a fixed bed (0.02 m I.D., quartz) reactor. They report high catalytic activity of calcined limestones for NO reduction by hydrogen and carbon monoxide:

$$NO + CO \xrightarrow{\text{catalyst}} CO2 + 1/2\ N2$$

$$NO + H2 \xrightarrow{\text{catalyst}} H2O + 1/2\ N2$$

$$NO + 5/2\ H2 \xrightarrow{\text{catalyst}} NH3 + H2O$$

In view of this finding it is interesting to note that Martens and Van Koppen (1983) have performed fluidized bed experiments in which a batch of fresh dolomite was fed into the bed during continuous feeding of coal (anthracite). As many others Martens found that in general the <NOx> was somewhat reduced at the presence of limestone / dolomite in the bed. However, simultaneous observations of the NOx and SO2 concentrations at the flue exit made clear that this is only true at the presence of SO2. For

those situations where the <SO2> is small (say less than 20 ppm) the NOx concentration at the flue exit is approximately the maximum that is theoretically possible on basis of fuel nitrogen.

3.2.5 CO-oxidation in the gas phase

Chaung (1982), Martens et al. (1983) and Martens (1983) and (1984) obtained by experiment time averaged CO concentration profiles along the freeboard. The experimental results showed high CO concentrations (up to 5%) near the fluidized bed surface and in the splash zone. Higher up the CO concentration decreased, although no complete burn-out was obtained. Martens (1984) also found the lateral distribution of the time averaged gas species composition just above the the fluidized bed surface to vary considerably with lateral distance. See figure 3-1 for a typical plot. The oxygen concentration is highest in the central region and the CO-concentration is highest near the wall. This phenomenon can well be explained by assuming an oxygen-rich bubbling phase feeding the central region and a CO-rich emulsion phase feeding the wall region. Indeed, Horio et al. (1982) determined the contour lines of the local average superficial bubble velocity at various bed heights and found the values in the central region to be well above those near the wall. Further the higher solids and char concentrations in the wall layer may play a role.

The CO conversion in the gas phase dependends on:

* The macro-mixing of the gas (the overall mixing process).
* The micro-mixing of the gas (mixing in the molecular scale).
* The kinetics, the gas species concentrations and the temperature.

Further, CO production from gas-particle reactions occurs.

The freeboard CO-oxidation studies can be divided into the following categories:

* Studies regarding the overall micro- and macro-mixing,
* Studies regarding the kinetics for uniform gas composition,
* Studies assuming plug-flow.

1) Studies regarding the overall micro- and macro-mixing.
Rajan and Wen (1980) divided the freeboard into a number of perfectly mixed compartments of equal size. The compartment size was based on the Peclet number obtained from the correlation of Wen and Fan (1975):

$$\frac{1}{Pe_D} = \frac{1}{Re_D\, Sc_g} + \frac{Re_D\, Sc_g}{192} \qquad Re_D < 2000 \qquad (3\text{-}2a)$$

$$\frac{1}{Pe_D} = \frac{3.E7}{Re_D^{2.1}} + \frac{1.35}{Re_D^{1.8}} \qquad Re_D > 2000 \qquad (3\text{-}2b)$$

The dimensionless numbers are defined as:

$$Pe_D = \frac{\bar{v}_g\, D_f}{\mathbb{D}_h} \qquad (3\text{-}3)$$

$$Re_D = \frac{\rho_g\, \bar{v}_g\, D_f}{\eta_g} \qquad (3\text{-}4)$$

$$Sc = \frac{\eta_g}{\rho_g \, \mathbb{D}_{O2-N2}} \qquad (3\text{-}5)$$

The average compartment size is calculated from:

$$h_f = \frac{2 \, \mathbb{D}_h}{\bar{v}_g} \qquad (3\text{-}6)$$

$\mathbb{D}_h$ is the axial dispersion coefficient.

Hot-wire measurements of Horio et al. (1980) and Pemberton and Davidson (1983) in the freeboard at ambient temperature showed that (section 2.2.7) :

* The turbulent intensity in the freeboard is proportional to the erupting bubble size.
* The turbulence decays along the freeboard with height.

The latter has also been confirmed by Havenaar (1982) with laser-doppler velocity measurements at ambient temperature and under combustion conditions. Assuming that the dissipation of the bubble induced turbulence, the low frequency eddies, can be related to the state of macro-mixing and assuming that the subsequent micro-mixing is relatively fast, then the overall mixing is primarily dependent on bubble size and freeboard height. These parameters, however, cannot be found in equation (3-2).

2) Studies regarding the kinetics for uniform gas composition.

a) Global kinetics:

Global kinetics are widely used in combustion engineering in order to overcome the lack in knowledge of the true chemical mechanisms and/or to simplify complicated and detailed kinetics. The global CO-oxidation rate is commonly expressed as:

$$r_{CO} = A \, C_{CO}^{a} \, C_{H2O}^{b} \, C_{O2}^{c} \exp\left(\frac{-E}{R\,T}\right) \qquad (3\text{-}7)$$

Table 3-2 summarizes the parameters of interest from various authors. Chaung (1982) demonstrated that the reaction orders used in most global expressions depend on the investigators' choise of reaction sets for partial equilibrium of the OH gas species. Partial equilibrium in a reacting system is said to exist when certain fast reactions are dynamically balanced even though the system as a whole is not in thermodynamic equilibrium. An overview of global kinetics for freeboard modeling used by various authors is given in table 3-3. The CO-oxidation modeling result of Wells et al. (1981) and Martens et al. (1983) showed rapid CO consumption. Rajan and Wen (1980) did not report CO-oxidation results. The main shortcomings of global kinetics are:

* The assumption of complete combustion and no reverse reactions. This results in an over-estimation of the total heat produced, because actually the fuel gas species reaches equilibrium with the oxidant and is not fully consumed.
* Global reaction mechanisms assume the energy to become available instantly. The first reaction steps of the actual combustion mechanism, however, are endothermic, resulting in a delay in fuel consumption and heat release. On the contrary global reaction mechanisms show (in an adiabatic system) at the initial period a temperature increase that promotes further reaction.

b) Detailed kinetics:

Martens (1981) performed model calculations with a set of 80 reversible reactions involving 28 gas species. The mechanism of the reactions was taken from the work of Paauw et al. (1979) (see table 2-4) and the computer program used ('CEC 80') was a modification of Pratt's (1974) 'PSR'. Martens initially showed that a wet gas mixture containing CO at 1.E5 Pa and 1073 K in an adiabatic system will develop stable ignition and combustion. An example from his results is visualized in figure 3-2. Initial molar gas fractions were: 0.025 CO, 0.027 O2, 0.039 H2O, 0.115 CO2, 300 ppm NO, the remaining being N2. The heat capacity of the gas was 1260 J/(kg.K). The CO-oxidation in the well-mixed gas phase proceeds rapidly (say within 0.1 s) resulting in a temperature increase of 195 K. Significant CO conversion occurs after the formation of high OH and H concentrations.

Chaung (1982) reported that the CO-oxidation is quenched at or below 950 K as was demonstrated by Hardy and Lyon (1980), and that the conversion is dependent on the initial CO concentration. In this view it is interesting to note that Martens using his model dit not find stable ignition of CO below 975 K. The experimental work of Gibbs et al. (1975) on fluidized bed coal combustion leads to the same findings.

Chaung performed calculations on CO-oxidation using a set of 22 reversible reactions involving 10 reactants (see table 3-6) which is a simplification of Westbrook's (1977) set involving 28 reversible reactions. He showed that the empirical global rate equation of Dryer and Glassman (1974) overpredicts CO burnout while the assumption of partially equilibrated OH leads to far too low oxidation rates. Chaung further argued that the high solids concentration affects the CO-oxidation by providing a large surface area for heterogeneous radical recombination. At 1100 K and for the particles sizes of interest diffusion of the OH radical to the particle surface was shown to be the limiting step. For a single particle the total OH consumption rate thus can be simplified to:

$$r_{OH,p} \leq Sh_p \, \mathbb{D}_{OH\text{-}gas} \, \pi \, d_p \, C_{OH,\infty} \qquad (3\text{-}8)$$

Model calculations in the temperature range 975 K to 1100 K, isothermal conditions, using mono-size particles of 0.3E-3 m and 1.E-3 m, showed that the heterogeneous radical recombination reaction on CO-oxidation becomes noticable for values A/V of 0.1 1/m and 1.0 1/m , the latter for the coarser particles. The A/V was defined as:

$$\frac{A_p}{V_f} = \frac{\text{total external particle surface}}{\text{reactor volume}} \qquad (3\text{-}9)$$

Heterogeneous radical recombination reactions were shown to govern the CO-oxidation reaction at an A/V ratio beyond 1000 1/m for the lower temperatures and a particle size of 1.E-3 m. The CO-oxidation-temperature relation elaborated from the work of Chaung is presented in figure 3-3. The A/V is 100 1/m and 1000 1/m respectively and the gas residence time 3.6 s. It can be seen that there is no significant conversion at temperatures around 900 K. Above 1100 K the CO-oxidation is completed, and the gas species can be thought to have reached an equilibrium with some CO unconverted. Unconverted CO increases with increasing A/V and decreasing temperatures. In the region 900 - 1100 K the temperature and particle surface area dependency of CO-oxidation is high. In section 2.4 the freeboard particle volume fraction is demonstrated to be in the order of 2.E-2. The particle volume fraction near the wall will be somewhat higher, because of

the dense layer of descending particles. For comparison: for Chaungs' model result on 1.E-3 m particles an A/V of 100 1/m correspond with a particle volume fraction of 1.7E-2. From these considerations one may conclude that the heterogeneous radical recombination in the freeboard has no keen effect on CO-oxidation for temperatures above 1000 K. In the fluidized bed the A/V ratios are much higher than in the freeboard. There one may expect that this phenomenon hampers the CO-oxidation process considerably, which may explain the large concentrations of CO in the bed.

3) Studies assuming plug-flow.

These studies assume perfect micro- and macro-mixing in a thin horizontal slice moving upward with the average velocity of the gas.

With their global reaction mechanism and plug flow reactor model Martens et al. (1983) and Wells et al. (1981) found a sharp reduction in the CO concentration just off the surface of the fluidized bed. These authors derived a differential energy balance along the freeboard based on:

* Heat generation resulting from gas-solid and gas-gas reactions.
* Radiation of particles to the wall.
* Convection and radiation from the gas to the wall.
* Convective heat transport with the gas.
* Martens also included convective heat transport by the ballistically moving particles in his model, and heat transfer from the particles.

Due to the rapid CO combustion Wells et al. found a step in the freeboard temperature of 20 K for an initial molar gas fractions of about 0.0015 (which is rather too low). Martens et al. found a step in the freeboard temperature of 8 K with initially 0.025 CO. They further found the experimentally determined CO-oxidation to be much slower than the predicted one, and the large solids fluxes in the freeboard, with their large heat capacities, to counteract any temperature change (see section 3.3.2).

Freeboard modeling results were obtained by Martens (1981) and Chaung (1982) using a detailed set of reaction mechanisms in conjunction with plug-flow. See table 3-4 and 3-5. Martens' energy balance included:

* Heat generation resulting from reactions.
* Convective heat transport by the gas.
* Heat transfer to fluxes of particles with the following approximative assumptions:
  Exponential decay of particle entrainment as a function of freeboard height (see equation 2-5) where F_0 = 3.3 kg/(s.m2), F_∞ =4.0E-4 kg/(s.m2) and a = 4.7 (1/m).
  Particles traversing a reactor (slice) have a residence time that is too short for considerable heat transfer (they leave the reactor at their original temperature).
  Particles changing direction in a reactor (slice) have a residence time long enough for completion of the heat exchange with the gas (they leave the reactor at a temperature equal to that of the gas).

The gas and the initial particle temperatures were 1073 K, particle density 2600 kg/m3, particle heat capacity 800 J/(kg.K), heat capacity of the gas 1260 J/(kg.K), fluidization velocity 1 m/s, pressure 1.01E5 Pa. The molar gas fractions at the fluidized bed surface were: CO=0.025, O2=0.027, H2O=0.039, CO2=0.115, NO=300ppm and the remaining N2. The model result is visualised in figures 3-4a and b. The conclusions were: The CO reacts fast and the high particle mass fluxes transport the larger portion of the heat generated towards the fluidized bed. Although the model does not predict the slow progress of the CO-oxidation it does predict the trend of the temperature increase (sup-

pression) in the freeboard satisfactorily. Chaung (1982) performed model calculations on CO-oxidation and solid-gas reactions (including radical recombination reactions) and compared results with measurements from the MIT AFBC. The reader is left in doubt about freeboard temperatures (presumably the freeboard was set isothermal) and the A/V ratio or the particle volume fraction as a function of the freeboard height. The CO concentration profile of the predictions and the experiments were in rough agreement. Significant hydrocarbon species were found immediately above the fluidized bed surface. Reactions between these hydrocarbons and radical species were conjectured to further deplete the radical pool and hence reduce the initial CO-oxidation rate in the freeboard.

3.3 The one-dimensional freeboard model

3.3.1 Modeling gas-particle reactions

In general the overall rate equation for a reaction accounts for both physical transport steps and reaction steps:

* Diffusion of the gaseous reactant to the surface of the particle through the gasfilm surrounding the particle.
* Diffusion of the gaseous reactant through the pores or blankets of ashes.
* Reaction of the gaseous reactant with the solid.
* Diffusion of the gaseous product through the blanket of ashes to the exterior surface of the solid.
* Diffusion of the gaseous product through the gasfilm surrounding the particle into the bulk of the gas.
* Reactions of the gaseous product with gaseous reactants during the diffusion steps.

Consider the following overall reaction:

$$A(gas) + B(gas) + C(solid) \longrightarrow G(gas) + E(gas) + F(solid)$$

* The resistances to reaction can be considered to occur in series.
* Any diffusional resistance in the boundary layer of the particle is limited to the gaseous species A, diffusing towards the particle.
* Gas-gas reactions occuring in the boundary layer of the particle are lumped to the particle surface area by means of an effectiveness factor Φ_p.
* The reaction is first order with respect to A and is irreversible.
* The reaction is based on unit internal or external particle surface area.
* The true reaction rate and the internal diffusion rate is "lumped" to the characteristic surface area that has a uniform concentration of A. If required an effectiveness factor is defined.
* The particles are spherical.
* Steady state.

By diffusion the flux of i to the surface is given by:

$$r_{d,i,p} = k_{d,i,p} A_p (C_i(\infty) - C_i(d_p)) \qquad (3\text{-}10)$$

where the mass transfer coefficient of A reads:

$$k_{d,i,p} = \frac{Sh_p \mathbb{D}_{i\text{-}N2}}{d_p} \qquad (3\text{-}11)$$

and the particle surface area:

$$A_p = \pi\, d_p^2 \qquad (3\text{-}12)$$

For a single sphere in an extensive flowing fluid Rowe and al. (1965) find:

$$Sh_p = 2 + 0.69\, Re_p^{0.5}\, Sc_f^{0.33} \qquad (3\text{-}13)$$

where:

$$Re_p = \frac{\rho_f\, v_r\, d_p}{\eta_f} \qquad 0 < Re_p < 2000 \qquad (3\text{-}14)$$

and:

$$Sc_f = \frac{\eta_f}{\rho_f\, \mathbb{D}_{i\text{-}N2}} \qquad (3\text{-}15)$$

This relation can be used as a first approximation of the true situation: a cloud or an aggregate of particles. The reaction rate of species i by reaction j at the effective particle surface area is given by:

$$r_{i,j,p} = k_{i,j,p}\, A_{p,e}\, C_i(d_p) \qquad (3\text{-}16)$$

where the reaction rate is expressed by Arrhenius' law:

$$k_{i,j,p} = k_{0,i,j,p}\, T^n \exp\left(\frac{-E_{i,j}}{R\, T_p}\right) \qquad (3\text{-}17)$$

For the case of spheroidal particles and surface reaction the particles' surface area is derived from the mass-equivalent spherical particle. For the processes in series, at steady state, the flow rate to the surface is equal to the reaction rate at the surface:

$$r_{i,j} = r_{d,i,p} = r_{i,j,p} \qquad (3\text{-}18)$$

From equations (3-10), (3-16) and (3-18) follows:

$$r_{i,j,p} = \frac{1}{\left(\frac{1}{k_{d,i,p}\, A_p} + \frac{1}{k_{i,j,p}\, A_{p,e}}\right)}\, C_i(\infty) \qquad (3\text{-}19)$$

The global chemical reactions to be considered in the freeboard are:

Φ_p C + O2 ——> $(2\Phi_p\text{-}2)$ CO + $(2\text{-}\Phi_p)$ CO2 (j=1)

2 C + O2 ——> 2 CO (j=6)

C + CO2 ——> 2 CO (j=2)

1/2 C + NO ——> 1/2 CO2 + 1/2 N2 (j=3)

C + NO ——> CO + 1/2 N2 (j=7)

CaO + SO2 + 1/2 O2 ——> CaSO4 (j=4)

For reactions 1,3,6 and 7 table 3-1 summarises the correlations and reaction mechanisms used or found by various authors, and those used in this work for the freeboard model. The SO2 reaction mechanism (j=4) was modeled after Rajan (1978) but no reasonable freeboard model results could be obtained as no boundary conditions at the bed-freeboard interface on SO2 and limestone conversion were available. Therefore no further emphasis will be laid on this subject here.

It has been pointed out in section 3.2.1 that at the carbon surface CO and CO2 are primary products, and at least some combustion occurs in the boundary-layer. The primary CO/CO2 ratio p is correlated in the model by a modification of Arthur and Phillips et al. (see Laurendeau (1978)). These authors write:

$$p_p = A \exp(-B/T_p) \qquad (3\text{-}20)$$

where at low pressures: A=316 and B=3000 - 4500 K, and at high pressures: A=3162 and B=6000 - 9500 K. The constants used by Rajan and Wen (1980), Rajan (1981), Chaung (1982), Martens et al. (1983) and in this work are: A=2500 and B=6240 K. These values originate from the experimental work of Arthur (1956), for two different carbons and for temperatures between 730 and 1170 K. Chaung (1982), starting from the double film theory of Caram and Amundson (1977), concludes that Arthur's correlation is applicable only for small particles. Wen and Dutta (1978) propose a correlation to estimate the mechanism factor, Φ_p, by a linear interpolation between small particle sizes and large particle sizes:

$$\Phi_p = \frac{2p_p + 2}{p_p + 2} \qquad d_p < 50.E\text{-}6 \text{ m} \qquad (3\text{-}21a)$$

$$\Phi_p = \frac{2p_p + 2}{p_p + 2} - \frac{p_p (d_p - 50.E\text{-}6)}{0.95E\text{-}3 (p_p + 2)} \qquad 50.E\text{-}6 \text{ m} < d_p < 1.E\text{-}3 \text{ m} \qquad (3\text{-}21b)$$

$$\Phi_p = 1 \qquad d_p > 1.E\text{-}3 \text{ m} \qquad (3\text{-}21c)$$

This relation is used by Rajan and Wen (1980), Rajan (1981), Martens et al. (1983) and in this work because of simplicity. However, it should be noted that the elementary step controlling the CO combustion reaction (CO + OH ——> CO2 + H) might be affected by radical recombination reactions (Chaung (1982)) or by pressure.

For the char combustion, the particle temperature is calculated from the thermal equilibrium with the surroundings. This equilibrium temperature follows from:

$$\dot{Q}_{ip} = \dot{Q}_{cpg} + \dot{Q}_{rps} \qquad (3\text{-}22)$$

Each of the terms is a function of the particle temperature. As a first approximation we have:

$$\dot{Q}_{ip} = r_{ip} H_i^0 \qquad (3\text{-}23)$$

$$\dot{Q}_{cpg} = \alpha_{cpg} \pi d_p^2 (T_p - T_g) \qquad (3\text{-}24)$$

$$\dot{Q}_{rps} = \pi d_p^2 \varepsilon_p \sigma_b (T_p^4 - T_s^4) \qquad (3\text{-}25)$$

where:

$$\alpha_{cpg} = \frac{Nu_p \lambda_f}{d_p} \qquad (3\text{-}26)$$

and (Rowe et al. (1965)):

$$Nu_p = 2 + 0.6 Re_p^{0.5} Pr_f^{0.33} \qquad (3\text{-}27)$$

Further:

$$Re_p = \frac{\rho_f v_r d_p}{\eta_f} \qquad (3\text{-}28)$$

and:

$$Pr_f = \frac{\eta_f Cp_f}{\lambda_f} \qquad (3\text{-}29)$$

In table 3-6 the considered reaction mechanisms and convective properties are given as used by various authors.
Notes:

1) The non-steady temperature state of a burning char particle can be determined after section 4.3.2 for constant particle boundary conditions.
2) The effective temperature of the surrounding of a particle is, due to the non-isothermal gas-particle cloud somewhere in-between the gas, the particles and the wall temperature. For a transparent gas and low particle volume fraction the wall has to be taken for the surrounding temperature, whereas for high particle density the particle temperature, that for most cases is approximately equal to the gas temperature, can be taken as the surrounding temperature.

3.3.2 Modeling of CO-oxidation in the gas phase

From the literature review of section 3.2.5 one can conclude that the CO-oxidation in the freeboard has not been modeled satisfactorily. The slow progress in CO-oxidation cannot be predicted from the described global reaction mechanisms so far used, detailed reaction mechanisms or even detailed reaction mechanisms including radical recombination reactions alone. The axial dispersion coefficient is expected to give poor results, as it does not encompass all parameters.

To bridge these shortcomings we focuss our attention on the fluctuating and lateral distribution of the gas species concentrations at the fluidized bed surface and the decay of the mixing in the freeboard. These aspects have not been taken into account yet. To do so an approach is taken in which all these effects are 'lumped' on a single parameter.

With respect to the gas the freeboard is divided into two parallel gas flows. The nature of the gas flows is hypothesized as follows:

* A homogeneous CO-rich gas phase originating from the particle dense phase of the fluidized bed.
* A homogeneous oxygen-rich gas phase originating from the particle lean phase of the fluidized bed.

The gas phases interchange matter. The degree of mixing of CO in the oxygen rich phase is described by a simple cumulative mixing term:

$$\dot{n}_{mix,h} = A_{bed}\, v_s\, C_{CO,0}\, (1-e^{-a\, h_f}) \qquad (3\text{-}30)$$

At the fluidized bed surface the gas phases are assumed to be completely separated. Far above the fluidized bed surface the phases are well mixed.

$$\dot{n}_{mix,0} = 0$$

$$\dot{n}_{mix,\infty} = A_{bed}\, v_s\, C_{CO,0}$$

The time averaged transfer rate of CO to the oxygen rich phase in a slice of the freeboard with upper limit h_u and lower limit h_l, is then defined follows:

$$\dot{n}_{mix,h_u-h_l} = A_{bed}\, v_s\, C_{CO,0}\, (e^{-a\, h_l} - e^{-a\, h_u}) \qquad (3\text{-}31)$$

The CO-mixing term has to be seen as a model parameter. For use in the model, the value of the mixing parameter a is fitted from 'average' CO concentrations along the freeboard of the fluidized bed combustor 'MAGMA' (Martens (1984)). The fuels used for the experiments were Niederberg AG anthracite (F.R.G.) and a South-African bituminous coal. The trend of the spatially resolved CO concentration normalised to the maximum value at the fluidized bed surface is visualized in figure 3-5. The normalised CO concentration resulting from values of the mixing parameter a=1, 1.5 and 2 are visualized in the same figure. If the CO-oxidation rate were much larger than the mixing rate, then, choosing a proper value of a should lead to similar curves for both the model and the experiments. Although no perfect fit can be obtained a value of a=1.25 1/m upto 1.75 1/m might be considered reasonable for the present state of knowledge. Note that for the bituminous coal run considerable amounts of CH4 and H2 were present in the splash zone and for the anthracite run considerable amounts of char were elutriated. These circumstances may have affected the CO-combustion mechanism. In further research the mixing term defined here may be connected to the low frequency eddies induced by the bubbling or jetting phenomena at the fluidized bed surface. The turbulent intensity is:

* proportional to the bubble size at the fluidized bed surface (Horio et al. (1980)), Pemberton and Davidson (1983)),
* inversely proportional to freeboard height (Horio et al. (1980)), or decaying in an approximately exponential way (Pemberton and Davidson (1983)).

Therefore the parameter a is presumably related to the bubble diameter, the bubble frequency and the bed diameter.

In a simple model a global reaction mechanism is more appropriate than detailed reaction mechanisms. To predict the CO-oxidation after the mixing of the two gas phases we follow Hottel (1965):

$$CO + 0.5\ O2 \longrightarrow CO2 \qquad (j=5)$$

where:

$$r_{ch,CO} = 1.902E6\ C_{CO}^{1.0}\ C_{H2O}^{0.5}\ C_{O2}^{0.3}\ \exp\left(\frac{-804.7}{T_g}\right) \qquad (3\text{-}32)$$

For the calculations the freeboard is divided into a number of compartments. The reactions are assumed to occur in the full compartment volume. This is not consistent with the assumption of the two parallel gas flows, but can hardly be avoided as detailed knowledge about the gas flow is lacking. The effects of these inaccuracies are implicitly accomodated for in the value of the empirical mixing parameter.

3.3.3 The mass balance

3.3.3.1 Introduction

For analytical purpose the freeboard is divided into a number of perfectly stirred reactors in series with, in principle arbitrary diameter and height. The contents is well stirred and uniform throughout. The exit fluid stream has the same composition and temperature as the fluid within the reactor. The application covers:

* the mixed reactor (1 constant flow stirred tank reactor, CFSTR),
* the plug flow reactor (infinity CFSTR in series),
* the cascade of CFSTR reactors.

The mass and molar flow rate of the gas changes in the reactor as a consequence of the gas-gas and the gas-solid reactions:

* Gas-solid reactions lead to mass changes of the gas phase and the solid phase in both directions.
* Conversions lead to an increase or decrease of the number of molecules depending on the stochiometry of the reactions.

For the gas both effects are analytically covered by the molar balance and the known specific molar weights of the gas species. For the particles the change in mass is the more importent one as the particle motion is influenced by the change of drag force to gravity force rate. (See also section 2.3.) The following combustion mechanisms can be selected in the model:

* constant density and changing size (shrinking particle),
* changing density and constant size (shrinking density),
* both changing density and size.

More details are presented in section 3.3.3.3.

3.3.3.2 The molar balance of the gas phase

3.3.3.2.1 The general balance of the gas phase

In this work the following gas species (index i) are considered:

	Ar	CO	CO2	H2O	N2	NO	O2	SO2
i=	1	2	3	4	5	6	7	8

The global reactions (index j) that may occur are (see section 3.3.1):

Φ_p C + O2 ——> $(2\Phi_p - 2)$ CO + $(2 - \Phi_p)$ CO2 (j=1)

C + CO2 ——> 2 CO (j=2)

1/2 C + NO ——> 1/2 CO2 + 1/2 N2 (j=3)

CaO + SO2 + 1/2 O2 ——> CaSO4 (j=4)

CO + 1/2 O2 ——> CO2 (j=5)

Reaction 5 is a gas-gas reaction (see section 3.3.2), the other ones are gas solid reactions. The molar balance of any species i concerns the molar

flow rate of the gas via the reactor boundaries and any conversion j within the reactor (see figure 3-6):

$$\dot{n}_{i,g}(n-1) + \dot{n}_{i,5}(n) + \sum_{p=1}^{p=np} \sum_{j=1}^{j=4} \dot{n}_{i,j,p}(n) = \dot{n}_{i,g}(n) \qquad (3\text{-}33)$$

3.3.3.2.2 Reactor conversion rate and the stochiometry of the reaction

An analytic solution of the molar flow rates can easily and straightforward been found when we arrive at a set of simultaneous linear equations. Therefore the molar flow rates are transformed into linear expressions of molar concentrations and pseudo proportional factors. The factors themselves are weak functions of the molar concentrations, the temperatures and the particle trajectories. The proportionality factors are based first on previously set conditions and altered subsequently with calculation results until convergence.

The steady-state molar consumption rate of species i by reaction j for each particle that traverses the boundaries of the reactor n per unit of time reads:

$$\dot{n}_{i,j,p}(n) = 1\ r_{i,j}(n)\ t_p(n) \qquad (3\text{-}34)$$

where t_p is the residence time of the particle. For analytical purposes (3-34) is transformed with use of equation (3-19) into:

$$\dot{n}_{i,j,p}(n) = a_{i,j,p}(n)\ C_i(n) \qquad (3\text{-}35)$$

where the pseudo-proportionality factor:

$$a_{i,j,p}(n) = \frac{-1\ t_p(n)}{\frac{1}{k_{d,i,p}\ A_p} + \frac{1}{k_{i,j,p}\ A_p}} \qquad (3\text{-}36)$$

Now each of the gas-solid reactions j=1 until 4 is discussed. The O2 conversion for each char particle traversing the reactor boundary per unit of time is expressed by (3-36) where i=O2 , j=1 and:

$$k_{d,O2,p}(n)\ A_p(n) = \pi\ d_p(n)\ Sh_p(n)\ \mathbb{D}_{O2\text{-}N2}(n) \qquad (3\text{-}37)$$

$$k_{O2,1,p} = \pi\ d_p^2(n)\ \frac{596}{\Phi_p(n)}\ T_p(n)\ \exp\left(\frac{-17967}{T_p(n)}\right) \qquad (3\text{-}38)$$

The stochiometry of the reaction leads to:

$$\dot{n}_{CO,1,p}(n) = -\ (2\Phi_p(n) - 2)\ a_{O2,1,p}\ C_{O2}(n) \qquad (3\text{-}39)$$

and:

$$\dot{n}_{CO2,1,p}(n) = -\ (2 - \Phi_p(n))\ a_{O2,1,p}\ C_{O2}(n) \qquad (3\text{-}40)$$

The CO2 conversion for each char particle traversing the boundary of reactor n per unit of time is expressed by (3-36) where i=CO2 , j=2 and:

$$k_{d,CO2,p}(n)\ A_p(n) = \pi\ d_p(n)\ Sh_p(n)\ \mathbb{D}_{CO2-N2}(n) \qquad (3\text{-}41)$$

$$k_{CO2,2,p}(n) = \pi\ d_p^2(n)\ 4.1E6\ \exp\left(\frac{-29787}{T_p(n)}\right) \qquad (3\text{-}42)$$

The stochiometry of the reaction leads to:

$$\dot{n}_{CO,2,p}(n) = -\ 2\ a_{CO2,2,p}(n)\ C_{CO2}(n) \qquad (3\text{-}43)$$

The NO conversion for each char particle traversing the boundary of reactor n per unit of time is expressed by equation(3-36) where i=NO , j=3 and:

$$k_{d,NO,p}(n)\ A_p(n) = \pi\ d_p(n)\ Sh_p(n)\ \mathbb{D}_{NO-N2}(n) \qquad (3\text{-}44)$$

$$k_{NO,3,p}(n) = \pi\ d_p^2(n)\ 1.3E5\ \exp\left(\frac{-17111}{T_p(n)}\right) \qquad (3\text{-}45)$$

The stochiometry of the reaction leads to:

$$\dot{n}_{CO2,3,p}(n) = -\ 1/2\ a_{NO,3,p}\ C_{NO}(n) \qquad (3\text{-}46)$$

$$\dot{n}_{N2,3,p}(n) = -\ 1/2\ a_{NO,3,p}\ C_{NO}(n) \qquad (3\text{-}47)$$

The SO2 conversion from each char particle traversing per unit time the reactor boundary is expressed by equation(3-36) where i=SO2 , j=4 and:

$$k_{d,SO2,p}(n)\ A_p(n) = \pi\ d_p(n)\ Sh_p(n)\ \mathbb{D}_{SO2-N2}(n) \qquad (3\text{-}48)$$

$$k_{SO2,4,p} = \frac{\pi}{6}\ d_p^3(n)\ 4900\ \exp\left(\frac{-8807}{T_p(n)}\right)\ f(d_p(n),\text{conversion}) \qquad (3\text{-}49)$$

The stochiometry of the reaction leads to:

$$\dot{n}_{O2,4,p}(n) = 1/2\ a_{SO2,4,p}\ C_{SO2}(n) \qquad (3\text{-}50)$$

The steady state molar conversion rate of gas-gas reaction j=5 referring to species i=CO is expressed as:

$$\dot{n}_{CO,5}(n) = a_{CO,5}(n)\ C_{CO}(n) + \dot{n}_{CO,mix}(n) \qquad (3\text{-}51)$$

where:

$$a_{CO,5}(n) = -\ A_f(n)\ (h_f(n) - h_f(n-1))\ k_{CO,5}(n) \qquad (3\text{-}52)$$

and:

$$k_{CO,5}(n) = 1.902E6\ C_{H2O}^{0.5}(n)\ C_{O2}^{0.3}(n)\ \exp\left(\frac{-\ 804.7}{T_g(n)}\right) \qquad (3\text{-}53)$$

and:

$$\dot{n}_{CO,mix}(n) = A_{bed}\, v_s\, C_{CO,0}\, (e^{-a\, h_f(n-1)} - e^{-a\, h_f(n)}) \qquad (3\text{-}54)$$

The stochiometry of the reaction leads to:

$$\dot{n}_{O2,5}(n) = 1/2\; a_{CO,5}\; C_{CO}(n) \qquad (3\text{-}55)$$

and:

$$\dot{n}_{CO2,5}(n) = -\; a_{CO,5}(n)\; C_{CO}(n) \qquad (3\text{-}56)$$

The molar flow rate of each gas species i (i=1 through 8) at the boundary of the reactor is expressed as:

$$\dot{n}_{i,g}(n-1) = a_g(n-1)\; C_i(n-1) \qquad (3\text{-}57)$$

$$\dot{n}_{i,g}(n) = a_g(n)\; C_i(n) \qquad (3\text{-}58)$$

where:

$$a_g(n-1) = A_f(n-1)\; v_g(n-1) \qquad (3\text{-}59)$$

and:

$$a_g(n) = A_f(n)\; v_g(n) \qquad (3\text{-}60)$$

3.3.3.2.3 The balance in linear expressions of the molar concentrations

For the proportionality factors developed in section 3.3.3.2.2. and molar concentrations equation (3-33) the molar balance can be expressed as follows:

for gas species Ar:

$$a_g(n-1)\; C_{Ar}(n-1) - a_g(n)\; C_{Ar}(n) = 0 \qquad (3\text{-}61)$$

for gas species CO:

$$a_g(n-1)\; C_{CO}(n-1) + (a_{CO,5}(n) - a_g(n))\; C_{CO}(n)$$

$$+ \sum_{p=1}^{p=np} 2\; a_{CO2,2,p}(n)\; C_{CO2}(n)$$

$$+ \sum_{p=1}^{p=np} (2\Phi_p(n) - 2)\; a_{O2,1,p}(n)\; C_{O2}(n) = 0 \qquad (3\text{-}62)$$

for gas species CO2:

$$a_g(n-1)\, C_{CO2}(n-1) + \left(\sum_{p=1}^{p=np} a_{CO2,2,p}(n) - a_g(n) \right) C_{CO2}(n)$$

$$+ \sum_{p=1}^{p=np} 1/2\, a_{NO,3,p}(n)\, C_{NO}(n)$$

$$+ \sum_{p=1}^{p=np} (2 - \Phi_p(n))\, a_{O2,1,p}(n)\, C_{O2}(n) = 0 \qquad (3\text{-}63)$$

for gas species H2O:

$$a_g(n-1)\, C_{H2O}(n-1) - a_g(n)\, C_{Ar}(n) = 0 \qquad (3\text{-}64)$$

for gas species N2:

$$a_g(n-1)\, C_{N2}(n-1) - a_g(n)\, C_{N2}(n)$$

$$+ \sum_{p=1}^{p=np} 1/2\, a_{NO,3,p}(n)\, C_{NO}(n) = 0 \qquad (3\text{-}65)$$

for gas species NO:

$$a_g(n-1)\, C_{NO}(n-1) + \left(\sum_{p=1}^{p=np} - a_{NO,3,p}(n) - a_g(n) \right) C_{NO}(n) = 0 \qquad (3\text{-}66)$$

for O2:

$$a_g(n-1)\, C_{O2}(n-1) + 1/2\, a_{CO,5}(n)\, C_{CO}(n)$$

$$+ \left(\sum_{p=1}^{p=np} - a_{O2,1,p}(n) - a_g(n) \right) C_{O2}(n)$$

$$+ \sum_{p=1}^{p=np} 1/2\, a_{SO2,4,p}(n)\, C_{SO2}(n) = 0 \qquad (3\text{-}67)$$

for gas species SO2:

$$a_g(n-1)\, C_{SO2}(n-1) + \left(\sum_{p=1}^{p=np} a_{SO2,4,p}(n) - a_g(n) \right) C_{SO2}(n) = 0 \qquad (3\text{-}68)$$

The boundary condition for the gas species i entering the freeboard read:

$$a_g(0)\ C_i(0) = a_g(bed)\ C_i(bed) \qquad (3\text{-}69)$$

For N reactors in series the i(N+1) molar concentrations have to be solved:

$$\begin{array}{ccccccc} C_1(0), & C_1(1), & C_1(2), & \ldots\ldots\ldots\ldots\ldots, & C_1(N) \\ \vdots & \vdots & \vdots & \vdots & \vdots & \vdots \\ C_i(0), & C_i(1), & C_i(2), & \ldots\ldots\ldots\ldots\ldots, & C_i(N) \end{array}$$

The number of equations is i(N+1):
N (reactors) for each gas species i,
1 boundary condition of each gas species i at the bed level.
This system of simultaneous linear equations can be solved by Gauss elimination as the number of unknowns equals the number of independent equations.

3.3.3.3 The material balance of the particles

During char combustion carbon burns off and the inert material of the particle (ash) remains. The total mass of the particle consists of the mass of char and ash. For the boundary conditions of the particle in reactor n we define (see figure 3-7).

$$m_p(m-1) = m_{p,char}(m-1) + m_{p,ash} \qquad (3\text{-}70)$$

and:

$$m_p(m) = m_{p,char}(m) + m_{p,ash} \qquad (3\text{-}71)$$

The particles' mass is defined as:

$$m_{p,ash} = \rho_{p,ash}\ V_{p,ash} \qquad (3\text{-}72)$$

$$m_{p,char}(m-1) = \rho_{p,char}(m-1)\ V_{p,char}(m-1) \qquad (3\text{-}73)$$

$$m_{p,char}(m) = \rho_{p,char}(m)\ V_{p,char}(m) \qquad (3\text{-}74)$$

The total volume of the particle is given by:

$$V_p(m-1) = V_{p,char}(m-1) + V_{p,ash} \qquad (3\text{-}75)$$

$$V_p(m) = V_{p,char}(m) + V_{p,ash} \qquad (3\text{-}76)$$

The char mass consumption of the particle in reactor n reads:

$$\Delta m_p(n) = m_p(m-1) - m_p(m) = m_{p,char}(m-1) - m_{p,char}(m) \qquad (3\text{-}77)$$

where:

$$\Delta m_{p,char}(n) = t_c(n)\, M_c \qquad (3\text{-}78)$$

$$\left(\frac{1}{\Phi(n)}\, r_{O2,1,p}(n) + r_{CO2,2,p}(n) + 1/2\, r_{CO,3,p}(n)\right)$$

The maximal volume reduction is obtained for constant char density:

$$\Delta V_{max,p,char}(n) = \frac{\Delta m_{p,char}(n)}{\rho_{p,char}(m-1)} \qquad (3\text{-}79)$$

Actually the combustion of char leads to an unknown combination of density and volume reduction. To meet this uncertainty mathematically we define the shrinking factor Φ_{sh};

$$\Phi_{sh}(n) = \frac{\Delta V_p(n)}{\Delta V_{p,max}(n)} \qquad (3\text{-}80)$$

The limits are:

$\Phi_{sh} = 1$ ———> shrinking core

$\Phi_{sh} = 0$ ———> shrinking density

From equations (3-77) through (3-80) follows the char density of the particle leaving reactor n:

$$\rho_{p,char}(m) = \frac{\rho_{p,char}(m-1)\, m_{p,char}(m-1)}{-\Delta m_p(n)\, \Phi_{sh} + m_{p,char}(m-1)} \qquad (3\text{-}81)$$

The mass and density of the limestone or dolomite particles is assumed to be constant throughout the freeboard.

3.4 Model predictions and verification

In this section model predictions concerning mass transfer and chemical reactions are compared with the experiment of firing anthracite in the 'MAGMA' (Martens (1984)). The experimental result concerning the 'average' gas species concentrations as a function of freeboard height is given in figure 3-8. The model results concerning the particle behaviour, volume fraction and entrainment correspond with the results outlined later in section 2.4. The temperature distribution in the freeboard obtained from the experiment as well as from the model is discussed in section 4.4. In addition to table 2-3 further freeboard boundary conditions are listed in table 3-7.

Results on average CO, O2 and NO concentrations from both the model calculations and the experiment are visualized in figures 3-9a, b and c. In the figures the markers of the model results are positioned at the half-width of the stirred reactors in series. The model result on CO-concentration shows CO to be negligible in the active (mixed) phase and the confined (un-mixed) phase to dominate. This indicates the CO originating from the confined phase and the CO originating from the char reactions to react fast

with oxygen. The similarity in the profiles of the model and the experiment, as well as the deviations along the freeboard should not be surprising as the mixing parameter is merely a fitted model parameter. The qualitative agreement in the O2 profiles of the model compared to the experiment is satisfactory, but the absolute difference between them is too high. The over-estimation of the CO-oxidation in the model automatically goes with the larger oxygen consumption. Possible causes for the differences are:

1) a lower 'true' overall (anthracite-) char reactivity compared to the model input,
2) a higher effective (anthracite-) char density compared to the model input, resulting in smaller effective char surface area (for constant char mass),
3) the smaller amount of char particles elutriated according to the experiment, as compared to the model (by a factor of 10; see section 2.4).

These possible causes indicate on which topics further research is required.

The absolute NO reduction along the freeboard is well predicted although in the splash and the dense disengaging zone the reduction is somewhat overpredicted, and slightly underpredicted higher-up.

The cumulative oxygen and NO conversion as a function of char-particle size is illustrated in figure 3-10. It is found that the smaller particles contribute considerably because of their large surface area per unit mass and further because of their lower resistance to diffusion. The Boudoir-reaction ($C + CO_2 \longrightarrow 2\ CO$) is found to be of no-importance, because of the low reaction rate (too low temperature). For the conditions investigated globally it can be stated that the residence time of the single char particle during its trajectory in the freeboard is too short to obtain complete burnout before elutriation.

3.5 Conclusions and recommendations

The method of book-keeping the char particles' residence time in each compartment has been combined with heterogeneous reactions: char-O2, char-CO2 and char-NO and an homogeneous overall reaction CO-O2. The reaction rate constants used in the model were deduced from literature. They may suffer from large deviations because of the type of coal used and the relatively low temperatures for which the correlations are employed.

It has been demonstrated that the OH-radical recombination reaction, as modeled by Chaung (1982), alone is not responsible for the observed slow progress in freeboard CO-oxidation. Therefore it is suggested that CO-mixing is the rate determining step, and as a first approximation has been modeled as such.

In spite of some uncertain input values and the uncertainties of the experimental result (lateral distribution of particle fluxes and gas species concentrations) the model has been found to qualitatively predict the chemical phenomena in the freeboard satisfactorily. To achieve quantitative predictions further research is required amongst others on:

* details of the gas flow near the bed surface,
* lateral distribution effects of particles and gas species, and
* detailed chemical reaction mechanisms in the gas phase.

3.6 List of symbols

A	constant	-
	frequency factor	$mol^{1-x}.m^{3x-3}.s^{-1}$.
	surface area	m2
a	mixing parameter	1/m
	coefficient	m3/s
B	constant	K
b	constant	-
C	molar concentration	mol/m3
Cp	specific heat at constant pressure	J/(kg.K)
D	diameter	m
d	diameter	m
E	activation energy of reaction	J/mol
H^0	heat of reaction	J/mol
h	height	m
k	reaction rate	m/s
	reaction rate	1/s
k_0	frequency factor	$m/(s.k^n)$
M	molecular weight	kg/mol
m	mass	kg
	position of particle at reactor boundary	-
Nu	Nusselt number	-
n	power	-
	reactor number or boundary of reactor	-
$\dot{n}$	molar flow rate	mol/s
	molar flow rate	mol/(s.particle)
Pe	Peclet number	-
Pr	Prandtl number	-
p	CO/CO2 ratio	-
$\dot{Q}$	heat flux	J/s
R	universal gas constant	J/(mol.K)
Re	Reynolds number	-
r	reaction rate	mol/(s.particle)
	reaction rate	mol/(s.m3)
Sc	Schmidt number	-
Sh	Sherwood number	-
T	temperature	K
t	time	s
V	volume	m3
v	velocity	m/s

GREEK SYMBOLS

$\mathbb{D}$	diffusion coefficient	m2/s
	dispersion coefficient	m2/s
ε	emissivity	-
Φ	mechanism factor for char combustion	-
	mechanism factor for shrinking	-
η	viscosity	kg/(m.s)
λ	thermal conductivity	W/(m.K)
π	3.1415926535	-
ρ	density	kg/m3
σ	Stefan Boltzmann constant	W/(m2.K4)

SUBSCRIPTS

bed fluidized bed
c carbon
cp combustion of particle
cpg convection from particle to gas
ch chemical reaction
d diffusion
e effective
f mean physical properties in gas film
freeboard
g gas
h height
i gas species i
summation index
j reaction j
summation index
mix mixing
np total number of particles involved
p particle
rps radiation from particle to surroundings
s surrounding
superficial
sh shrinking
0 initial or reference
∞ infinity

3.7 References

Arthur, J.A.
Reactions between carbons and oxygen.
Trans. Faraday Soc. 47, pp. 164/178 (1957).

Borgwardt, R.H.
Kinetics of the reaction of SO2 with calcined limestone.
Environ. Sci. Tech., 4, pp. 59 (1970).

Beer, J.M., Sarofim, A.F., Sharma, P.K., Chaung, T.Z., Sandhu, S.S.
Fluidized coal combustion: the effect of sorbent and coal feed particle size upon the combustion efficiency and NOx emission.
Fluidization, Grace and Matsen, (eds.), pp. 185/194.
Plenum Press, New York (1980).

Caram, H.S. and Amundson, N.R.
Diffusion and reaction in a stagnant boundary layer about a carbon particle. Ind. Eng. Chem. Fundamentals 16, pp. 171/181 (1977).

Chan, L.K.
Kinetics of nitric oxide - carbon reactions under fluidized bed combustor conditions.
Dissertation. Massachusetts Institute of Technology.
Cambridge, MA., USA (1980).

Chan, L.K., Sarofim, A.F., Beer,J.M.
Kinetics of the NO-carbon reaction at fluidized bed combustor conditions.
Combustion and Flame, Vol. 52, No. 1, pp. 37/46, The Journal of the Combustion Institute (1983).

Chaung, T.Z.
Particle entrainment and chemical reactions in the freeboard of a fluidized bed coal combustor.
Dissertation. Massachusetts Institute of Technology.
Massachusetts, MA., USA (1982).

Chirone, R. and Paullilo, D.
Fragmentation of particles of various coals in high temperature fluidized bed combustor.
Presentation of Annual Congress of the Combustion Institute, Italian Section. Anacapri, Italy (1981).
Chirone, R., Cammarota, A., D'Amore, M., Massimilla, L.
Fragmentation and attrition in the fluidized combustion of a coal.
Proc. of the 7th Int. Conf. on Fluidized Bed Combustion. pp. 1023/1030.
National Technical Information Service , US Department of Commerce. Springfield, VA., USA (1983).
Dryer, F.L., Glassman, I.
High-temperature oxidation of CO and CH4.
14th Symposium (Intnl.) on Combustion, The Combustion Institute, pp. 987/1003 (1974).
Duxbury, J., Pratt, N.H.
A shock tube study of NO kinetics in the presence of H2 and fuel-N.
15th Int. Symp. on Combustion, pp. 843/855.
The Combustion Institute, Pittsburg, PA. (1975).
Edwards, H.W.
Interaction of nitric oxide with graphite.
AIChE Symposium series No. 126, Vol.68. AIChE Symposium Series, Vol. 68, No. 126, pp. 91 (1972).
Field, M.A., Gill, D.W., Morgan, B.B., Hawksley, P.G.W.
Combustion of pulverised coal.
BCURA, Leatherhead, UK (1967).
Furusawa, T., Kunii, D., Tsujimura, M., Tsunoda, M.
Calcined lime and in situ formed char as catalysts for "NO" reducing gases.
Proc. of the 7th Int. Conf. on Fluidized Bed Combustion, pp. 525/533.
National Technical Information Service , US Department of Commerce. Springfield, VA., USA (1983).
Gibbs, B.M., Pereira, F.J., Beer, J.M.
Coal combustion and NO formation in an experimental fluidised bed
Institute of Fuel, Symposium Series, no. 1, Fluidised combustion. London, UK (1975).
Havenaar, P.
Theoretisch en experimenteel stromingsonderzoek in het vrijboord van een AFBC.
Rapport EV-1248, Laboratory for Thermal Power Engineering.
Delft University of Technology. Delft, The Netherlands (1982).
Horio, M., Mori, S., Muchi,I.
A model study for the development of low NOx fluidized bed coal combustors.
Proc. of the 5th Int. Conf. on Fluidized Bed Combustion, pp. 605/623. Washington, DC., USA (1977).
Horio, M., Liu, J., Muchi, I.
Particle behavior in the fluidized bed grid zone, bubbling zone and freeboard.
in: Fluidization, Science and Technology, pp 112/123.
edited by: Kwauk, M. and Kunii, D.
Gordon and Breach, Science Publishers, New York (1982).
Hottel. H.C., Williams, G.C., Nerheim, N.M., Schneider, G.R.
Combustion of carbon monoxide and propane.
10th Symp. (Intnl.) on Combustion, The Combustion Institute, pp. 111/121 (1965).

Howard, J.B., Williams, G.C., Fine, D.H.
Kinetic of carbon monoxide oxidation in postflame gases.
14th Symp. (Intnl.) on Combustion, The Combustion Institute, pp. 975/986 (1973).

Kozlov, G.I.
On high-temperature oxidation of methane.
7th Symposium (Intnl.) on Combustion, The combustion Institute, pp. 142/149 (1959)

Laurendeau, N.M.
Heterogeneous kinetics of coal char gasification and combustion.
Prog. Energy Combust. Sci., Vol. 4., pp. 221/270.
Pergamon Press, UK (1978).

Lavrov, N.V.
Nank Uzb SSR, 25, 9 (1968).

Louis, J.F., Tung, S.E.
Modeling of fluidized-bed combustion of coal.
Quarterly technical progress report, August 1, 1977 - October 31, 1977.
Massachusetts Institute of Technology. Cambridge, MA., USA (1977).

Lyon, R.K., Hardy, J.E.
Paper presented in the 73rd AIChE Annual Meeting.
Chicago, USA (1980).

Martens, F.J.A.
Fluide bed verbranding: Vrijboord.
Lecture notes 'College Steenkooltechnologie M18'. Rapport EV-1358.
Delft University of Technology. Delft, The Netherlands (1981).

Martens, F.J.A., Op den Brouw, H., Van Koppen, C.W.J.
The behaviour of the freeboard region of a fluidized bed coal combustor.
Proc. of the 7th Int. Conf. on Fluidized Bed Combustion, pp. 1054/1063.
National Technical Information Service , US Department of Commerce.
Springfield, VA., USA (1983).

Martens, F.J.A., Van Koppen, C.W.J.
Experimental study of the freeboard region in a fluidized bed coal combustor.
Verbrennung und Feuerungen, 11. Deutscher Flammentag.
VDI-Bericht Nr. 498, pp. 101/106. VDI-Verlag, Duesseldorf, BRD (1983).

Martens, F.J.A.
Experiments with the atmospheric fluidized bed combustor 'MAGMA'.
Rapport EV-1333, Laboratory for Thermal Power Engineering.
Delft University of Technology, Delft, The Netherlands (1984).

Myerson, A.L.
The reduction of nitric oxide in simulated combustion effluents by hydrocarbon-oxygen mixtures.
15th Int. Symp. on Combustion, pp. 1085/1092.
The Combustion Institute. Pittsburg, PA., USA (1975).

Oguma, A.N., Yamada, N., Furusawa, T., Kunii, D.
Reduction Reaction rate of char with NO.
Preprint for 11th Fall Meeting of Soc. of Chem. Eng., pp. 121.
Japan (1971).

Paauw, Th.T.A., Heidweiler, D.J., Van Koppen, C.W.J.
Die bildung von Stickstofoxiden bei industriellen Erdgasverbrennungsprozessen.
Verbrennung und Feurungen, 9. Deutscher Flammentag.
VDI-Bericht 346, pp. 55/66. VDI-Verlag, Duesseldorf (1979).

Pemberton, S.T., Davidson, J.F.
Elutiation of fine particles from bubbling fluidized beds.
Proc. 4th Int. Conf. on Fluidization. pp. 275/282.
Eds. Kunii, D. and Toei, R., Publications Department AIChE, New York (1983).

Pillai, K.K.
The influence of coal type on devolatilization and combustion in fluidized beds.
Journal of the Institude of Energy, pp. 142/150, (September 1981).

Pratt, D.T.
PSR - A computer program for calculation of steady flow, homogeneous combustion reaction kinetics.
Bulletin 336, Washington State University.
Engeneering Extension Service Pullman, Washington DC (1974).

Rajan, R.R. and Wen, C.Y.
A comprehensive model for fluidized bed coal combustors.
AIChE Journal, Vol. 26, No. 4, pp. 642/655 (1980).

Rajan, R.R.
Simulation of fluidized bed coal combustors.
Dissertation. West Virginea University. Morgantown, W-VA., USA (1978).

Rowe, P.N. , Claxton, K.T., Lewis, J.B.
Heat and mass transfer from a single sphere in an extensive flowing fluid.
Trans. Instn. Chem. Engrs., Vol. 43, pp. T14/31, (1965).

Smith, I.W.
Kinetics of combustion of size-graded pulverized fuels in the temperature range 1200-2270 K.
Combustion and flame 17, pp 303/314 (1971)

Soete, De G.G., Giorgetti, Ch., Queraud, A.
Mechanisms of nitric oxide reduction on solid particles (comparative study on coal and char particles).
Techniques d'Application Energetiques, Laboratoire d'Aerothermique Fondamentale, Rueil Malmaison, France (1980).

Song, Y.H.
Fate of fuel nitrogen during pulverized coal combustion.
Sc.D. Thesis. Massachusetts Institute of Technology.
Cambridge, MA., USA (1978).

Thurgood, J.R. and Smooth L.D.
Volatiles combustion.
in: Pulverised-Coal Combustion and Gasification
Smooth, L.D. and Pratt, D.T. (eds.), pp. 169/182.
Plenum Press, New York (1979).

Wen, C.Y. and Dutta, S.
Rate of coal pyrolyses and gasification reactions.
in: Coal conversion technology.
Wen, C.Y. and Lee (eds.),
Addison-Wesley Publishing Co (1978).

Wen, C.Y., Fan, L.T.
Model for flow systems and chemical reactors.
Dekker, New York (1975).

Wells, J.W., Culver, M.H., Krishnan,R.P.
Tennesee Valey Authority atmospheric fluidized bed combustor simulation interim annual report 1980.
Oak Ridge National Laboratory. Oak Ridge, Tennesee, USA (1981).

Williams, G.C., Hottel, H.C., Morgan, A.C.
The combustion of methane in a jet-mixed reactor.
12th Symp. (Intnl.) on Combustion, The Combustion Institute, pp. 913/925 (1969).
Yamazaki, S., Hiratsuka, M., Fujitani, Y.
Study of high temperature gas reaction of NO-CH_4 (-CO) mixtures by means of molecular beam sampling-mass filter system.
Combustion Science and Technology, Vol. 20., pp. 25/32 (1979).

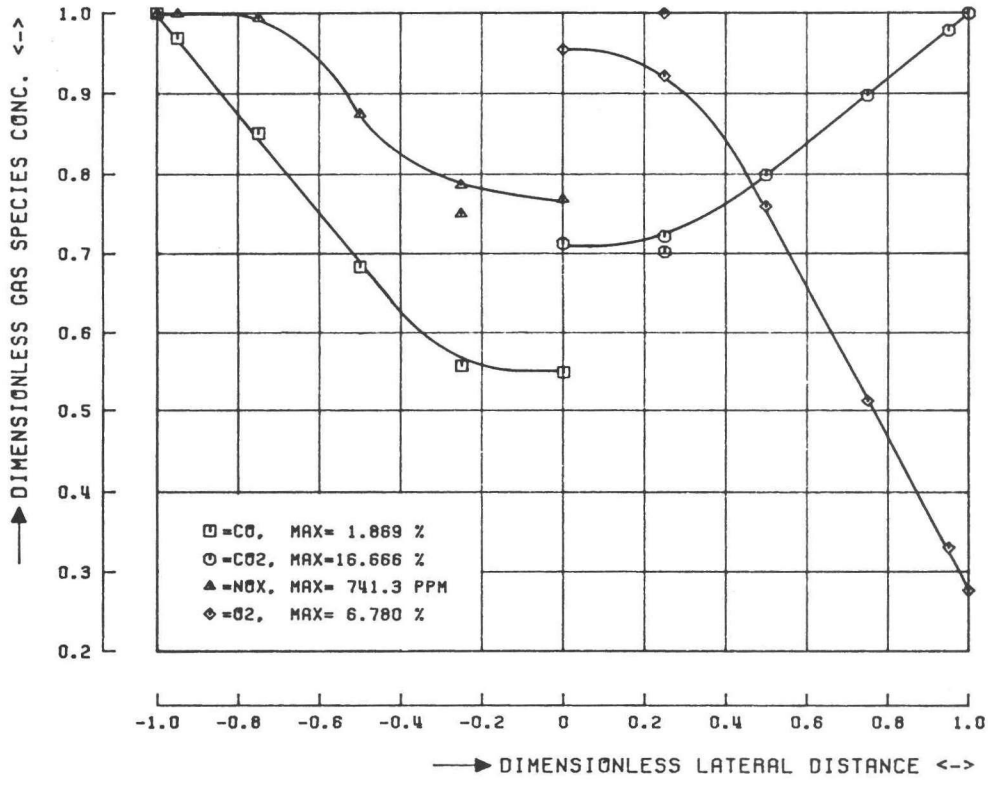

Figure 3-1.
Typical lateral distribution of the time averaged gas species composition. (fuel: South-African bituminous coal, v_s=1 m/s, v_{mf}=0.16 m/s)

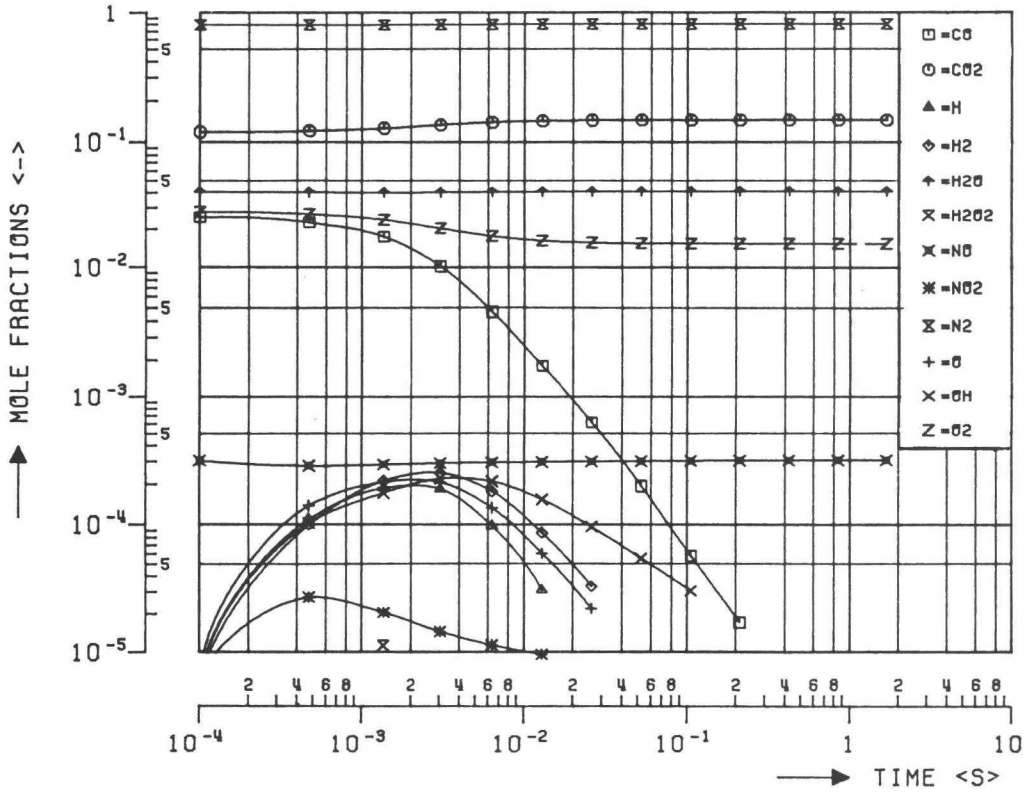

Figure 3-2a.
Example of time resolved CO-oxidation. Prediction from detailed reaction mechanism model for adiabatic conditions (from Martens (1981)). Course of temperature at 1.E5 Pa and 1073 K, initially.

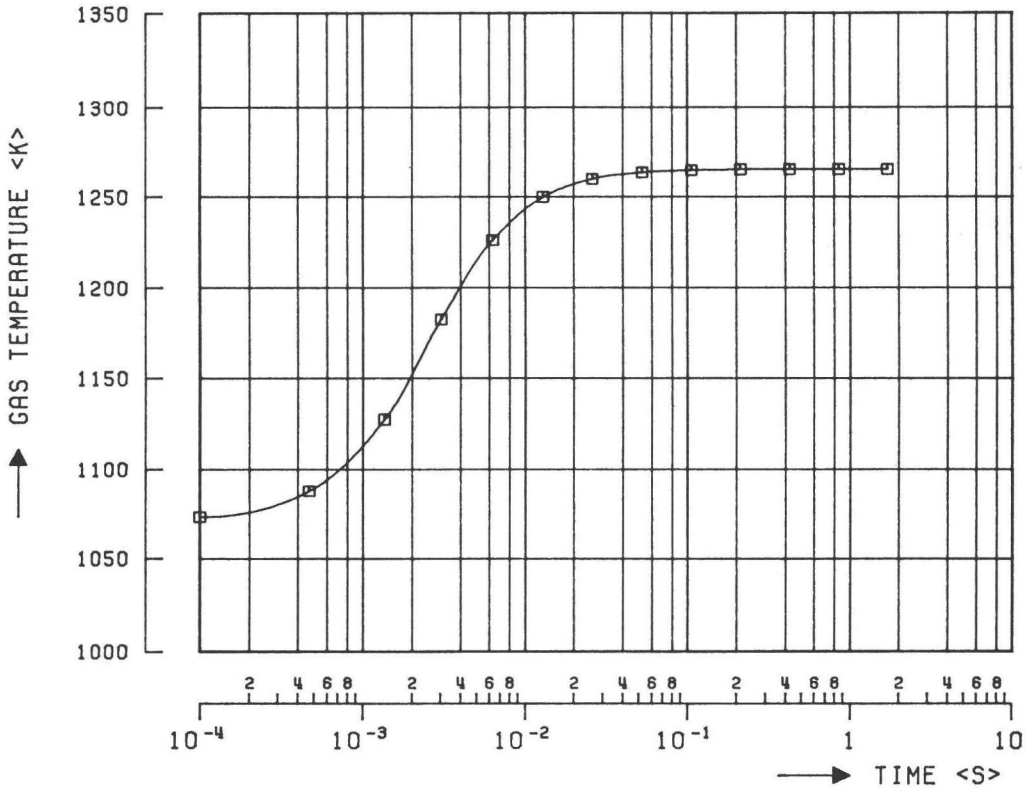

Figure 3-2b.
Example of time resolved CO-oxidation. Prediction from detailed reaction mechanism model for adiabatic conditions (from Martens (1981)). Molar gas fractions at 1.E5 Pa and 1073 K, initially.

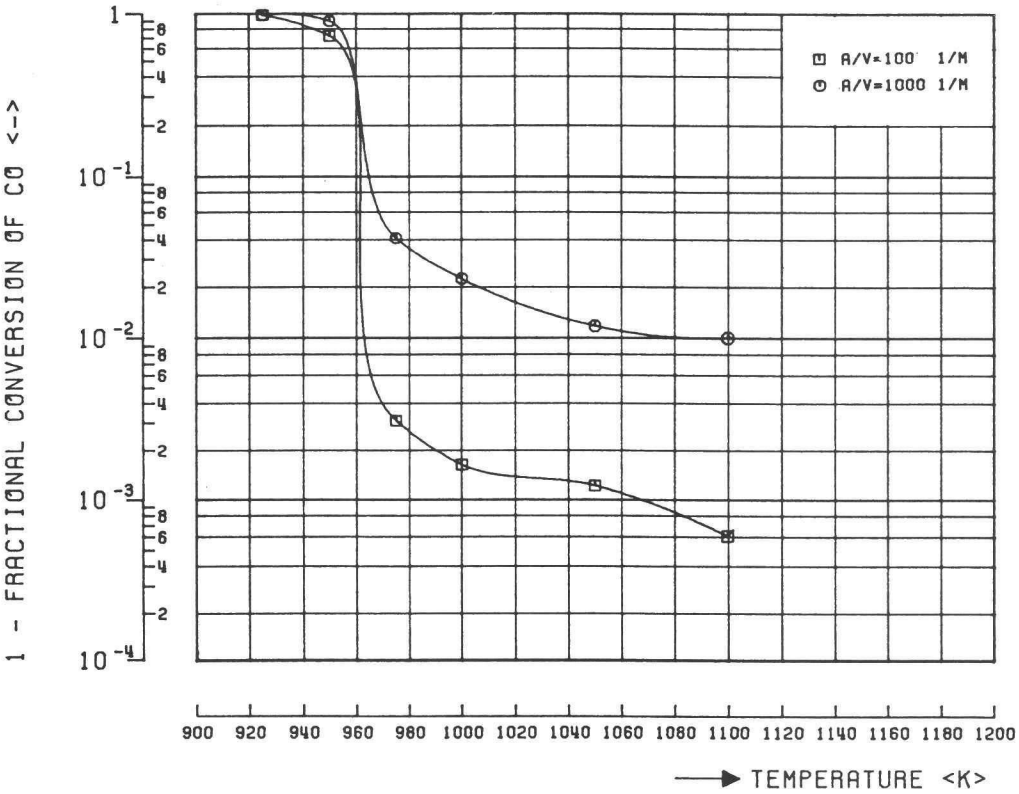

Figure 3-3.
Effect of the presence of solid particles on CO-oxidation (elaborated from Chaung (1982)).

pressure	1.01E5 Pa
mean particle size	1.E-3 m
isothermal condition	
gas residence time	3.6 s
A/V	100 and 1000
C O2,initial	0.06
C CO,initial	0.03
C CO2,initial	0.12
C H2O,initial	0.06

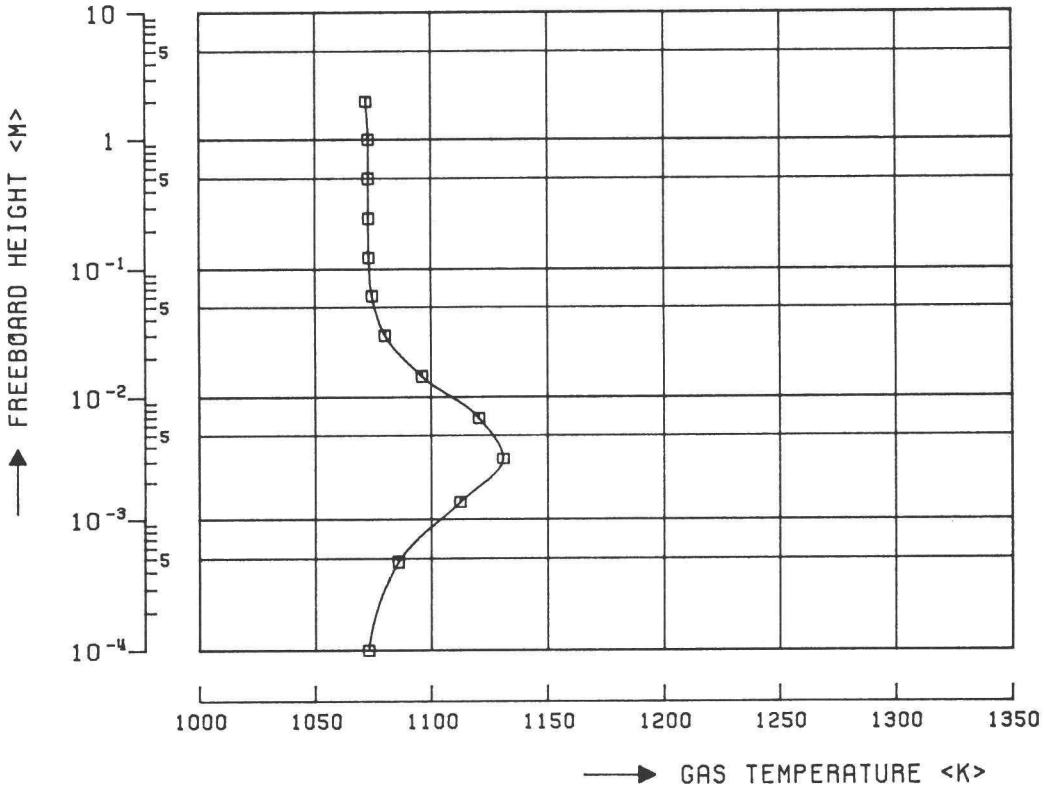

Figure 3-4a.
Example of CO-oxidation along the freeboard. Adiabatic plug-flow reactor, including effect of particle-gas heat transfer (from Martens (1981)). Course of temperature at 1.E5 Pa and 1073 K, initially.

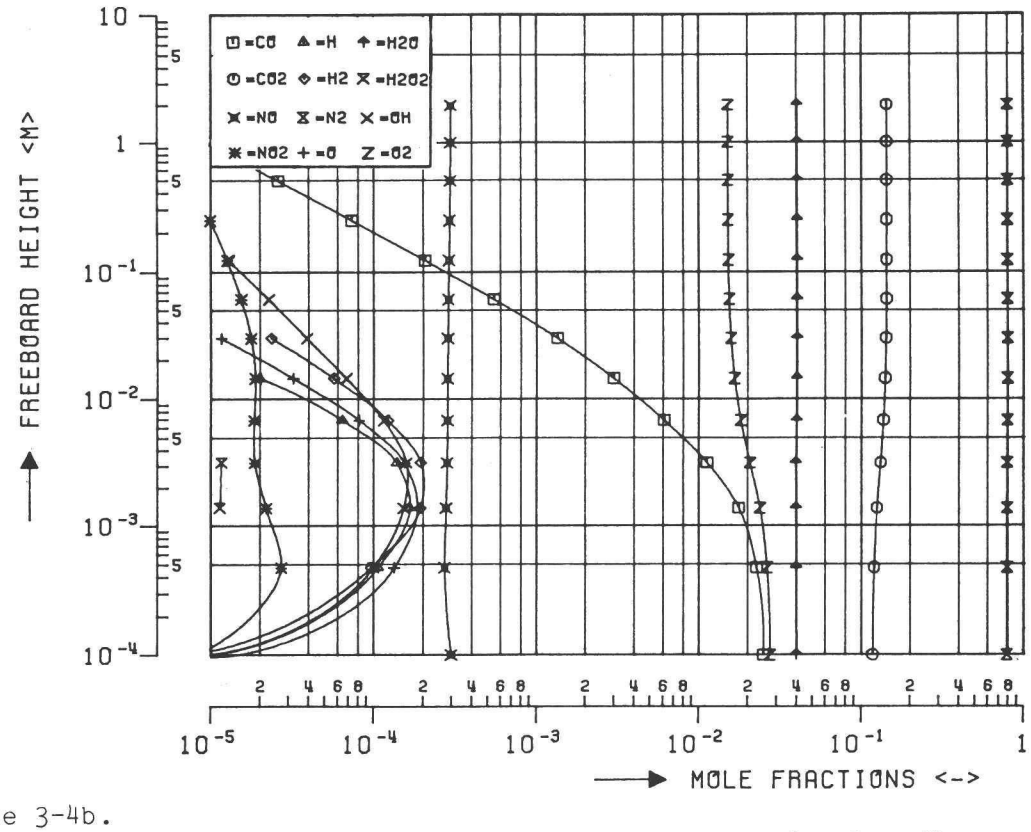

Figure 3-4b.
Example of CO-oxidation along the freeboard. Adiabatic plug-flow reactor, including effect of particle-gas heat transfer (from Martens (1981)). Molar gas fractions at 1.E5 Pa and 1073 K, initially.

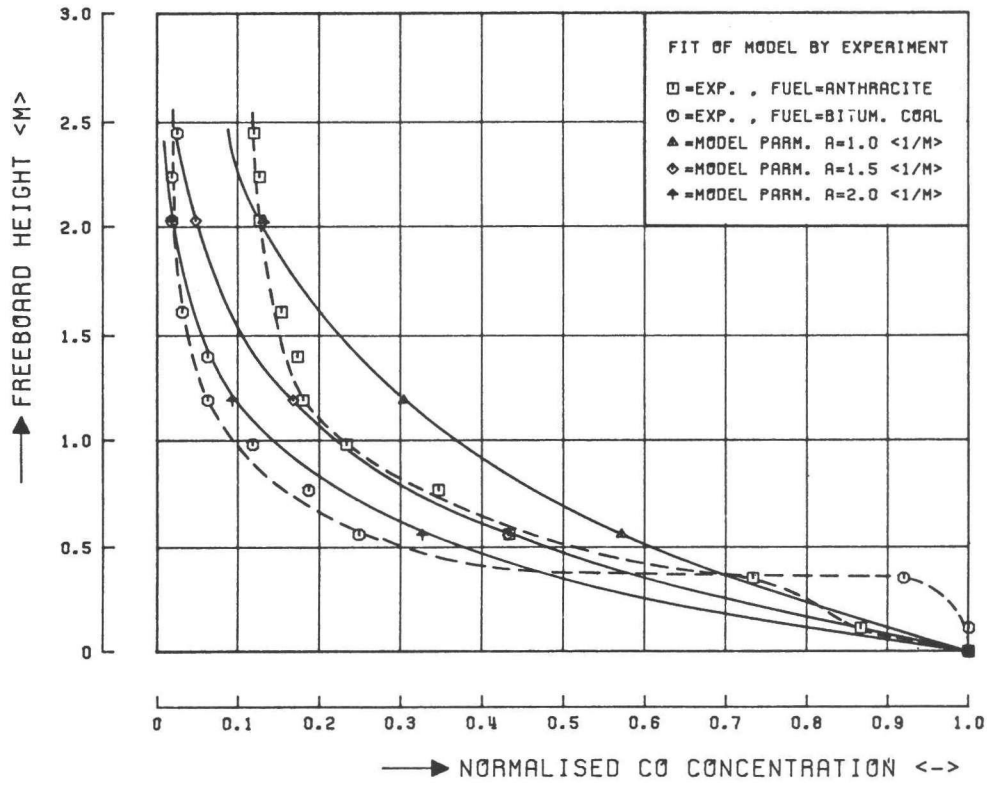

Figure 3-5.
Trial of fitting the experimentally determined CO decay in the freeboard by a mixing parameter.

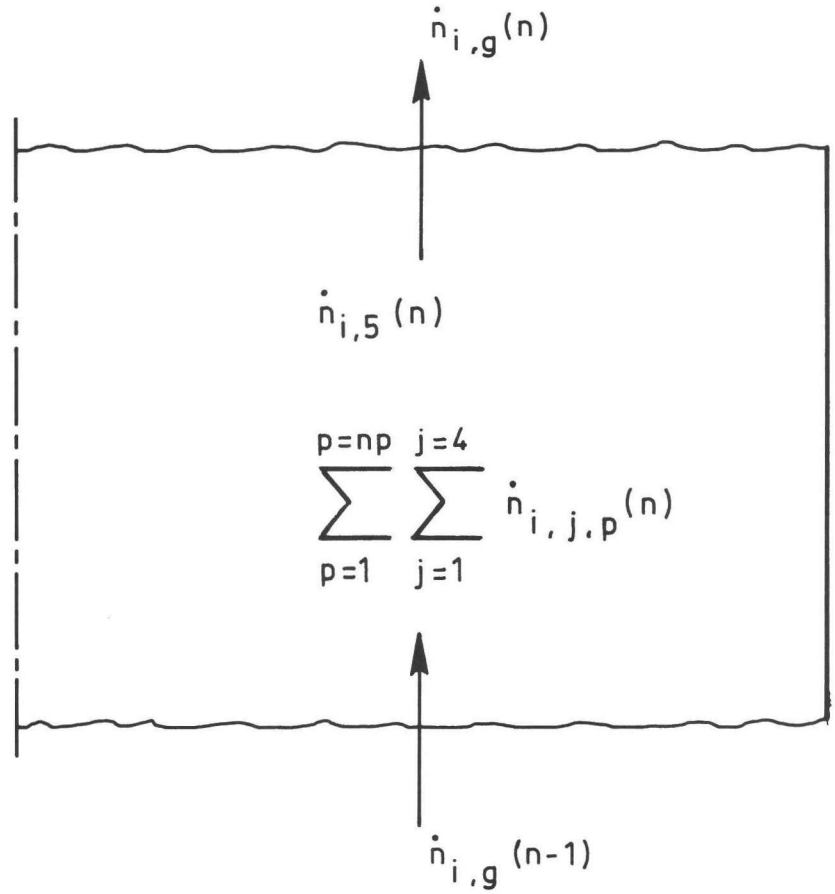

Figure 3-6.
Molar balance of gas species i in reactor n.

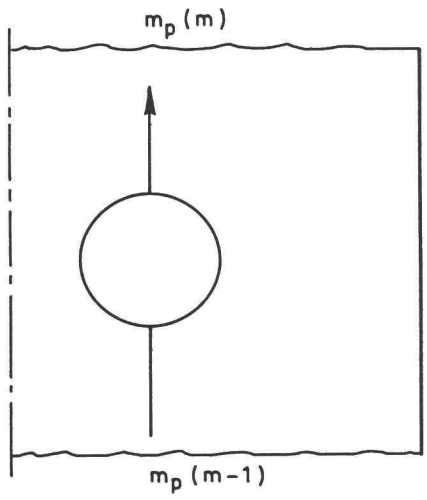

a) continously rising particle

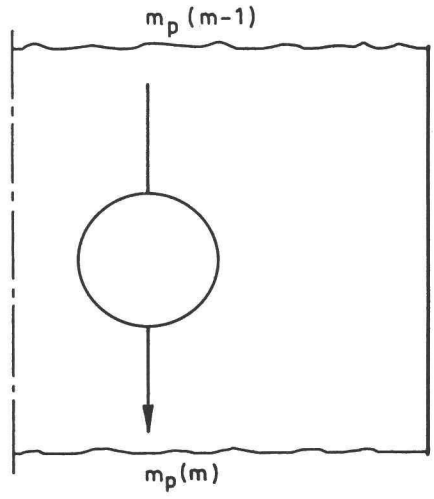

b) continuously descending particle

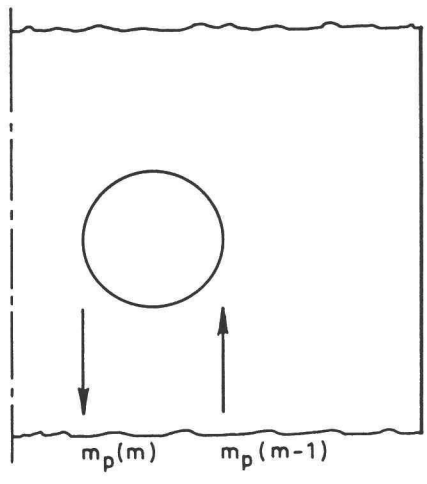

c) initially rising and
finally descending particle

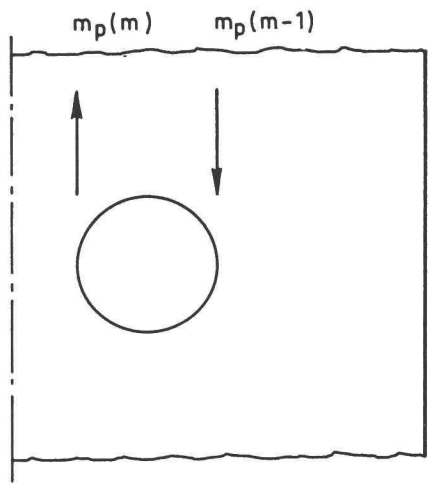

d) initially descending and
finally rising particle

Figure 3-7.
Nomenclature of a particle traversing reactor n.

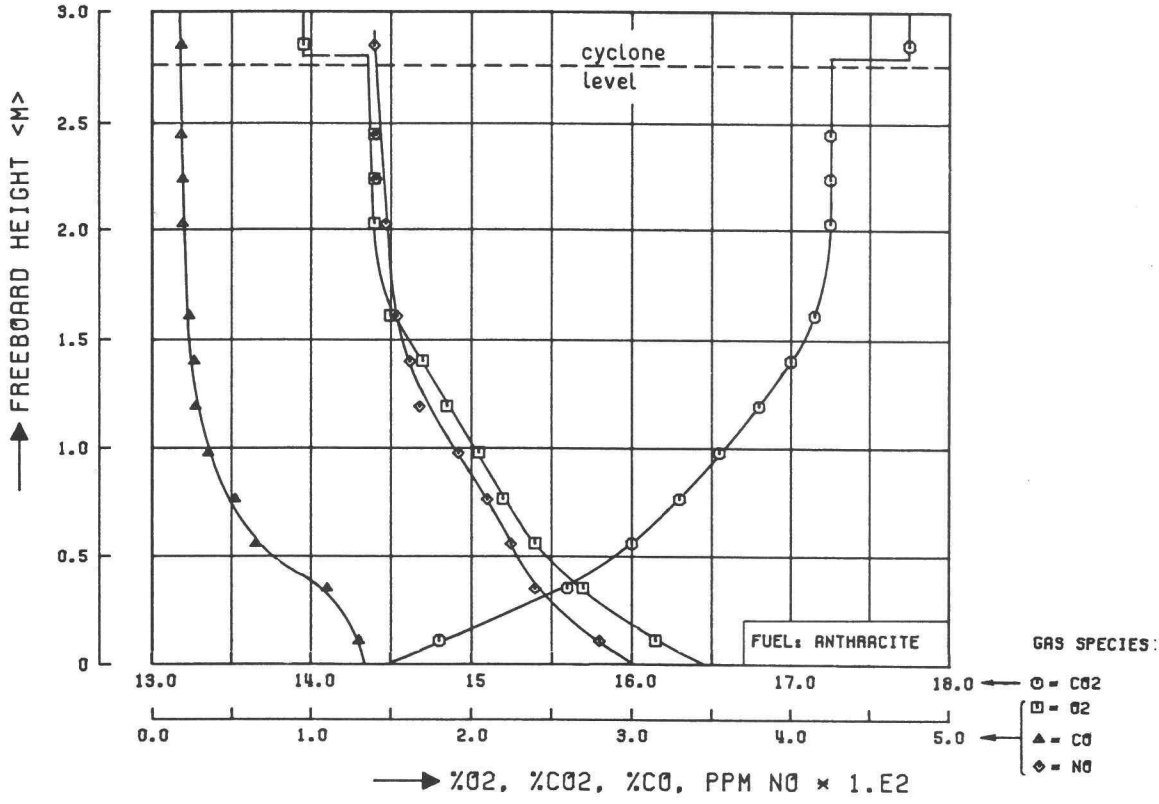

Figure 3-8.
Gas concentrations in the centre of the freeboard as a function of height (fuel: anthracite, further conditions tables 2-3 and 3-7).

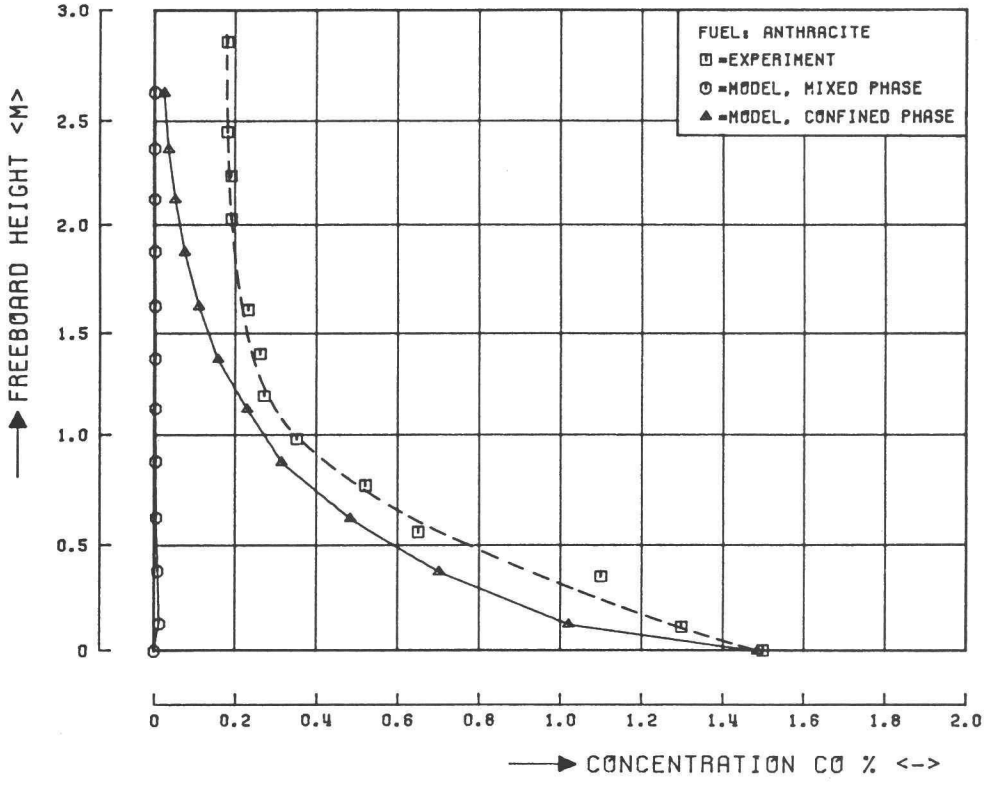

Figure 3-9a.
Comparison of calculated and experimental CO-concentration in the freeboard as a function of height.

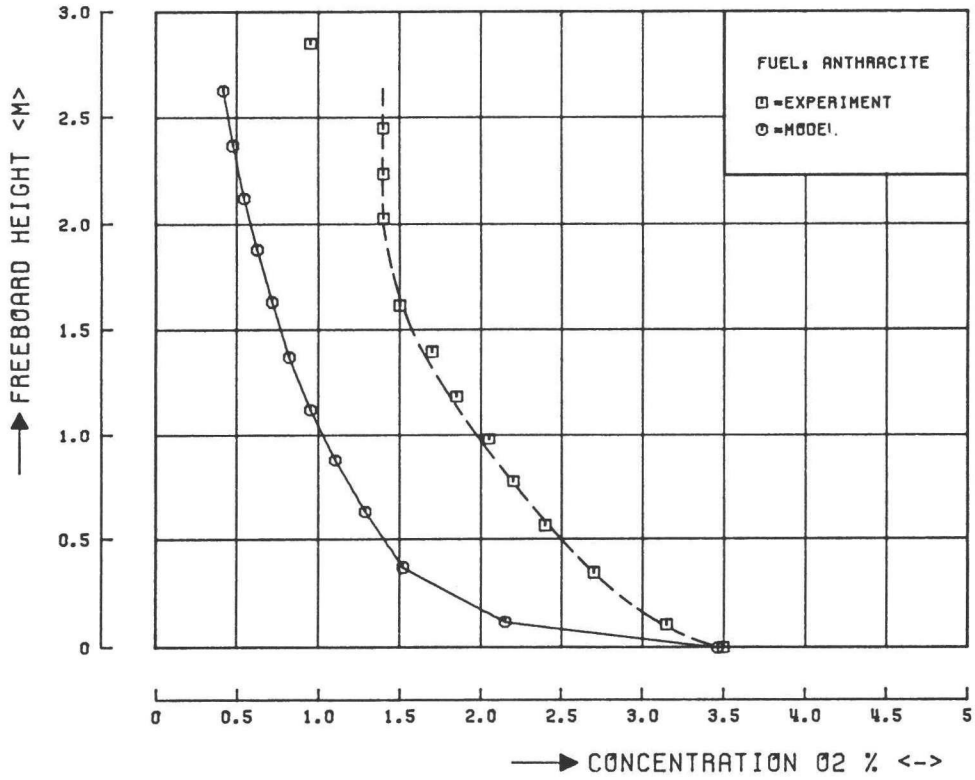

Figure 3-9b.
Comparison of calculated and experimental O2-concentration in the freeboard as a function of height.

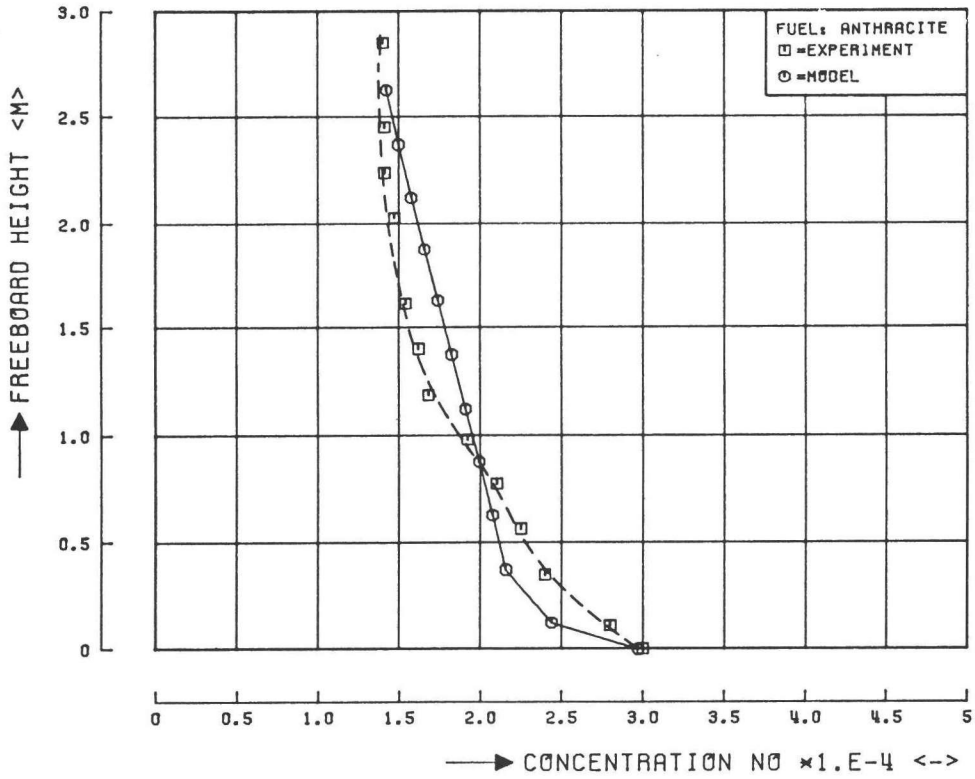

Figure 3-9c.
Comparison of calculated and experimental NO-concentration in the freeboard as a function of height.

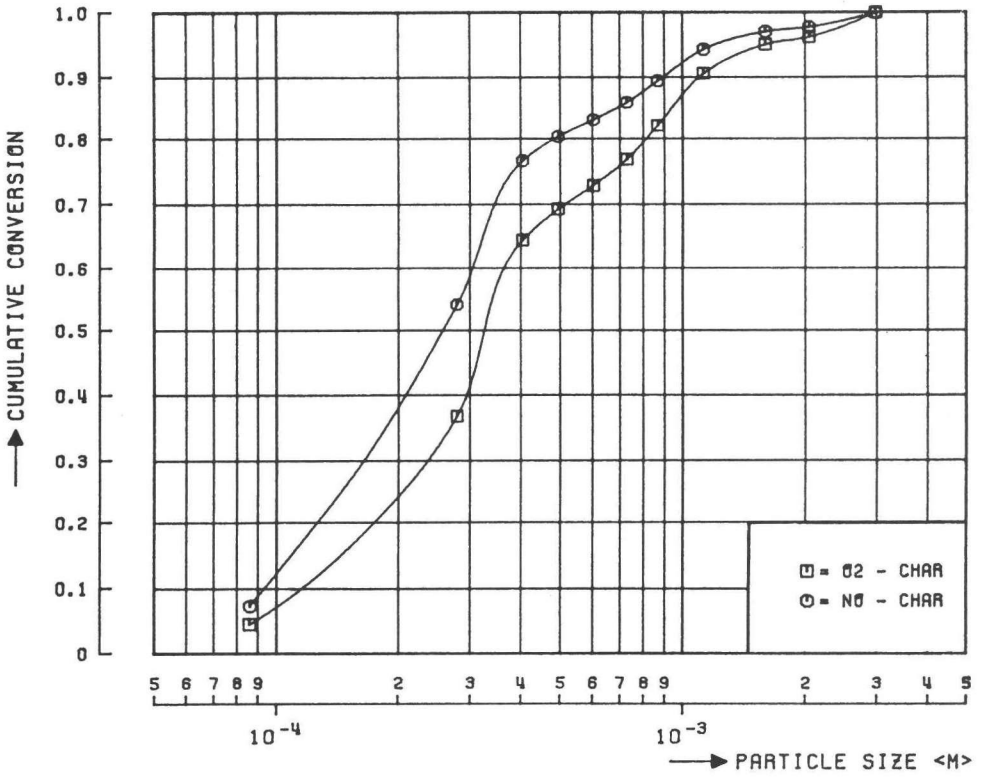

Figure 3-10. Cumulative O2 and NO conversion by char in the freeboard as a function of particle size (for reactions see table 3-1).

Table 3-1. Overall gas-particle reactions in the freeboard after various authors.

reaction no. j	reference	first order with i	Sh p	$k_{0,i,j}$ $<\frac{m}{n}>$ $s.K$	$E_{i,j}$ T p <K>	n	surf. area i=int e=ext	references, remarks
1	Rajan and Wen (1980)	O2	2	$\frac{596}{\Phi}$	17967	1	e	kin. based on Field (1967) Φ eq. (3-21)
1	Martens et al. (1983) and this work	O2	eq. 3-13	$\frac{596}{\Phi}$	18000	1	e	based on Rajan and Wen (1980). Φ eq. (3-21) kin. based on Field (1967)
6	Wells et al. (1981)	O2	2	0.0228	8052	1	e	kin. based on Smith (1971)
3	Rajan and Wen (1980), Rajan (1981)	CO2	∞	4.1E6	29787	0	e	kin. based on Caram et al. (1977)
3	Wells et al. (1981)	CO2	2	4.1E8	29794	0	e	kin. based on Caram et al. (1977) and Horio et al. (1977)
3	this work	CO2	eq. 3-13	4.1E6	29787	0	e	kin. based on Caram et al. (1977)

To be continued on next page.

Continued from previous page.

reaction no. j	reference	first order with i	Sh p	$k_{0,i,j}$ $\left\langle \frac{m}{n} \right\rangle$ s.K	$\frac{E_{i,j}}{T_p}$ <K>	n	surf. area i=int e=ext	remarks
3	Rajan and Wen (1980), Rajan (1981)	NO	2	5.24E5 error, must be 1.3E5	17117	0	e	kin. based on Oguma et al. (1971) and Horio et al. (1977)
3	Martens et al. (1983) and this work	NO	eq. 3-13	1.3E5	17111	0	e	kin. based on Horio et al. (1977)
3	Wells et al. (1981) chapter 4	NO	2	1.3E5	17111	0	e	kin. based on Horio et al. (1977)
	chapter 5	NO	2	5.9E-9 error must be 5.9E-6	9814	1	e error must be i	kin. based on Louis and Tung (1977), origin. from Chan (1977)
3+7	Chaung (1982)	NO	∞	5.95E-6	3801 type or print error, must be 9815	1	i	kin. based on Chan (1977) for T<1016 K
				4.10E-3	16454	1	$\frac{m^2}{kg}$ 6.0E5 subbituminous coal 1.5E5 bituminous coal	Song (1978) for T>1016 K

Table 3-2.
Summary of empirical global rate expressions for wet CO-oxidation. From Chaung (1982) (converted into S.I. units).
* Kozlov's concentrations are expressed as mol fractions, and not as mol/m3.

reference	temp. range <K>	press. <Pa>	A $x=a+b+c$ $\frac{mol^{1-x}}{m^{3-3x}.s}$	E/R <K>	a CO <->	b H2O <->	c O2 <->
Hottel and al. (1965)	1280 / 1535	2.5E4 / 1.0E5	1.902E6	804.7	1.0	0.5	0.3
Williams and al. (1969)	1400 / 1800	0.3E5 / 1.1E5	1.8E7	12573	1.0	0.5	0.5
Howard and al. (1974)	840 / 2360	1.0E5	1.3E7	15088	1.0	0.5	0.5
Lavrov (1968)	1063 / 1593	1.0E5	5.692E7	14233	1.0	0.5	0.25
* Kozlov (1969)	970 / 1370	1.0E5	$x=0$ $\frac{1.04E12}{T^{2.5}}$	16094	1.0	0.5	0.25
Dryer and Glassman (1974)	1030 / 1230	1.0E5	1.23E10	20117	1.0	0.5	0.25

Table 3-3.
Summary of global reaction rate expressions used for freeboard modeling by various authors (values converted into S.I. units).

freeboard modeling reference	CO-oxidation global react. mechanism reference	A x=a+b+c $\frac{mol^{1-x}}{m^{3-3x}.s}$	E/R <K>	a CO <->	b H2O <->	c O2 <->
Rajan (1978) and Rajan and Wen (1980)	Hottel and al. (1965)	1.9E6	8053	1	0.5	0.3
Martens and al. (1983)	Hottel and al. (1965)	1.902E6	8056	1	0.5	0.3
Wells and al. (1981)	Howard and al. (1981)	1.8E7	15080	1	0.5	0.5

Table 3-4.
Rate constant set for computer modeling of hydrocarbon combustion. From Paauw et al. (1979) (converted into S.I. units).

REACTION MECHANISM	RATE CONSTANT SET		
$r = 10^{A} T^{n} \exp\left(\frac{-E}{RT}\right)$ mol <------> m3.s	10 logA	n <->	E/R <K>
H + CH4 <--> CH3 + H2	20.10	0.0	5985.91
H + CH4 <--> CH3 + H2	20.10	0.0	5985.91
CH4 + M <--> CH3 + H + M	23.30	0.0	44477.56
O + CH4 <--> CH3 + OH	19.30	0.0	4642.68
OH + CH4 <--> CH3 + H2O	19.48	0.0	3019.63
CH3 + O <--> CH2O + H	20.41	0.0	1006.54
CH3 + O2 <--> CH2O + OH	17.95	0.0	5988.92
CH2O + M <--> CO + H2 + M	22.32	0.0	17604.93
CH2O + OH <--> HCO + H2O	19.36	0.0	503.27
CH2O + O <--> HCO + OH	19.00	0.0	503.27
HCO + M <--> H + CO + M	18.30	0.50	14392.55
HCO + O2 <--> CO + HO2	19.48	0.0	0.0
HCO + OH <--> CO + H2O	19.00	0.0	0.0
CO + OH <--> CO2 + H	13.18	1.30	-387.52
CO + O + M <--> CO2 + M	19.60	0.0	0.0
CO + O2 <--> CO2 + O	19.20	0.0	20623.55
CO + HO2 <--> CO2 + OH	19.70	0.0	11575.23
HO2 + OH <--> O2 + H2O	19.70	0.0	0.0
HO2 + O <--> O2 + OH	19.70	0.0	0.0
HO2 + H <--> O2 + H2	19.44	0.0	352.29
HO2 + H <--> OH + OH	20.44	0.0	956.21
H + O2 + H2 <--> HO2 + H2	21.70	0.0	-503.27
H + O2 + M <--> HO2 + M	21.30	0.0	-503.27
H + O2 + H2O <--> HO2 + H2O	22.50	0.0	-503.27
OH + OH + M <--> H2O2 + M	21.00	0.0	-2566.68
H + O2 <--> O + OH	20.34	0.0	8334.17
O + H2 <--> H + OH	16.26	1.00	4509.31
O + H2O <--> OH + OH	19.76	0.0	9063.91
H + H2O <--> H2 + OH	19.92	0.0	10095.62
H + OH + M <--> H2O + M	28.30	-2.00	0.0
H + H + M <--> H2 + M	24.65	-1.0	0.0
O + H + M <--> OH + M	21.76	0.0	-1399.09
H2 + O2 <--> OH + OH	19.23	0.0	24217.40
O + O + M <--> O2 + M	21.67	-0.28	0.0
NO + O + M <--> NO2 + M	21.10	0.0	-473.07
CO + NO2 <--> CO2 + NO	19.51	0.0	16104.68
NO + HO2 <--> NO2 + OH	20.60	0.0	0.0
O + NO2 <--> NO + O2	19.00	0.0	301.96
H + NO2 <--> NO + OH	19.48	0.0	0.0
NO + M <--> O + N + M	26.60	-1.50	75002.44

To be continued on next page.

Continued from previous page.

REACTION MECHANISM	RATE CONSTANT SET		
$r = 10^{A}\ T^{n}\ \exp\left(\frac{-E}{R\,T}\right)$ $\left\langle \frac{mol}{m^3.s} \right\rangle$	10^{logA}	n <->	E/R <K>
O + N2 <--> N + NO	20.13	0.0	37946.61
N + O2 <--> O + NO	15.81	1.00	3145.44
N2O + M <--> N2 + O + M	20.70	0.0	29189.72
N2O + O <--> NO + NO	20.00	0.0	14192.24
OH + N <--> NO + H	19.60	0.0	0.0
N2O + O <--> N2 + O2	20.00	0.0	14192.24
N2O + H <--> N2 + OH	19.58	0.0	6341.21
C + O2 <--> CO + O	19.60	0.0	0.0
CH + H <--> C + H2	17.95	0.69	805.23
CH + O2 <--> HCO + O	18.70	0.0	0.0
CH + N2 <--> HCN + N	17.90	0.0	5535.98
CH2 + H <--> CH + H2	19.00	0.0	0.0
CH2 + OH <--> CH + H2O	19.00	0.0	0.0
CH2 + O2 <--> HCO + OH	18.90	0.0	0.0
CH3 + OH <--> CH2 + H2O	18.60	0.0	0.0
CH3 + N <--> HCN + H2	16.80	0.50	0.0
CH3 + NO <--> HCN + H2O	17.80	0.0	0.0
CH + NH3 <--> HCN + H + H2	20.00	0.0	0.0
HCN + OH <--> CO + NH2	19.20	0.0	9562.15
CN + H2O <--> HCN + OH	17.50	0.0	0.0
CN + H2 <--> HCN + H	19.70	0.0	11323.60
CN + NO <--> CO + N2	20.04	0.0	4026.17
HCN + O <--> CNO + H	18.70	0.0	4076.50
CN + O2 <--> CNO + O	19.40	0.0	9058.88
CN + OH <--> CNO + H	20.60	0.0	3522.90
CN + CO2 <--> CNO + CO	18.60	0.0	0.0
CNO + O <--> CO + NO	18.00	0.0	0.0
CNO + H <--> CO + NH	19.00	0.0	0.0
NH3 + O <--> OH + NH2	18.20	0.0	3019.63
NH3 + OH <--> H2O + NH2	18.70	0.0	1006.54
NH3 + H <--> H2 + NH2	18.60	0.0	5032.71
NH2 + O <--> OH + NH	18.20	0.0	3019.63
NH2 + OH <--> H2O + NH	18.55	0.0	1006.54
NH2 + H <--> H2 + NH	19.00	0.0	5032.71
NH + O <--> OH + N	19.70	0.0	3019.63
NH + OH <--> H2O + N	19.20	0.0	1006.54
NH + H <--> H2 + N	20.20	0.0	5032.71
NH2 + NH2 <--> NH3 + NH	19.80	0.0	1811.78
NH + NH <--> H2 + N2	20.00	0.0	0.0
NH + NO <--> N2 + OH	18.40	0.0	0.0
NH2 + NO <--> N2 + H2O	18.40	0.0	0.0

Table 3-5.
Rate constant set for computer modeling of wet CO combustion. From Chaung (1982) (converted into S.I. units).

REACTION MECHANISM	RATE CONSTANT SET		
$r = 10^{A} T^{n} \exp\left(\frac{-E}{R T}\right)$ $\left\langle \frac{mol}{m^3.s} \right\rangle$	$10^{\log A}$	n <->	E/R <K>
H + O2 <--> OH + O	20.27	0.0	8454.
OH + H2 <--> H + H2O	19.34	0.0	2589.
CO + OH <--> CO2 + H	13.11	1.30	-385.
OH + H2O2 <--> H2O + HO2	19.00	0.0	906.
O + H2 <--> H + OH	16.26	1.0	4478.
H + H2O2 <--> HO2 + H2	18.23	0.0	1902.
HO2 + CO <--> CO2 + OH	20.00	0.0	11573.
H + HO2 <--> OH + OH	20.40	0.0	956.
H + HO2 <--> H2 + O2	19.40	0.0	352.
O + H2O <--> OH + OH	19.53	0.0	9239.
OH + HO2 <--> H2O + O2	19.70	0.0	503.
O + HO2 <--> O2 + OH	19.70	0.0	503.
HO2 + HO2 <--> H2O2 + O2	19.00	0.0	503.
H2 + O2 <--> OH + OH	20.90	0.0	22493.
CO + O2 <--> CO2 + O	17.50	0.0	18920.
O + O + M <--> O2 + M	21.59	-0.25	0.
H2 + M <--> H + H + M	19.79	0.0	48307.
CO + O + M <--> CO2 + M	21.77	0.0	2063.
H2O + M <--> H + OH + M	22.34	0.0	52886.
H + O2 + M <--> HO2 + M	21.22	0.0	-503.
O + H + M <--> OH + M	21.90	0.0	0.
OH + O + M <--> HO2 + M	23.00	0.0	0.

Table 3-6. Reaction mechanism and convective properties for calculation of the particle temperature.

reaction no. j	reference	$\dot{Q}_{ip}$ <J/s>	Nu_p <->	remarks
2	Wells et al.(1981)	$r_{C\text{-}CO}\, H^{0}_{C\text{-}CO}$	2	in radiation term: surrounding temp. = gas temperature.
1	Rajan and Wen(1980), Rajan (1981)	$(2\Phi\text{-}1)\, r_{C\text{-}CO}\, H^{0}_{C\text{-}CO} + (2\text{-}2/\Phi)\, r_{C\text{-}CO2}\, H^{0}_{C\text{-}CO2}$	2	in radiation term: surrounding temp. = gas temperature.
1	this work	$(2\Phi\text{-}1)\, r_{C\text{-}CO}\, H^{0}_{C\text{-}CO} + (2\text{-}2/\Phi)\, r_{C\text{-}CO2}\, H^{0}_{C\text{-}CO2}$	eq. 3-27	in radiation term: surrounding temp. = wall temperature.

Table 3-7.
Input values for the model (see also table 2-3).

Volume fraction of gas species at the fluidized bed surface:	
Ar	0.0000 <->
CO	0.0150 <->
CO2	0.1450 <->
H2O	0.0150 <->
NOx	0.0003 <->
O2	0.0350 <->
SO2	0.0000 <->
CO-mixing parameter a	1.5 <1/m>
char burning mechanism Φ	shrinking size

4 THE HEAT ECONOMY IN THE FREEBOARD

4.1 Introduction

A proper freeboard heat economy is of particular interest for the firing of high volatile fuel and/or for pressurized combustion, because of the potency of high chemical heat release per unit reactor volume. The chemical heat release, governed by CO-oxidation and char combustion, leads to an increased temperature, which on its turn again determines the conversion rates. As the absorption of SO2 by limestone or dolomite is restricted to a narrow temperature regime, temperature excursions, especially to a much higher temperature level, can not be tolerated. Furthermore the freeboard wall lifetime is affected by the temperature level, the temperature distribution and any temperature excursions.

4.2 Experiments

In chapter 3 (see figure 3-8) it was shown that significant combustion occurs in the freeboard of a fluidized bed coal combustor, especially in the lower part, the so-called splash zone.

Martens and Van Koppen (1983) and Martens (1984) found the chemical heat release in the freeboard to be not reflected in the temperature increase of the gas and the heat losses via the freeboard wall. They demonstrated the existence of a strong upwind heat transfer by maintaining an air fluidized bed at high temperature (1070 K) by the burning of natural gas in the freeboard (maximum temperature 1330 K). Their global energy balance is visualized in figure 4-1. It was found that back-radiation and / or recirculation of heated gas from the freeboard towards the bed did not contribute essentially to the upwind heat transfer. Some 70% of the combustion heat generated in the freeboard was carried towards the bed by recirculating particles, in particular from the splash zone (see also figures 2-2 and 2-7 for the flux of descending solids as a function of freeboard height). Consequently the temperature increase of the gas was suppressed, particularly in the lower freeboard region. After disengagement of the particles, however, any combustion leads to a considerable temperature increase of the gas. From their gas species concentration measurements in the freeboard, when firing anthracite and bituminous coal, they concluded that the total and the distribution of the heat release was dependent on fuel type and excess air ratio. The heat release in the freeboard was 10% - 15% of the total in the combustor. As can be seen in figure 4-2 the temperature increase in the freeboard is relatively small. To illustrate these results one of their experiments, firing anthracite, is considered in more detail. From the gas species concentration (figure 3-8) the global trend of the chemical heat release was determined along the freeboard with height. See figure 4-3. The chemical heat release commensurates with an adiabatic gas temperature increase of 230 K. The actually freeboard gas and wall temperatures obtained are visualized in figure 4-4. The freeboard gas temperature increases is up to 33 K. The lateral distribution of the freeboard temperatures was shown to be uniform. The contours of the isotherms were relatively flat, except very near to the freeboard wall. Later this experiment will serve a further comparison of the model with the experiment (section 4.4).

4.3 The one-dimensional freeboard model

4.3.1 Introduction

Parts of 'FAME', the one-dimensional freeboard model that has been developed for a pressurized fluidized bed combustor, were discussed already in the two foregoing chapters. The scope of this section is to describe

the backgrounds of the heat economy as incorporated in 'FAME'. One of the aims is to perform a total freeboard energy balance on the level of a 'laboratory calculation', with all possible but at the same time practical refinements. The total energy balance can be seen as the result of the interconnected balances of the individual particles, the gas and the freeboard wall. The model of the energy balance adopted for this work is given in figure 4-5.

As regards the gas the operating conditions in the freeboard of a fluidized bed combustor can lead to:

* temperatures of 900 - 1300 K
* pressures up to 30.E5 Pa
* concentrations of CO2 from 10 - 20 %
  CO from 0 - 5 %
  H2O from 2 - 10 %

With respect to the particles it can lead to:

* 0 - 5 % of particles in the gas by volume,
* with a large variety of particle sizes, ranging from 0 to 10.E-3 m. and a variety in shapes,
* the bulk of the particles being in the size range of 0.5E-3 to 5.E-3 m, and
* the particle cloud being non-isothermal.

The main assumptions for a standard volume, i.e. a compartment of the freeboard are:

* the gas is well mixed and isothermal,
* particles are uniformly distributed,
* there is no net contribution of radiation to the heat transfer across the boundaries of the volume, except for the wall (in other words longitudinal temperature gradients are small compared to the lateral ones),
* there is no net radiation from the gas to the particle cloud, or from individual particles to each other, unless via the wall (quasi isothermal).

This last assumption is valid when the temperature difference between gas and particles is small compared to the temperature difference between gas/particles and wall.

4.3.2 Radiation of heat

4.3.2.1 The total net radiation of a gas-particle cloud to a wall

The emissive and absorptive behaviour of an isothermal volume radiator may be characterised by relating its radiation to a replacement body and assigning to each point of its envelope an emissivity and absorptivity. The total net rate of radiation of heat from a non-grey isothermal volume-emitter to an isothermal grey enclosure can, according to Vortmeyer (1977), be approximated by:

$$\dot{Q}_{rvw} = \frac{A_w \varepsilon_w \varepsilon_v \sigma_b T_v^4}{1 - (1-\varepsilon_w)(1-\alpha_v)} - \frac{A_w \varepsilon_w \alpha_v \sigma_b T_w^4}{1 - (1-\varepsilon_w)(1-\alpha_v)} \qquad (4\text{-}1)$$

4.3.2.2 The total net radiation of individual components to a wall

The total net energy flux from a volume radiator (gas suspended with a cloud of particles) to its wall is the summation of the net contributions of the individual particles and of the gas to the wall. The net rate of heat transfer from the individual components to the wall can be related to variables such as temperatures, emissivities and absorptivities.

Assume that we have a uniform suspension of grey particles (dust) in a non-grey radiating gas. The overall emissivity and the overall absorptivity of the isothermal cloud of optical thickness L_v is defined as:

$$\varepsilon_{g+d} = 1 - \exp(-k_{a,g+d}\, L_v) \qquad (4\text{-}2)$$

and:

$$\alpha_{g+d} = 1 - \exp(-k_{e,g+d}\, L_v) \qquad (4\text{-}3)$$

The optical thickness L_v is defined as the radius of the hemisphere which produces the same flux of radiant heat as the shape in question. Values of L_v have been determined for various shapes in Hottel and Sarofim (1967) and Vortmeyer (1977). For crude calculations one can use the relation (Vortmeyer (1977)):

$$L_v = 0.9\, \frac{4\, V_v}{A_v} \qquad (4\text{-}4)$$

For a cilinder with a ratio of height to diameter larger than 0.5 the error due to the approximation after equation (4-4) is less than 5%.

The overall absorption coefficient and the overall emission coefficient is the arithmetic sum of the coefficients of the single components. That is:

$$k_{a,g+d} = k_{a,g} + k_{a,d} \qquad (4\text{-}5)$$

where:

$$k_{a,d} = \sum_{p=1}^{p=np} k_{a,p} \qquad (4\text{-}6)$$

and:

$$k_{e,g+d} = k_{e,g} + k_{e,d} \qquad (4\text{-}7)$$

where:

$$k_{e,d} = \sum_{p=1}^{p=np} k_{e,p} \qquad (4\text{-}8)$$

As the particles are assumed to be grey radiators one may define for all particles:

$$k_{e,p} = k_{a,p} = k_p \qquad (4\text{-}9)$$

When a volume emitter is not isothermal its temperature function and its optical thickness are interlinked in the relation for the rate of emission by the cloud. Thus for the emissivity and temperature of the non-isothermal cloud the overall emissivity and temperature have to be taken of the isothermal cloud having the same absorption coefficient and the same rate of emission (Field et al. (1967). The rate of radiant emission by the volume in which component i has an absorption coefficient k and a temperature T can be approximated by assigning to the volume an absorption coefficient k given by the sum of absorption coefficient of the components and a mean temperature T given by the relation:

$$T_{g+d}^4 = \frac{k_{a,g}\, T_g^4 + \sum_{p=1}^{p=np} k_{a,p}\, T_p^4}{k_{a,g} + \sum_{p=1}^{p=np} k_{a,p}} \qquad (4\text{-}10)$$

The rate of absorption by the cloud can be expressed in a temperature function and an optical thickness:

$$T_w^4 = \frac{k_{e,g}\, T_w^4 + \sum_{p=1}^{p=np} k_{e,p}\, T_w^4}{k_{e,g} + \sum_{p=1}^{p=np} k_{e,p}} \qquad (4\text{-}11)$$

The procedure implied in equations (4-10) and (4-11) does not in fact describe the physical processes. However, it can provide convenient approximations to calculate the contribution of each component to the total net rate of radiation of heat to the wall. Note that there is no net radiation of heat from one of the components of the gas-particle cloud to the other unless by radiation via the wall. Substition of the equations (4-10) and (4-11) in equation (4-1) and substituting the subscript v for g+d gives:

$$\dot{Q}_{rvw} = \frac{A_w\, \varepsilon_w\, \varepsilon_{g+d}\, \sigma_b}{1 - (1-\varepsilon_w)(1-\alpha_{g+d})} \cdot \frac{k_{a,g}\, T_g^4 + \sum_{p=1}^{p=np} k_{a,p}\, T_p^4}{k_{a,g} + \sum_{p=1}^{p=np} k_{a,p}} \qquad (4\text{-}12)$$

$$- \frac{A_w\, \varepsilon_w\, \alpha_{g+d}\, \sigma_b}{1 - (1-\varepsilon_w)(1-\alpha_{g+d})} \cdot \frac{k_{e,g}\, T_w^4 + \sum_{p=1}^{p=np} k_{e,p}\, T_w^4}{k_{e,g} + \sum_{p=1}^{p=np} k_{e,p}}$$

The total net rate of heat transport (equation (4-12)) can be calculated by taking the arithmetic sum of the contributions of all individual components. Therefore we define:

$$\dot{Q}_{rvw} = \dot{Q}_{rgw} + \sum_{p=1}^{p=np} \dot{Q}_{rpw} \qquad (4\text{-}13)$$

in which:

$$\dot{Q}_{rpw} = \frac{A_w\, \varepsilon_w\, \varepsilon_{g+d}\, \sigma_b}{1 - (1-\varepsilon_w)(1-\alpha_{g+d})} \cdot \frac{k_{a,p}\, T_p^4}{k_{a,g+d}} \qquad (4\text{-}14)$$

$$- \frac{A_w\, \varepsilon_w\, \alpha_{g+d}\, \sigma_b}{1 - (1-\varepsilon_w)(1-\alpha_{g+d})} \cdot \frac{k_{e,p}\, T_w^4}{k_{e,g+d}}$$

and:

$$\dot{Q}_{rgw} = \frac{A_w \varepsilon_w \varepsilon_{g+d} \sigma_b}{1 - (1-\varepsilon_w)(1-\alpha_{g+d})} \frac{k_{a,g} T_g^4}{k_{a,g+d}} \tag{4-15}$$

$$- \frac{A_w \varepsilon_w \alpha_{g+d} \sigma_b}{1 - (1-\varepsilon_w)(1-\alpha_{g+d})} \frac{k_{e,g} T_w^4}{k_{e,g+d}}$$

The determination of the emission/absorption coefficients of the individual components is discussed below.

4.3.2.3 The emission/absorption of a particle cloud

4.3.2.3.1 Radiative transfer in a non-scattering particle cloud

The relation for the emission/absorption coefficient of a suspension of grey non-scattering particles in a non-scattering gas in terms of the sizes and concentration of the particles is according to Vortmeyer (1977):

$$k_{d,ns} = \sum_{i=1}^{p=np} k_{p,ns} \tag{4-16}$$

where:

$$k_{p,ns} = \varepsilon_p A_p n_{p,v} \tag{4-17}$$

Next each of the variables in equation (4-17) is discussed.

The emissivity of particles containing oxides is strongly dependent on grain size, trace additives and temperature. Most oxides normally have grains in the size range where a decrease in grain size leads to a decrease in emissivity (Hottel and Sarofim (1967)). Beyond particle diameters of 6.E-6 m the emissivity increases again. Generally a decrease in temperature results in an increase in emissivity. For computer calculations one can obtain, roughly, from Hottel and Sarofim (1967) for silica sand:

$$\varepsilon_p = 1.3 + 0.2 \, {}^{10}\log d_p - 0.6 \, {}^{10}\log \left(\frac{T_p}{1283}\right) \tag{4-18}$$

for:

$$1.E\text{-}5 \text{ m} < d_p < 1.E\text{-}3 \text{ m} \tag{4-19}$$

$$1000 \text{ K} < T_p < 1840 \text{ K} \tag{4-20}$$

$$0 < \varepsilon_p < 1 \tag{4-21}$$

Maximum error is 30% of the absolute value.

The projection surface of the particle with diameter d_p on a plane is defined as:

$$A_p = \frac{\pi}{4} d_p^2 \tag{4-22}$$

Consider the case that each second one spherical particle enters a volume with cross section area A_V and height h_V. The particle traverses the volume with a residence time t. The particle number density of the single

particle in the volume

$$V_v = A_v \, h_v \tag{4-23}$$

is:

$$n_{p,v} = \frac{1 \; t_p}{V_v} \tag{4-24a}$$

Equation (4-24a) then implies that equation (4-14) refers to the flux of heat from all particles to the wall per unit of time as experienced by the wall. The flux of heat as experienced by all particles per unit of time given by equation (4-14) is implied with:

Section 4.3.2

$$n_{p,v} = \frac{1}{V_v} \tag{4-24b}$$

4.3.2.3.2 Radiative transfer in a scattering particle cloud

The absorption equation on which the derivations in section 4.3.2.3.1 are based assumes the change of intensity to be given by:

$$dI = - I \, k \, dL \tag{4-25}$$

However, particles scatter radiation as well as absorb it. The scattering ability of the medium may be characterised by a scattering coefficient s and an absorption (or emission) coefficient k so that:

$$dI = - I \, (k + s) \, dL \tag{4-26}$$

The treatment of scattering, including the detailed angular distribution of scattered intensity is very complicated (Hottel and Sarofim (1967)) and far to comprehensive to be included in a first order approximative model. To get some idea of the magnitude of the effects of scattering we apply some crude calculations that are more compatible with the present state of knowledge on our subject.

A simple approach suited to the analysis of one dimensional transfer problems has been elaborated by Biermann and Vortmeyer (1969). They describe the behaviour of a non-scattering uniform particle cloud as:

$$\varepsilon_{d,ns} = 1 - \exp(- k_{d,ns} \, L_v) \tag{4-27}$$

For the scattering particle cloud ε is reduced and takes the form:

$$\varepsilon_{d,sc} = (1 - \sigma) \, \frac{1 + \exp(- k_{d,ns} \, L_v \sqrt{1 + 2R})}{1 + \sigma \exp(- k_{d,ns} \, L_v \sqrt{1 + 2R})} \tag{4-28}$$

where:

$$\sigma = \frac{- 1 + \sqrt{1 + 2R}}{1 + \sqrt{1 + 2R}} \tag{4-29}$$

R is the ratio of the efficiency factor for scattering to the efficiency factor for absorption. The scattering phenomena is related to the geometry

of the particles and the radiation wave length. One can define the dimensionless number p_p:

$$p_p = \frac{\pi\, d_p}{\lambda_r} \qquad (4\text{-}30)$$

Small particles such as soot in flames, are smaller than the wave lengths important for thermal emissions (d_p < 0.5E-6 m and λ_r = 2.E-6 - 7.E-6 m) that p_p < 1. For these particles scattering is negligible. In the region p_p = 1 the calculations are complex (Van der Hulst (1957)). It is well established (Field and al. (1967), Biermann and Vortmeyer (1969)) that for coal and ash particles, say with diameters beyond 30.E-6 m, so that p_p > 25, R has a value less than but almost equal to 0.2. This condition may be satisfactory for the freeboard where the greater part of the solids has a size above 100.E-6 m. If equation (4-28) is used for calculating ε, within the region $0 \leq (k.L) < 1$ and $0 < R < 0.4$, one notices that, compared with equation (4-27), the relative difference is less than 5%. For practical reasons here a multiplication factor for scattering is introduced giving the ratio of the effective overall coefficient of absorption to the overall coefficient of absorption of the identical non-scattering cloud:

$$f_{sc} = \frac{e^{\log(1 - \varepsilon_{d,sc})}}{k_{d,ns}\, L_v} \qquad (4\text{-}31)$$

Then we can define:

$$k_p = f_{sc}\, k_{p,ns} \qquad (4\text{-}32)$$

for use in equation (4-9).

4.3.2.4 The emission/absorption coefficient of combustion gases

Carbon monoxide, carbon dioxide and water vapour, the predominant products of fossil-fuel combustion, contribute most to the process of thermal radiation of gases (Vortmeyer (1977), Hottel and Sarofim (1967), Edwards and Balakrishnan (1973), Hines and Edwards (1968)). Molecular gas radiation properties are complex due to the many orders of magnitudes of variation in the spectral emission/absorption coefficients with wavenumber. Regions of intense absorption, called absorption bands, are due to the interaction of radiation with the vibration modes of the gas molecules. The true gas spectral absorption coefficient can vary greatly over a number of wavelengths, called lines. Each line of each gas is located at a specific wavenumber and consequently the lines of different gases form a particular and complex array. When the spectral bands within which the radiant absorption or emission by respective gases (partly) coincide, corrections have to be made.

Following the frame-work of Edwards and al. (1973), Venema (1981) developed the computer program 'GEAC' which permits calculation of the emission/absorption coefficient of a homogeneous gas containing carbon monoxide, carbon dioxide and water vapour over a large range of total and partial pressures. The remaining gas components such as nitrogen and oxygen are highly diathermal.

The computer program 'GEAC' is incorporated in the freeboard model 'FAME' and the underlying theory is described below. For a mixture of emitting/absorbing gases with overlapping bands the emission/absorption coefficient is very nearly equal to the sum of the emission/absorption coefficients (Edwards and al. (1973)).

$$k_{g,\nu,mix} = \sum_{i=1}^{i=ng} \sum_{j=1}^{j=nb} k_{g,\nu,i,j} \qquad (4\text{-}33)$$

The summation covers, in principle, all absorption bands j of all species i. The monochromatic emission/absorption coefficient of a homogeneous gas for the i-th species and j-th narrow absorption band is given by (Edwards and al. (1973)):

$$k_{g,\nu,i,j} = \frac{-\left(\frac{s}{d}\right)_{i,j} \rho_i}{\left(1 + \frac{\left(\frac{s}{d}\right)_{i,j} \rho_i L_v}{\beta_{i,j} P_{e,i}}\right)^{0.5}} \qquad (4\text{-}34)$$

The broadening pressure effective on the i-th species is written as:

$$P_{e,i} = \left(\frac{P}{P_o} + \frac{P_i}{P_o}(b_i - 1)\right)^n \qquad (4\text{-}35)$$

A wide exponential band correlation is used to describe the relation between

$$\left(\frac{s}{d}\right)_{n,i,j} \quad \text{and} \quad \beta_{i,j}$$

as a function of wavenumber ν inside each band:

$$\left(\frac{s}{d}\right)_{\nu,i,j} = \frac{s}{d}_{\nu,i,j}(\alpha_{i,j}, \omega_{i,j}, \nu_{i,j}) \qquad (4\text{-}36)$$

The model is then a description of values of:

$$\alpha_{i,j},\ \beta_{i,j} \text{ and } \omega_{i,j} \text{ versus temperature.}$$

The parameter α is the integrated band intensity, i.e. the integrated (s/d) over all ν. The band width parameter ω is the width of the spectral interval in which (s/d) is larger than (1/e) times its maximum value. The fraction of total power contained within the spectral region occupied by the j-th band of species i, between the upper and lower wavenumber ν amounts to (Czerney and Walther (1961)):

$$f(u_{i,j}) = \frac{15}{\pi^4} \int_{u_l}^{u_u} \frac{u^3\, du}{\exp(u) - 1} \qquad (4\text{-}37)$$

where:

$$u_{i,j} = \frac{h\, c\, \nu_{i,j}(T_g, P_i, P, L)}{k_b\, T_s} \qquad (4\text{-}38)$$

T_s and T_g are the source (emitter) respectively gas temperature.

From equation (4-37) and (4-38) we can define the fractional function of the first kind:

$$f\left(\frac{\nu}{T_s}\right) = \sum_{i=1}^{i=ng} \sum_{j=1}^{j=nb} f(u_{i,j}) \qquad (4\text{-}39)$$

The spectral calculation is subsequently carried out (using equation (4-33) to find k) and numerically integrated with respect to ν to find the total emissivity/absorptivity. Returning to the radiative heat transfer from the wall to the gas we find:

$$T_s = T_w \tag{4-40}$$

so that the absorptivity reads:

$$\alpha_{g,mix}(T_w,T_g,P_{i=1,ng},P,L_v) = \tag{4-41}$$

$$\int_0^1 (1-\exp(k_{g,\nu,mix}(T_g,P_{i=1,ng},P,L_v)\ L_v))\ df(\frac{\nu(T_g,P_{i,ng},P,L_v)}{T_w})$$

For the radiative heat transfer from the gas to the wall we find:

$$T_s = T_g \tag{4-42}$$

so that the emissivity reads:

$$\varepsilon_{g,mix}(T_g,P_{i=1,ng},P,L_v) = \tag{4-43}$$

$$\int_0^1 (1-\exp(k_{g,\nu,mix}(T_g,P_{i=1,ng},P,L_v)\ L_v))\ df(\frac{\nu(T_g,P_{i,ng},P,L_v)}{T_g})$$

For the case of a gas-particle cloud the contribution of the gas to the total emission/absorption coefficient, defined by equations (4-5) and (4-7), is given by:

$$k_{a,g} = \frac{e_{\log(1\ -\ \varepsilon_{g,mix})}}{L_v} \tag{4-44}$$

and:

$$k_{e,g} = \frac{e_{\log(1\ -\ \alpha_{g,mix})}}{L_v} \tag{4-45}$$

4.3.2.5 The emissivity of a stainless steel wall

For an oxidized stainless steel wall the emissivity is fitted by a polynomial expression from a graphical presentaion after Hoogendoorn (1979):

$$\varepsilon_w = 0.8556 - 3.571E\text{-}6\ T_w + 3.393E\text{-}8\ T_w^2 \tag{4-46}$$

for:

$$500\ K < T_w < 1300\ K \tag{4-47}$$

The maximal error is 4%.

4.3.3 Unsteady heat conduction in a sphere

4.3.3.1 Introduction

For cases such as pneumatic conveying of solids in reactors the contribution of the solids on the overall heat balance can be enormous. Relative to the gas the solids often have a high mass flux at similar specific heat capacity. For the fluidized bed coal combustor of our interest the ratio of particle mass flux and gas mass flux at the fluidized bed-freeboard interface is in the order of 100 and at the freeboard outlet in the order of 0.01. Generally for gases the thermal energy transport by mixing is fast and surpasses conduction. In solids thermal energy transport takes place by conduction. Dependent on geometry, physical properties and residence time the exchange of heat can be complete or not.

In the freeboard temperatures change with height and the particles are subject to unsteady heat transfer. In this section an analytical expression is developed to describe this process for a spherical particle, selected for reasons of simplicity, and starting from the following problem: A homogeneous sphere of solid material, initially at a uniform temperature, is suddenly immersed in a volume of well-stirred gas of constant temperature. The wall surrounding the volume is at a constant temperature. The outer surface of the solid acts as a source of heat. The non-steady state involves transfer of heat to the solid material and surrounding gas and wall. Given the particle residence time it is desired to find the heat transmitted:

* from the particle surface to the gas by convection,
* from the particle surface to the wall by radiation,
* from the particle surface to the interior of the solid by conduction.

4.3.3.2 Basic equations at the particle surface

The rate of heat flow at the wall of the solid can be calculated from:

$$\dot{Q}_{cp}(t) = - \lambda_p A_p \left(\frac{\delta T_p(t)}{\delta r}\right)_{r=R_p} \qquad (4\text{-}48)$$

Note that $T_p(t)$ refers to the surface of the particle.

Heat can be liberated or absorbed at the solid surface.
Here the general linearised case is treated in which:

$$\dot{Q}_{sp}(t) = A_p \, (c1 \; T_p(t) - c2) \qquad (4\text{-}49)$$

where c1 and c2 are constants.
The case may refer to systems in which at the solid surface reaction, evaporation or condensation takes place. However the geometry and the physical properties of the solid must remain unchanged; at least the changes must be acceptably slow.

The heat flow across the solid-gas interface by convection is defined as:

$$\dot{Q}_{cpg}(t) = \alpha_{cpg}\, A_p\, (T_p(t) - T_g) \qquad (4\text{-}50)$$

where α_{cpg} is obtained with use of equations 3-26 upto 29.

In general the net radiation of heat flow between the particle surface and the wall, both at constant temperatures, is expressed as

$$\dot{Q}_{rpw} = c3\, T_p^4 - c4\, T_w^4 \qquad (4\text{-}51)$$

in which c3 and c4 are constants. See equation (4-14). This equation is modified (for numerical convenience) into the product of the characteristic temperature difference and the proportionality factor (pseudo heat transfer coefficient)

$$\dot{Q}_{rpw}(t) = \alpha_{rpw}\, A_p\, (T_p(t) - T_w) \qquad (4\text{-}52)$$

where

$$\alpha_{rpw} = \frac{c3\, T_p^4(0) - c4\, T_w^4}{A_p\, (T_p(0) - T_w)} \qquad (4\text{-}53)$$

Note that the proportionality factors α in equations (4-50) and (4-52) are based on the particle conditions at t_p=0.

4.3.3.3 Total energy balance

The total amount of heat transmitted to the interior of the solid during the particles' residence time t_p

$$Q_{cp}(t_p) = \int_0^{t_p} \dot{Q}_{cp}(t)\, dt \qquad (4\text{-}54)$$

can be related to the change in enthalpy.
Assume that the physical properties ρ_p and Cp_p of the particle are constant. Hence we can write

$$Q_{cp}(t_p) = -\, \rho_p\, Cp_p\, V_p\, (\bar{T}_p(t_p) - T_p(0)) \qquad (4\text{-}55)$$

The calorific mean particle temperature reads

$$\bar{T}_p(t_p) = \frac{\int_{V_p} (\rho_p\, Cp_p\, T_p(r,t_p))\, dV_p}{\int_{V_p} (\rho_p\, Cp_p)\, dV_p} \qquad (4\text{-}56)$$

Note that $T_{r,t}$ refers to the internal particle temperature.

The principle of conservation of energy enables a relation for the non-steady state to be obtained. Integrating equations (4-49), (4-50) and (4-52) over the residence time and combining the result with equation (4-55) according to figure 4-6 gives

$$Q_{cp}(t_p) = Q_{sp}(t_p) + Q_{cpg}(t_p) + Q_{rpw}(t_p) \qquad (4\text{-}57)$$

$$Q_{sp}(t_p) = A_p\, t_p\, \left(c1\, \frac{\int_0^{t_p} T_p(t)\, dt}{t_p} - c2\right) \qquad (4\text{-}58)$$

$$Q_{cpg}(t_p) = \alpha_{cpg}\, A_p\, t_p \left(\frac{\int_0^{t_p} T_p(t)\, dt}{t_p} - T_g\right) \qquad (4\text{-}59)$$

$$Q_{rpw}(t_p) = \alpha_{rpw}\, A_p\, t_p \left(\frac{\int_0^{t_p} T_p(t)\, dt}{t_p} - T_w\right) \qquad (4\text{-}60)$$

The problem is thus reduced to that of finding the solution for

either $\bar{T}_p(t_p)$ or $\dfrac{\int_0^{t_p} T_p(t)\, dt}{t_p}$

4.3.3.4 The particle temperature

For the interior of a solid the equation of energy, after insertion of Fourier's law of heat conduction, becomes

$$\rho_p\, Cp_p \frac{\delta T_p(r,t)}{\delta t} = (\nabla \lambda_p\, \nabla T_p(r,t)) \qquad (4\text{-}61)$$

Assuming the thermal conductivity to be constant (4-61) becomes

$$\frac{\delta T_p(r,t)}{\delta t} = a_p\, \nabla^2 T_p(r,t) \qquad (4\text{-}62)$$

In this relation the thermal diffusivity of the solid is defined as

$$a_p = \frac{\lambda_p}{\rho_p\, Cp_p} \qquad (4\text{-}63)$$

For the symmetrical temperature field of the sphere equation (4-15) becomes

$$\frac{\delta T_p(r,t)}{\delta t} = \frac{a_p}{r^2} \frac{\delta}{\delta r}\left(r^2 \frac{\delta T_p(r,t)}{\delta r}\right) \qquad (4\text{-}64)$$

The initial condition is

$$T_p(r,0) = T_p(0) = \text{constant for } t \leq 0 \qquad (4\text{-}65)$$

The boundary condition at $r=R_p$ is determined by

$$\dot{Q}_{cp}(t) = \dot{Q}_{sp}(t) + \dot{Q}_{cpg}(t) + \dot{Q}_{rpw}(t) \qquad (4\text{-}66)$$

Substitution of equations (4-48), (4-49), (4-50) and (4-52) into (4-66) gives

$$\left(\frac{\lambda_p}{\alpha_{tot}} \frac{\delta T_p(t)}{\delta r} + T_p(t)\right)_{r=R_p} = T_\infty \qquad \text{for } t > 0 \qquad (4\text{-}67)$$

where the value

$$T_\infty = \frac{\alpha_{cpg}\, T_g + \alpha_{rpw}\, T_w + c2}{\alpha_{tot}} \qquad \text{for } \alpha_{tot} \neq 0 \qquad (4\text{-}68)$$

and

$$\alpha_{tot} = \alpha_{cpg} + \alpha_{rpw} + c1 \qquad (4\text{-}69)$$

It is convenient to introduce dimensionless quantities. The dimensionless temperature:

$$\Theta_p(\xi,\tau) = \frac{T_p(r,t) - T_\infty}{T_p(0) - T_\infty} \qquad (4\text{-}70)$$

The dimensionless length:

$$\xi = \frac{r}{R_p} \qquad (4\text{-}71)$$

The dimensionless time (Fourier number):

$$\tau = \frac{a_p\, t}{R_p^2} \qquad (4\text{-}72)$$

The Biot number Bi gives the ratio between the resistance against heat transfer inside the solid and outside of the solid:

$$Bi_p = \frac{\alpha_{tot}\, R_p}{\lambda_p} \qquad (4\text{-}73)$$

Then the differential equation (4-64), the initial and boundary condition, equation (4-65) respectively (4-66) becomes:

$$\frac{\delta\Theta_p(\xi,\tau)}{\delta\tau} = \frac{1}{\xi^2}\,\frac{\delta}{\delta\xi}\left(\xi^2\,\frac{\delta\Theta_p(\xi,\tau)}{\delta\xi}\right) \qquad (4\text{-}74)$$

$$\Theta_p(\xi,0) = 1 \text{ for } \tau \leq 0 \qquad (4\text{-}75)$$

$$\left(\frac{1}{Bi_p}\,\frac{\delta\Theta_p(\xi,\tau)}{\delta\xi} + \Theta_p(\xi,\tau)\right)_{|\xi|=1} = 0 \text{ for } \tau > 0 \qquad (4\text{-}76)$$

The calorific mean dimensionless temperature is defined as:

$$\bar{\Theta}_p(\tau) = 3\int_0^1 \Theta_p(\xi,\tau)\,\xi^2\,\delta\xi \qquad (4\text{-}77)$$

In many unsteady state heat conduction problems the solution is found in the form of infinite series. The series obtained for this problem are given by Martin (1984) and are listed in appendix 2. The use of the infinite series is unwieldy for practical calculations. In practice Θ_p can be approximated by (Martin (1984)):

$$\bar{\Theta}_p(\tau) = \exp\left(\frac{-3\tau}{\frac{1}{Bi_p} + \frac{1}{Nu(\tau)}}\right) \qquad (4\text{-}78)$$

where:

$$Nu(\tau) = \left(\left(\frac{\pi^2}{3}\right)^2 + \left(\frac{4}{\pi\,\tau}\right)\right)^{0.5} \qquad (4\text{-}79)$$

The difference between Θ_p calculated from equation (4-78) and the solution obtained in appendix 3 with the use of the first 40 terms of the infinite series is always less than 3%. See figure 4-7. Substitution of equation (4-70) into (4-77) yields:

$$\bar{T}_p(t) = \bar{\Theta}_p(t)\ T_p(0) + (1-\bar{\Theta}_p(t))\ T_\infty \qquad (4\text{-}80)$$

or with (4-68) and (4-69)

$$\bar{T}_p(t) = \bar{\Theta}_p(t)\ T_p(0) + (1-\bar{\Theta}_p(t))\ \frac{\alpha_{cpg}\ T_g + \alpha_{rpw}\ T_w + c2}{a_{cpg} + a_{rpw} + c1} \qquad (4\text{-}81)$$

4.3.3.5 The time mean particle surface temperature

Substitution of the value of the mean particle temperature of equation (4-81) into (4-56) up to (4-60) and rewriting in terms of $T_p(0)$, T_g, T_w and c2 gives:

$$\frac{\int_0^{t_p} T_p(t)\,dt}{t_p} = \frac{\rho_p\ Cp_p\ V_p\ (1-\bar{\Theta}_p)}{\alpha_{tot}\ A_p\ t_p}\ T_p(0) \qquad (4\text{-}82)$$

$$+ \frac{\alpha_{cpg}}{\alpha_{tot}}\left(\frac{-\rho_p\ Cp_p\ V_p\ (1-\bar{\Theta}_p)}{\alpha_{tot}\ A_p\ t_p} + 1\right) T_g$$

$$+ \frac{\alpha_{rpw}}{\alpha_{tot}}\left(\frac{-\rho_p\ Cp_p\ V_p\ (1-\bar{\Theta}_p)}{\alpha_{tot}\ A_p\ t_p} + 1\right) T_w$$

$$+ \frac{1}{\alpha_{tot}}\left(\frac{-\rho_p\ Cp_p\ V_p\ (1-\bar{\Theta}_p)}{\alpha_{tot}\ A_p\ t_p} + 1\right) c2$$

This equation permits the calculation of the true mean particle surface temperature over the residence time of the particle in the standard volume.

4.3.3.6 The solution of the separate flows of thermal energy

The total amount of heat transmitted to the solid material is given by equations (4-56) and (4-81):

$$Q_{cp}(t_p) = -\rho_p\ Cp_p\ V_p\ (1-\bar{\Theta}_p) \left(\frac{\alpha_{cpg}\ T_g + \alpha_{rpw}\ T_w + c2}{\alpha_{tot}} - T_p(0)\right) \qquad (4\text{-}83)$$

The heat liberated by the source is determined by equations (4-58) and (4-82):

$$Q_{sp}(t_p) = \frac{c1\ \rho_p\ Cp_p\ V_p\ (1-\bar{\Theta}_p)}{\alpha_{tot}}\ T_p(0) \qquad (4\text{-}84)$$

$$+ \frac{c1\ \alpha_{cpg}}{\alpha_{tot}} \left(\frac{-\ \rho_p\ Cp_p\ V_p\ (1-\bar{\Theta}_p)}{\alpha_{tot}} + A_p\ t_p\right) T_g$$

$$+ \frac{c1\ \alpha_{rpw}}{\alpha_{tot}} \left(\frac{-\ \rho_p\ Cp_p\ V_p\ (1-\bar{\Theta}_p)}{\alpha_{tot}} + A_p\ t_p\right) T_w$$

$$+ \frac{1}{\alpha_{tot}} \left(\frac{-\ c1\ \rho_p\ Cp_p\ V_p\ (1-\bar{\Theta}_p)}{\alpha_{tot}} - (\alpha_{cpg} + \alpha_{rpw})\ A_p\ t_p\right) c2$$

For the heat transmitted from the particle to the gas by convection we can write from equations (4-59) and (4-82):

$$Q_{cpg}(t_p) = \frac{\alpha_{cpg}}{\alpha_{tot}}\ \rho_p\ Cp_p\ V_p\ (1-\bar{\Theta}_p)\ T_p(0) \qquad (4\text{-}85)$$

$$+ \frac{\alpha_{cpg}^2}{\alpha_{tot}} \left(\frac{-\ \rho_p\ Cp_p\ V_p\ (1-\bar{\Theta}_p)}{\alpha_{tot}} - \frac{\alpha_{rpw} + c1}{\alpha_{cpg}}\ A_p\ t_p\right) T_g$$

$$+ \frac{\alpha_{cpg}\ \alpha_{rpw}}{\alpha_{tot}} \left(\frac{-\ \rho_p\ Cp_p\ V_p\ (1-\bar{\Theta}_p)}{\alpha_{tot}} + A_p\ t_p\right) T_w$$

$$+ \frac{\alpha_{cpg}}{\alpha_{tot}} \left(\frac{-\ \rho_p\ Cp_p\ V_p\ (1-\bar{\Theta}_p)}{\alpha_{tot}} + A_p\ t_p\right) c2$$

Combining equations (4-60) and (4-82) gives an analogous expression for the thermal energy transmitted from the solid to the wall by radiation:

$$Q_{rpw}(t_p) = + \frac{\alpha_{rpw}}{\alpha_{tot}}\ \rho_p\ Cp_p\ V_p\ (1-\bar{\Theta}_p)\ T_p(0) \qquad (4\text{-}86)$$

$$+ \frac{\alpha_{cpg}\ \alpha_{rpw}}{\alpha_{tot}} \left(\frac{-\ r_p\ Cp_p\ V_p\ (1-\bar{\Theta}_p)}{\alpha_{tot}} + A_p\ t_p\right) T_g +$$

$$+ \frac{\alpha_{rpw}^2}{\alpha_{tot}} \left(\frac{- \rho_p \, Cp_p \, V_p \, (1-\bar{\theta}_p)}{\alpha_{tot}} - \frac{\alpha_{cpg} + c1}{\alpha_{rpw}} A_p \, t_p \right) T_w$$

$$+ \frac{\alpha_{rpw}}{\alpha_{tot}} \left(\frac{\rho_p \, Cp_p \, V_p \, (1-\bar{\theta}_p)}{\alpha_{tot}} + A_p \, t_p \right) c2$$

For each particle traversing the freeboard, with a residence time calculated according to section 2.3, the linear relations in the temperatures can now be written (equations (4-83) up to (4-86)). These relations are treated further in section 4.3.5 in order to solve the total energy balance in the freeboard.

4.3.4 Heat transfer via the freeboard wall

4.3.4.1 Introduction

Actual application of the model 'FAME' requires modeling of the freeboard wall as a heat sink. For the intended comparison of the model with experiment the heat transfer problem concerns the heat losses via the freeboard wall of the 'MAGMA' (see Martens (1984)). This freeboard wall is a long vertical cylinder made up of layers of various materials, each with its own physical properties. For analytical purposes the freeboard is subdivided into a number of reactors in series. At the inner (reactor) side of the wall the heat transfer is governed by radiation and forced convection of a gas that contains large quantities of solid particles. At the outer side the heat transfer is governed by radiation as discussed earlier and free convection to the surroundings at ambient temperature.

In this section it is shown how the various resistances to heat transfer are combined into a total resistance. The physical properties of the materials and / or fluids are discussed in appendix 1. The main purpose of this section is to illustrate some particular problems that arise in the application of standard heat transfer knowledge to a freeboard and how the results link up with the phenomena discussed before. Reading this section and section 4.3.5 may be omitted if only a general judgement on the validity of the model is pursued (see section 4.4).

4.3.4.2 Basic equations

The assumptions that are made are the following:

* stationary state
* radial symmetry
* axial heat fluxes in the composite walls may be neglected

In figure 4-8 a composite wall is shown made up of three materials of different thicknesses and different thermal conductivities. The composite materials are: 1 stainless steel, 2 ceramic wool, 3 rockwool. Surface 01 is in convective and conductive contact with a fluid containing gas and particles and in radiative contact with a volume emitter containing gas and particles. Surface 34 is in convective and radiative contact with a fluid respectively a surface at the ambient temperature.

Two questions arise for the investigation of the non-radiative heat transmission between the inner wall and the flowing mixture of gas and solids. Firstly: how will the heat transfer be distributed over the gas and solids, and secondly, how will the solids influence the lateral transport of heat. Stockburger (1966) has studied this phenomenon and from his work some conclusions are drawn for the present investigation. The specific

heat and the density of the gas and solids, the particle volume fraction, the geometry of the confinement, the gas velocity and most of all the surface mean (Sauter) particle size determine the distribution of heat between gas and solids. The larger the particles the lower the heat transmitted to them. This phenomenon is related to the heat conduction of the gas and solids as discussed in the last few sections. It also appears that above a certain particle size their influence on the lateral heat transfer is negligible. Such essentially, because large particles do not respond to turbulent velocity and temperature fluctuations and can not penetrate into the thermal boundary sublayer. Returning to the freeboard analysis it can be shown that for the present investigation the particle size in the splash and dense disengaging zone is such that the effect of the particles is limited. Only higher-up in the freeboard there may be a small increase of the heat transfer. This effect, however, will be neglected, i.e. it is assumed that the particles do not influence the radial (non-radiative) heat transfer at the wall.

For the heat transfer due to forced convection at the inner wall 01 the following correlations quoted in Bird et al. (1960) is used in 'FAME':

$$Nu'_{fc} = 0.026\ Re_D^{0.8}\ Pr_f^{0.33}\ \left(\frac{\eta_g}{\eta_w}\right)^{0.14} \qquad 1.E4 < Re_D < 1.E5 \qquad (4\text{-}87)$$

which may be corrected for the transient boundary layer by means of a multiplication factor:

$$Nu_{fc} = Nu'_{fc}\ \left(1 + \left(\frac{D_{01}}{H_f}\right)^{0.7}\right) \qquad (4\text{-}88)$$

where:

$$Re_D = \frac{\rho_f\ \bar{v}_g\ D_{01}}{\eta_f} \qquad (4\text{-}89)$$

and:

$$Pr_f = \frac{\eta_f\ Cp_f}{\lambda_f} \qquad (4\text{-}90)$$

The heat flux is then given by:

$$\dot{Q}_{cgw,01} = \alpha_{cgw,01}\ A_{w,01}\ (T_g - T_{w,01}) \qquad (4\text{-}91)$$

where:

$$\alpha_{cgw,01} = \frac{Nu_{fc}\ \lambda_f}{D_{01}} \qquad (4\text{-}92)$$

The influence of the contacting of the particles with the wall is not incorporated in the model and neither is any effect of the wall layer.

The net rate of radiation of heat from a non-grey isothermal volume emitter to an isothermal grey wall was discussed in section 4.3.2 and follows from equation (4-1).

$$\dot{Q}_{rvw,01} = \frac{A_{w,01}\ \varepsilon_{w,01}\ \sigma_b\ (\varepsilon_v\ T_v^4 - \alpha_v\ T_{w,01}^4)}{1 - (1-\varepsilon_{w,01})\ (1 - \alpha_v)} \qquad (4\text{-}93)$$

In section 4.3.2 the temperature of the volume emitter was expressed in terms of the gas and the individual particle temperatures. For calculations it is convenient to modify equation (4-93) to the product of characteristic temperature difference and the proportionality factor for the gas as well as for the individual particles. See equations (4-13) through (4-15). This yields:

$$\dot{Q}_{rpw,01} = \dot{Q}_{rgw,01} + \sum_{p=1}^{p=np} \dot{Q}_{rpw,01} \qquad (4\text{-}94)$$

$$\dot{Q}_{rgw,01} = \alpha_{rgw,01}\ A_{w,01}\ (T_g - T_{w,01}) \qquad (4\text{-}95)$$

$$\dot{Q}_{rpw,01} = \alpha_{rpw,01}\ A_{w,01}\ (T_p - T_{w,01}) \qquad (4\text{-}96)$$

where:

$$\alpha_{rgw,01} = \frac{\varepsilon_{w,01}\ \varepsilon_{g+d}\ \sigma_b\ (k_{a,g}\ T_g^4 - k_{e,g}\ T_{w,01}^4)}{(1 - (1-\varepsilon_{w,01})(1-\alpha_{g+d}))\ (T_g - T_{w,01})} \qquad (4\text{-}97)$$

and

$$\alpha_{rpw,01} = \frac{\varepsilon_{w,01}\ \varepsilon_{g+d}\ \sigma_b\ (k_{a,p}\ T_p^4 - k_{e,p}\ T_{w,01}^4)}{(1 - (1-\varepsilon_{w,01})(1-\alpha_{g+d}))\ (T_p - T_{w,01})} \qquad (4\text{-}98)$$

For layers with constant thermal conductivity the heat flux becomes (see f.i. Bird et al. (1960)):

$$\dot{Q}_{c,j} = \alpha_{c,j}\ A_{w,ij}\ (T_{w,ij} - T_{w,jk}) \qquad (4\text{-}99)$$

where:

$$\alpha_{c,j} = \frac{2\ \bar{\lambda}_j}{D_{ij}\ e^{\log(D_{jk}/D_{ij})}} \qquad (4\text{-}100)$$

and where: j = 1, 2, 3 and i = j-1 and k = j+1. As the thermal conductivity of the insulation materials (ceramic and rockwool) are functions of the temperature, determination of a solution of the heat flux becomes time-consuming. A reasonable accurate description of the system is obtained by approximating the true physical situation by a subdivision of the layers. An effective mean thermal conductivity being determined on the basis of a temperature profile in the material.

The net radiation rate from the outer (grey) wall to the surroundings via the transparent air follows from (4-1) and the assumption:

$$\varepsilon_v = \alpha_v = 1 \qquad (4\text{-}101)$$

resulting in:

$$\dot{Q}_{rgw,34} = A_{w,34}\ \varepsilon_{w,34}\ \sigma_b\ (T^4_{w,34} - T^4_s) \qquad (4\text{-}102)$$

Modifying this equation into the product of the characteristic temperature difference and the proportionality factor yields:

$$\dot{Q}_{rgw,34} = \alpha_{rgw,34}\ A_{w,34}\ (T_{w,34} - T_s) \qquad (4\text{-}103)$$

where:

$$\alpha_{rgw,34} = \varepsilon_{w,34}\ \sigma_b\ (T^2_{w,34} + T^2_s)\ (T_{w,34} + T_s) \qquad (4\text{-}104)$$

At the outer freeboard wall the heat is usually transported upward by free convection. Following the work of Börner (1977) the dimensionless quantities for the vertical cilinder are written:

$$Gr_H = \frac{g\ H^3_f\ \beta_s\ (T_{w,34} - T_s)}{\eta_f} \qquad (4\text{-}105)$$

$$Pr_f = \frac{\eta_f\ Cp_f}{\lambda_f} \qquad (4\text{-}106)$$

and the functional relationship Nu = Nu(Gr,Pr) is represented in 'FAME' by:

$$Nu_{nc,H} = 0.8 + 0.1\ (Gr_H\ Pr_f)^{0.33} + 0.3\ (Gr_H\ Pr_f)^{0.25}$$
$$1.E\text{-}4 < (Gr_H\ Pr_f) < 1.E12 \qquad (4\text{-}107)$$

$Nu_{nc,H}$, the Nusselt number of the cilinder, yet independent of its diameter, has to be transformed into the true mean Nusselt number $Nu_{nc,D}$. The functional relationship is:

$$Nu_{nc,D} = Nu_{nc,D}\ (Nu_{nc,H}, H_f\ /\ D_{34}) \qquad (4\text{-}108)$$

and is presented in a graph (Börner (1977)). For computational purposes this graph is represented in 'FAME' by:

$$Nu_{nc,D} = 3.0\ 10^{(0.1\ a_1)} \qquad (4\text{-}109)$$

where:

$$a_1 = a_2 + (11.618 - 0.844\ a_2 + 0.0165\ a^2_2)\ (7.43E\text{-}4 +$$
$$3.47E\text{-}4\ a_3 - 5.21E\text{-}6\ a^2_3 + 2.68E\text{-}8\ a^3_3) \qquad (4\text{-}110)$$

and:

$$a_2 = 10^{\,10\log(Nu_{nc,H}/3.0)} \qquad (4\text{-}111)$$

$$a_3 = H_f \,/\, D_{34} \qquad (4\text{-}112)$$

for: $0 < H_f/D_{34} < 100$, and $3 < Nu_{nc,H} < 300$. The overall heat flux at the outer wall by natural convection is then given by:

$$\dot{Q}_{cgw,34} = \alpha_{cgw,34}\, A_{w,34}\, (T_{w,34} - T_s) \qquad (4\text{-}113)$$

where:

$$\alpha_{cgw,34} = \frac{Nu_{nc,D}\ \lambda_f}{D_{34}} \qquad (4\text{-}114)$$

4.3.4.3 Overall heat flux via the wall

Conservation of energy at the fluid-solid or solid-solid interfaces, according to figure (4-7) implies:

$$\dot{Q}_w = \dot{Q}_{c,1} = \dot{Q}_{c,2} = \dot{Q}_{c,3} = \dot{Q}_{cgw,34} + \dot{Q}_{rgw,34} \qquad (4\text{-}115)$$

The total heat flux via the wall may be found by addition of equations (4-99), (4-103) and (4-113) for $(T_{w,01} - T_s)$, given equation (4-115) the geometrical relation:

$$A_{w,ij} = \pi\, D_{ij}\, h_f \qquad (4\text{-}116)$$

for: $j = 1, 2, 3, 4$ and $i = j - 1$. This yields:

$$\dot{Q}_w = \alpha_w\, A_{w,01}\, (T_{w,01} - T_s) \qquad (4\text{-}117)$$

where:

$$\alpha_w = \frac{1}{\sum_{j=1}^{j=3} \frac{D_{01}}{D_{ij}\,\alpha_{c,j}} + \frac{D_{01}}{D_{34}\,(\alpha_{cgw,34} + \alpha_{rgw,34})}} \qquad (4\text{-}118)$$

and $i = j - 1$.

The problem of finding the heat flux via the freeboard wall of each reactor in series is thus reduced to that of solving:

$$\dot{Q}_w = \dot{Q}_{cgw,01} + \dot{Q}_{rgw,01} + \sum_{p=1}^{p=np} \dot{Q}_{rpw,01} \qquad (4\text{-}119)$$

according to figure 4-9 where:

$$\dot{Q}_w = \alpha_w\, A_{w,01}\, (T_{w,01} - T_s) \qquad (4\text{-}120)$$

$$\dot{Q}_{cgw,01} = \alpha_{cgw,01} A_{w,01} (T_g - T_{w,01}) \qquad (4\text{-}121)$$

$$\dot{Q}_{rgw,01} = \alpha_{rgw,01} A_{w,01} (T_g - T_{w,01}) \qquad (4\text{-}122)$$

$$\dot{Q}_{rpw,01} = \alpha_{rpw,01} A_{w,01} (T_p - T_{w,01}) \qquad (4\text{-}123)$$

The equations (4-119) through (4-123)) are solved in the context of the total freeboard energy balance. See section 4.3.5. A set of ostensibly linear functions of the temperatures T_g, T_p, T_s, and $T_{w,01}$ are realised, in which the alfa' s are weak functions of the temperatures. Therefore the calculation of the heat flux follows an iterative procedure until (usually rapid) convergence.

4.3.5 The freeboard energy balance

4.3.5.1 Introduction

In the freeboard the material balance and the energy balance are tied up, because heat is generated by the reactions.

For analytical purpose the freeboard is divided into a number of compartments in series. For convenience the same subdivision of compartments is taken as in section 3.3.3 for the material balance. The pattern of gas flow in each compartment is a steady state well-mixed flow, the exit fluid stream from this reactor having the same temperature as the fluid within the reactor. In 'FAME' the number of compartments may be selected to yield either:

* the mixed reactor (1 constant flow stirred tank reactor CFSTR),
* the plug flow reactor (infinite number of CFSTR in series),
* the cascade of CFSTR reactors.

The particle trajectory computations in each compartment follow from ballistic considerations for a plug flow of gas (see section 2.3).

For reactor n conservation of energy leads to (see figure 4-10):

$$\dot{Q}_{sg}(n-1) + \sum_{p=1}^{p=np} \dot{Q}_{sp}(m-1) + \dot{Q}_s(n) = \qquad (4\text{-}124)$$

$$\dot{Q}_{sg}(n) + \sum_{p=1}^{p=np} \dot{Q}_{sp}(m) + \dot{Q}_w(n)$$

(m-1) refers to particles that enter reactor n, and m refers to particles that leave reactor n; m covers both types of particle movements: rising and descending. For each particle m can be interpreted as the current variable that indicates the position of the particle in the reactors, as a function of time.

For each compartment the total energy balance can be made up from the interconnected component energy balances of:

* the gas,
* the wall,
* the individual particles.

4.3.5.2 The energy balances of the gas, the wall and the particles

Conservation of energy for the gas in any reactor n implies, after figure 4-11:

$$\dot{Q}_{sg}(n-1) + \sum_{p=1}^{p=np} \dot{Q}_{cpg}(n) + \dot{Q}_{r}(n) = \dot{Q}_{sg}(n) + \dot{Q}_{cgw}(n) + \dot{Q}_{rgw}(n) \qquad (4\text{-}125)$$

Conservation of energy for the wall of any reactor n implies, after figure 4-12:

$$\dot{Q}_{cgw}(n) + \dot{Q}_{rgw}(n) + \sum_{p=1}^{p=np} \dot{Q}_{rpw}(n) = \dot{Q}_{w}(n) \qquad (4\text{-}126)$$

As mentioned before the longitudinal radiation of heat is neglected; anyhow this radiation is much smaller than the convection term. Conservation of energy for each particle that traverses the boundaries of any reactor n per unit of time yields, after figure 4-13a through d:

$$\dot{Q}_{sp}(m-1) = \dot{Q}_{sp}(m) + \dot{Q}_{cpg}(n) + \dot{Q}_{rpw}(n) \qquad (4\text{-}127)$$

4.3.5.3 The heat flow rates in linear expressions of the temperatures

In general the temperature differences in the freeboard are small compared to the temperature level. This permits linearisation of the heat transfer equations in the temperature and subsequent calculation of the separate heat flows by solving a set of simultaneous linear equations.

The enthalpy flow rates with the gas read:

$$\dot{Q}_{sg}(n-1) = A_{f}(n-1)\ \rho_{g}(n-1)\ v_{g}(n-1)\ H_{g}(n-1) \qquad (4\text{-}128)$$

and:

$$\dot{Q}_{sg}(n) = A_{f}(n)\ \rho_{g}(n)\ v_{g}(n)\ H_{g}(n) \qquad (4\text{-}129)$$

The change in enthalpy flow rate with the gas in any reactor is found by substracting equation (4-129) from (4-128). For numerical convenience the heat capacity and the mass flow of the gas are taken constant within in a reactor. Then:

$$\dot{Q}_{sg}(n-1) - \dot{Q}_{sg}(n) = a_{sg}(n)\ T_{g}(n-1) - a_{sg}(n)\ T_{g}(n) \qquad (4\text{-}130)$$

where:

$$a_{sg}(n) = A_{f}(n)\ \rho_{g}(n)\ v_{g}(n)\ Cp_{g}(n) \qquad (4\text{-}131)$$

Because of the steady state assumed the inert solid mass flows entering and leaving any reactor are equal. The associated convective enthalpy flows read:

$$\dot{Q}_{sp}(m-1) = 1\ \rho_{p}(m-1)\ V_{p}(m-1)\ H_{p}(m-1) \qquad (4\text{-}132)$$

and:

$$\dot{Q}_{sp}(m) = 1\ \rho_{p}(m)\ V_{p}(m)\ H_{p}(m) \qquad (4\text{-}133)$$

The change in enthalpy flow rate with the particles is found by substracting (4-133) from (4-132). For numerical convenience the change in enthalpy flow rate is approximated in 'FAME' by:

$$\dot{Q}_{sp}(m-1) - \dot{Q}_{sp}(m) = a_2(n)\, T_p(m-1) - a_2(n)\, T_p(m) \qquad (4\text{-}134)$$

where:

$$a_{sp}(n) = \rho_p(m)\, V_p(m)\, Cp_p(m) \qquad (4\text{-}135)$$

The convective heat transfer rate from the gas to the wall is expressed as (see equation (4-121)):

$$\dot{Q}_{cgw}(n) = a_3(n)\, T_g(n) - a_3(n)\, T_w(n) \qquad (4\text{-}136)$$

where:

$$a_{cgw}(n) = \alpha_{cgw}(n)\, A_w(n) \qquad (4\text{-}137)$$

The net radiative heat flow rate from the gas to the wall is given by a pseudo heat transfer coefficient and a characteristic temperature difference (see equation (4-122)):

$$\dot{Q}_{rgw}(n) = a_4(n)\, T_g(n) - a_4(n)\, T_w(n) \qquad (4\text{-}138)$$

where:

$$a_{rgw}(n) = \alpha_{rgw}(n)\, A_w(n) \qquad (4\text{-}139)$$

The convective heat transfer rate from the particle to the gas for each particle traversing the reactor boundary per unit of time (see equation (4-85)) leads to:

$$\dot{Q}_{cpg}(n) = a_{cpg1}(n)\, T_p(m-1) + a_{cpg2}(n)\, T_g(n) + a_{cpg3}(n)\, T_w(n) \qquad (4\text{-}140)$$

where:

$$a_{cpg1}(n) = \frac{\alpha_{cpg}(m-1)}{\alpha_{cpg}(m-1) + \alpha_{rpw}(m-1)} \qquad (4\text{-}141)$$

$$(\rho_p(m)\, Cp_p(m)\, V_p(m)\, (1-\bar{\theta}_p(n)))$$

$$a_{cpg2}(n) = \frac{\alpha^2_{cpg}(m-1)}{\alpha_{cpg}(m-1) + \alpha_{rpw}(m-1)} \qquad (4\text{-}142)$$

$$\left(\frac{-\rho_p(m)\, Cp_p(m)\, V_p(m)\, (1-\bar{\theta}_p(n))}{\alpha_{cpg}(m-1) + \alpha_{rpw}(m-1)} - \frac{\alpha_{rpw}(m-1)}{\alpha_{cpg}(m-1)}\, A_p(n)\, t_p(n)\right)$$

$$a_{cpg3}(n) = \frac{\alpha_{cpg}(m-1)\ \alpha_{rpw}(m-1)}{\alpha_{cpg}(m-1) + \alpha_{rpw}(m-1)} \qquad (4\text{-}143)$$

$$\left(\frac{-\rho_p(m)\ Cp_p(m)\ V_p(m)\ (1-\bar{\theta}_p(n))}{\alpha_{cpg}(m-1) + \alpha_{rpw}(m-1)} + A_p(n)\ t_p(n)\right)$$

The pseudo heat transfer relation of (4-86) leads to an analogous expression for the net radiative heat flow rate from the solids to the wall:

$$\dot{Q}_{rpw}(n) = a_{rpw1}\ T_p(m-1) + a_{rpw2}\ T_g(n) + a_{rpw3}\ T_w(n) \qquad (4\text{-}144)$$

where:

$$a_{rpw1}(n) = \frac{\alpha_{rpw}(m-1)}{\alpha_{cpg}(m-1) + \alpha_{rpw}(m-1)} \qquad (4\text{-}145)$$

$$(\rho_p(m)\ Cp_p(m)\ V_p(m)\ (1-\bar{\theta}_p(n)))$$

$$a_{rpw2}(n) = \frac{\alpha_{cpg}(m-1)\ \alpha_{rpw}(m-1)}{\alpha_{cpg}(m-1) + \alpha_{rpw}(m-1)} \qquad (4\text{-}146)$$

$$\left(\frac{-\rho_p(m)\ Cp_p(m)\ V_p(m)\ (1-\bar{\theta}_p(n))}{\alpha_{cpg}(m-1) + \alpha_{rpw}(m-1)} + A_p(n)\ t_p(n)\right)$$

$$a_{rpw3}(n) = \frac{\alpha^2_{rpw}(m-1)}{\alpha_{cpg}(m-1) + \alpha_{rpw}(m-1)} \qquad (4\text{-}147)$$

$$\left(\frac{-\rho_p(m)\ Cp_p(m)\ V_p(m)\ (1-\bar{\theta}_p(n))}{\alpha_{cpg}(m-1) + \alpha_{rpw}(m-1)} - \frac{\alpha_{cpg}(m-1)}{\alpha_{rpw}(m-1)}\ A_p(n)\ t_p(n)\right)$$

Note that the right hand sides of equations (4-143) and (4-146) are identical. The source of heat in the reactor is defined as:

$$\dot{Q}_s(n) = \dot{Q}_r(n) + \dot{Q}_{sp}(n) \qquad (4\text{-}148)$$

where the heat flow rate due to reaction is defined as (see section 3.3.3):

$$\dot{Q}_r(n) = \dot{Q}_{r,co}(n) + \sum_{p=1}^{p=nc} \dot{Q}_{r,p}(n) \qquad (4\text{-}149)$$

and for the convective heat flow rate with the char particles:

$$\dot{Q}_{sp}(n) = \sum_{p=1}^{p=nc} \dot{Q}_{sp}(m-1) - \sum_{p=1}^{p=nc} \dot{Q}_{sp}(m) \qquad (4\text{-}150)$$

In (4-150) the heat flow rates are defined by (4-135) and the steady state (equilibrium) temperatures are calculated according to equation (3-24). The heat flow rate at the outer reactor wall to the surroundings is, according equation (4-120), expressed as:

$$\dot{Q}_w(n) = a_w(n)\ (T_w(n) - T_s(n)) \qquad (4\text{-}151)$$

where:

$$a_w(n) = \alpha_w(n)\ A_w(n) \qquad (4\text{-}152)$$

4.3.5.4 Formation of a set of simultaneous linear equations

For each reactor substituting equations (4-130), (4-136), (4-138) and (4-140) into (4-125) results in:

$$\begin{aligned} & a_{sg}(n)\ T_g(n-1) \\ & + (-a_{sg}(n) - a_{cgw}(n) - a_{rgw}(n) + \sum_{p=1}^{p=np} a_{cpg2}(n))\ T_g(n) \\ & + (a_{cgw}(n) + a_{rgw}(n) + \sum_{p=1}^{p=np} a_{cpg3}(n))\ T_w(n) \\ & + (\sum_{p=1}^{p=np} a_{cpg1}(n)\ T_p(m-1)) = \dot{Q}_s(n) \end{aligned} \qquad (4\text{-}153)$$

For each reactor substituting equations (4-136), (4-138), (4-144) and (4-152) into (4-126) leads to:

$$\begin{aligned} & (a_{cgw}(n) + a_{rgw}(n) + \sum_{p=1}^{p=np} a_{rpw2}(n))\ T_g(n) \\ & + (-a_{cgw}(n) - a_{rgw}(n) + \sum_{p=1}^{p=np} a_{rpw3}(n) - a_w(n))\ T_w(n) \\ & + (\sum_{p=1}^{p=np} a_{rpw1}(n)\ T_p(m-1)) = -a_w(n)\ T_s(n) \end{aligned} \qquad (4\text{-}154)$$

The temperature T_s in the right hand side of (4-154) is a boundary condition. For each particle traversing the reactor n substitution of equations (4-134), (4-140) and (4-144) into (4-127) leads to:

$$\begin{aligned} & (-a_{cpg2}(n) - a_{rpw2}(n))\ T_g(n) + (-a_{cpg3}(n) - a_{rpw3}(n))\ T_w(n) \\ & + \sum_{p=1}^{p=np} ((a_{sp}(n) - a_{cpg1}(n) - a_{rpw1}(n))\ T_p(m-1)) \\ & + \sum_{p=1}^{p=np} (-a_{sp}(n)\ T_p(n)) = 0 \end{aligned} \qquad (4\text{-}155)$$

The boundary conditions of the gas and all the particles entering the first freeboard reactor read:

$$T_g(0) = T_{bed} \qquad (4\text{-}156)$$

and:

$$T_p(0) = T_{bed} \qquad (4\text{-}157)$$

For N reactors in series 2N+1 temperatures have to be solved:

$$T_g(0),\ T_g(1),\ \ldots\ldots\ldots,\ T_g(N)$$
$$T_w(1),\ T_w(2),\ \ldots\ldots\ldots,\ T_w(N)$$

For one particle traversing M reactors, M+1 temperatures have to be solved:

$$T_p(0),\ T_p(1),\ \ldots\ldots\ldots,\ T_p(M)$$

The number of equations is:
- N for the gas volume
- N for the wall
- 1 boundary condition for the the gas at the bed surface
- M for each particle traversing M reactors
- 1 for each particle at the fluidized bed surface

It can be shown that for all particle and reactor numbers the number of equations and unknowns equals. Therefore this system of simultaneous linear equations can be solved by Gauss elimination, as implemented in 'FAME'.

4.4 Model predictions and verification

4.4.1 Introduction

In this section model predictions and experimental results on firing anthracite in the 'MAGMA' (Martens (1984)) are compared. Attention focusses on the heat economy. The input values, respectively results concerning particle trajectories can be found in section 2.4 and results concerning the chemical conversions in section 3.4. In addition to table 2-3 and 3-7 further boundary conditions and physical properties are listed in table 4-1. All physical properties not mentioned are calculated according to appendix 1. Regarding the heat economy two cases will be treated:

1) The full model trial, i.e. the chemical heat release along the freeboard as calculated according to section 3.4 (resulting in figure 4-14).
2) The model trial without chemical heat release but with a source of heat along the freeboard as determined from the chemical conversions found in the experiment (see figure 4-14 or 4-2).

The differences between the two cases mainly result from:
* The overprediction of the chemical heat release by char combustion in the lower 0.5 m of the freeboard.
* The underprediction of the chemical heat release, presumably from char combustion, above a height of 1 m upto 1.5 m.
* The overprediction of the chemical heat release from char combustion and CO-oxidation above a height of 2 m.

The model result of both cases is only slightly affected by the input data of the chemical heat release. Therefore only case 1 is treated in more detail. For case 2 only the overall freeboard energy balance and the temperature profiles of the gas and the wall will be presented.

4.4.2 Radiative emissivity

The calculated radiative emissivity of the gas-particle cloud is shown in figure 4-15. The ratio of gas to total emissivity is visualized in figure 4-16. In the splash-zone and the beginning of the dense disengaging zone the total emissivity is almost 1 (the maximum theoretically possible) and the contribution of the gas to the total emissivity is negligible. The process of particle disengagement (see figure 2-12) leads to a decrease of

particle volume fraction (see figure 2-13) and hence to a decrease in particle cloud emissivity. Therefore the total emissivity decreases with height, and the emissivity ratio shifts from the regime ruled by the particle holdup to the regime ruled by the gas species components. At freeboard heights above 1.25 m the entrainment becomes uniform. The total emissivity attains a value of 0.12 and the emissivity is ruled by the gas (emissivity ratio 72%). In this connection it should be noted that the model overpredicts the entrainment; so the gas may even be more dominant than calculated.

4.4.3 Heat transfer via the freeboard wall

Results on heat transfer coefficients and characteristic temperature differences are visualized in figures 4-17 and 4-18. In the splash and the dense disengaging zone the overall radiative particle-wall (pseudo) heat transfer coefficient is highest and the characteristic temperature difference lowest. Along the freeboard the particle wall heat transfer coefficient gradually decreases by somewhat more than one order of magnitude, to become uniform when the entrainment becomes constant as confirmed by the emissivity curve. The characteristic temperature difference increases by somewhat less than one order of magnitude. The radiative gas-wall heat transfer coefficient is lowest in the splash zone (lowest emissivity ratio, less transparency), increases in the disengaging zones (increasing emissivity ratio), to become constant when the entrainment (figure 2-12) becomes constant. The characteristic temperature difference between gas and wall and particles and wall develop similarly along the freeboard with height. The temperature difference between the gas and the particle cloud for case 2 is not negligibly small. One of the assumptions of the model concerns the quasi isothermal gas particle cloud and implies actually no particle-gas or particle-particle net heat fluxes. So the freeboard gas may exchange a net radiative flux of heat with the particles. Consequently the particles will experience more heat-up and the gas temperature will be lower than calculated. The heat transfer coefficient for forced convection is small compared to the total heat transfer coefficient. The heat transfer coefficient in the first freeboard region is highest because of the transient thermal boundary layer (equation (4-88)).

4.4.4 Particle trajectories and heat transfer

From figure 4-19, showing the history for some particles, it can be concluded that the convective heat transfer is of overall importance and more so for the smallest particles than for the larger. Although small, the radiative heat transfer coefficient increases in the higher freeboard regimes (above 0.5 m) for all sizes, as the particle cloud becomes more transparent there. The dimensionless particle temperature differs strongly for the particles considered; small particles rapidly attain gas temperature, while for the larger particles the dimensionless time is too short to lead to considerable temperature increase. See figure 4-20a and b. Although the temperature increase is not spectacular the large particle fluxes result in large enthalpy flows and largely suppress any temperature increase due to chemical reactions. This is born out by the energy balance.

4.4.5 Overall freeboard energy balance

The model calculations lead to the following overall freeboard energy balances:

	case 1	case 2
net downward enthalpy flow with rising - descending particles:	69.1%	54.4%
net enthalpy flow with elutriated particles:	0.9%	1.4%
net enthalpy flow increase with the gas:	10.7%	16.4%
heat loss via the freeboard wall:	19.3%	27.8%
	+	+
total chemical heat release in the freeboard:	100.%	100.%
or in W/m2:	1.67E4	1.10E4
The adiabatic gas temperature increase without particles would be:	344 K	245 K

4.4.6 Comparison of temperature profiles

Temperature profiles resulting from the experiment and the model calculations, case 1 and 2, are visualized in figure 4-21. The gas temperature in the freeboard increases for the experimental result by maximally 33 K and for the model result, case 1 by 36 K, and case 2 by 58 K, respectively. The agreement of the various results is promising. This in view of the following:

* For case 1 the agreement is excellent except for the overestimation of the gas and wall temperatures higher-up in the freeboard. The over-estimation is due to the overprediction of the chemical heat release there.
* For case 2 the difference between the actual and numerical determined gas temperature is maximally 35 K which is 15% of the maximal temperature increase of the gas in an adiabatic system. The model possibly underestimates the net enthalpy recycle rate to the bed by 15% of the total heat released. The gas and wall temperature profiles of the experiment and the model develop similarly with height.
* Many uncertainties exist on the true value at the boundaries of the system.
* The lateral and time dependent effects of gas species concentrations and particle fluxes are neglected.
* Particle-particle and particle-gas radiation is neglected.

4.5 Conclusions and recommendations

1) At large freeboard heights, above 1.75 m in the 'MAGMA', the heat flux via the freeboard wall exceeds the heat generated by chemical reaction. The contribution to the heat flux from the entrained particles may be neglected as the ratio of solids mass flow and gas mass flow is low (< 0.1). Below this level the chemical heat release exceeds the heat flow via the freeboard wall (2.5E3 W/(m2.layer)). The ascending particle flux is cold (relative to the gas) and these particles heat up. The reverting and descending particles continue exchanging heat with the gas. They may heat-up or cool-down depending on particle history, size, residence time, etc.

2) The intermediate region, 0.5 - 1.5 m in the 'MAGMA', is typified as a dilute particle disengagement zone. The solid fluxes are not sufficient to prevent the freeboard gas temperature from rising considerably. The temperature increase in this region is sensitive to the chemical heat release, to the solids fluxes and thereby sensitive to the initial particle velocity distribution.

3) At small freeboard heights, 0 - 0.5 m in the 'MAGMA', the particle mass fluxes are large (splash zone, dense disengaging zone). There the chemical heat release is almost completely consumed by particles finally returning to the fluidized bed.

4) In general the heat economy in the splash-zone and the dense disengaging zone is governed by the solids. The effect of any source or sink of heat will be reduced. This should also apply to the effect of a heat exchanger inside the freeboard, unless it would limit the particles' penetration.

5) The conclusions just mentioned follow from experiment and calculations for just a few cases. The semi-quantitative agreement between experiments and predictions justify some confidence in more general validity of 'FAME'.

4.6 List of symbols

A	surface area	m2
a	thermal diffusivity	m2/s
a_1	variable defined in equation (4-110)	-
a_2	variable defined in equation (4-111)	-
a_3	variable defined in equation (4-112)	-
a_i	coefficient	W/K
Bi	Biot number	-
b	selfbroadening coefficient	-
Cp	heat capacity at constant pressure	J/(kg.K)
c	speed of light	m/s
c1	coefficient	W/(m2.K)
c2	coefficient	W/m2
c3	coefficient	W/K4
c4	coefficient	W/K4
D	diameter	m
d	particle diameter	m
e	2.71828	-
f	multiplication factor for scattering	-
Gr	Grashof number	-
g	gravitational acceleration	m/s2
H	enthalpy	J/kg
	total characteristic (freeboard) height	m
h	Plancks' constant	m.K
	height	m
I	intensity of radiation	W/m2
i	gas component	-
k	coefficient of absorption and emission	1/m
k_b	Boltzmann constant	J/K
L	optical thickness	m
M	total number of transitions of a particle in the reactors	-
m	position of particle at reactor boundary	-
N	total number of reactors	-
Nu	Nusselt number	-
n	reactor number or boundary of reactor	-
	particle number density	1/m3
	exponent in (4-35)	-
$P_{e,i}$	partial pressure parameter def. by (4-34)	-
P	absolute pressure	Pa
Pr	Prandtl number	-
p	dimensionless number defined by eq. (4-30)	-
Q	energy flow	J

$\dot{Q}$	net rate of heat transport	J
R	rate of efficiency factor for scattering to	
	efficiency factor for absorption	-
	radius of sphere	m
r	radial distance in spherical coardinates	m
Re	Reynolds number	-
s	coefficient of scattering	-
s/d	mean line intensity to line spacing ratio	m2/kg
T	temperature	K
$\overline{T}$	calorific mean temperature	K
t	time	s
u	dimensionless number defined by eq. (4-37)	-
V	volume	m3
v	velocity	m/s

GREEK SYMBOLS

α	absorptivity	-
	integrated band intensity	m/kg
	heat transfer coefficient	W/(m2.K)
β	line width parameter	-
β	thermal coeff. of volumetric expansion	1/K
ε	emissivity	-
η	viscosity	kg/(m.s)
λ_r	wavelength of electromagnetic radiation	m
λ	thermal conductivity	W/(m.K)
ν	wave number	1/m
π	3.14159	-
ρ	density	kg/m3
σ_b	Stefan Boltzmann constant	W/(m2.K4)
σ	factor defined by eq. (4-29)	-
∇	nabla operator	
Θ	dimensionless temperature	-
$\overline{\Theta}$	calorific mean dimensionless temperature	-
τ	Fourier number	-
ω	band with parameter	-
ξ	dimensionless radial coordinate	-

SUBSCRIPTS

1	1st term
2	2nd term
3	3rd term
a	absorption
c	conduction
co	CO combustion
cp	conduction in particle
cr	chemical reaction
cgw	convection gas to wall
cpg	convection from particle to gas
D	diameter
d	dust
e	emission
f	freeboard
	mean physical properties in the gasfilm
fc	forced convection
g	gas
g+d	combined gas and particles (dust)

H total freeboard height
i general summation index
j general summation index
k general summation index
l lower wavenumber
mix mixture of gas species
nb total number of absorption bands involved
nc total number of char particles involved
natural convection
ng total number of gas species involved
np total number of particles involved
ns non-scattering
o reference
p particle
r chemical reaction
rgw radiation gas to wall
rpw radiation particle to wall
rvw radiation volume to wall
s surrounding
source
sc scattering
sg convective heat flow with the gas
sp convective heat flow with the particle
source of particle
tot total (see equation (5-22))
u upper wavenumber
v volume
volume emitter
w wall
ν wavenumber
∞ limit at a long time (see equation (5-21)
0,1 quantity evaluated at section "0", "1", etc.
01 quantity evaluated at the transition of section "0" to section "1", etc.

OVERLINES

- average value

4.7 References

Biermann, P., und Vortmeyer, D.
Wärmestrahlung staubhaltiger Gase.
Wärme- und Stoffübertragung, 2, pp. 193/202 (1969).

Bird, R.B., Stewart, W.E., Lightfoot, E.N.
Transport phenomena.
Wiley International Edition, New York (1960).

Börner, H.
Konvektiver Wärme-übertragung bei freier laminarer und turbulenter Strömung an senkrechten Wänden und waagerechten Zylindern.
VDI-Wärmeatlas, 3. Auflage, pp.Fa1/3.
VDI-Verlag, Düsseldorf, BRD (1977).

Czerney, M. and Walther, A.
Tables of the fractional functions for the Planck radiation law.
Springer, Berlin (1961).

Edwards, D.K. and Balakrishnan, A.
Thermal radiation by combustion gases.
J. of Heat and Mass Transfer, Vol. 16, pp. 25/40 (1973).

Field, M.A., Gill, D.W., Morgan, B.B., Hawksley, P.G.W.
Combustion of pulverised coal.
The British Coal Utilisation Research Association.
Leatherhead, UK (1967).

Hines, W.S. and Edwards, D.K.
Infrared absorptivities of mixtures of carbon dioxide and water vapour.
Chemical Engineering Prog. Symp. Series 64, pp. 173/180 (1968).

Hoogendoorn, C.J.
Warmteoverdracht door straling.
Syllabus bij Kollege C-51, Technische Natuurkunde.
Technische Hogeschool Delft.
Delft (1979).

Hottel, H.C. and Sarofim, A.F.
Radiative transfer.
McGraw-Hill, New York (1969).

Hulst, Van de H.C.
Light scattering by small particles.
Wiley and Sons (1957).

Martens, F.J.A.
Experiments with the atmospheric fluidized bed combustor 'MAGMA'.
Rapport EV-1333, Laboratory for Thermal Power Engineering.
Delft University of Technology, Delft, The Netherlands (1984).

Martin, H.
Instationäre Wärmeleitung in ruhenden Körpern.
VDI-Wärmeatlas, 4. Auflage, pp. Ec1/20.
VDI-Verlag, Düsseldorf, BRD (1984).

Stockburger, D.
Der Wärmeaustausch zwischen einer Rohrwand und einem turbulent strömenden Gas-Feststoff Gemisch (Flugstaub).
VDI-Forschungsheft 518.
VDI-Verlag, Düsseldorf, BRD (1966).

Venema, E.K.
Fluide bed verbranding onder druk: Warmtewisselaar ontwerp aspecten, Warmteoverdracht in bed en freeboard.
Rapport EV-1218, Technische Hogeschool Delft.
Delft (1981).

Vortmeyer, D.
VDI-Wärmeatlas, 3. Auflage, pp. Kc1/11.
VDI-Verlag, Düsseldorf, BRD (1977).

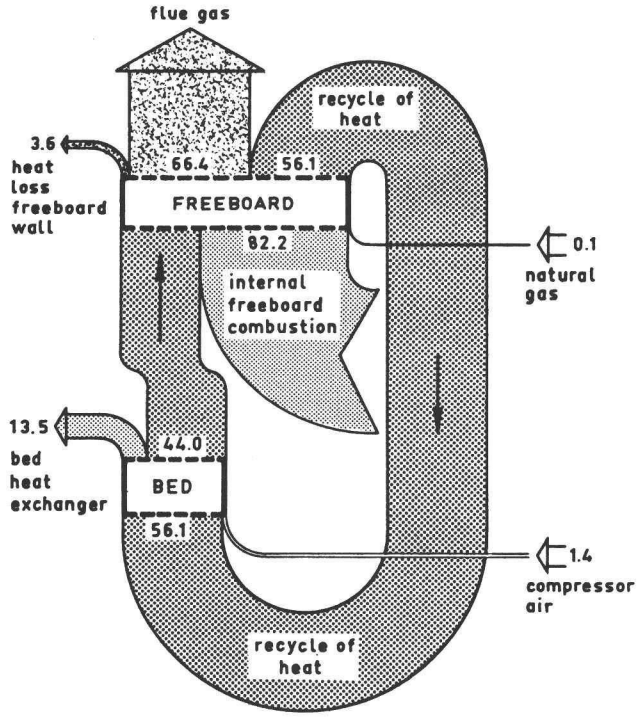

Figure 4-1.
Global energy balance of the freeboard (fuel: natural gas; after Martens and Van Koppen (1983)). Numbers in kW.

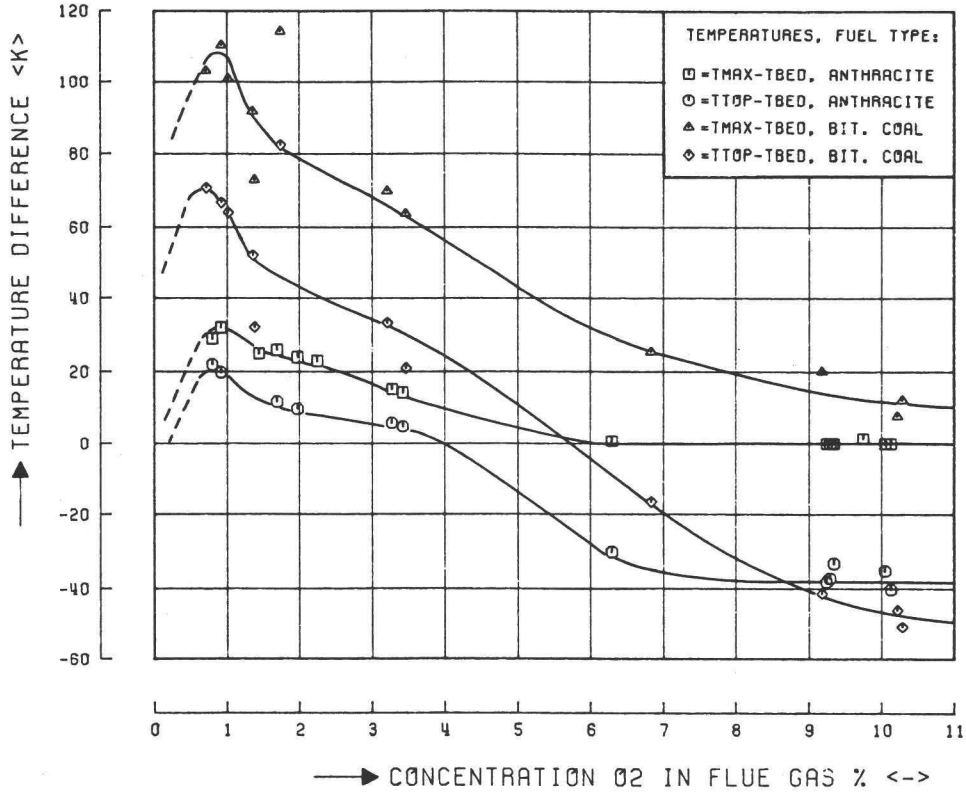

Figure 4-2.
Temperature increase in the freeboard as a function of flue gas oxygen concentration (from Martens (1984)).

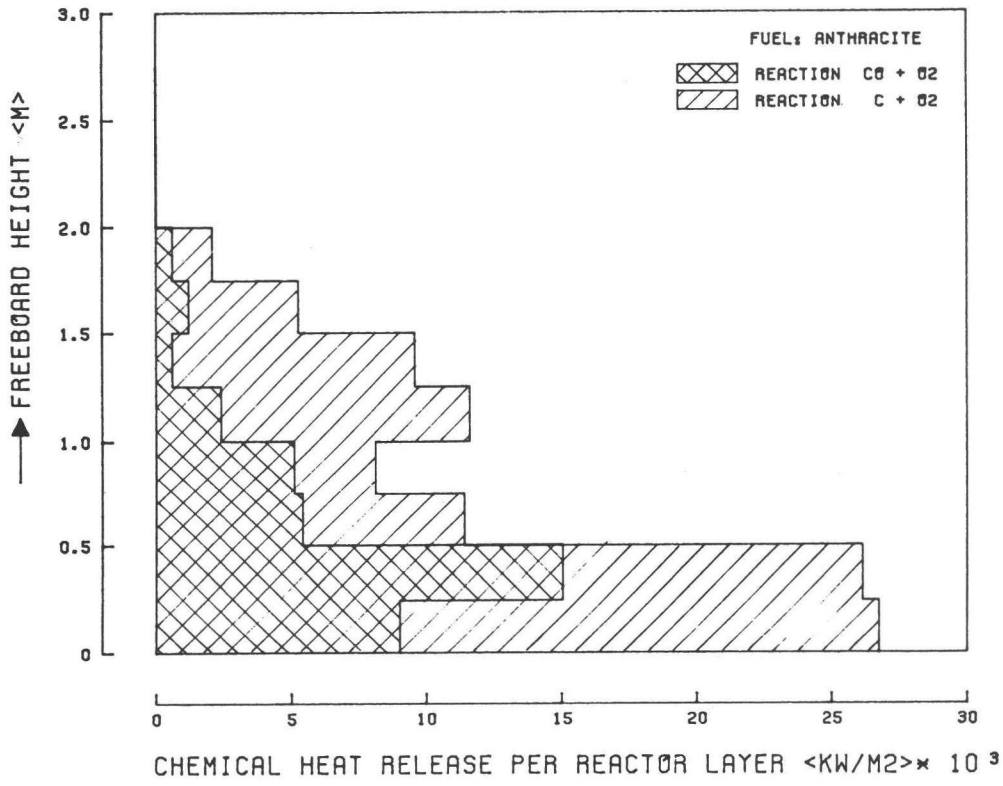

Figure 4-3.
Chemical heat release in the freeboard as a function of height (fuel: anthracite; after Martens (1984)). Depth of each reactor layer 0.25 m.

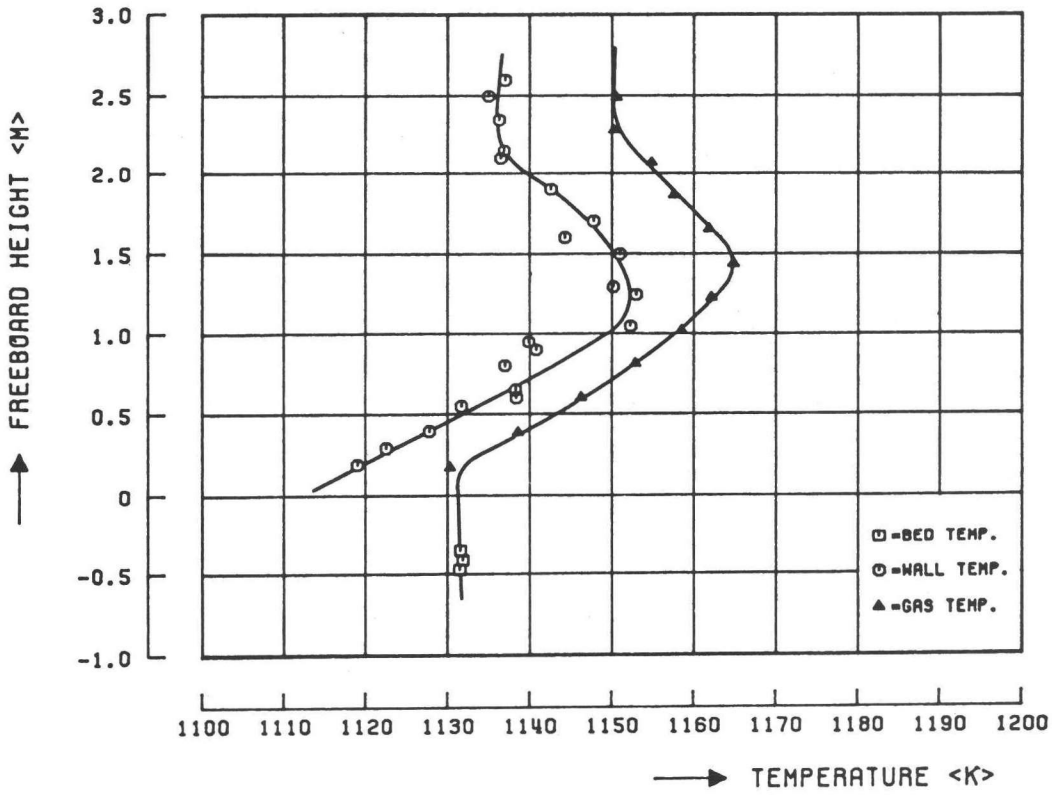

Figure 4-4.
Gas and wall temperatures as a function of freeboard height (fuel: anthracite; after Martens and Van Koppen (1983)).

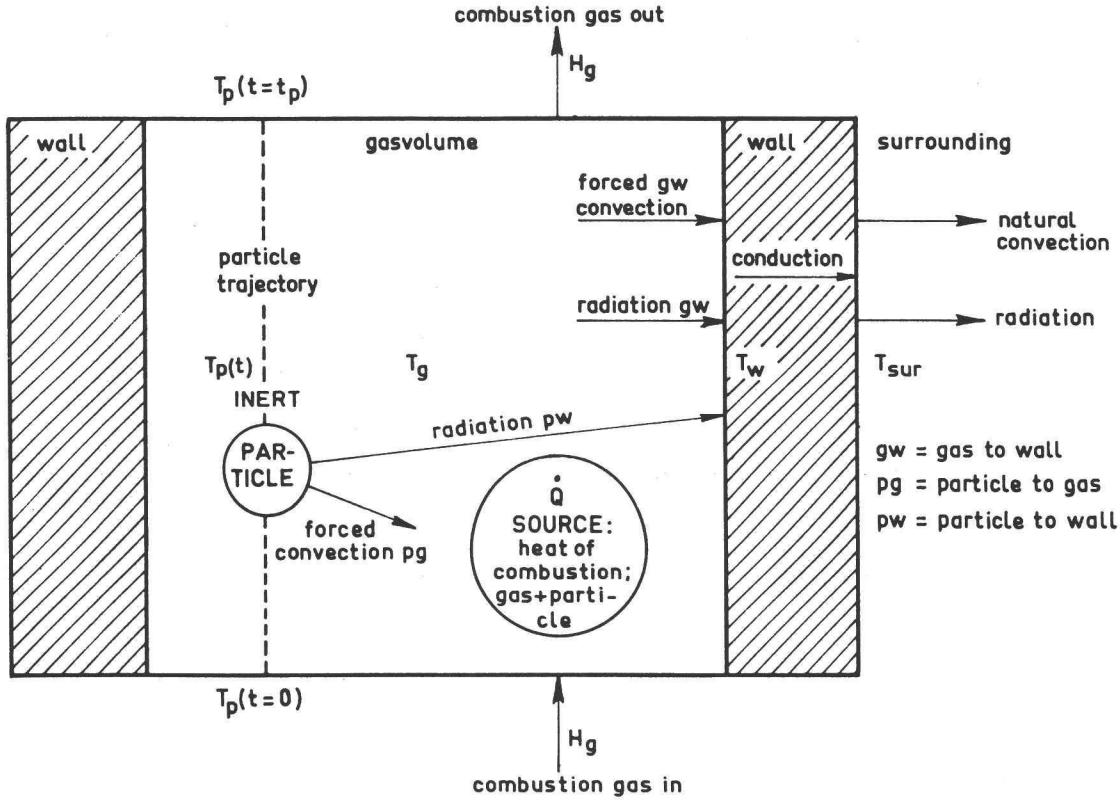

Figure 4-5.
Model of the heat economy in a freeboard compartment.

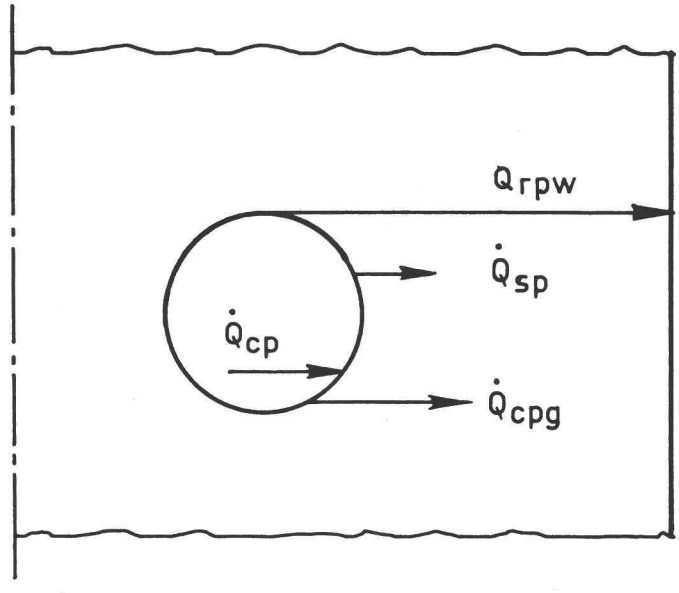

Figure 4-6.
Heat flows at the surface of a particle.

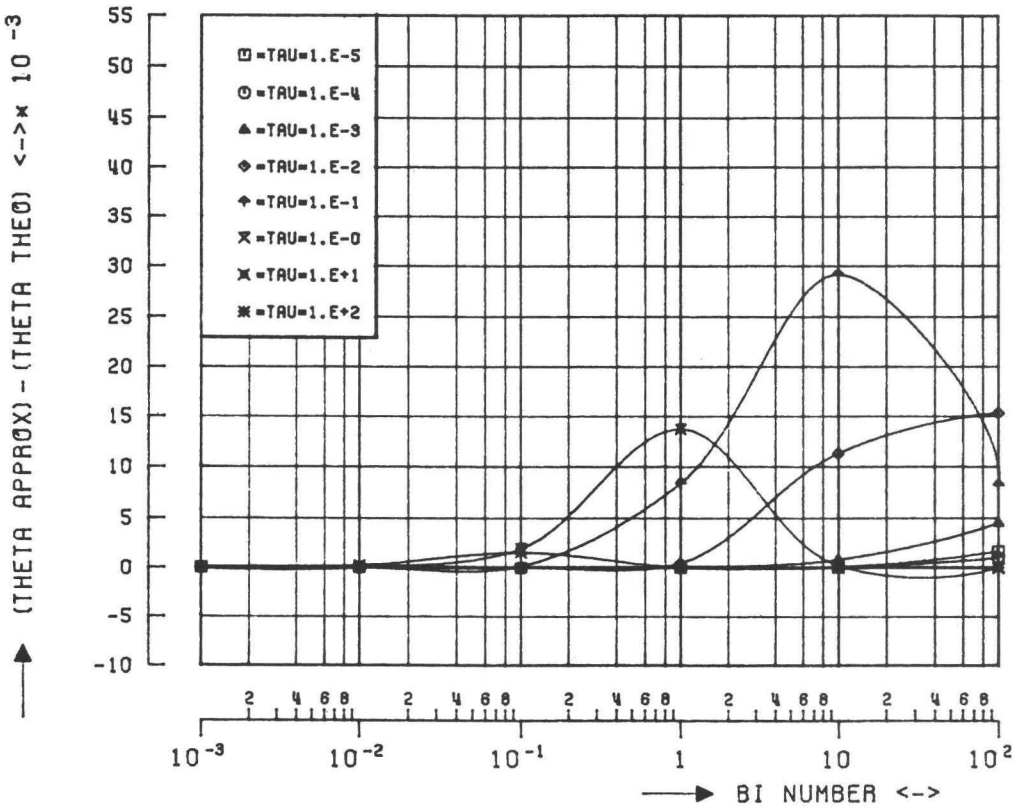

Figure 4-7.
The absolute difference between approximated and theoretical dimensionless mean particle temperature as a function of Biot number and limited τ - range.

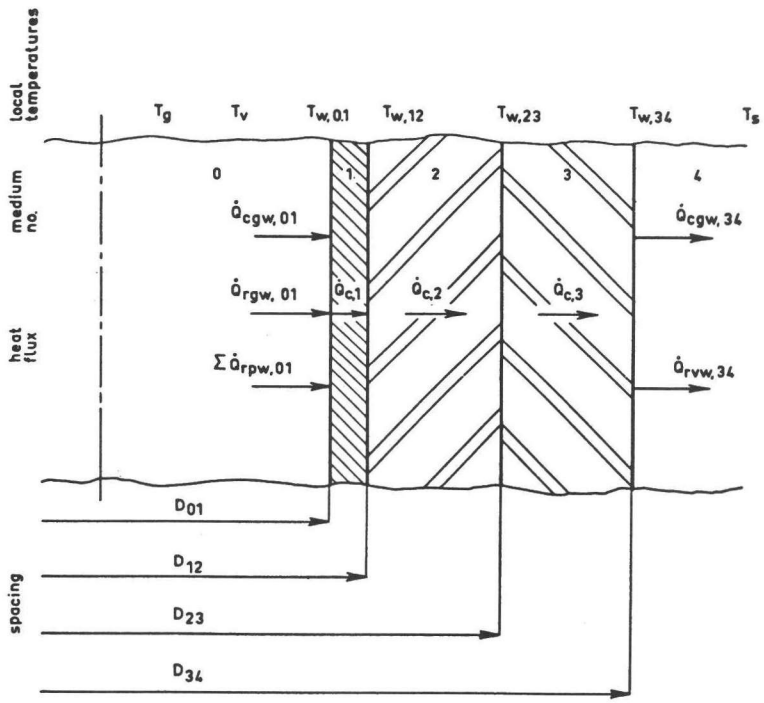

Figure 4-8.
Heat flux via the composite freeboard wall.

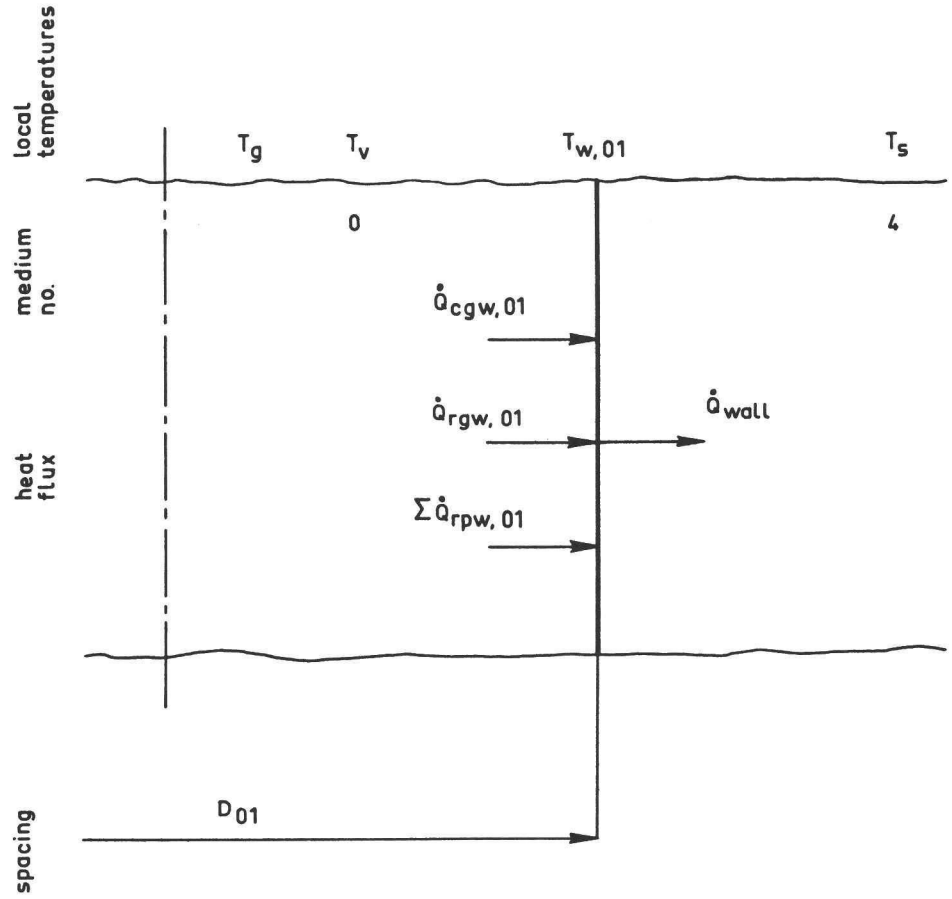

Figure 4-9.
Simplified representation of the heat flux via the freeboard wall.

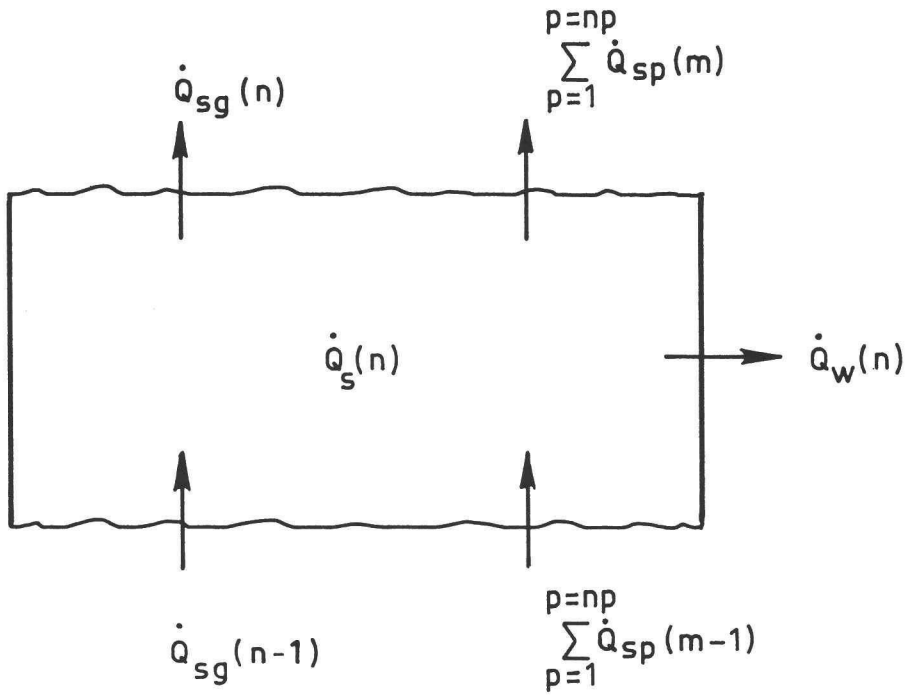

Figure 4-10.
The overall compartment energy balance.

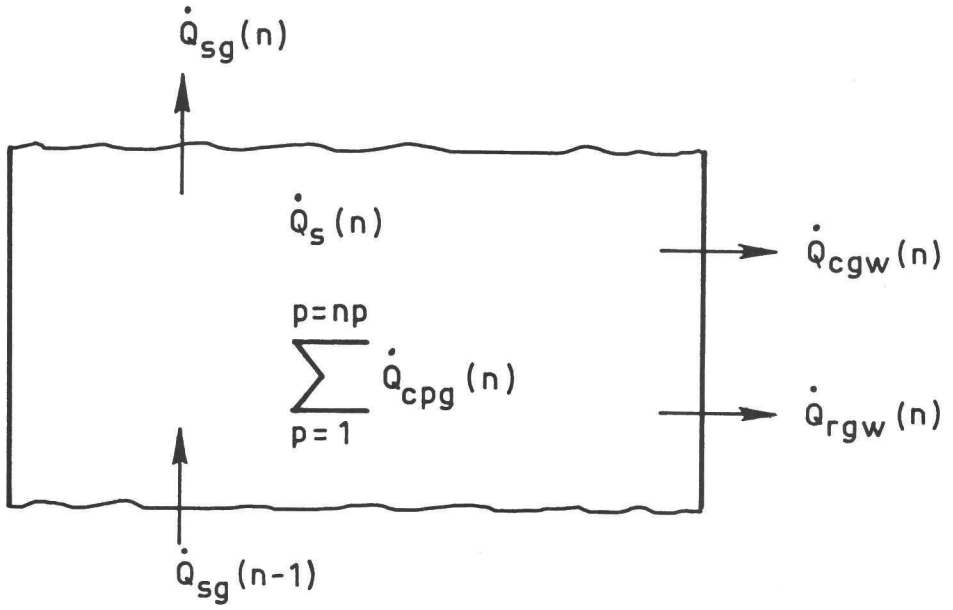

Figure 4-11.
The energy balance of the gasvolume.

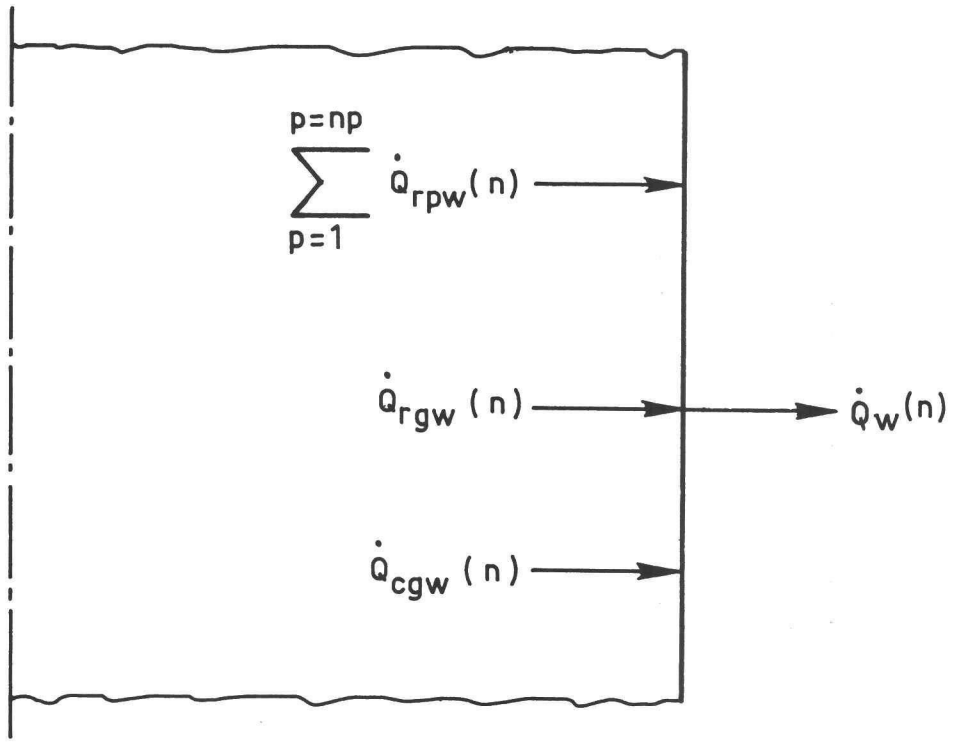

Figure 4-12.
The energy balance of the reactor wall.

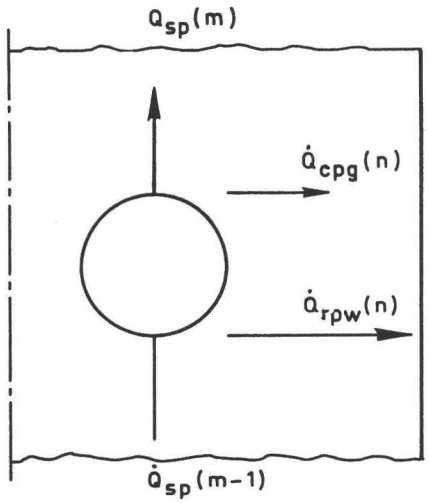

a) continously rising particle

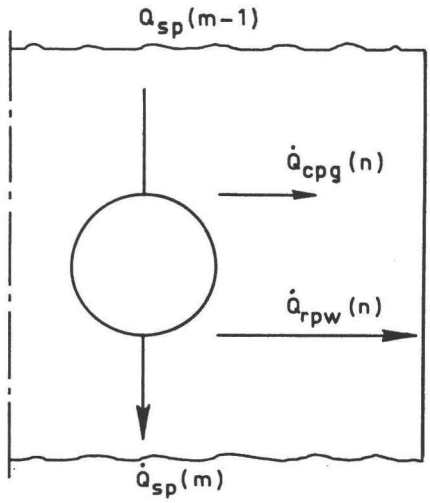

b) continuously descending particle

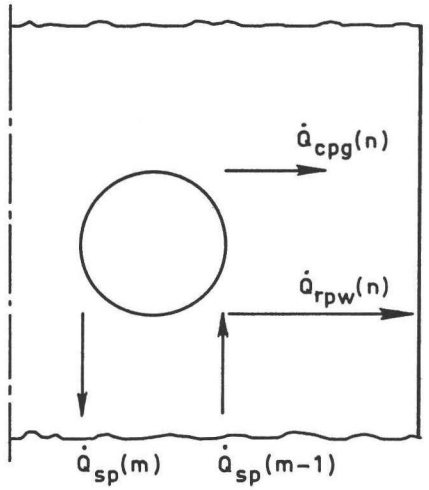

c) initially rising and
finally descending particle

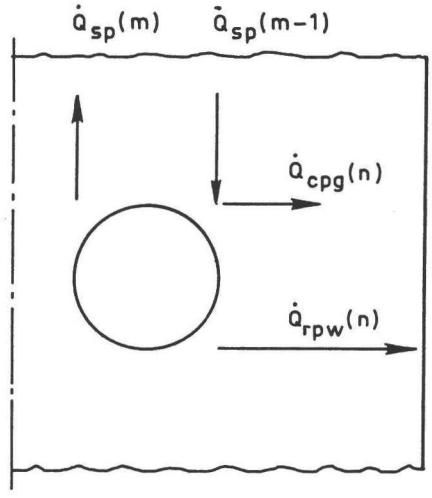

d) initially descending and
finally rising particle

Figure 4-13.
The energy balance of a particle.

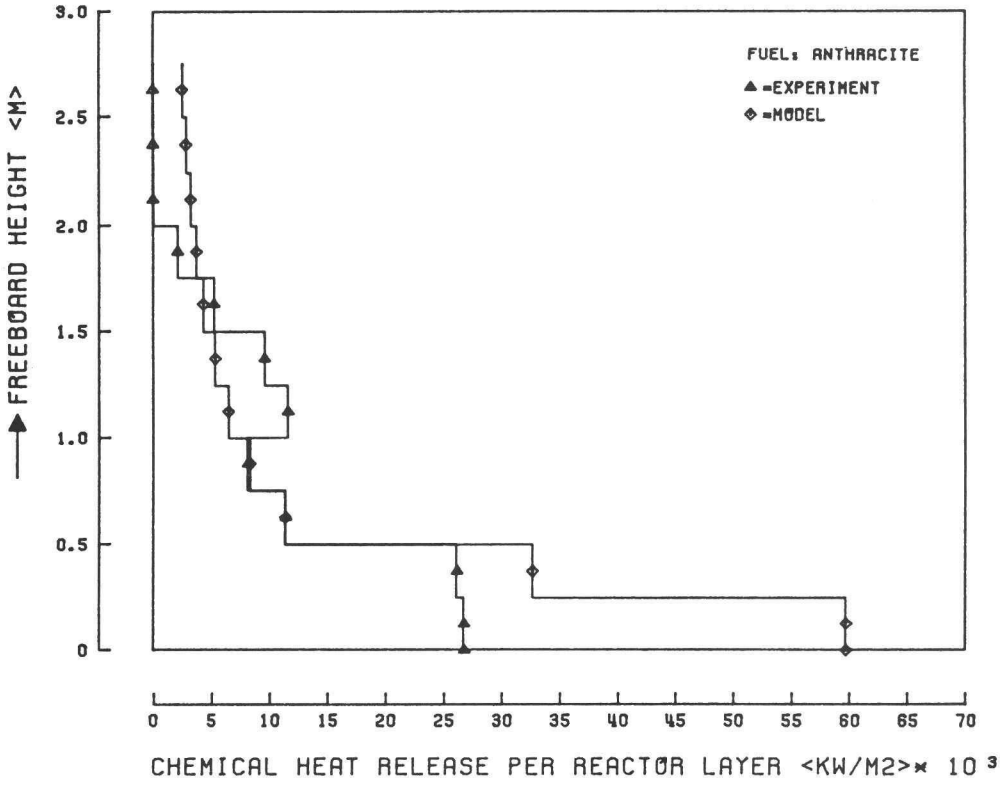

Figure 4-14.
Chemical heat release in the freeboard as a function of height (model and experiment). Depth of each reactor layer is 0.25 m.

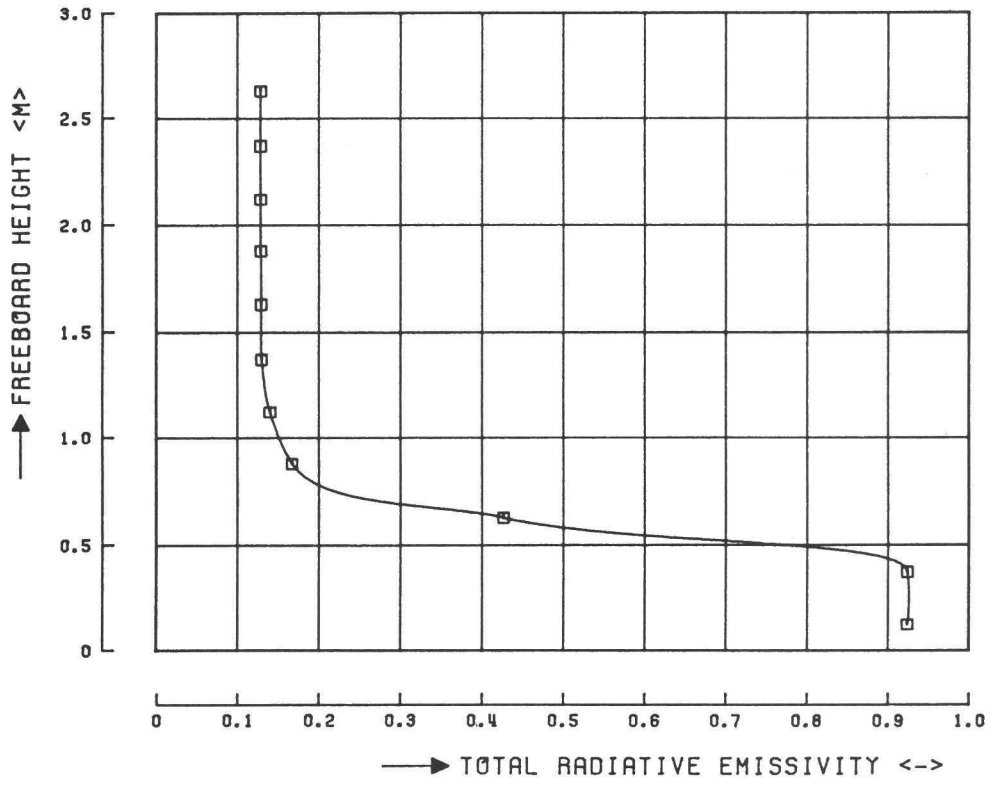

Figure 4-15.
Radiative emissivity of the (total) gas-particle cloud as a function of freeboard height.

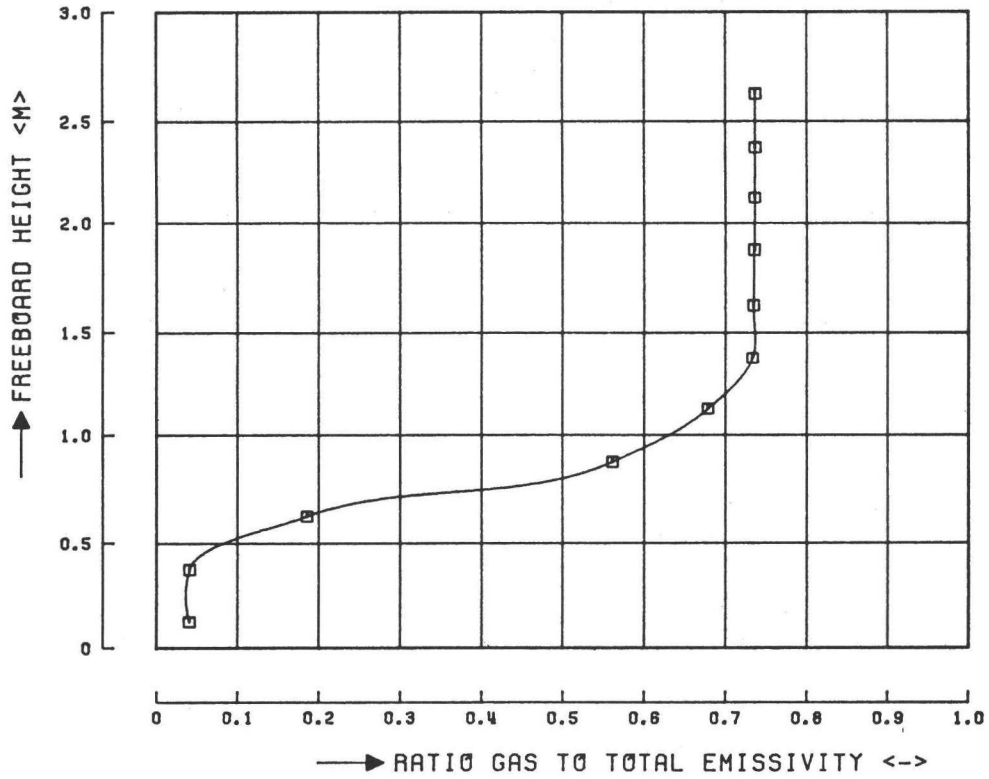
FREEBOARD HEIGHT <M>
3.0
2.5
2.0
1.5
1.0
0.5
0
0 0.1 0.2 0.3 0.4 0.5 0.6 0.7 0.8 0.9 1.0
RATIO GAS TO TOTAL EMISSIVITY <->
Figure 4-16.
Ratio of gas to total emissivity as a function of freeboard height.

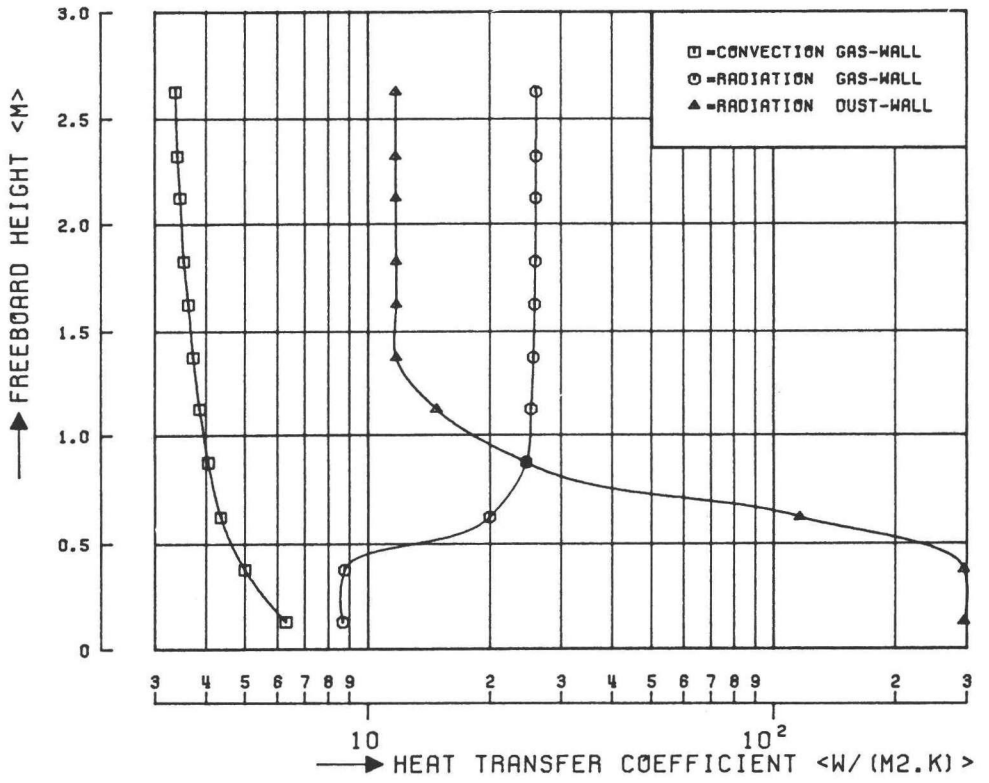
FREEBOARD HEIGHT <M>
3.0
2.5
2.0
1.5
1.0
0.5
0
□ =CONVECTION GAS-WALL
○ =RADIATION GAS-WALL
▲ =RADIATION DUST-WALL
3 4 5 6 7 8 9 2 3 4 5 6 7 8 9 2 3
10
10²
HEAT TRANSFER COEFFICIENT <W/(M2.K)>
Figure 4-17.
Convective and radiative 'pseudo' heat transfer coefficients as a function of freeboard height.

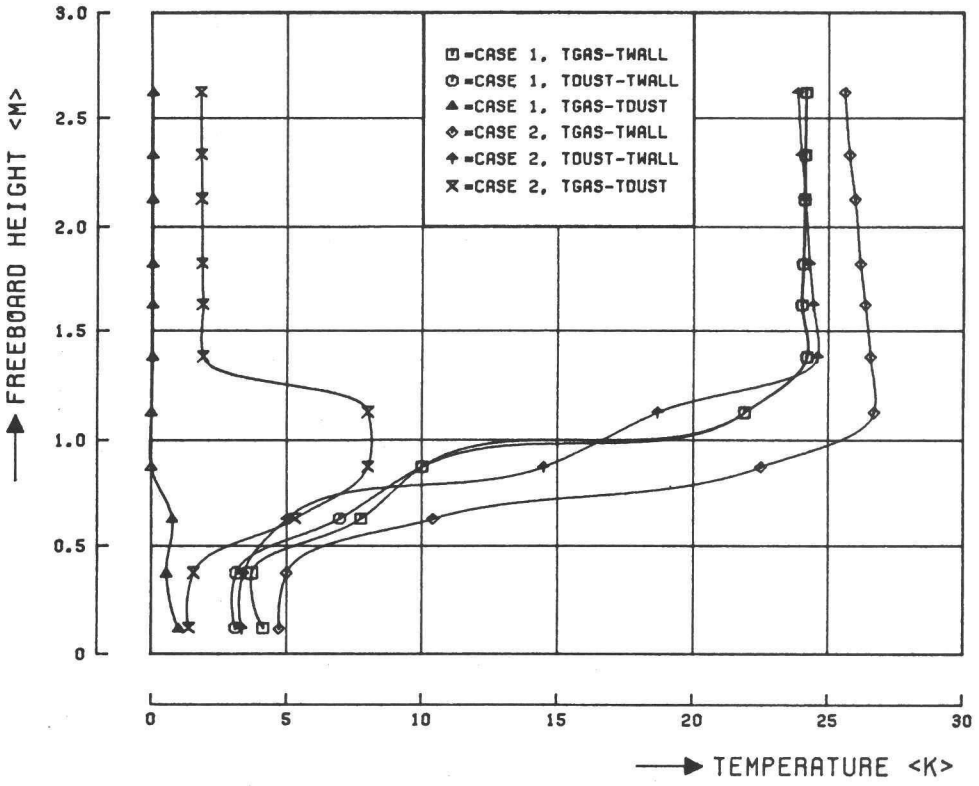

Figure 4-18.
Characteristic temperature differences as a function of freeboard height.
For definition of cases see text, section 4.4.1.

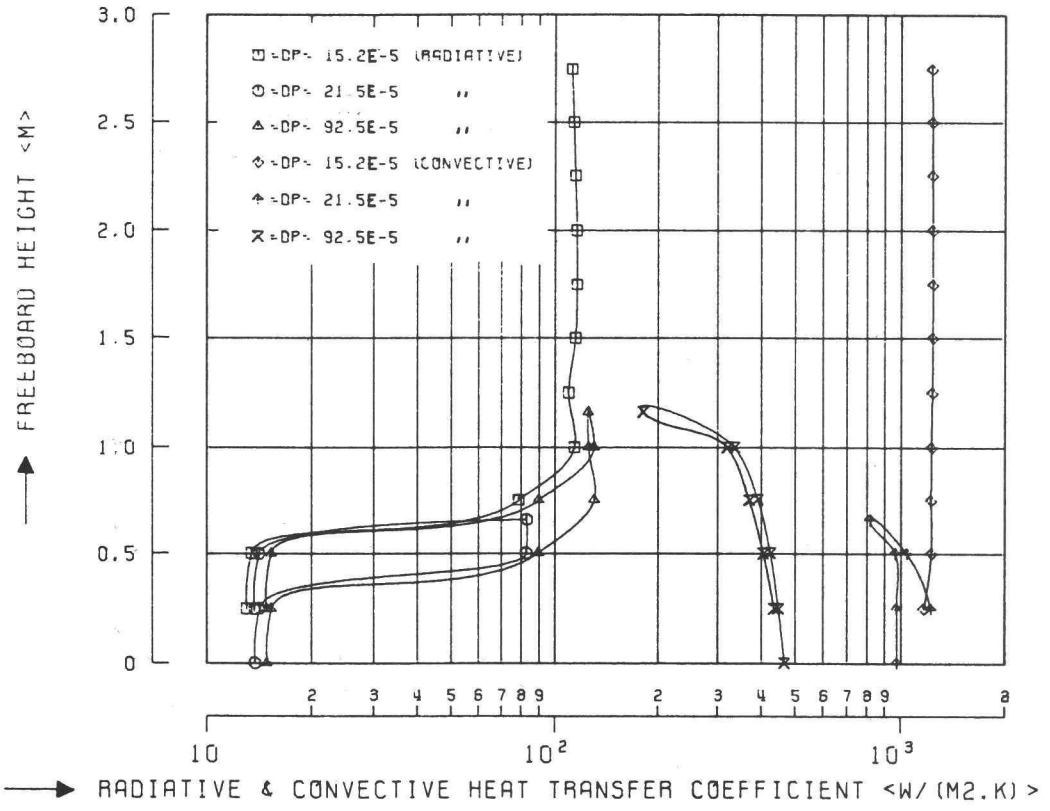

Figure 4-19.
Convective and radiative heat transfer coefficients as a function of freeboard height for various particle trajectories.

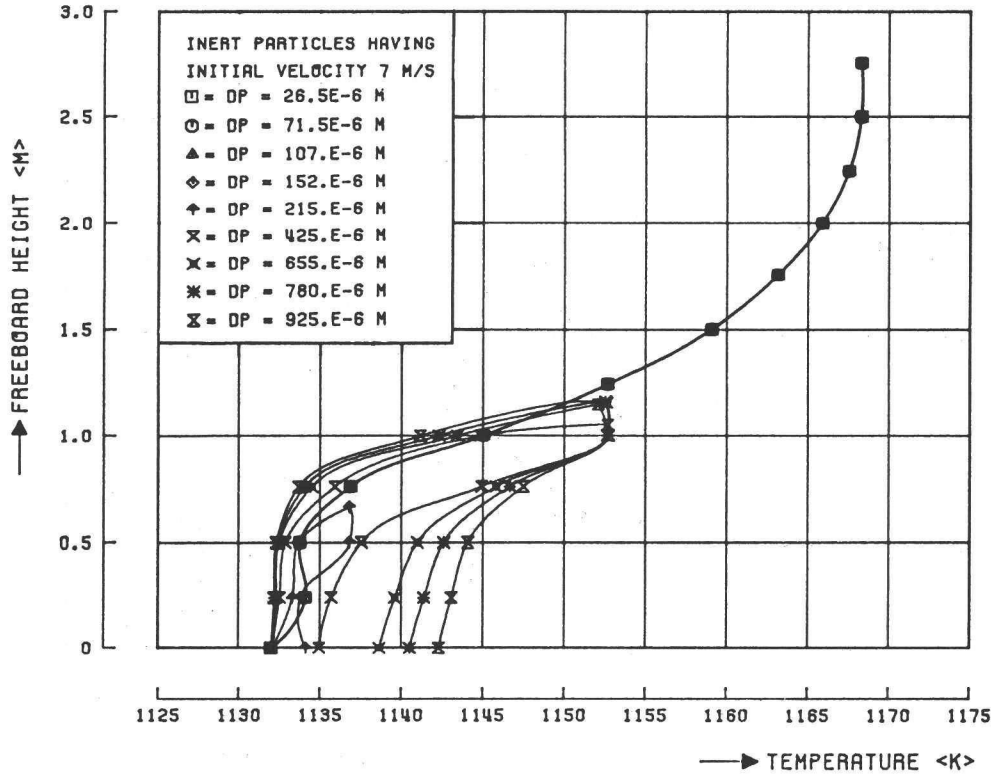

Figure 4-20a.
Inert particle temperature as a function of freeboard height; various particle sizes, initial particle velocity 7 m/s.

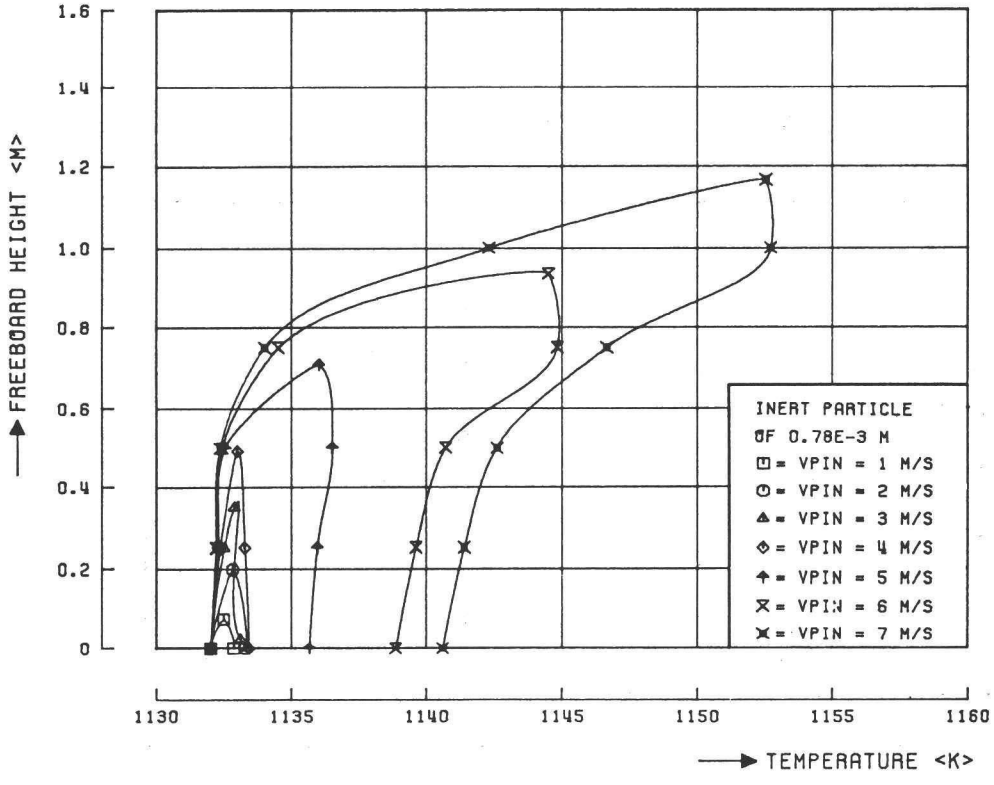

Figure 4-20b.
Inert particle temperature as a function of freeboard height; various initial particle velocities, particle size 0.78E-3 m.

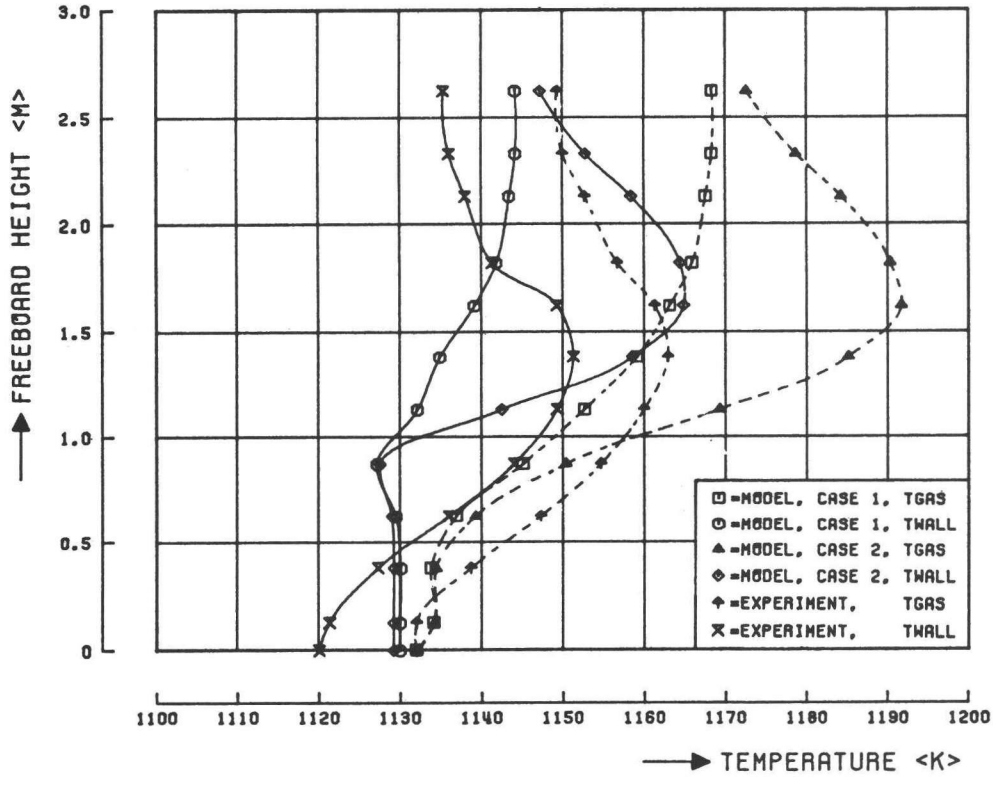

Figure 4-21.
Temperatures of the gas and the wall as a function of freeboard height (experimental data and model result).

Table 4-1.
Input values for the model (see also table 2-3 and 3-7)

internal freeboard diameter	0.390 <m>
wall data:	
1) stainless steel wall	
thickness	0.003 <m>
divided into (model) layers	1
2) ceramic wool	
thickness	0.040 <m>
divided into (model) layers	5
3) rock-wool	
thickness	0.100 <m>
divided into (model) layers	5
temperature of the surroundings	300 <K>
specific heat of solid at Tbed	1134. <J/(kg.K)>
thermal conductivity of solid particles	1.5 <W/(m.K)>

ACKNOWLEDGEMENTS

I am grateful to all who have made my stay at the Delft University of Technology joyful and fruitful. The experience and the enthousiasm of many people at the Laboratory for Thermal Power Engineering and the Laboratory of Chemical Technology contributed to this essentially.

I want to thank professor C. van Koppen and D. Boersma for their advice, support and their confidence. They gave me the opportunity of executing the project on freeboard phenomena and the allowance to visit the various conferences and research institutes abroad.

W. Middelkoop, K. Vis and H. Op den Brouw contributed essentially to the work reported. I am greatly indebted to them for their encouragement and their friendship.

I want to thank professors C. van Koppen and P. van den Berg. Their suggestions and constructive criticism helped formulate this thesis.

Many thanks to my wife Saskia for her encouragement, her patience and her concern for my well being.

This thesis is supported by the Delft University of Technology.

SAMENVATTING

VERSCHIJNSELEN IN HET VRIJBOORD BOVEN EEN KOLENGESTOOKT WERVELBED

Een stationair, een-dimensionaal model van verschijnselen in het vrijboord is ontwikkeld, bestaande uit een combinatie van vereenvoudigde voorstellingen van fysische en chemische verschijnselen.
Het model is in staat, uitgaande van de omstandigheden aan de oppervlakte van het wervelbed een voorspelling te doen omtrent deeltjestransport, stofoverdracht in de gasfase, chemische omzettingen en warmteoverdracht als functie van de hoogte boven het wervelbed.
Het transport van deeltjes is gebaseerd op ballistische beschouwingen met in achtname van o.a. de zwaartekracht, meesleepkracht en traagheidskracht.
Daarbij is het mogelijk de massastromen en verblijftijd van de vaste stof als functie van de vrijboordhoogte te bepalen. Op basis van deze gegevens worden de reacties van het gas met de vaste stof en het warmtetransport bepaald.
De stroming van het gas wordt gemodelleerd volgens een serieschakkeling van ideaal geroerde reactoren. Een mengparameter bepaalt de mate van stofoverdracht tussen de zuurstofrijke gasstroom uit de bellenfase en de koolmonoxide rijke gasstroom uit de emulsiefase van het wervelbed, eventueel gevolgd door chemische reacties.
De mate van chemische omzetting van zuurstof, kooldioxide en stikstofoxiden met cokes-deeltjes wordt bepaald door de snelheid waarmee gasdiffusie door de grenslaag van het deeltje gevolgd door een eerste orde chemische reactie aan het koolstofoppervlakte plaats vindt.
De quasi-stationaire warmtebalans resulteert uit de mate van het vrijkomen van de reactiewarmte, het convectieve transport van voelbare warmte via het gas en de deeltjes, de mate van convectieve warmteoverdracht van gas naar deeltjes en reactorwand, en de stralingswarmteoverdracht van gas en deeltjes naar de reactorwand.
Tijdens de baan van een deeltje door het vrijboord wordt warmte naar dat deeltje overgedragen. De hoeveelheid warmte wordt bepaald door de warmteweerstand in het deeltje, de warmteweerstand in de grenslaag om het deeltje, de lokale gas- en reactorwandtemperatuur en vooral de verblijftijd.
De beschikbare literatuur over vrijboordverschijnselen is, voor zover nuttig, herzien en in verband gebracht met de vele aannamen die in het model gemaakt zijn. Een algehele schaarste aan experimentele resultaten maakt een meer complexe aanpak van het model nog niet zinvol.
Een modelberekening is gedetailleerd beschreven.
De randvoorwaarden die genomen zijn aan het wervelbedoppervlak zijn gebaseerd op metingen verricht aan een experimenteel wervelbed.
Een samenhangend beeld van de vele verschijnselen in het vrijboord is ontstaan. Daarnaast komen de mate van chemische omzetting en warmteoverdracht in het model redelijk met die van de experimentele resultaten overeen.
Aangetoond is dat het vrijboord een integraal deel van het wervelbed systeem vormt. De bijdrage van de verbranding en de NOx-reductie is aanzienlijk.
De warmte die vrijkomt bij de chemische omzettingen wordt voor een belangrijk deel door recirculerende deeltjes opgenomen en teruggevoerd naar het bed.

A P P E N D I X 1

1 PHYSICAL PROPERTIES

In this chapter the analytic treatment of the physical properties of the gases and the solid materials of interest is worked out in detail.

1.1 Physical properties of gas

1.1.1 Thermo-physical properties of a multi component gas

1.1.1.1 Introduction

The present section describes a method for calculating the following thermo-physical properties of a multi-component gas at the low density limit:

* density
* viscosity
* thermal conductivity
* specific heat
* enthalpy
* binary diffusivity.

Once computerised the procedure can be applied to a wide variety of multi-component gases and for a wide temperature and pressure range. Such because the effect of pressure on the viscosity, thermal conductivity and diffusivity of a mixture of gases is not significant in certain regions of pressure and temperature. For instance at high reduced temperatures (> 1) and low reduced pressures (< 0.5). The viscosity, thermal conductivity and diffusivity of a gas then approache a definite limit: the low density limit.

The reduced properties of a multi component gas are commonly expressed as a fraction of the critical properties according to:

$$T_r = \frac{T_{mix}}{\sum_{i=1}^{i=ng} x_i \, T_{c,i}} \qquad (1\text{-}1)$$

and:

$$P_r = \frac{P_{mix}}{\sum_{i=1}^{i=ng} x_i \, P_{c,i}} \qquad (1\text{-}2)$$

The critical properties of the considered gas species are listed in table 1-1. Estimation of the applicability of the calculations over a pressure range for the pressurized fluidized bed combustor of our current interest leads to:

$$1.E5 \text{ Pa} < P_{mix} < 100.E5 \text{ Pa}$$

for:

* $T_{mix} = 1150$ K
* stochiometric combustion conditions
* a pressure effect on viscosity and thermal conductivity of maximal 5% of the true value.

The basic equations for the described procedure are taken from Reid et al. (1977) and Bird et al. (1960) and are given below with only limited comment.

1.1.1.2 Molecular weight

The molecular weight of a mixture of gases is defined as:

$$M_{mix} = \frac{\sum_{i=1}^{i=ng} x_i M_i}{\sum_{i=1}^{i=ng} x_i} \qquad (1\text{-}3)$$

The specific molecular weights for the considered chemical species are given in table 1-2.

1.1.1.3 Density

Assuming all gases to be ideal and neglecting interactions among the phases the equation of state for the mixture is:

$$\frac{P_{mix}}{\rho_{mix}} = \frac{R\, T_{mix}}{M_{mix}} \qquad (1\text{-}4)$$

and the density:

$$\rho_{mix} = \frac{M_{mix}\, P_{mix}}{R\, T_{mix}} \qquad (1\text{-}5)$$

1.1.1.4 Viscosity at the low density limit

Based on Sutherland's kinetic theory Wilke approximates the viscosity in a series expansion:

$$\eta_{mix} = \sum_{i=1}^{i=ng} \frac{x_i \eta_i}{\sum_{j=1}^{j=n} x_j \Psi_{ij}} \qquad (1\text{-}6)$$

in which:

$$\Psi_{ij} = \frac{1}{\sqrt{8}} \left(1 + \frac{M_i}{M_j}\right)^{-0.5} \left(1 + \left(\frac{\varepsilon_i}{\varepsilon_j}\right)^{0.5} \left(\frac{M_j}{M_i}\right)^{0.25}\right)^2 \qquad (1\text{-}7)$$

and (after converting in S.I. units):

$$\eta_i = 8.4401\text{E-}25 \frac{\sqrt{M_i\, T_{mix}}}{\sigma_i^2\, \Omega_{v,i}} \qquad (1\text{-}8)$$

Neufeld et al. propose an empirical equation for the collision integral

which is convenient for computer application:

$$\Omega_{v,i} = \frac{A}{(T^*)^B} + \frac{C}{\exp(D\,T^*)} + \frac{E}{\exp(F\,T^*)} \qquad (1\text{-}9)$$

where:

$$T^* = \left(\frac{k}{\varepsilon}\right)_i T_{mix} \qquad (1\text{-}10)$$

and:

A = 1.16145 <->
B = 0.14874 <->
C = 0.52487 <->
D = 0.77320 <->
E = 2.16178 <->
F = 2.43787 <->

The remaining parameters to be obtained are σ and (ε/k) of the individual gas species. These parameters are named after Lennard-Jones. For the considered species they are listed in table 1-3. Omitting extraordinary mixtures, the comparison of experimental and calculated values indicates that the error is usually less than 2%.

1.1.1.5 Thermal conductivity at the low density limit

The thermal conductivity of a gas mixture of non polar gases at the low density limit may be estimated by a method analogous to that given for the viscosity:

$$\lambda_{mix} = \sum_{i=1}^{i=ng} \frac{x_i\,\lambda_i}{\sum_{j=1}^{j=n} x_j\,\Psi_{ij}} \qquad (1\text{-}11)$$

The coefficients Ψ are identical with those that appear in the viscosity equation (1-6). The semi-empirical method developed by Euken for the thermal conductivity of a poly-atomic gas at low density is used:

$$\lambda_i = \left(Cp_i + \frac{5\,R}{4\,M_i}\right) \varepsilon_i \qquad (1\text{-}12)$$

This equation also includes the mono-atomic formula. Comparison with experimental data indicate an average deviation of about 4% for mixtures containing nonpolar poly-atomic gases.

1.1.1.6 Diffusivity for binary gas systems at the low density limit.

The diffusivity or diffusion coefficient for a binary gas at the low density limit can be estimated with confidence from theory. The relation used is derived from elementary kinetic theory, but contains important correcting factors (converted into S.I. Units):

$$\mathbb{D}_{AB} = 5.953\text{E-}24\,\frac{T^{1.5}\left(\frac{M_A + M_B}{M_A\,M_B}\right)^{0.5}}{P\,\sigma_{AB}^2\,\Omega_D} \qquad (1\text{-}13)$$

Analogous to the viscosity calculations the relation of Neufeld et al. is used:

$$\Omega_D = \frac{A}{(T^*)^B} + \frac{C}{\exp(D\,T^*)} + \frac{E}{\exp(F\,T^*)} + \frac{G}{\exp(H\,T^*)} \qquad (1\text{-}14)$$

where:

$$T^* = \left(\frac{k}{\varepsilon_{AB}}\right) T_{mix} \qquad (1\text{-}15)$$

and:

A = 1.06036 <->
B = 0.15610 <->
C = 0.19300 <->
D = 0.47635 <->
E = 1.03587 <->
F = 1.52996 <->
G = 1.76474 <->
H = 3.89411 <->

The combination rules for the Lennard Jones parameters are:

$$\frac{\varepsilon_{AB}}{k} = \left(\frac{\varepsilon_A}{k}\,\frac{\varepsilon_B}{k}\right)^{0.5} \qquad (1\text{-}16)$$

and:

$$\sigma_{AB} = \frac{\sigma_A + \sigma_B}{2} \qquad (1\text{-}17)$$

The error to be expected from this procedure is generally less than 10%.

For analytic purposes it is useful to simplify the procedure. The variation of the diffusion coefficient with temperature and pressure can be represented by (Field et al. (1967)):

$$\mathbb{D}_{ij} = \mathbb{D}_{ij} \left(\frac{T_{mix}}{T_{ref,ij}}\right)^{1.75} \left(\frac{P_{ref,ij}}{P_{mix}}\right) \qquad (1\text{-}18)$$

The reference temperature and pressure may be chosen arbitrarily. It is recomended however to take the reference conditions (calculated from equation (1-13)) as close as possible to the regime of application. Table 1-4 gives the reference temperatures and pressures and corresponding binary diffusion coefficients of interest.

1.1.1.7 Specific heat and enthalpy

For each gaseous species in the ideal-gas state, the thermodynamic functions specific heat and enthalpy as functions of the temperature are given in the form of least square coefficients as follows:

$$Cp_i^0 = R \sum_{j=1}^{j=5} a_{ij}\, T^{(j-1)} \qquad (1\text{-}19)$$

$$H_i^0 = R \sum_{j=1}^{j=5} \frac{a_{ij}\, T_{mix}^{j}}{j} \qquad (1\text{-}20)$$

The reference temperature for H_i^0 is 0 K.

The gas mixture combination rule leads to:

$$Cp_{mix} = \frac{\sum_{i=1}^{i=ng} x_i \, Cp_i^0}{M_{mix}} \qquad (1\text{-}21)$$

and:

$$H_{mix} = \frac{\sum_{i=1}^{i=ng} x_i \, H_i^0}{M_{mix}} \qquad (1\text{-}22)$$

The least square coefficients of the considered species are listed in table 1-5.

1.1.2 Thermal coefficient of volumetric expansion of air

The thermal coefficient of volumetric expansion of dry air at 1.E5 Pa as a function of temperature is expressed as:

$$\beta_{air} = \sum_{i=1}^{i=4} b_i \, (T_{air} - 273.15)^{(i-1)} \qquad (1\text{-}23)$$

for the temperature range:

$$273 \text{ K} < T_{air} < 1273 \text{ K}$$

where:

b_1 = 3.551382E-3 <1/K>
b_2 =-9.314647E-6 <1/K^2>
b_3 = 1.236424E-8 <1/K^3>
b_4 =-5.881232E-12 <1/K^4>

Values calculated from the polynomial expression deviate less than 5% from the experimental data given in Schunck (1977).

1.2 Thermo-physical properties of solids

1.2.1 Thermal conductivity of solids

The effective thermal conductivity of solids used in this work is given by the following polynomial expression:

$$\bar{\lambda}_s = \sum_{i=1}^{i=n} c_i^n \, (\bar{T}_s - 273.15)^{(i-1)} \qquad (1\text{-}24)$$

The coefficients and the appropriate temperature intervals are given in table 1-6.

1.2.2 Specific heat and enthalpy of silica

The specific heat and enthalpy of silica is expressed as:

$$Cp_s = \sum_{i=1}^{i=2} d_i \, T_s^{(i-1)} \qquad (1\text{-}25)$$

and:

$$H_s = \sum_{i=1}^{i=2} \frac{d_i \, T_s^{i}}{i} \qquad (1\text{-}26)$$

where:
d_1 = 0.783834E3 J/(kg.K)
d_2 = 0.41278 J/(kg.K2)
(from data General Electric (1982) for glass, silica) for:

$$370 \text{ K} < T_s < 1100 \text{ K}$$

1.2.3 Density of solids

The density of the solids of interest is listed in table 1-7.

1.3 List of symbols

A	coefficient	-
a_{ij}	coefficient	$1/K^{j-1}$.
B	coefficient	-
b_i	coefficient	$1/K^{i}$.
C	coefficient	-
Cp^0	specific heat at constant pressure	J/(mol.K)
Cp	specific heat at constant pressure	J/(kg.K)
c_i	coefficient	$W/(m.K^{i})$
d	coefficient	$J/(kg.K^{i})$
E	coefficient	-
F	coefficient	-
G	coefficient	-
H^0	enthalpy	J/mol
H	enthalpy	J/kg
	coefficient	-
M	molecular weight	kg/mol
P	pressure	Pa
R	gas constant	J/(mol.K)
T^*	dimensionless temperature	-
T	temperature	K
x	mol fraction	-

GREEK SYMBOLS

β	thermal coefficient of volum. expansion	1/K
$\mathbb{D}$	diffusion coefficient	m2/s
	coefficient	-
ε	characteristic energy	J
η	viscosity	kg/(m.s)
λ	thermal conductivity	W/(m.K)
ρ	density	kg/m3
σ	molecular diameter	m

Ψ interaction parameter
Ω collision integral for viscosity

INDICES

AB species A in species B
c critical
D diffusion
i summation index
component
j summation index
component
mix mixture of gas species
n summation index
ng total number of gas species involved
r reduced
ref reference
s solid
v viscosity

OVERHEADS

- average

1.4 References

Bird, R.B., Stewart, W.E., Lightfoot, E.N.
Transport Phenomena.
Wiley International Edition, New York (1960).

Field, M.A., Gill, D.W., Morgan, B.B., Hawksley, P.G.W.
Combustion of pulverised coal.
BCURA, Leatherhead U.K. (1967).

Forschungsinstitut für Wärmeschutz E.V. München.
Bestimmung der Wärmeleitfähigkeit der Drahtgeflechtmatte 160 Rockwool Lapinus BV, Roermond.
Prüfbericht F III 1/78.
München , B.R.D. (1978).

General Electric
Heat transfer and fluid flow data books. Transittal no. 37.
Schenetady, New York, USA (August 1982).

Gordon, S. and McBride, B.J.
Computer program for calculation of complex chemical equilibrium composition, rocket performance, incident and reflected shocks, and Chapman-Jouguet detonations.
NASA SP - 273, NASA Lewis Research Center , USA (1971).

Marks, L.S.
Mechanical engineers' handbook, 5th edition.
McGraw Hill, New York (1959).

Reid, R.C., Prausnitz, J.M., Sherwood, T.K.
The properties of gases and liquids
McGraw-Hill Book Company, New York (1977).

Schunck., M.
VDI-Wärmeatlas, pp. Db7.
VDI-Verlag, Düsseldorf, BRD (1977).

Tipton, C.R. Jr.
Reactor handbook, Volume 1 Materials, Second Edition.
Interscience Publishers, New York (1960).

Weast, R.C.
Handbook of chemistry and physics, 55th edition 1974-1975.
CRC-Press, Cleveland Ohio, USA (1974).

Table 1-1.
Critical temperature and pressure of some gases.
* from Reid and al (1977),
other data from Bird et al. (1960).

gas species formular	T c <K>		P c <Pa>	
Ar	151		48.6E5	
CO	133		34.0E5	
CO2	304		73.9E5	
H2O	647	*	217.6E5	*
NO	180		64.8E5	
N2	126		33.9E5	
O2	154		50.3E5	
SO2	430		78.8E5	

Table 1-2.
Molecular weights of some gas species,
after Gorden and McBride (1971).

gas species formular	molecular weight <kg/mol>
Ar	39.94800E-3
CO	28.01055E-3
CO2	44.00995E-3
H2O	18.01534E-3
NO	30.00610E-3
N2	28.01340E-3
O2	31.99880E-3
SO2	64.06277E-3

Table 1-3.
Lennard-Jones potentials as determined from viscosity data, from Reid et al. (1977).

gas species formular	σ <m>	ε/k <K>
Ar	3.542E-10	93.3
CO	3.690E-10	91.7
CO2	3.941E-10	195.2
H2O	2.641E-10	809.1
NO	3.492E-10	116.7
N2	3.798E-10	71.4
O2	3.467E-10	106.7
SO2	4.112E-10	335.4

Table 1-4.
Reference temperature , pressure and binary diffusion coefficients.

binary gas mixture	T ref <K>	P ref <Pa>	binary diffusion coefficient <m2/s>	reference
O2 - N2	1100	1.01325E5	1.88E-4 1.86E-4	Field et al. (1971) calculated
CO2 - N2	1100	1.01325E5	1.45E-4 1.46E-4	Field et al. (1971) calculated
NO - N2	1100	1.01325E5	1.86E-4	calculated
SO2 - N2	1100	1.01325E5	1.25E-4	calculated

Table 1-5.
Property data bank for determining specific heat and enthalpy of some gas species (data taken from Gorden and McBride (1971) and converted into S.I. units).

gas species formular	coefficients a_{ij} ; j=1 through 5 $\langle 1/K^{(j-1)} \rangle$ for: 1000 K < T$_{mix}$ < 5000 K ; 300 K < T$_{mix}$ < 1000 K
Ar	2.5000000E+00 ; 2.5000000E+00 0.0000000E+00 ; 0.0000000E+00 0.0000000E+00 ; 0.0000000E+00 0.0000000E+00 ; 0.0000000E+00 0.0000000E+00 ; 0.0000000E+00
CO	2.9840698E+00 ; 3.7100925E+00 1.4891389E-03 ; -1.6190964E-03 -5.7899683E-07 ; 3.6923593E-06 1.0364577E-10 ; -2.0319675E-09 -6.9353533E-15 ; 2.3953344E-13
CO2	4.4608040E+00 ; 2.4007797E+00 3.0981719E-03 ; 8.7350942E-03 -1.2392575E-06 ; -6.6070879E-06 2.2741325E-10 ; 2.0021862E-09 -1.5525955E-14 ; 6.3274039E-16
H2O	2.7167633E+00 ; 4.0701275E+00 2.9451374E-03 ; -1.1084499E-03 -8.0224374E-07 ; 4.1521180E-06 1.0226682E-10 ; -2.9637404E-09 -4.8472145E-15 ; 8.0702103E-13
NO	3.1890001E+00 ; 4.0459518E+00 1.3382281E-03 ; -3.4181783E-03 -5.2899316E-07 ; 7.9819192E-06 9.5919328E-11 ; -6.1139325E-09 -6.4847928E-15 ; 1.5919080E-12

To be continued on next page.

Continued from previous page.

gas species formular	coefficients a_{ij} ; j=1 through 5 $\langle 1/K^{(j-1)} \rangle$ for: $1000\ K < T_{mix} < 5000\ K$; $300\ K < T_{mix} < 1000\ K$
N2	2.8963194E+00 ; 3.6748257E+00 1.5154865E-03 ; -1.2081501E-03 -5.7235275E-07 ; 2.3240100E-06 9.9807398E-11 ; -6.3217565E-10 -6.5223570E-15 ; -2.2577253E-13
O2	3.6219535E+00 ; 3.6255985E+00 7.3618264E-04 ; -1.8782184E-03 -1.9652228E-07 ; 7.0554544E-06 3.6201558E-11 ; -6.7635137E-09 -2.8945627E-15 ; 2.1555993E-12
SO2	5.2451363E+00 ; 3.2665339E+00 1.9704204E-03 ; 5.3237901E-03 -8.0375770E-07 ; 6.8437549E-07 1.5149969E-10 ; -5.2810059E-09 -1.0558005E-14 ; 2.5590450E-12

Table 1-6.
Thermal conductivity of various solid materials.

material	T min <K>	T max <K>	n	c until c i n <W/(m.K^{i})>	max. dev. %	reference
Ceramic fibre. Triton Kaowool rho= 128 kg/m3	550	1250	3	c1=0.020 c2=1.242E-4 c3=7.080E-8	5	supplier
Rockwool Lapinus BV Roermond. Drahtgeflecht matte. rho= 70 kg/m3	323	723	5	c1=2.999E-2 c2=2.443E-4 c3=-1.66E-6 c4=7.539E-9 c5=-8.00E-12	5	Forschungs institut München (1978)
Stainless steel 304 typ. value.			1	c1=34		Weast (1974)
Iron	1100	1100	1	c1=30		Weast (1974)
Sand	1093	1093	1	c1=1.5 - 1.7		Marks (1959)
Sandstone	273	273	1	c1=5.72		Weast (1974)
	373	373	1	c1=4.46		
	473	473	1	c1=3.78		

Table 1-7.
Density of solid materials.

material	density <kg/m3>	reference
Silica sand	2600	Tipton (1960)
Anthracite	1400	Tipton (1960)

A P P E N D I X 2

2 UNSTEADY STATE HEAT CONDUCTION IN A SPHERE

2.1 Solution in an infinite series expansion

A homogeneous sphere of solid material, initially at a uniform temperature, is suddenly immersed in a volume of constant temperature. It is desired to find the solid temperature as a function of time and position. The differential equation and the initial and boundary conditions in dimensionless quantities read:

$$\frac{\delta\Theta}{\delta\tau} = \frac{1}{\xi^2}\frac{\delta}{\delta\xi}\left(\xi^2\frac{\delta\Theta}{\delta\xi}\right) \tag{2-1}$$

$$\Theta(\xi,0) = 1 \tag{2-2}$$

$$\frac{1}{Bi}\frac{\delta\Theta}{\delta\xi} + \Theta = \begin{matrix}1 \text{ for } \tau = 0\\ 0 \text{ for } \tau > 0\end{matrix} \tag{2-3}$$

The caloric dimensionless temperature is defined as:

$$\bar{\Theta} = 3\int_0^1 \Theta(\xi)\,\xi^2\,d\xi \tag{2-4}$$

The solution of the problem of determining $\Theta(\xi)$ and $\bar{\Theta}$ is found in the for of infinite series and is given by Martin (1984):

$$\Theta = \sum_{i=1}^{i=\infty} C_i(m_i)\, f(m_i\,\xi)\, \exp(-m_i^2\,\tau) \tag{2-5}$$

$$\bar{\Theta} = \sum_{i=1}^{i=\infty} C_i(m_i)\, D(m_i\,\xi)\, \exp(-m_i^2\,\tau) \tag{2-6}$$

where:

$$m_i = (1-Bi)\frac{\sin m_i}{\cos m_i} \tag{2-7}$$

and:

$$C_i(m_i) = 2\frac{\sin m_i - m_i\cos m_i}{m_i - \sin m_i\cos m_i} \tag{2-8}$$

$$D_i(m_i) = 3\frac{\sin m_i - m_i\cos m_i}{m_i^3} \tag{2-9}$$

$$f(m_i\,\xi) = \frac{\sin(m_i\,\xi)}{m_i\,\xi} \tag{2-10}$$

The first four roots of m_i are presented in table 2-1.

2.2 List of symbols

Bi	Biot number	-
C	coefficient	-
D	coefficient	-
f	coefficient	-
m	eigen value	-

GREEK SYMBOLS

ξ	dimensionless radial coordinate	-
Θ	dimensionless solid temperature	-
$\overline{\Theta}$	caloric mean dimensionless solid temp.	-
τ	Fourier number	-

SUBSCRIPTS

i	summation index

2.3 Reference

Martin, H.
Instationäre Wärmeleitung in ruhenden Körpern.
VDI-Wärmeatlas, 4. Auflage, pp. Ec1/20.
VDI-Verlag, Düsseldorf, BRD (1984).

Table 2-1
The first four roots of m as a function of Bi (after Martin (1984)).

Bi <->	m 1 <->	m 2 <->	m 3 <->	m 4 <->
0.000	0.000	4.493	7.725	10.904
0.001	0.055	4.494	7.725	10.904
0.002	0.077	4.494	7.725	10.904
0.005	0.122	4.495	7.726	10.905
0.010	0.173	4.496	7.727	10.905
0.020	0.242	4.498	7.728	10.906
0.050	0.385	4.504	7.732	10.908
0.100	0.542	4.516	7.739	10.913
0.200	0.759	4.538	7.761	10.923
0.500	1.166	4.604	7.790	10.950
1.000	$\pi/2$	$3\,\pi/2$	$5\,\pi/2$	$7\,\pi/2$
2.000	2.030	4.913	7.979	11.085
5.000	2.569	5.354	8.303	11.335
10.000	2.836	5.717	8.659	11.658
20.000	2.986	5.978	8.983	12.003
50.000	3.079	6.158	9.239	12.320
∞	π	$2\,\pi$	$3\,\pi$	$4\,\pi$

A P P E N D I X 3

3 UNSTEADY STATE HEAT CONDUCTION IN A SPHERE

3.1 Approximate solution

A homogeneous sphere of solid material, initially at a uniform temperature is suddenly immersed in a volume of constant temperature. It is desired to find an approximation of the calorific mean dimensionless solid temperature (Martin (1984)).

The inner and outer particle heat transfer coefficients are defined by:

$$\dot{Q}_i(t) = \alpha_i(t)\, A_p\, (\bar{T}_p(t) - T_p(R)) \qquad (3\text{-}1)$$

$$\dot{Q}_o(t) = \alpha_o\, A_p\, (T_p(R) - T_\infty) \qquad (3\text{-}2)$$

The particle energy balance yields:

$$\dot{Q}_p(t) = \dot{Q}_i(t) = \dot{Q}_o(t) \qquad (3\text{-}3)$$

so that substitution of $T_p(R)$ from equation (3-2) into (3-1) yields:

$$\dot{Q}_p(t) = \alpha(t)\, A_p\, (\bar{T}_p(t) - T_\infty) \qquad (3\text{-}4)$$

where:

$$\frac{1}{\alpha(t)} = \frac{1}{\alpha_o} + \frac{1}{\alpha_i(t)} \qquad (3\text{-}5)$$

The particle energy balance related to the particle enthalpy gives:

$$\dot{Q}_p(t) = -\rho_p\, Cp_p\, V_p\, \frac{d\bar{T}_p(t)}{dt} \qquad (3\text{-}6)$$

From equations (3-4) and (3-6) we find:

$$\int_{\bar{T}_p(0)}^{\bar{T}_p(t_p)} \frac{d\bar{T}_p}{\bar{T}_p(t) - T_\infty} = \qquad (3\text{-}7)$$

$$\int_0^{t_p} -\frac{A_p}{\rho_p\, Cp_p\, V_p\, \left(\frac{1}{\alpha_o} + \frac{1}{\alpha_i(t)}\right)}\, dt$$

Assume that $\alpha_i(t)$ is only a weak function of time then integration of equation (3-7) gives, approximately:

$$\frac{\bar{T}_p(t_p) - T_\infty}{T_p(o) - T_\infty} = \exp\left(\frac{-A_p\, t_p}{\rho_p\, Cp_p\, V_p\, \left(\frac{1}{\alpha_o} + \frac{1}{\alpha_i(t)}\right)}\right) \qquad (3\text{-}8)$$

$\alpha_i(t)$ can be approximated for all t by:

$$\alpha_i(t) = (\alpha_i^2(o) + \alpha_i^2(\infty))^{0.5} \qquad (3\text{-}9)$$

where:

$$\alpha_i(o) = \left(\frac{4}{\pi}\,\frac{\lambda_p}{\rho_p\, Cp_p}\right)^{0.5} \qquad (3\text{-}10)$$

and:

$$\alpha_i(\infty) = \frac{\pi^2}{3}\,\frac{\lambda_p}{R} \qquad (3\text{-}11)$$

Now we define:

$$\bar{\theta}(t_p) = \frac{\bar{T}_p(t_p) - T_\infty}{T_p(o) - T_\infty} \qquad (3\text{-}12)$$

$$\tau_p = \frac{\lambda_p}{\rho_p\, Cp_p}\,\frac{t_p}{R^2} \qquad (3\text{-}13)$$

$$Bi_p = \frac{\alpha_o\, R}{\lambda_p} \qquad (3\text{-}14)$$

Then substituting equations (3-9) to (3-14) into (3-8) gives:

$$\bar{\theta}(t_p) = \exp\left(-\frac{A_p\, R}{V_p}\,\frac{\tau_p}{\frac{1}{Bi_p} + \frac{1}{\left(\left(\frac{\pi^2}{3}\right)^2 + \frac{4}{\pi}\,\frac{1}{\tau_p}\right)^{0.5}}}\right) \qquad (3\text{-}15)$$

3.2 List of symbols

A	surface area	m2
Bi	Biot number	-
Cp	heat capacity at constant pressure	J/(kg.K)
$\dot{Q}$	rate of energy flow	W
R	radius of sphere	m
T	Temperature	K
$\bar{T}$	calorific mean tempearture	K
t	time	s
V	volume	m3

GREEK SYMBOLS

α	heat transfer coefficient	W/(m2.K)
$\overline{\Theta}$	calorific mean dimensionless temperature	-
λ	thermal conductivity	W/(m.K)
π	3.14159	-
ρ	density	kg/m3
τ	Fourier number	-

SUBSCRIPTS

i	inner
o	outer
p	particle

-

3.3 Reference

Martin, H.
Instationäre Wärmeleitung in ruhenden Körpern.
VDI-Wärmeatlas, 4. Auflage, pp. Ec1/20.
VDI-Verlag, Düsseldorf, BRD (1984).

Stellingen behorende bij het proefschrift
FREEBOARD PHENOMENA IN A FLUIDIZED BED COAL COMBUSTOR

Het verdient aanbeveling de subsidies en verordeningen die differentiëren naar het individuele inkomen te dereguleren en slechts de loon- en inkomstenbelasting af te stemmen op de integrale individuele draagkracht.

De introductie van vergassingssystemen voor de energievoorziening zal niet zozeer door de brandstofprijzen worden bepaald als wel door de investerings- en bedrijfskosten bij conventionele energiesystemen die zullen voortvloeien uit stringente emissienormen.

Men wordt geacht de wet te kennen.
Echter, de uitvoering van de wet zou practisch onmogelijk zijn wanneer een ieder bekend zou zijn met de mogelijkheden die de wet biedt.

Computersystemen in instellingen voor wetenschappelijk onderwijs dienen zowel de mogelijkheden voor technisch wetenschappelijk rekenen als uitgebreide tekstverwerking te bieden

Bij de invoering van het Fries als officiële taal maakt men zich schuldig aan snobisme. Het regionale taalgebruik zal op welwillende en informele basis beter gedijen dan door formele dwang.

Op grond van de Woonruimtebeschikking 1984 kunnen nagenoeg alle gemeenten bij het verlenen van een woonvergunning aan ingezetenen voorkeursrecht verlenen en/of aan niet-ingezetenen additionele eisen stellen. Door daarbij een koper te verplichten de woning tegen koopprijs aan ingezetenen aan te bieden wordt de vrucht van het onderhandelingsproces tussen koper en verkoper ontvreemd.

In het vrijboord van een wervelbedvuurhaard zijn stijghoogte, verblijftijd en thermische relaxatietijd van deeltjes van wezenlijk belang voor het opnemen en afvoeren van de bij chemische omzettingen vrijkomende warmte.
Dit proefschrift.

Behoudens een aantal uitzonderingen gaan de technisch wetenschappelijke ontwikkelingen op het gebied van de wervelbedverbranding voorbij aan milieu-aspecten.

Wervelbedverbrandingssystemen zijn nog niet gereed voor commerciële introductie. Fluidised combustion is it achieving its promise?
3rd International Fluidized Conference.
The Institute of Energy, London 1984.

Volgens Chaung is de radicaal-recombinatie-reactie aan vaste deeltjes mede bepalend voor de CO-verbrandingssnelheid en de uiteindelijke evenwichtssamenstelling van het gas.
Zijn conclusies voor omstandigheden als in het vrijboord zijn onjuist door het overschatten van de deeltjesconcentratie aldaar.
Op grond van zijn bevindingen zou evenwel de hoge CO-emissie van het wervelbed verklaard kunnen worden.
Chaung, T.Z. "Particle entrainment and chemical reactions in the freeboard of a fluidized bed coal combustor". Dissertation, Massachusetts Institute of Technology, Massachusetts, MA, USA (1982).